DOCTOR OF SCIENCE

The influence of structural details, geotechnical factors and environs on the seismic response of framed structures.

Madden, Patrick

Award date:
2014

DOCTOR OF SCIENCE

The influence of structural details, geotechnical factors and environs on the seismic response of framed structures.

Patrick Madden

2014

University of Dundee

The influence of structural details, geotechnical factors and environs on the seismic response of framed structures

Patrick Madden

A dissertation submitted for the degree of Doctor of Philosophy
December 2013

Department of Civil Engineering
School of Engineering, Physics & Mathematics
College of Art, Science & Engineering
University of Dundee

"*It takes an earthquake to remind us that we walk on the crust of an unfinished earth*."

Charles Kuralt

Declaration

I hereby declare that except where specific reference has been made to the work of others, the contents of this dissertation are wholly the result of my own original work. Neither this dissertation, nor any part of it, has been presented or is currently submitted in candidature for any other degree or qualification at this or any other University.

Patrick Madden (candidate)
December 2013

Dr. Jonathan Knappett (supervisor)
December 2013

Acknowledgements

Firstly I would like to express sincere gratitude to my supervisor Dr. Jonathan Knappett. Without his guidance I may never have undertaken post-graduate research. He inspired my interest in this particular field and gave me the belief that I could carry out this work. I am grateful for his continued support, encouragement and advice throughout the course of the project.

I would like to thank members of the geotechnical research group at the University of Dundee, whose assistance and feedback on various aspects of the project were always provided when requested.

I am very grateful to the technical staff within the Department of Civil Engineering at the University of Dundee, who skilfully manufactured the model components required for this research and assisted in operating the centrifuge boom during the centrifuge analysis.

I would like to thank the Northern Research Partnership and the EPSRC, whose financial support grants made this research possible.

To my close friends, both here in Dundee and further afield, I would like to thank you for your unwavering support and motivation throughout my post-graduate experience. A special thank you must be given to Tony Allison whose ‘pep talks’ and support were a true inspiration.

Finally I would like to thank my family, whose love, support and understanding throughout my entire education made this all possible.

Abstract

Seismic events around the globe directly affect all ranges of structures, from complex and expensive ‘skyscrapers’ to simple frame structures, the latter making up a higher proportion of the number of structures affected as they are a much more common type of structure. The impact of a seismic event can be devastating, especially if adequate predictions of their impact and imposed structural response are not made during the design stage of the structure. Knowing what response to expect allows the engineer to design the structure to survive an event and protect the occupants. The structural response to a seismic event is very complex and can be affected by a wide range of structural, geotechnical and environ parameters. While larger, expensive structures make use of expensive, time consuming, finite element analytical procedures to determine their response the cheaper, simpler, frame structures have to make do with existing, simplified, spectral method predictions.

This research firstly involves finite element analysis of simple frame structures, considering different structural and geotechnical parameters which may influence the seismic response, namely the stiffness of the structural joints, the geometry of the structure (influencing the individual structural element flexibility) and the foundation conditions (fixed base or shallow foundations with soil structure interaction). A range of frames, of varying geometry, are considered which mobilise different amounts of inter-storey drift, local rotation and global rotation response. The influence of soil structure interaction (SSI) and frame rigidity (i.e. the properties of the joints) on the response behaviour is investigated. The finite element database is then used to validate improved methods for predicting the spectral response parameters, specifically the natural period and damping of equivalent single degree of freedom (SDOF) systems, which include the effects of frame rigidity, geometry and SSI.

Dynamic centrifuge testing is also carried out in order to further validate the improved spectral model for the case of real soil with shear dependant stiffness. The physical model testing is also extended to consider how environs, such as other structures in close proximity, influence the response of a structure.

Table of contents

Notations

Symbol	**Description**
Roman:	
a_g	Peak ground acceleration at top of bedrock
a_{gf}	Peak ground acceleration at top of soil, free field
B	Foundation width
c	Cohesive strength of the soil
c'	Cohesion yield stress
D	Embedment depth of found
E	Modulus of Elasticity
e	Embedment depth of found
e_{min}	Minimum void ratio of the soil
e_{max}	Maximum void ratio of the soil
e_o	Initial void ratio of the soil
F	Force
f	Far end of beam under consideration
f_j	Beam restraint demand factor
f_n	Natural frequency
G	Shear modulus of soil
G_0	Small strain shear modulus of soil
H	Height of structure
H_s	Depth of soil layer
h_{CM}	Height to centre of mass
I_b	Second moment of area beam
I_c	Second moment of area column
i	Storey level, 1 at ground, 2 at first floor…etc
K_i	Rotational stiffness at end of column i

K_0	Lateral earth pressure
K_R	Foundation rotational stiffness
Kx	Foundation lateral stiffness
k_{col}	Individual column stiffness
k_{eq}	Structural lateral stiffness
k_{fr}	Foundation local rotational stiffness
k_{fx}	Foundation horizontal stiffness
k_{fz}	Foundation vertical stiffness
$k_{f\phi}$	Foundation global rotational stiffness
k_j	Rotational stiffness of a joint
k_s	Total column stiffness for storey s
L_b	Length of beam (distance between columns)
L_c	Length of column
L_{crit}	Critical length rocking foundation
L_f	Foundation length
M	Moment
M_{eq}	Equivalent mass for a structure
M_j	Mass of storey j
M_p	Moment capacity
M_s	Moment magnitude of an earthquake
m	mode
N_c	Bearing capacity factor for cohesion
N_q	Bearing capacity factor for embedment
N_γ	Bearing capacity factor for self weight
n	Near end of beam under consideration
p'	Mean confining stress in soil
p_a	Reference stress
q	Bearing pressure of the structure
q_f	Bearing capacity of the foundation
R	Fixity factor

R_1	Fixity factor at ground level
R_2	Fixity factor at 1st storey level
R_m	Fixity factor mean value
r_d	Stress reduction factor
r_x	Foundation area
S	Soil amplification factor
S_{De}	Elastic displacement response spectrum
$S_{De\ s,\ m}$	Elastic displacement response spectrum for storey s mode m
$S_{De\ m}$	Elastic displacement response spectrum for mode m
S_e	Horizontal elastic response spectrum
s	storey
T_n	Natural period of a fixed base structure
$T_{n,i}$	First mode natural period of a fixed base structure
$T_{n,j}$	Second mode natural period of a fixed base structure
$T_{n,ssi}$	Natural Period of a structure founded on soil
V	Vertical load
V_s	Shear wave velocity
w	Inter-building spacing coefficient
x	Horizontal measurement
$\bar{y}$	Modal coordinate
z	Vertical measurement

Greek:

β_x	Rectangular footing horizontal coefficient
β_z	Rectangular footing vertical coefficient
β_ϕ	Rectangular footing rotation coefficient
Γ_m	Modal participation factor
γ	Shear strain
γ_s	Unit weight of soil
Δ_e	Change in voids ratio

ΔH	Seismically induced settlement
Δ_z	Vertical displacement
ε_{vc}	Volumetric strain within the soil
ζ	Viscous damping ratio
ζ_f	Foundation damping factor
ζ_{soil}	Soil damping ratio
ζ_{ssi}	Viscous damping ratio with soil structure interaction
ζ_{st}	Structural damping by isolated structural elements
η	Damping correction factor
θ	Rotation angle
λ	Flexibility factor
v	Poisson's ratio
σ_{v0}	Total effective overburden stress
σ'_{h0}	Horizontal effective stress
σ'_{v0}	Vertical effective stress
τ_{av}	Average shear stress
φ	Friction angle of soil
ψ	Dilation angle of soil

Chapter 1

Introduction

1.1 Global seismic impact

The risk of seismic activity is an ever-present global problem. The global seismic hazard map, Figure 1.1, illustrates, for the entire globe, the peak ground accelerations expected from a 475 year return period earthquake occurring at that location. This return period represents a typical level of earthquake history that would be used in design for a 'no collapse' condition.

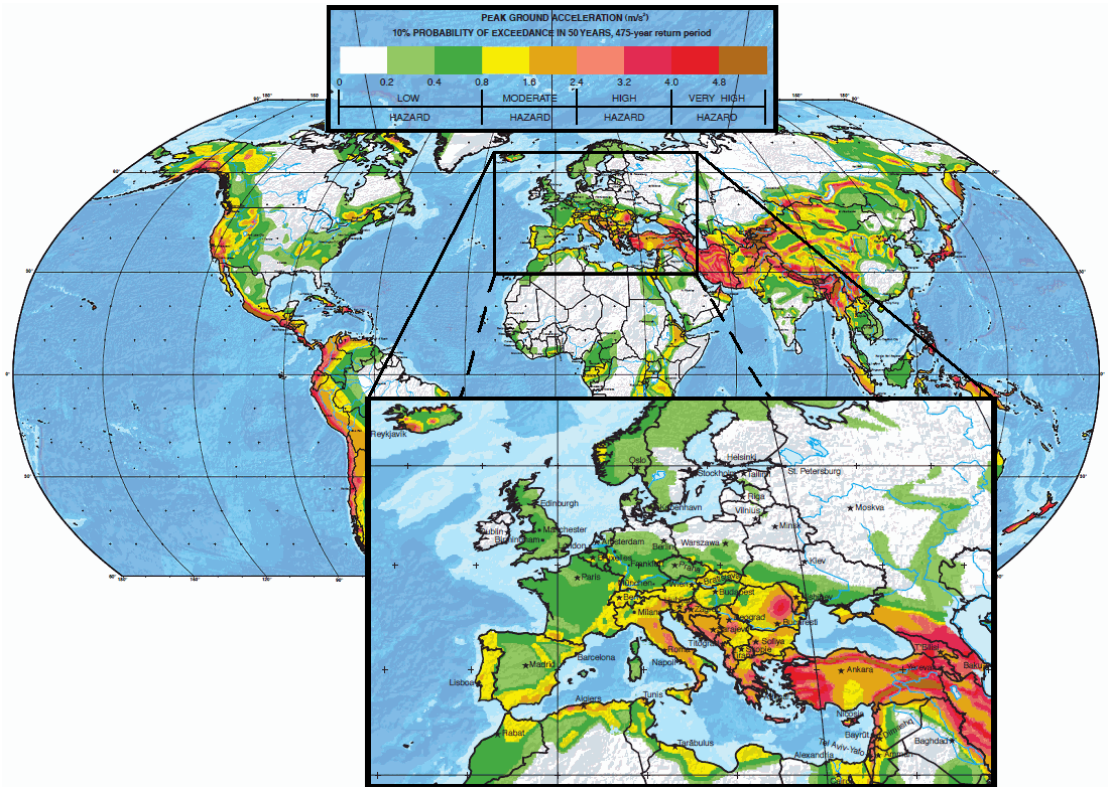

Figure 1.1 Global seismic hazard map after (Glardini *et al.*, 1999)

Europe, in Figure 1.1, has been enlarged to highlight that a large area of the continent, primarily covered by Eurocode design, is prone to 'moderate' to 'high' hazard risk. There are many cities and other urbanised areas already existing in earthquake prone regions. There is a need to fully understand the seismic hazard in such areas and a continued need to redevelop parts of these settlements or enlarge them.

During an earthquake, buildings and the ground they stand on are subjected to seismic ground motion as the principal loading. This loading is transferred through each part of the system onto the next causing vibration within the building, leading to damage and even collapse of parts of the building, or the whole system, if the shaking is severe enough. Examples of earthquake induced damage to European, framed buildings are outlined in Figure 1.2. In turn this damage endangers the lives of people in the area. The effect of seismic activity on buildings has therefore always been a major concern for civil engineers in Europe and indeed around the world.

Figure 1.2 Top left: Damage to Hotel Degli Abruzzi, L'Aquila, Italy, 2009 (www.emsc-csem.org), Top right: four storey partial building collapse Greece, 1999 (www.itsak.gr), Bottom left: collapsed building Kocaeli, 1999 (www.eepimap.com), Bottom right: Building collapse Aigion, Greece 1995 (www.eepimap.com).

1.2 Designing structures for seismic loading

Over the years many different novel methods of protecting structures from seismic loading have been developed. These include, but are not limited to, liquid mass dampers, fluid viscous dampers and base isolation techniques, which are shown in Figure 1.3. While these mechanisms do indeed protect the structure from seismic motions they are complex systems which are expensive to install, a cost which is often excessive compared to the cost of the overall structure.

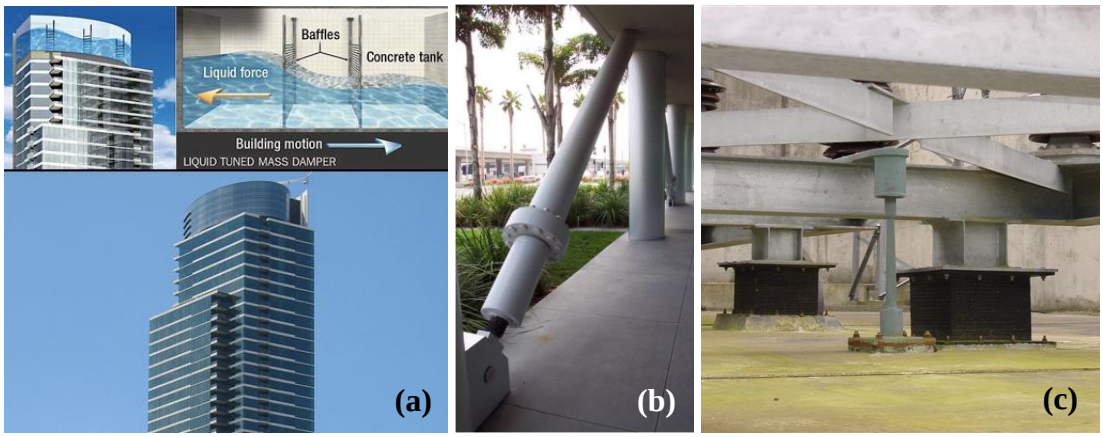

Figure 1.3 (a) Liquid mass damper, One Rincon Hill (www.techeblog.com) (b) Fluid Viscous Dampers (www.seismico.com) (c) base isolation elements (www.seismicisolation.com)

These methods therefore are usually reserved for high-rise, high-value structures. Low rise, lower-value structures have to rely on structural element design and geometry in order to provide a suitable level of seismic resilience. By adapting these parameters a building more suitable to surviving a seismic event, with limited structural damage, can be designed. Therefore it is important for an engineer to be able to accurately predict how structures, of different geometries and different structural make up, will respond to seismic loading. Finite element analysis can be a powerful tool in analysing the response of a structural system to a seismic event; however this method of analysis comes at a high cost and can take a long time to develop and analyse. As a result this method is also often reserved solely for high-rise, high-value structures. Low - Medium rise structures, which make up a large proportion of the structures in seismically active zones and are often the structures in which collapse/damage is observed, rely on simpler, spectral based methods of analysis in order to predict their response. While these methods are indeed simpler they can still produce representative results, thanks to the level of research that has

formed the background for their development. However all too often these calculations are overly simplified, disregarding certain characterises of the system which may prove beneficial or detrimental to the system's response.

1.3 Outline of thesis

The main objectives for this research are

i) To produce improved methods for determining the spectral response of framed structures accounting for semi-rigid construction, frame geometry and soil structure interaction.

ii) To investigate how the responses parameters may be affected by the presence of adjacent structures, (Structure soil structure interaction).

These objectives will be addressed over seven chapters as follows:

- Chapter 2: Introduces the basic principles behind the design of structures in seismic prone areas and reviews the current state-of-the-art understanding of seismic structural performance in both isolated and grouped scenarios.

- Chapter 3: Presents the design of the structural frames that are to be analysed. It also outlines the method of modelling the structures within the finite element package ABAQUS/CAE, along with analysis procedures for conducting (virtual) pseudo-static push-over tests, determining natural frequencies of the soil-structure systems and conducting full dynamic analyses in the time domain.

- Chapter 4: Outlines an improved spectral prediction method for estimating a system's peak seismic response. It then reports, compares and discusses the results from the finite element analyses. Finally the results from the finite element analyses are used to validate the new spectral prediction method.

- Chapter 5: Details centrifuge model tests that were carried out on both independent and adjacent buildings on soil, subjected to seismic loading. It outlines the centrifuge modelling principles that were adhered to, the facility

that was utilised, the modelling techniques required for the testing to be carried out and the method of analysis that was followed.

- Chapter 6: Discusses the observations of the centrifuge tests, the response of the structures and the factors affecting the response. It extends the spectral method of predicting the response of structures to earthquake loading, presented in Chapter 4, in order to incorporate the non-linear behaviour of real soil and also allows spectral prediction of settlement. A validation of this improved method is subsequently presented against the centrifuge data for isolated structures. Finally it looks at how adjacent structures (environs) affect the response of the structures.

- Chapter 7: Summarises the findings and comments on their implications in terms of the design of structures subjected to seismic loading. Suggestions for future research are also outlined.

Chapter 2

Literature Review

2.1 Introduction

This chapter will introduce the basic principles behind the design of structures in seismic prone areas and the current understanding of their seismic performance.

2.2 Spectral seismic design to Eurocode 8

Eurocode 8: Design of structures for earthquake resistance, (BSI, 2008b), outlines, in Section 1, its purpose as to ensure that "*human lives are protected, damage is limited, and structures important for civil protection remain operational*". It further enforces this in Section 2 where it states that structures have a no-collapse requirement, whereby they are required to withstand the design seismic action, of an event with a 475 year return period, without local or global collapse and retain structural integrity and residual load bearing capacity after the seismic event. A damage limitation requirement is also outlined as a structure's ability to withstand a smaller scale, larger probability of occurrence seismic motion with a 95 year return period, without the occurrence of damage and the associated limitations of use.

For routine design Eurocode 8, (BSI, 2008b), outlines a simple spectral analysis method in which the horizontal elastic inertial response, $S_e(T_n)$, of a structure, is determined from the following expressions:

$$0 \le T_n \le T_B : S_e(T_n) = a_g S\left[1 + \frac{T_n}{T_B}\left((\eta 2.5) - 1\right)\right] \qquad \textbf{Equation 2.1}$$

$$T_B \le T_n \le T_c : S_e(T_n) = a_g S \eta 2.5 \qquad \textbf{Equation 2.2}$$

$$T_C \le T_n \le T_D : S_e(T_n) = a_g S \eta 2.5 \left[\frac{T_C}{T_n} \right] \qquad \textbf{Equation 2.3}$$

$$T_D \le T_n \le 4s : S_e(T_n) = a_g S \eta 2.5 \left[\frac{T_C T_D}{T_n^{\,2}} \right] \qquad \textbf{Equation 2.4}$$

This prediction is based on the design ground acceleration at the top of the bedrock, a_g, for the earthquake event in question (i.e. a 'no collapse' event or a 'damage limitation' event), the soil amplification factor, S, which is related to the ground type (see Table 2.1), the natural period of the structure T_n, the damping correction factor η:

$$\eta = \sqrt{10/(5+\zeta)} \ge 0.55 \qquad \textbf{Equation 2.5}$$

where ζ is the viscous damping ratio of the structure, and by T_B, T_C and T_D which are defined in Table 2.1 for different ground types.

The elastic displacement response spectra, $S_{De}(T_n)$ is also defined in Eurocode 8, (BSI, 2008b), clause 3.2.2.2, and is obtained by a direct transformation of the elastic acceleration response spectrum, $S_e(T_n)$, using Equation 2.6

$$S_{De}(T_n) = S_e(T_n) \left[\frac{T_n}{2\pi} \right]^2 \qquad \textbf{Equation 2.6}$$

The effects of structural dynamic properties (T_n and η) and ground type (including site effects) are summarised in Figure 2.1.

Ground Type	***S***	***T_B(s)***	***T_C(s)***	***T_D(s)***
A	1.0	0.15	0.4	2.0
B	1.2	0.15	0.5	2.0
C	1.15	0.2	0.6	2.0
D	1.35	0.2	0.8	2.0
E	1.4	0.15	0.5	2.0

Table 2.1 Ground type dependent ground factors and limiting periods

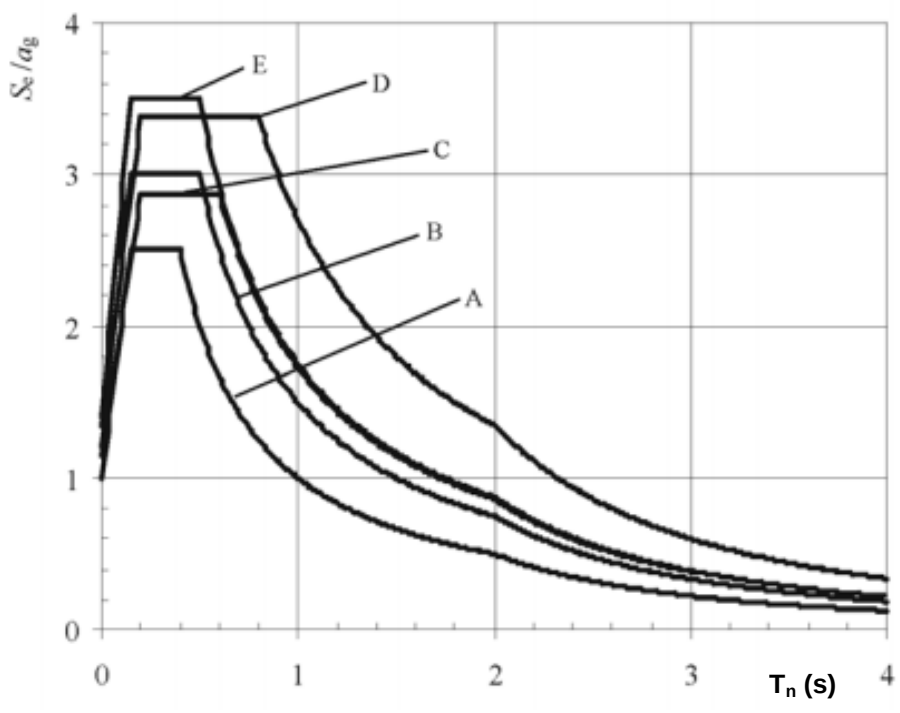

Figure 2.1 Type 1 elastic response spectra for ground types A to E (5% damping), (BSI, 2008b)

While the ground type will affect the general shape of the spectrum the calculations for predicting the horizontal elastic response spectrum are also based around the natural period and damping of the structure. The accuracy of this response spectrum is therefore linked directly to the accuracy in predicting these parameters.

Most other seismic building codes from around the world also permit response spectrum analysis procedures for the dynamic analysis of structures constructed in a similar way. While an exact comparison between the different elastic response spectra from the different codes is difficult, as each code has been developed differently, Chopra (2011) provides a general spectral shape comparison for the response spectrum developed in the National Building Code of Canada (NBCC), (CCBFC, 2010), the Mexico Federal District Code (MFDC), (GFD, 2004), the International Building Code-United States (IBC), (ICC, 2009) and Eurocode 8, (BSI, 2008b), which is presented in Figure 2.2. The elastic response spectrum, S_e , has been normalised relative to its value at zero period in order to remove any difference in peak ground acceleration implied by the different spectral shapes while still providing a direct comparison of spectral shapes. The spectral shapes have been presented for ground types similar to that of ground type C in Eurocode 8, (BSI, 2008b), with 5% structural damping. While none of the codes are exact copies of one another the

general shape of each is similar, with the scale of the European, Canadian and USA codes proving most similar after normalisation.

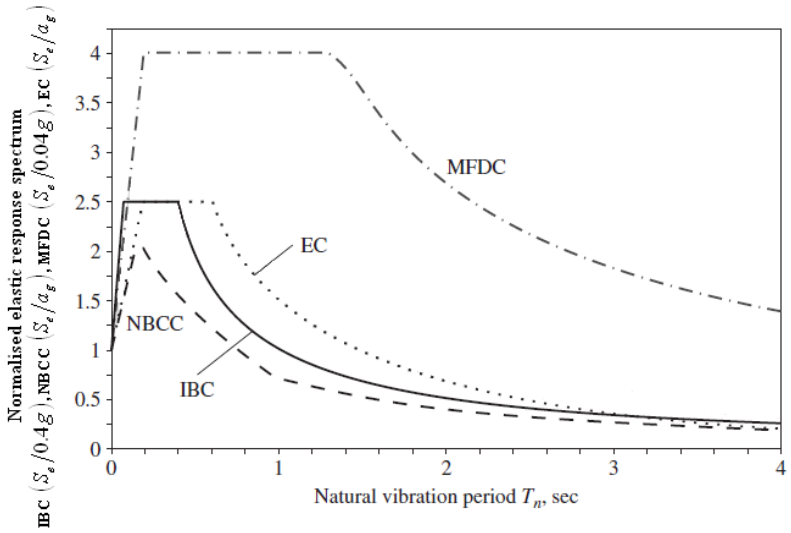

Figure 2.2 Comparison of the elastic response spectra from different codes after (Chopra, 2011)

The Eurocode 8, (BSI, 2008b), method for calculating the natural period of the structure utilises Rayleigh's principle, (Chopra, 2011), for modelling a multi degree of freedom (MDOF) structure by an equivalent single degree of freedom system representing the response in the first or fundamental model of vibration, where the natural period is given by:

$$T_n = 2\pi\sqrt{\frac{M_{eq}}{k_{eq}}} \qquad \textbf{Equation 2.7}$$

where:

$$M_{eq} = \sum_{s-storeys} M_s\left(\bar{y}_s\right)^2 \qquad \textbf{Equation 2.8}$$

$$k_{eq} = \sum_{s-storeys} k_s\left(\bar{y}_s - \bar{y}_{s-1}\right)^2 \qquad \textbf{Equation 2.9}$$

In Equations 2.8 and 2.9 $\bar{y}$ represents the modal coordinate considered for that storey from the mode shape. For each storey, *s*, M_s is the mass of the storey and k_s is the summation of the stiffness provided by all the individual columns, k_{col}, making up the storey. Traditionally k_{col} is calculated from Equation 2.10(a) or 2.10(b) depending

on whether the joint connecting the column to the mass is considered fixed or pinned respectively.

$$\textbf{(a)} \quad k_{col} = 12\frac{EI_c}{L_c^3} \qquad \textbf{(b)} \quad k_{col} = 3\frac{EI_c}{L_c^3} \qquad \textbf{Equation 2.10}$$

A MDOF structure will have multiple possible mode shapes which can be represented by individual SDOF systems. By obtaining the T_n for each mode that is to be considered the displacement response for each mode, S_{Dem}, can be obtained from the design spectra outlined previously. The true response of a MDOF system will be a combination of the response in each of the possible modes. In order to calculate an accurate combination of the modal responses a modal participation factor must first be obtained from Equation 2.11.

$$\Gamma_m = \frac{\sum_{s-storeys} M_s \bar{y}_s}{\sum_{s-storeys} M_s \bar{y}_s^2} \qquad \textbf{Equation 2.11}$$

The displacement of each storey in each mode, $S_{Des,m}$, can be found using the spectral displacement for the mode, S_{Dem}, the modal coordinate, $\bar{y}_s$ and the modal participation factor, Γ_m, as shown in Equation 2.12

$$S_{Des,m} = \Gamma_m \bar{y}_s S_{Dem} \qquad \textbf{Equation 2.12}$$

In order to combine the effect of each mode considered and obtain the overall displacement predicted for a MDOF system, the square root of the sum of the squares method, (SRSS), is used, Equation 2.13.

$$S_{De} = \sqrt{\sum_{m-\text{modes}} \left(\Gamma_m \bar{y}_s S_{Dem} \right)^2} \qquad \textbf{Equation 2.13}$$

This provides accurate response estimates, (Chopra, 2011), for structures with well spaced natural frequencies that can be considered independent of one another by satisfying Equation 2.14, (BSI, 2008b).

$$T_{n,j} = 0.9T_{n,i}$$ **Equation 2.14**

where: $T_{n,i}$ is the natural period of a given mode

$T_{n,j}$ is the natural period of the subsequent mode

In general, due to the low frequency input to the system by most earthquakes, it is the first mode shape, and therefore the first natural period, that is of most importance when considering the response. In many cases it is therefore sufficient to only account for the first mode during analysis.

This method gives an estimation of the natural period of the structure, assuming that the columns are the only flexible elements; however, it does not account for the flexibility applied to the frame through its joint system, flexure of the beams/floors or any soil structure interaction. Furthermore the damping correction factor considered in Eurocode 8, (BSI, 2008b), only considers the viscous damping of the structure itself and not the additional damping from the soil-structure interaction.

2.3 Semi-rigid (steel) structures

Additional flexibility and damping may be introduced into the structure through flexibility of the horizontal structural elements (e.g. the beams) and the joint systems connecting the beams and columns.

2.3.1 Joint systems used in steel frame construction

The forces and moments that build up in a moment resisting frame, both under static and seismic loading, will be transmitted from one structural member to another through the joint system. Therefore it is important that the joints' ability to transmit these loads is taken into account. Equation 2.10 does somewhat consider the joint system when estimating the natural period of a structure; however, it only considers the two extreme cases of either fully fixed or fully pinned. A fully fixed joint implies that full slope continuity exists between the beam and column and that full gravity moment is transferred between the members, whereas in a fully pinned case the beam behaves as a simply supported member with the column carrying no gravity moment from the beam, (Chen *et al.*, 1991). While conventional analysis and design of steel frameworks is usually carried out under these assumptions evidence from

experimental observations, (Goverdhan, 1983; Davison *et al.*, 1987; Chen *et al.*, 1989), show that they will overly simplify the system and that all connections used in practice possess rotational stiffness which falls between these extreme cases. Even if the joint is designed to match these extreme cases the stiffness of each individual joint will be affected by multiple factors; some of the most important ones outlined by Barakat (1988) and Chen *et al.* (1986) are highlighted below:

- Material discontinuity of the connection assemblage
- Local yielding of some component parts
- Stress and strain concentrations caused by holes, fasteners and bearing contacts of elements used
- Local buckling of flanges and/or web of beam/column
- Overall geometric changes under the influence of applied loads.

Abdalla *et al.* (1995) provided data on 44 tests carried out on a wide range of steel beam to column connections tested by multiple parties independent of one another. A summary of the details of these tests is given in Table 2.2, with the different joint compositions shown schematically in Figure 2.3.

Data from these tests, in terms of the global moment-rotation behaviour (i.e. describing the flexibility of the joints) is compiled and compared in Figure 2.4. From this figure it is evident that none of the considered joints match the extreme fixed or pinned cases. The moment reached within the joints in Figure 2.4 has been normalised by the moment capacity of the weakest structural element, beam or column, as recommended under Eurocode 3, (BSI, 2008a), for steel structures. However for some of the tests it was seen that this moment capacity was exceeded. This may have been due to the influence of the very stiff 'stubby' beam or column elements utilised within the tests being less influential than they would be in a real frame. While this does not affect the stiffness of the joint itself it would result in the test measuring the maximum moment capacity of the joint itself, rather than the stronger structural member(s) to which it is connected. In such cases the moment building up in the joint has been normalised by the maximum capacity achieved by the joint.

Overlaid onto Figure 2.4 are the regions of joint behaviour specified by Eurocode 3, (BSI, 2008a). The initial stiffness of each joint, before moment capacity has been reached and a plastic hinge forms, falls within either a 'nominally fixed'

zone, a zone within which Eurocode 8, (BSI, 2008b), recommends treating the joint as fully fixed, or at the upper end of the 'semi rigid' zone, the zone which lies between the nominally fixed and nominally pinned cases. The composition of joint system appears to heavily influence the stiffness of the joints, with the end plate type clustering within the nominally fixed region. The double web angle type joints appear more flexible and remain within the semi-rigid zone and the header plate type joints are more variable but still remain between the nominally fixed and semi-rigid zones. Therefore considering a joint as either fully fixed or fully pinned would not necessarily fully represent the actual behaviour of the structure.

No. of Tests	*Author*	*Column*	*Beam*
Double Web Angle			
2	Davison *et al.* (1987)	W6"×6"×16"	W10"×4"×15"
Top and Seat Cleat			
1	Davison *et al.* (1987)	W6"×6"×16"	W10"×4"×15"
1	Maxwell *et al.* (1981)	305×305 UC 97	457×191 UB 67
Extended End Plate			
2	Davison *et al.* (1987)	W6"×6"×16"	W10"×4"×15"
9	Zandonini *et al.* (1988)	99.0	IPE 300
2	Moore *et al.* (1986)	W6"×6"×16"	W10"×4"×15"
Flush End Plate			
3	Davison *et al.* (1987)	W6"×6"×16"	W10"×4"×15"
5	Philips *et al.* (1981)	W 200 × 100	W 250 × 33
Header Plate			
7	Aggarwal (1990b)	W8"×8"×31"	W8"×4"×17"
1	Davison *et al.* (1987)	W6"×6"×16"	W10"×4"×15"
Header plate & seat angle			
2	Aggarwal (1990b)	W8"×8"×31"	W8"×5.25"×17"
Double web and seat angle			
2	Davison *et al.* (1987)	W6"×6"×16"	W10"×4"×15"
9	Aggarwal (1990a)	W8"×8"×31"	W8"×5.25"×17"

Table 2.2 Database test summary

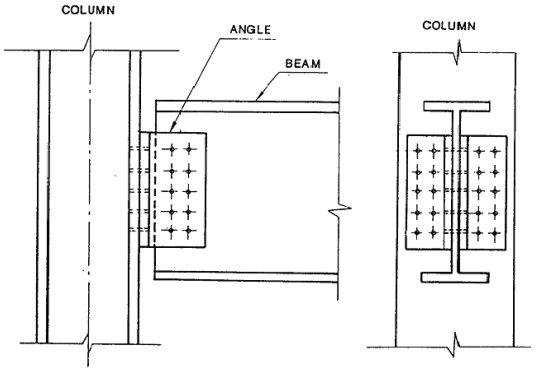

(a) Double web-angle connection

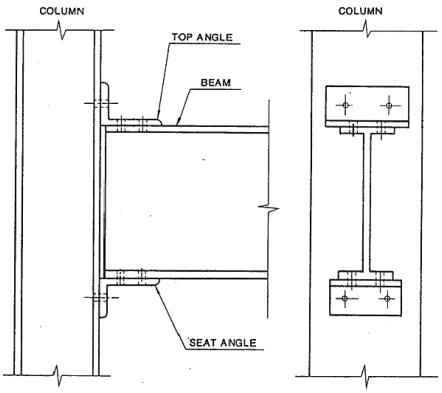

(b) Top and seat angle connection

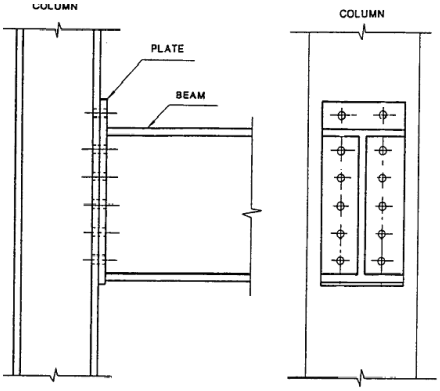

(c) Extended end plate (tension side) connection

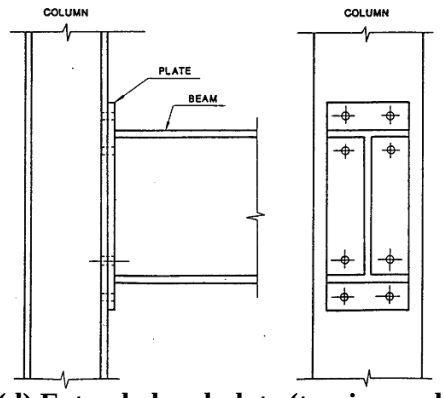

(d) Extended end plate (tension and compression side) connection

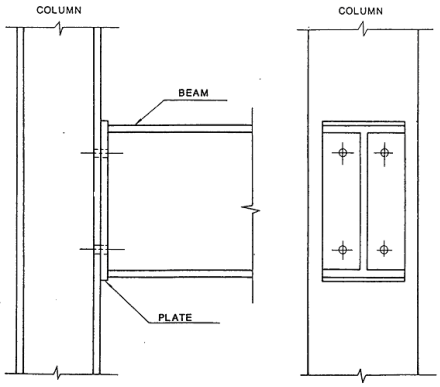

(e) Flush end plate connection

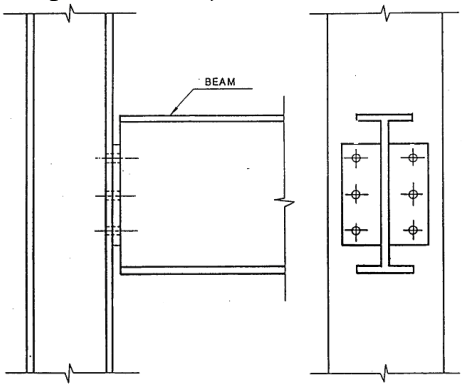

(f) Header plate connection

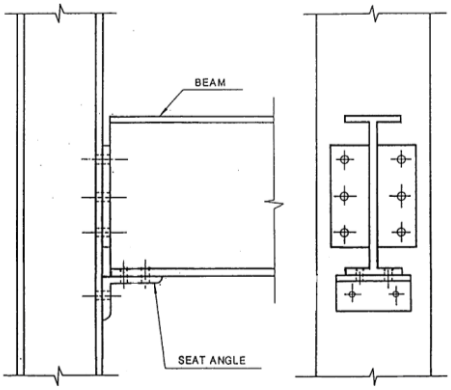

(g) Header and seat angle connection

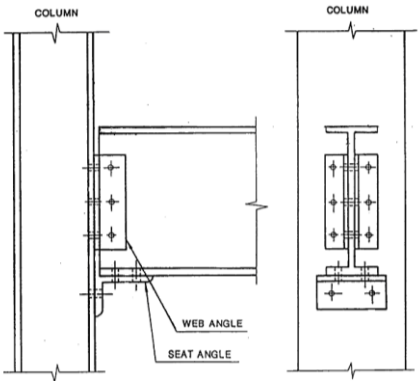

(h) Double web and seat angle connection

Figure 2.3 Database joint systems tested, after (Abdalla *et al.*, 1995)

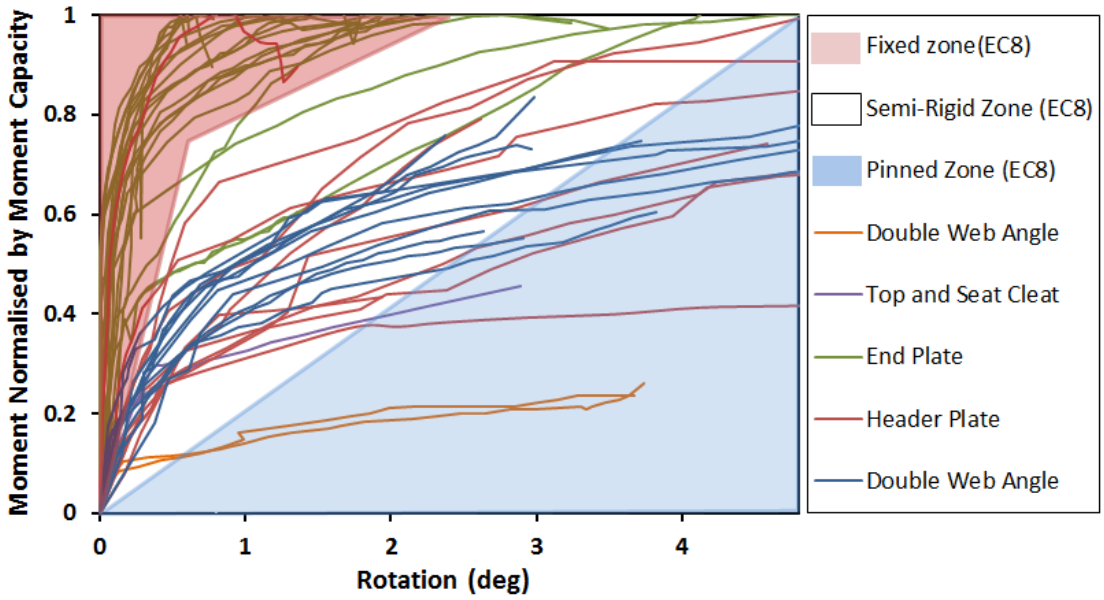

Figure 2.4 Normalised Moment-Rotation data from (Abdalla *et al.*, 1995) database

2.3.2 Structural element flexibility

In addition to the joint system, the structural elements of the columns and beams will also introduce flexibility to the system. While the Eurocode 8, (BSI, 2008b), method considers the stiffness of the column sections in its calculation it does not consider the second order effects on the stiffness of the column.

It also fails to consider the flexibility added to the system by the beam. By simply considering the beam as part of a rigid mass on top of the column it ignores this flexibility which may have an effect on the overall response, an effect that may be more prominent the longer the span of the beam element.

In order to consider the local second order effects on the stiffness of the column different authors have proposed different factors that account for this reduction in stiffness including LeMessurier (1977), Chen *et al.* (1991) and Hellesland (2009). It has been generally accepted that a value of this factor of between 1 and 1.22, applied to the sway stiffness, can be used for different degrees of deformation of a column.

"Flexibility factors" are used by Hellesland (2009) to correct for the increased flexibility of a column with given rotational end restraints based on the stiffness of the beam-joint connection. These are based on "fixity factors", outlined in Hellesland, (2008), which were developed for a free sway condition. These fixity factors are directly proportional to the first order end moment condition and can be written in

terms of relative rotational restraint flexibility factors, defined by Hellesland *et al.* (1996). Figure 2.5 , after Hellesland (2008), shows the variation of the "flexibility factor", λ, with reference to the "fixity factors", R, (R_{MIN} being the smaller and R_{MAX} being the larger of the first order rotational restraint fixity factors at either end of a member). Fixity factors range from $R = 0$ for a rotationally pinned end case to $R = 1$ for a rotationally fixed end case.

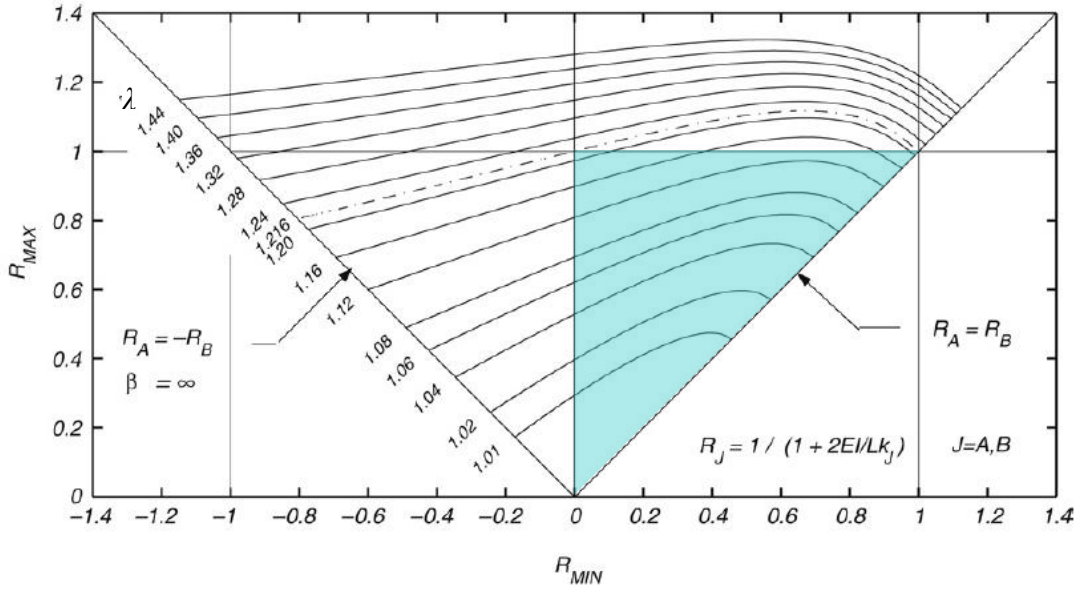

Figure 2.5 Variations in flexibility factor with fixity factors after (Hellesland, 2008)

In Figure 2.5 results in the lower right quadrant, shaded blue (where $0 < R_{MIN} < 1$ and $0 < R_{MAX} < 1$), represent bending shapes with positive restraints at both ends and double curvature bending – the flexibility factor in this case generally falls between 1 and 1.22. As mentioned above this range of between 1 and 1.22 has been previously stated as being generally acceptable as a flexibility factor for different degrees of deformation of a column. It would indeed be acceptable for similar stiffness columns in unbraced, regular frames where deflection matches the double curvature mode, however for irregular unbraced frames whose irregular loading caused a single curvature mode with negative restraints at one end of the column, as would fall into the bottom left segment of Figure 2.5, this factor could increase to 1.33. Furthermore in cases where the rotational restraint stiffness of the joint is very high the R_{MAX} value may exceed 1, further increasing the flexibility factor. Therefore by calculating the flexibility factor based on the fixity factors a more accurate factor can be calculated rather than assuming a value of between 1 and 1.22.

To combat the additional flexibility of the joint system and the structural beams, various authors, (Wang, 1983; Chen *et al.*, 1991; Xu *et al.*, 2002; Hellesland, 2009), have all proposed methods of calculating the rotational restraint stiffness at the end of a column. These methods include the rotational stiffness of the connection assembly itself as well as a restraining stiffness provided by the beams that are connected into that particular joint, using the individual beams' flexural stiffness as a variable. This allows consideration of multiple beams framing into a single column and also allows for different end connection rigidities at each end of the same beam. Combining the rotational stiffness of the joint and restraining stiffness of the beam in one equation allows for a near end pinned connection beam to introduce a zero multiplication term to the equation, therefore also removing the beam restraining stiffness as it is unable to influence the connected column through a pinned joint, (Xu *et al.*, 2002). This value of rotational restraint stiffness can then be used to calculate the fixity factors mentioned above, an example of this calculation will be given later in Chapter 4, Section 4.2.1.

The fixity factors presented by Hellesland (2008) allow for the rotational restraint stiffness values to be incorporated directly into calculations. Therefore by utilising the equation derived by Hellesland (2008) to compute the first order lateral stiffness of the columns, an equation which includes the fixity factors to account for the second order effects on the column stiffness, which in turn include the rotational stiffness of the connection and adjoining beams, all of the additional steel frame and second order effects, can be derived.

While these methods may account for the additional structural flexibility within a semi-rigid frame, there will also be additional flexibility introduced into the frame behaviour by soil structure interaction through the foundations that needs to be considered.

2.4 Soil structure interaction (SSI)

The concept of soil structure interaction, henceforth referred to as SSI, was developed in stages throughout the early 20th century with advances in SSI analysis gaining speed in the mid 20th century. This progression was born out of the advances in nuclear power and offshore industries and spurred on by the need to improve seismic safety after events observed during the 1967 earthquake in Caracas and the 1970

earthquake at Gediz, Turkey, involving the collapse of structures considered safe under fixed base conditions, (Dowrick, 1977).

SSI is a concept that Kausel (2010) describes as the "*static and dynamic phenomena mediated by a compliant soil and a stiffer super-structure*". Generally speaking, for the dynamic case at least, when a building is forced into a partnership with a soil, through its foundations, both the structure and the soil's reaction to the seismic loading will develop in accordance with each other due to the requirement of kinematic compatibility at their interface, ultimately changing their response. This effectively is known as the 'soil structure interaction effect' and it generates a very different structural response than that of the same structure, excited by the same seismic motion, but with its foundations fixed.

Despite it being widely recognised, (Wolf, 1985; Mylonakis *et al.*, 2000; Shakib *et al.*, 2004; Pitilakis *et al.*, 2008) among others, that the seismic response of a structure will be directly affected by the inherent flexibility of the soil with which it interacts, it is still common to use fixed-base structural response in seismic analysis of routine building structures. Even where it is considered, it is recommended that SSI effects only need be considered for relatively soft soils or structures having a high aspect ratio (tall compared to their width). It is considered negligible and can be ignored when considering structures founded on rock or very stiff soils, (BSI, 2008b; Pala *et al.*, 2008).

2.4.1 Primary effects of SSI on seismic structural response

The two principal factors responsible for the difference in seismic response, when considering SSI compared to the fixed base consideration, have been outlined by Veletsos *et al.* (1974) and Jennings *et al.* (1972) among others as:

- The additional horizontal, rotational and vertical flexibility of the foundations introduces more degrees of freedom and directly influences the dynamic characteristics of the structure, principally through a lengthening of the natural period of the structure.
- Vibrational energy of the flexibly supported structure may be dissipated by radiation damping through the soil.

The factors outlined above can be represented in the 'replacement oscillator approach' for elastic interaction effects, presented by Mylonakis *et al.* (2000) and depicted in Figure 2.6., where:

K_{eq} = structural lateral stiffness

K_R = foundation rotational stiffness

K_X = foundation lateral stiffness

ζ_{st} = damping ratio of a rigidly supported structure

ζ_{soil} = soil damping ratio

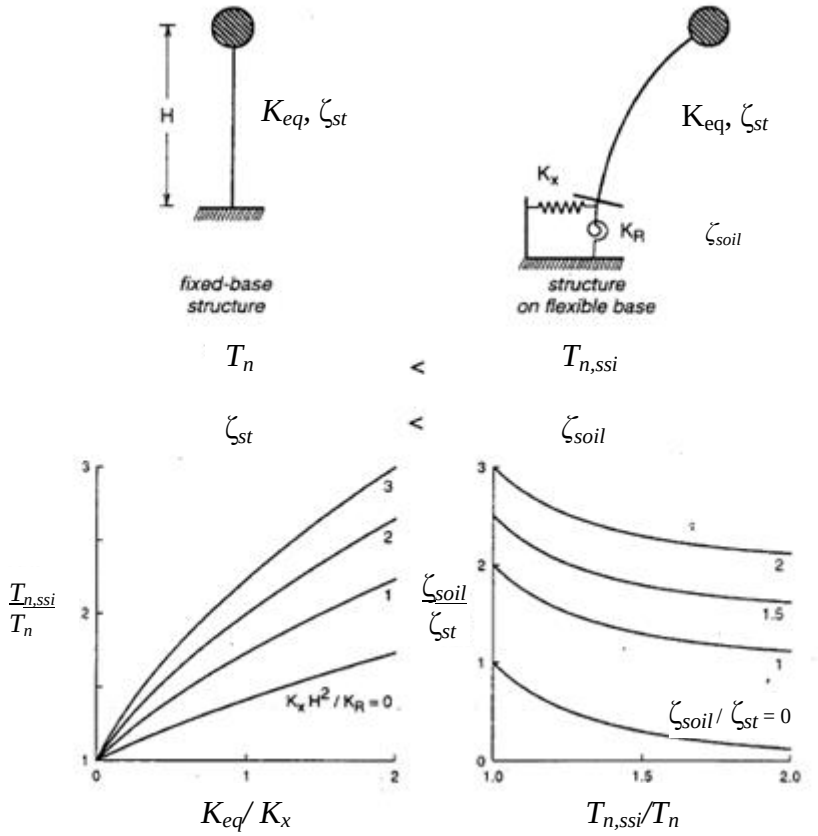

Figure 2.6 Effect of soil structure interaction on fundamental natural period and effective damping of a structure, after (Mylonakis *et al.*, 2000)

The main effect that these SSI factors have on the structure, as reported in Jennings *et al.* (1972) for the case of a single storey building on flexible foundations, is that the fundamental natural frequency of the structure is always shortened when SSI was considered. This has the effect of lengthening the natural period of the structure. At the same time as increasing the natural period of the structure, SSI also increases the damping available to the system. These two factors act in opposition when it comes to determining the seismic response, a longer period generally acting to

increase the response while the increased damping acts to reduce the response. Apart from extreme cases where taller slender structures with high flexibility, prone to large increase in natural period under SSI conditions, are supported on soft soils with naturally low damping, Eurocode 8, (BSI, 2008b), generally assumes that SSI will be beneficial (Figure 2.7) and therefore does not require consideration. This practice is sometimes considered an unsafe simplification, (Mylonakis *et al.*, 2000), and can lead to unsafe design for both foundations and superstructure as it may result in masking an increased seismic demand placed on the structure resulting from SSI, as happened in the Mexico City earthquake (1985).

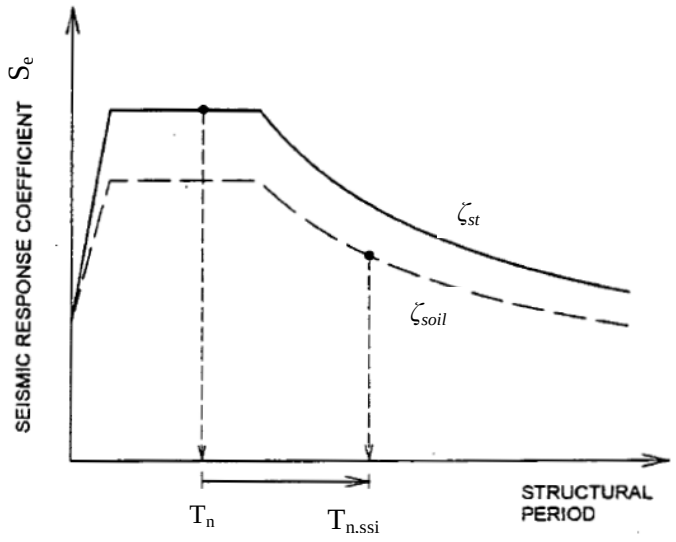

Figure 2.7 Reduction in seismic response due to SSI, after (Mylonakis *et al.*, 2000)

Elements within the structure itself, and the foundation system, may introduce similar large increases of the natural period of the system (e.g. due to additional flexibility from the joints/beams) without making the required improvements to damping the system that would be required in order to ensure that the SSI effect was beneficial. Accurately predicting the period lengthening and damping changes that a structure undergoes incorporating structural flexibility and SSI is therefore considered to be of high importance.

2.4.2 Estimation of primary SSI effects

The effect of period lengthening has been documented in field results by Stewart *et al.* (1999). They compiled and analysed 77 independent strong motion data sets from 57 building sites in California and Taiwan. A wide selection of structures were analysed

with different structural and environmental factors presented in Table 2.3. Within the table "Class A" sites refer to sites that contained both free field acceleration information and structural acceleration data from both the foundation and roof of the structure. "Class B" sites did not contain any free field data. The observed period lengthening ratio and foundation damping factor are presented in Figure 2.8.

Structural/Environmental factor	***Number of structures***
Data set:	
Class A	46
Class B	13
Foundation:	
Rock site	12
Soil site	4
Pile Found	23
Strip/Raft/Grade beam	34
No embedment	36
Single level basement	14
Multi level basement	7
Structure:	
1 – 4 storey	17
5 – 11 storey	27
> 11 storey	13
Lateral force resisting system:	
Masonry/concrete shear wall	19
Dual wall/frame system	11
Concrete frames	4
Steel frames	19
Base isolated frames	4

Table 2.3: Variable structural and environmental factors within data after Stewart *et al.* (1999)

Due to the large number of variables in Table 2.3 the period lengthening ratio and foundation damping factor are presented in terms of the dimensionless structure to soil stiffness ratio calculated by normalising the effective height of the structure, H, by the effective soil shear wave velocity, V_s, and the fixed base period, T_n. Stewart *et al.* (1999) acknowledge that there is a lot of scatter within the data and attribute it to factors such as aspect ratio and foundation embedment, type, shape and flexibility as well as the hysteric soil damping which varies with soil type.

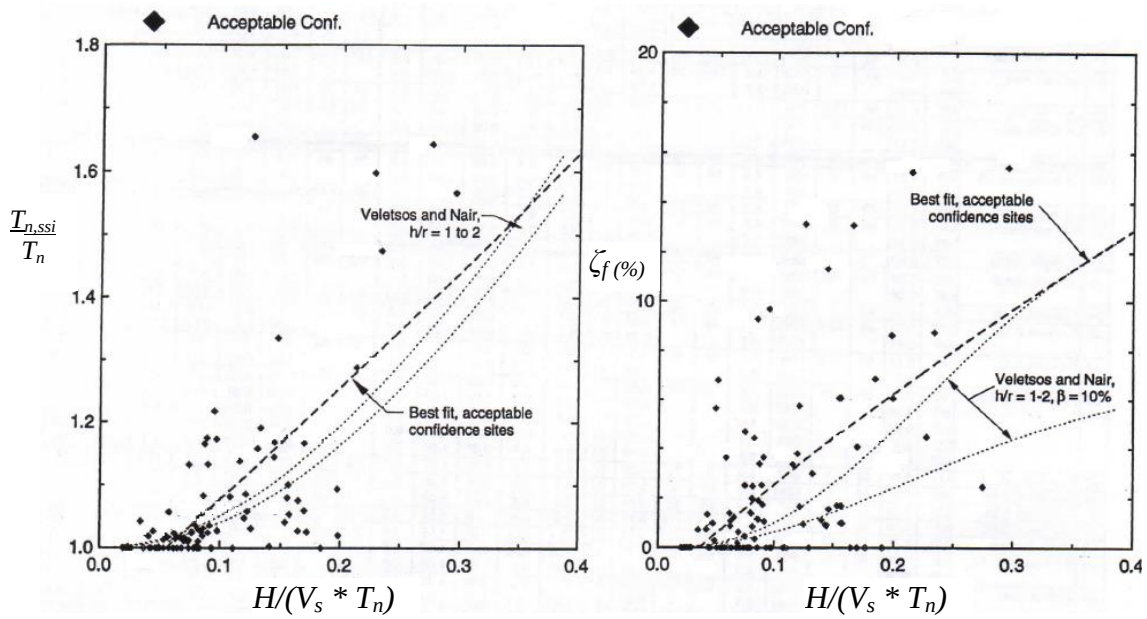

Figure 2.8 Observed period lengthening ratio and foundation damping factor (after Stewart *et al.* (1999))

Despite the scatter the best fit lines compare well with a simple relationship presented by Veletsos *et al.* (1975). This equation is presented below:

$$\frac{T_{n,ssi}}{T_n} = \sqrt{\left[1+\frac{k_{eq}}{k_{fx}}\left(1+\frac{k_{fx}h_{CM}^2}{k_{f\phi}}\right)\right]} \qquad \textbf{Equation 2.15}$$

In Equation 2.15 k_{eq} is the structural sway stiffness, and h_{CM} is the height to the centre of mass of the structure from the contact plane between the foundation and the soil. k_{fx} is the horizontal foundation stiffness and $k_{f\phi}$ the foundation's global rotational stiffness. The foundation damping factor is obtained after the equation by Veletsos *et al.* (1975) given as Equation 2.16:

$$\zeta_{ssi} = \zeta_f + \frac{\zeta_{st}}{\left(\frac{T_{n,ssi}}{T_n}\right)^3} \qquad \textbf{Equation 2.16}$$

where ζ_{st} is the structural damping provided by the structural elements of the frame and ζ_f is the foundation damping factor. Figure 2.9 shows more clearly the accuracy

of the Veletsos *et al.* (1974) and Veletsos *et al.* (1975) equations for period lengthening and foundation damping factor prediction. In Figure 2.9 the aforementioned method of prediction is used for the shallow foundations, while a method based on Bielak (1974) is used for the deep foundation predictions.

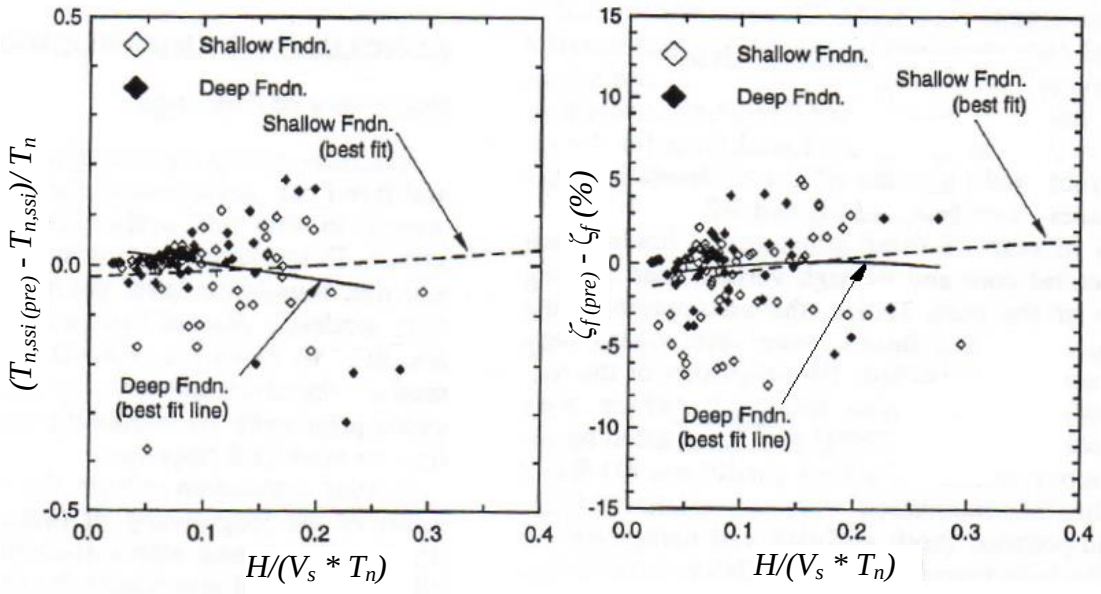

Figure 2.9 Errors in predicting period lengthening ratios and foundation damping factors (after Stewart *et al.* (1999))

While the scatter, mentioned previously, is still evident, the best fit line, especially for the shallow foundations, falls close to the 0 error datum. The amount of scatter for the predicted period lengthening generally falls within a range of ± 3%, however the foundation damping factor is much more difficult to predict and its range is generally between the ±8% error. As mentioned in section 2.4.1 the period lengthening and damping increase will have a direct impact on the seismic response of the structure.

2.4.3 Secondary effects of SSI

While SSI has a direct effect on the primary dynamic characteristics of a structure, as outlined in section 2.4.2., it also can introduce additional mechanisms of failure into a system that are not present for its fixed base counterpart. When considering the seismic performance of several tall slender structures during the 1960 earthquake in Chile and their apparent ability to outperform other "more stable" buildings, (Housner, 1963) proposed that foundation uplift and rocking may result in beneficial

radiation damping of the structures. He proceeded to show that the dynamic characteristics of a structure allowed to rock during a seismic event differed greatly from its fixed base counterparts.

The mechanism of rocking foundations resulting in uplift is shown in figure 2.10 (a) and (b). Figure 2.10 (a) highlights the critical length (L_{crit}) which will change as the rocking takes place, shown in more detail in 2.10 (b).

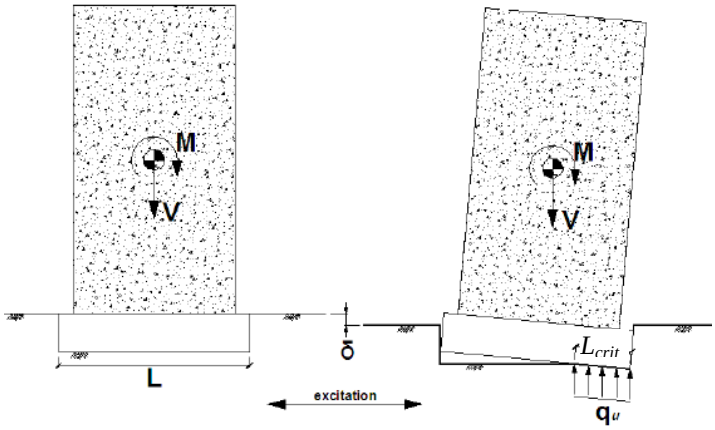

(a) Concept of a rocking foundation, (Algie *et al.*, 2010)

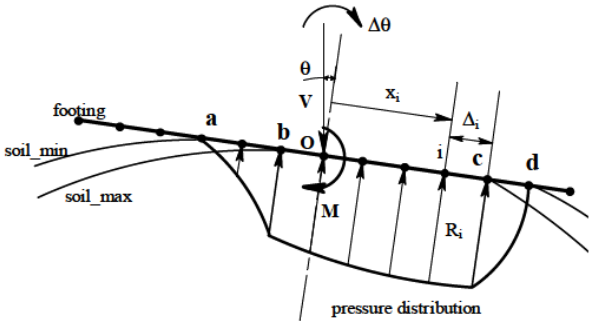

(b) Contact interface model for cyclic moment loading, (Gajan *et al.*, 2005)

Figure 2.10 (a) (b) Rocking foundation with uplift mechanism.

The rocking of the foundation can cause a rounding of the foundation soil which, as outlined by Gajan *et al.* (2005), can reduce the contact area between the foundation and the soil (defined by L_{crit}), inducing a nonlinear moment rotation relationship and therefore a reduction in overall stiffness. It can also result in a reduction in the bearing capacity of the foundation. Even without the rounding of the foundation soil the bearing capacity of a shallow foundation will be reduced when the foundation is subjected to rocking moments, horizontal loads, and particularly uplift, (Knappett *et al.*, 2006).

Current practice in the majority of seismic building codes is to produce strong rigid foundations that allow for no uplift or rocking to occur, (Ugalde *et al.*, 2007). In cases where it is considered to happen despite designing against it, its effects are neglected when considering the seismic response of the structure due to the presumption that neglecting the rocking mechanism will overestimate the seismic forces applied to the structural element and therefore result in a more conservative strength design, (Hung *et al.*, 2011). Therefore, current practices fail to take advantage of the possible benefits resulting from allowing rocking foundations.

Across the literature the benefits of rocking foundations are being reported. Through the centrifuge modelling of 50 models, of variable dimensions and system parameters, Gajan *et al.* (2005) highlighted that the dissipation of energy at the footing soil interface would reduce the demand on the structural elements of the system. Figure 2.11 shows the moment-rotation and settlement-rotation at the footing base centre, for one of the tests carried out. The large hysteresis loops of the moment-rotation curve show that a large amount of energy is being dissipated at the foundation/soil interface, with a degradation of the rotational stiffness.

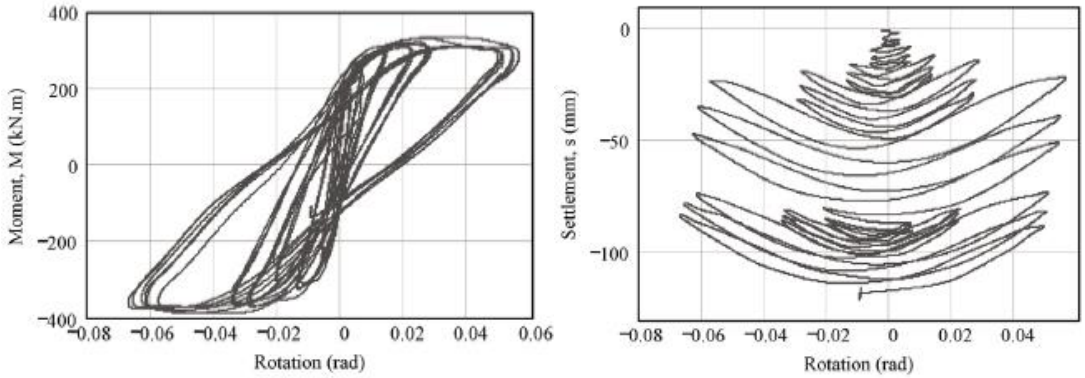

Figure 2.11 Moment rotation behaviour of footing soil interface (Gajan *et al.*, 2005)

The rate of settlement decreases due to embedment effects. Larger rotations result in increased uplift of the footing. This uplift creates a gap between the foundation and the soil, reducing the effective length of the footing and resulting in increased bearing pressure on the soil. As the soil around the footing still in contact with the soil does not remain elastic, a significant amount of energy is dissipated through its failure, (Ugalde *et al.*, 2007), which in turn increases the risk of uplift further. This uplift and bearing capacity failure may improve the damping of the structure, reducing the ductility demands on the structure and further protecting the superstructure, (Gajan *et al.*, 2008). Through their research into the response of bridge piers and field testing of

frame structures with shallow foundations, Hung *et al.* (2011) and Algie *et al.* (2010), respectively, also proposed that a rocking foundation and the bearing capacity failure may reduce the forces exerted on the super-structure and therefore protect the beams and columns from failure. Ugalde *et al.* (2007) summarised the main effects of rocking foundation as:

- Local bearing pressures increase resulting in plastic deformation of the soil around the footing resulting in additional hysteric damping;
- The act of rocking increases flexibility of the system and results in lengthening the natural period of the system;
- Peak moment demand in the column is limited by the moment capacity of the foundation, i.e. if the moment capacity of the foundation is lower than that of the columns, they will act as a fuse;
- Uplift of the foundation stores gravitational potential energy;
- The magnitude of settlement caused by rocking is dependant on the number of cycles and amplitude as well as the bearing capacity.

Ugalde *et al.* (2007) recommend that as a result of rocking foundations displaying excellent ductility, relatively small permanent deformations and their ability to "self centre" they can be used to reduce the demands on structural elements by dissipating energy through plastic deformation of the soil.

2.5 Structure soil structure interaction (SSSI)

Soil structure interaction describes how an isolated structure will respond to seismic excitation. However, a large percentage of buildings subjected to seismic loading exist in close proximity to other buildings. By considering these structures in isolation, certain mechanisms and effects on seismic response caused by the proximity of other structures may be missed. This effect, while it is based on similar principals as SSI, may be described more accurately as structure soil structure interaction, henceforth SSSI.

In his pioneering work on physically forcing a library building, on the Caltech campus, into vibration, Jennings (1970) observed that harmonic stationary records, picked up on seismographs a few kilometres away, corresponded with the building

period. Similar observations were made by Kanamori *et al.* (1991) and Kim *et al.* (2001) after the Colombia space shuttle re-entry to the atmosphere and the September 11th terrorist attacks on New York city respectively, also recorded by seismographs several kilometres away from the event. These events highlighted that the energy from a vibrating building could be efficiently transmitted into the soil as an outward propagating wave, (Bard *et al.*, 2006). If these external artificial events can induce such a response then a similar response could be expected from a structure vibrating due to a seismic event.

The effect of SSSI can be considered in two general ways, firstly by considering the effect of one structure on an adjacent structure or structures in its immediate vicinity and secondly by considering a wider city effect.

2.5.1 SSSI between adjacent structures

Research in the 1970's by Lee *et al.* (1973), investigating the SSSI between several adjacent nuclear reactor structures and by Wong *et al.* (1975) and Luco *et al.* (1973) addressing the anti-plane problem of interaction between infinite walls, helped define some of the main factors that could control the degree of interaction between structures, including:

- Relative foundation size
- The distance between the structures
- The mass of the superstructures
- The mass of the foundations
- Relative stiffness of the structure and soil

Since these early works there has been a wide range of research into the effects of SSSI, however with so many variables it is difficult to account for them all in any one analysis.

In their work looking at the through-soil interaction between nearby structures supported on pile groups in a three dimensional field Padrón *et al.* (2009) concluded that SSSI only really comes into effect when structures that have similar dynamic characteristics are in close proximity to one another, although whether the effect was

beneficial or not seemed to be more influenced by the spacing of the structures than their similarity/dissimilarity. When dissimilar structures were grouped together the effect of SSSI was less substantial. Similarly, Bard *et al.* (2006) proposed that while the overall effect of SSSI is beneficial due to the motion energy being reduced by the presence of the buildings, the effect of SSSI in adjacent structures was most evident in similar structures.

Padrón *et al.* (2009) proposed that when a short period structure was placed among a group of large period structures the effect was least favourable for the short structure. This ties in with Luco *et al.* (1973) and Wong *et al.* (1975) who proposed that SSSI is particularly important for a smaller and lighter structure when it is in interaction with a dissimilar large heavy structures. Analysing the effects of separation distance and relative mass of the structures through numerical parametric analysis to understand the nature of the interaction Bolisetti *et al.* (2011) noted that mass only affected the SSSI response when there was a large difference in the mass of the two structures, an overall increase in mass itself did not have much of an effect without the differential between two structures. More recent work by Aldaikh *et al.* (2011) confirmed this unfavourable effect on the smaller of the paired structures. Figure 2.12, from Aldaikh *et al.* (2011), shows that the response power spectra for the smaller building (top) increases when coupled with the larger building than when considered isolated. In doing so it has the effect of acting like a tuned mass damper for the larger building which sees its response power spectra reduce when considered alongside the smaller building.

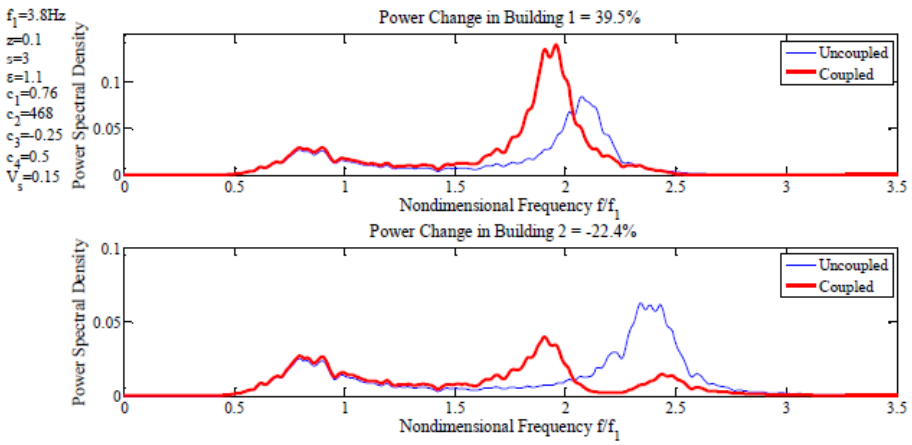

Figure 2.12 Response power spectra for total sway displacements for building 1 (small) and building 2 (large) due to Kanai Tajimi excitation, (Aldaikh *et al.*, 2011)

In their investigation of two adjacent 32 story buildings and their interaction through three different soil types, Yahyai *et al.* (2008) noticed that the SSSI increased the time period, base shear and displacements of the structures. Similar to Bolisetti *et al.* (2011) they concluded that the magnitude of the SSSI effects were dependent on the proximity of the structures to one another, and proposed that structures spaced 0.5 m – 2 m apart suffered the most interaction. Above 2 m spacing the effect proved negligible. At the closest distances the SSSI increased the lateral displacement three fold and the base shear twice, when compared to the isolated SSI systems. Luco *et al.* (1973), Wong *et al.* (1975) and Bolisetti *et al.* (2011) all agree that the spacing of the structures will directly influence the level of SSSI, although Bolisetti *et al.* (2011) suggest that the magnitude of this influence is not linear with increasing distance. Padrón *et al.* (2009) went further and proposed that the most unfavourable distance between the structures, where large amplifications were observed in the response of three and five aligned structures, was directly related to half the soil wavelength. Figure 2.13 from Aldaikh *et al.* (2011) shows how the spacing, and the difference in height of the two structures, influence the change in spectral power input to the structures. It suggests that the distance between the two structures that the SSSI is dependent on is based on *w*, the inter-building spacing coefficient which is used alongside the foundation width of the structure, B. Little effect was seen above 1.15*w*.

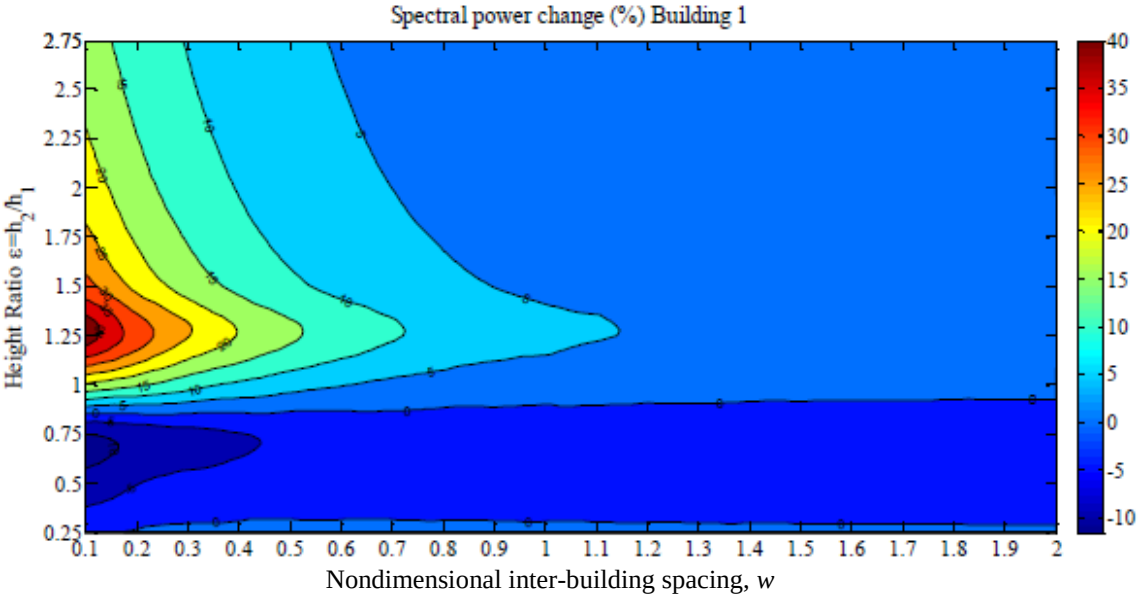

Figure 2.13 Effect of building spacing and building height ratio on the spectral power change after Aldaikh *et al.* (2011)

Considering the effects of SSSI through different soil types Fiorakis (2011) and Yahyai *et al.* (2008) showed that a denser soil minimises the effects of SSSI while the softer soils increase deterioration of the performance of the structure through SSSI.

The configuration and location of the structures also have an effect on how the SSSI manifests itself. Padrón *et al.* (2009) noted that Rayleigh waves in the direction of alignment of the structures resulted in the building that was first hit suffering the worst displacements while also shielding the other structures.

This section has shown that multiple factors need to be considered when considering SSSI effects on adjacent structures. Many of these variables require further research in order to fully understand their roles. The levels of complexity of SSSI do not stop at these factors however; what is known as the "city effect" is also a branch of SSSI which may require consideration, especially for large scale urban planning.

2.5.2 City Effect

When Wirgin *et al.* (1996) were analysing the records of Mexico's Michoacan 1985 earthquake they found discrepancies between the actual recorded response records and the response provided by classical computational methods they were using to replicate it. This prompted them to consider that some of the seismic energy transmitted into the buildings, during the earthquake, was being redistributed back into the soil, as previously highlighted by Jennings (1970) and others, and having an effect on multiple other buildings within its "neighbourhood", not just the adjacent structures. They referred to this as "site-city interaction", also known as the "city-effect".

From Menglin *et al.* (2011) and Bard *et al.* (2006) etc., it is evident that the complexities of interaction, the variables of the structures themselves, the distribution of the structures within a city and the soil make it difficult to accurately replicate the city effect. Limitations in current methods, which result in over-simplifications of the variables, produce representative but not conclusive analysis of the effect. However, even with these limitations, some advances have been made in the area.

After Wirgin *et al.* (1996) introduced the city effect they considered 2D numerical models in order to, quite accurately, describe the diffraction pattern of the

surface waves produced by the city effect. Later, Tsogka *et al.* (2003), in their idealised 2D model of a city comprised of homogenised blocks, Figure 2.14, were able to make a reasonable replication of the response resulting from the city effect, similar to that seen in Mexico city. The presence of the structural blocks clearly shows an increase in displacements throughout the system resulting from the structural vibration and interactions.

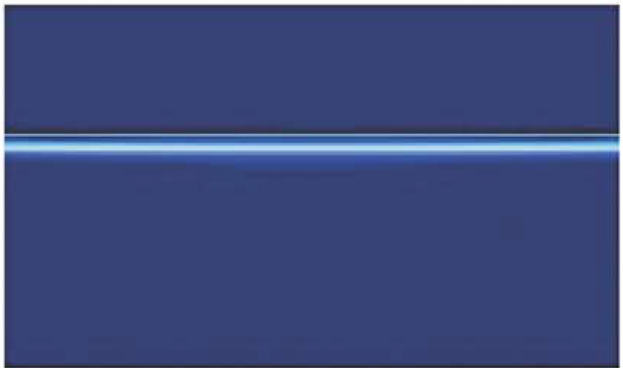

a)"city" with no structural blocks

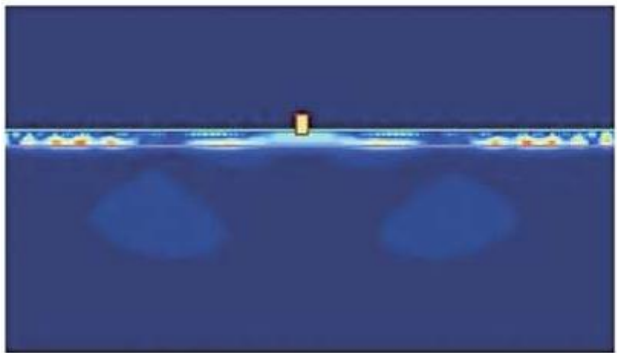

b) "city" with one block

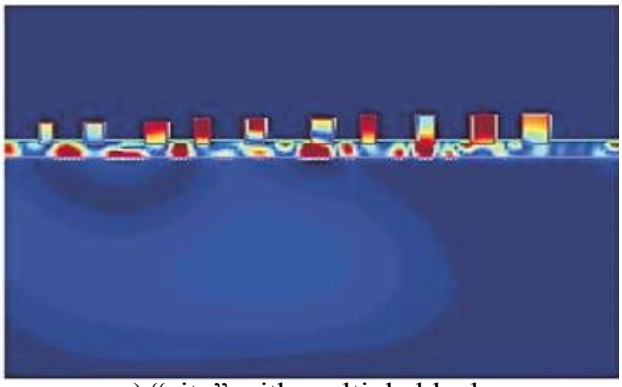

c) "city" with multiple blocks

Figure 2.14 Snapshot of total displacement field (red indicating high displacement, blue indicating low displacement) taken at the same time step of an identical earthquake applied to three "cities", after Tsogka *et al.* (2003)

The work carried out by Tsogka *et al.* (2003) forms part of the growing library of research into the impact of the city effect. The effect has been analysed through multiple different methods by Clouteau *et al.* (2001); Boutin (2004); Bard *et al.*

(2006) and Kham *et al.* (2006) among others, in order to try and understand the impact of the city on the buildings within a city and possibly highlight the parameters that control the effect. Some of these parameters and main observations, outlined in the research will be discussed here. Soil-structure frequency coupling, where the natural frequencies of both the soil and the structure are similar, allows a structure to more readily transmit its vibrations into the ground, (Kham *et al.*, 2006). While this occurred during the analysis of a "regular" homogenous city of similarly sized blocks with similar spacing, it was found to occur more often in an "irregular" city. The city types are shown in Figure 2.15.

The vibrations from the structures have been seen to modify the motion of other structures around it, radiating throughout the city, creating a site-city resonance. In turn this generates a "group effect" within the city which has been seen, (Kham *et al.*, 2006), to reduce the ground motion by up to 50% in idealised cases. This effect will be more pronounced for a homogenous city comprised of similarly sized buildings spaced evenly. A similar effect was also reported by Bard *et al.* (2006) in a homogenous building set case, whereby both the ground motion and building motion were reduced. An "irregular" city reduces this effect due to reduced coherency of buildings.

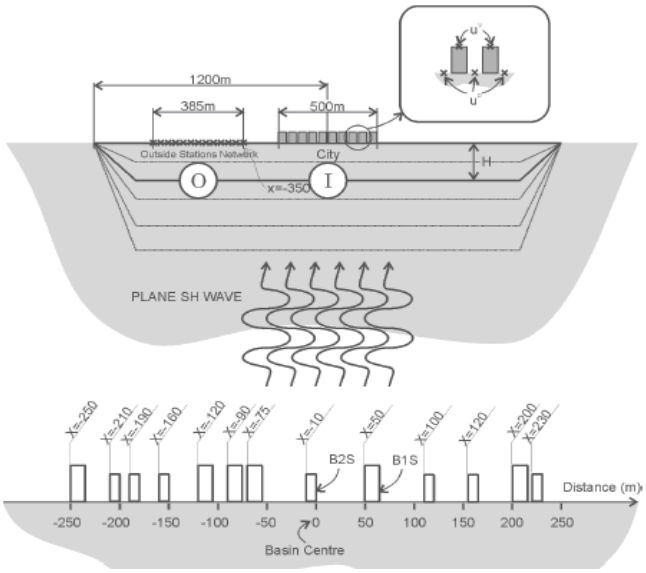

Figure 2.15 Regular (top) and irregular (bottom) site-city models considered by Kham *et al.* (2006)

Both Bard *et al.* (2006) and Kham *et al.* (2006) also noted that an increase in building density will enhance the city effect providing more optimal conditions for it to take effect. Kham *et al.* (2006) reported that an increase in ground motion was to be

seen outside the city limits due to the strengthening of the wave field radiated by the city. Similarly, Bard *et al.* (2006) noted that structures on the edge of the city were exposed to an increased ground motion resulting from the outward propagating waves.

Worryingly, Bard *et al.* (2006) pointed out that the city effect can also produce local "over-amplifications". The erratic pattern of the areas affected by these local events was not predictable but may explain random localised damage often seen during real seismic events, e.g. in Mexico City and Friuli, Italy. This explanation was reinforced by Groby *et al.* (2008) who observed that the modifications of the frequency-domain response resulting from the city effect was found to be substantial and give rise to anomalous features, peak motion amplifications, large durations etc, similar to those observed during the Mexico City earthquake 1985. Uenishi (2010) showed that the unique structural damage pattern caused by the 1976 Friuli, Italy, earthquake can also be accredited to the city effect.

Some of these variables may impact on what Ghergu *et al.* (2009) refer to as an overall city frequency. The city frequency does not depend on the number of buildings within a city but rather on the properties of the buildings within the city such as aspect ratio, building type and soil densities etc.

Research into the city effect is still at an early stage, due to the complexities of its analysis, but preliminary research is showing that the effect is real, complex and has a great impact on the response of structures within an urban environment. While the scope of this research will consider the SSSI effects of adjacent structures it does not cover the city effect due to the complexities of analysis requiring vast amounts of time.

2.6 Analysis techniques for SSI

SSI lends itself easily to multiple methods of analysis, some of which are more complex than others. Numerical and theory-based (analytical) methods have been used in the past, e.g. (Veletsos *et al.*, 1975); (Chen *et al.*, 2013); (Spyrakos *et al.*, 2009). While analytical methods do not lend themselves easily to allow for multiple changes within an analysis or complex boundary conditions they are required in order to simplify complex models, making them more manageable and allowing simple predictions to be made in routine design. In order to prove that they accurately

represent the more complex parameters within a soil structure system, and validate their use in predictions, they must be compared to more complex analyses which do accurately model these variables.

2.6.1 Finite Element Analysis

The finite element method is able to model realistic and complicated systems which may prove difficult to replicate in analytical terms. It is able to model multiple general parameters such as interactions between parts of a system and complex boundary conditions as well as extensively detailed material properties. In doing so realistic models are created that can be modified to represent almost any system, as shown by Dutta *et al.* (2002); Yazdchi *et al.* (1999); Hügel *et al.* (2008) and Grondin (2004). Multiple finite element packages are available for modelling structural and geotechnical systems, but only certain packages have the ability to accurately model both parts of the system as well as realistic interactions between the two. For this reason ABAQUS/CAE was chosen as the package of choice in the work described subsequently in Chapters 3 and 4.

2.6.2 Centrifuge Modelling

While finite element analysis has proven very successful in replicating complex soil structure interaction models its ability to accurately represent a real system must always be validated where possible to a physical model of the system. As Kutter *et al.* (2006) point out, relying on data from instrumented buildings is not always feasible due to the unpredictability of location and timing of seismic events. Centrifuge modelling of seismic soil structure interaction has been utilised to great success by various authors including Boulanger *et al.* (1999) and Ghosh *et al.* (2007) to name but two. The great advantage of centrifuge modelling of a SSI system is that a real soil can be used in the analysis and as the soil behaviour is stress dependent, (Brennan *et al.*, 2005); and not affected by scaling laws, (Weissman *et al.*, 1989). Therefore a centrifuge model ensures that the interaction between the soil and a prototype structure will match overall prototype system values.

2.7 Summary

This chapter has outlined current methods of predicting the seismic response of a structure, as well as outlining the current state of the art of research that has been undertaken into predicting the response. It has highlighted large gaps in the current routine methods of prediction that oversimplify the model considered and which may result in an inaccurate prediction model being used. The main variables that have been simplified out of the current method are:

- The flexibility of structural elements (columns, beams and joints) influencing the natural period of the structure;
- The additional flexibility and damping provided by the soil-structure-interaction of the system;
- The complex interaction that occurs when two structures interact with each other through the soil (SSSI).

It also considered the methods of analysis that are best suited to modelling these parameters so that a true representation of their influence can be obtained. The work presented in Chapters 3-6 will aim to address the issue of oversimplification in the prediction of the seismic response of the structure both within an individual structure (intra-structure effects) and in understanding its interaction with its surrounding environment (inter-structure effects).

Chapter 3

Numerical modelling of semi-rigid structures

3.1 Introduction

The main focus of this part of the research is to analyse how a semi-rigid structural steel frame interacts with underlying soil under seismic loading and how this interaction changes with the introduction of basic structural modifications (e.g. overall geometry and joint details) to the frame. In order to carry out this work different structural frames are considered, which must first be designed to conform to certain criteria (as highlighted below):

1. Firstly the frame must be structurally realistic, i.e. it must represent a section of frame designed by a structural engineer to withstand conventional static loading effects. In order to ensure a realistic representation is obtained, the frame will be designed to Eurocode 3, (BSI, 2008b), requirements.
2. The frame must also lend itself to individual structural changes without affecting the rest of the frame's structural form (e.g. so that a change in frame geometry does not require a complete re-design). This will enable the effects of the geometry of the frame to be investigated.
3. The joint system used must also realistically replicate the overall mechanical behaviour, i.e. the stiffness, of a real jointed or welded connection system. The joints used in this work will represent the behaviour of different Eurocode 3 joint classes.

Following a detailed presentation of the design of the frame structures, the modelling of planar frames within the finite element package ABAQUS/CAE is then described, along with analysis procedures for conducting (virtual) pseudo-static push-

over tests, determining natural frequencies of the soil-structure systems and conducting full dynamic analyses in the time domain. These analyses will be used to build a database of behaviour response against which an improved spectral method of response prediction can be validated.

3.2 Basic structural design to Eurocode 3

When considering the frame it is important to keep in mind the flexibility of the design that is required from the system. During the analysis it is essential that the frame gives an accurate representation of the differences in performance due to a specific individual change in the design.

For this analysis the main parameters considered that will influence the final design of the structure are (i) the structure's geometry, (ii) the soil/foundation interaction, and (iii) the stiffness of the structure's joint systems. The frame must therefore lend itself easily to being supported on the required foundation arrangements, be strong and stiff enough to incorporate joint systems of differing strength/stiffness without compromising the static stability/performance and be flexible enough to change its aspect ratio without the need for changing the sizes of the structural elements of the frame.

A simple single story, single bay, steel frame supporting a reinforced concrete slab and supported by concrete shallow foundations is being considered. The frame could subsequently be extended into a multi bay system many sections deep if required, but for this analysis the frame is being considered in its simplest form. A section of reinforced concrete slab is supported by a Universal Beam (UB) section, all of which is supported on two steel Universal Column (UC) sections. These columns are in turn fixed to the foundations. This frame has been designed to Eurocode 3 Standards, (BSI, 2008b); the calculations are outlined in Appendix A. The sections designed for the beam, slab and column supports are highlighted below in Table 3.1 with details for the UB and UC sections highlighted in Figures 3.1 and 3.2.

Section	*Dimensions*
Beam	610 × 305 × 149 UB
Column	254 × 254 × 107 UC
Reinforced (30N) Concrete Slab	0.360m deep (Main AS 1570mm²/m)
Strip Foundations	2m wide × 0.6m deep

Table 3.1 Section details for structural elements

Section: 610 x 305 x 149 UB							Elastic Modulus		Plastic Modulus	
Mass Per Meter kg/m	h mm	b mm	t_w mm	t_f mm	r mm	d mm	Axis x-x cm³	Axis y-y cm³	Axis x-x cm³	Axis y-y cm³
149.2	612.4	304.8	11.8	19.7	16.5	540.0	4111	611	4590	937

Figure 3.1 Sectional dimensions and properties for steel Universal Beam, after (Tata Steel, 2011)

Section: 254 x 254 x 107 UC							Elastic Modulus		Plastic Modulus	
Mass Per Meter kg/m	h mm	b mm	t_w mm	t_f mm	r mm	d mm	Axis x-x cm³	Axis y-y cm³	Axis x-x cm³	Axis y-y cm³
107.1	266.7	258.8	12.8	20.5	12.7	200.3	1310	458	1480	697

Figure 3.2 Sectional dimensions and properties for steel Universal Column, after Tata Steel (2011)

3.3 Parametric variations

3.3.1 Frame Geometry and Aspect Ratio

The frame itself follows the same layout, shown in Figure 3.3, for each analysis. The frame's span, L_b, and height, H, changes between analyses as required. The changes in dimensions are outlined in Table 3.2. Each of the elements are designed to support the largest of the frames carrying the heaviest loading, therefore they will be suitable for all other frames considered. While this approach overdesigns for the smaller frame it keeps the relative mass and stiffness of the frame elements comparable across all frames, allowing the specific changes made to the joints and foundations to be the main contributor to any differences observed in the frame's seismic response.

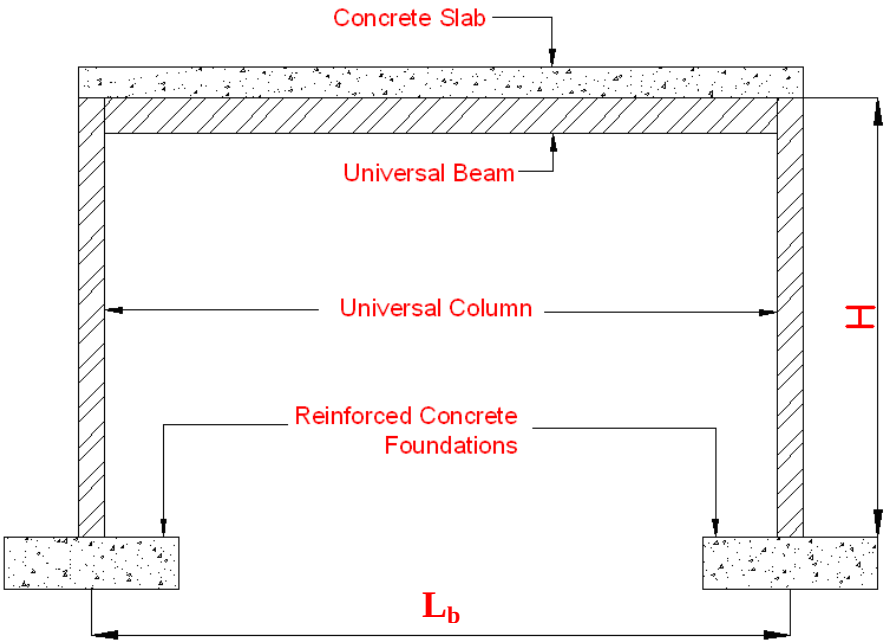

Figure 3.3 Basic composition of the frame

	Frame 1	*Frame2*	*Frame 3*
H (m)	3	5	5
L_b (m)	3	3	8
H/ L_b	1.00	1.67	0.63

Table 3.2 Dimension combinations considered

3.3.2 Joint properties

The joint system is one of the main structural design aspects being considered in this work, in terms of its influence on the seismic performance and soil-structure interaction (SSI). The beam-column joints (described below) are considered here. The joint between the foot of the column and the foundation is taken to be fully-fixed/rigid, with a capacity equal to the bending strength of the column section.

When considering the joint system the main factor affecting the design of the joint is its mechanical stiffness, the joints being designed so that failure occurs in the members connected through it, (BSI, 2008b). This stiffness ranges from the fully fixed case, in which the joint is considered to have an infinite rotational stiffness, k_j, to the fully pinned case, in which the joint is considered to have no rotational stiffness. Both extremes are first considered, i.e. taking the joints to be fully fixed (k_j = infinite), 'F', during one set of analyses and fully pinned ($k_j = 0$), 'P', in another. This brackets the structural response in defining how the joint system affects the overall system behaviour.

In reality a joint system would not necessarily fit either of these extreme cases exactly. Eurocode 3, (BSI, 2008b), suggests that a joint stiffness above a certain threshold can be considered fully fixed; similarly a joint with stiffness below a certain level can be considered fully pinned. Therefore, two further joint systems have been analysed whose stiffnesses lie directly on these limits. These limiting stiffness values are found by using a combination of Eurocode 3, (BSI, 2008b), Figure 6.9.8 and Eurocode 3 Equation (6.20), (BSI, 2008b), resulting in the criteria shown in Table 3.3. These joints can then be compared to the extreme idealised versions, which were previously outlined, so that the full range of nominally fixed, 'NF', and nominally pinned, 'NP', joints have been considered. This will highlight the validity of the Eurocode 3, (BSI, 2008b), assumptions on joint behaviour for use in seismic (rather than static) design. A fifth and sixth joint system are also considered. The fifth joint system's stiffness is taken as the point midway between the upper limit for pinned and the lower limit for fixed (the semi-rigid, 'SR', connection listed in Table 3.3). The need for a sixth joint stiffness to be analysed was highlighted after initial analyses of the previously described joints. This joint stiffness was taken as half-way between the 'semi rigid' state and the 'nominally pinned' state, and is referred to as moderately rigid, 'MR'. The chosen joint stiffnesses are highlighted in Figure 3.4.

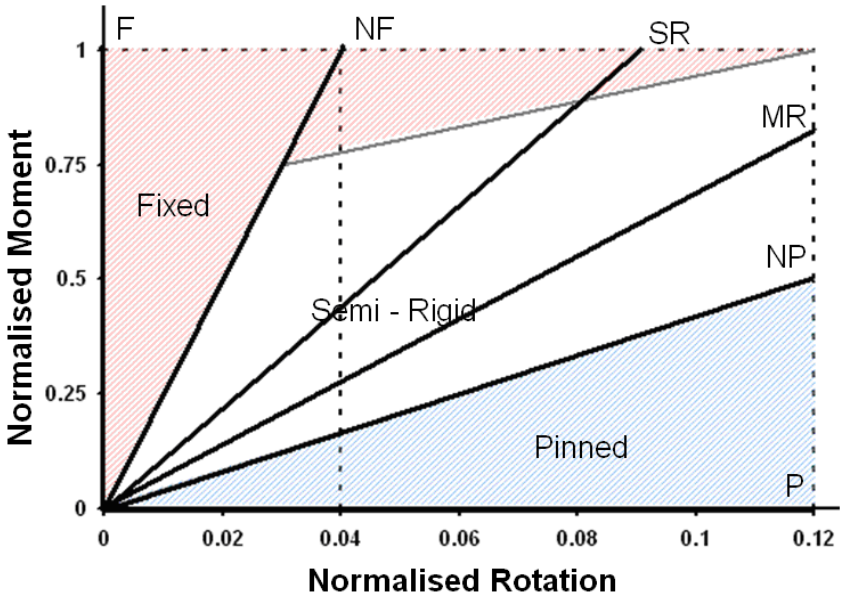

Figure 3.4 Selected Joint system stiffness

Joint	*Rotational stiffness*
Fixed	$k_j = \infty$
Nominally Fixed *	$k_j \geq 25\ EI_b/L_b$
Semi Rigid	$k_j \geq 12.5\ EI_b/L_b$
Moderately Rigid	$k_j \geq 6.5\ EI_b/L_b$
Nominally Pinned *	$k_j \geq 0.5\ EI_b/L_b$
Pinned	$k_j = 0$

Table 3.3 Joint stiffnesses considered [* indicates from Eurocode 3, (BSI, 2008b)]

Within the equations in Table 3.3, EI_b is the bending stiffness of the beam connected to the joint and L_b is the length (span) of the connected beam. The stiffness parameter k_j represents the secant rotational stiffness of the connection. The joint (moment) capacity is taken to be equal to that of the connecting beam or column, whichever is the lower (i.e. the joint has been designed to be stronger than the other frame elements).

3.3.3 Foundation design

Two foundation systems will be considered for the purpose of this research. The first is a fixed base case that matches Eurocode 8, Clause 3.1.2, Table 3.1, ground type "A" , (BSI, 2008b),where the foundation is essentially founded on rock. The second is

a SSI case, which matches ground type "E" from the same Table, where a medium dense sand deposit, 20m deep overlays a rock bed. The foundation itself is a 0.6m deep, 2m wide strip foundation made of reinforced (30N) concrete.

3.4 Continuum Finite Element Modelling

Following the design of the frame structure and the foundation system, the complete structural system is modelled numerically using the finite element package ABAQUS/CAE. ABAQUS/CAE is specifically designed for Computer Aided Engineering and holds an extensive library of elements giving it the capacity to accurately model virtually any structural or geotechnical component. Using the built in material generator the user can define and simulate the behaviour of almost any material required, including those of steel, reinforced concrete and soil. These material definitions can be applied to the individual model components. The model systems are comprised of the individual model components that are linked to one another by specified component interactions.

3.4.1 Modelling approach

The structural system being analysed was designed to Eurocode standards as outlined in Section 3.2. This model contains a definite axis of symmetry in both its construction and in its resistance to seismic loading. Therefore it is possible to recreate the system as a 2D plane strain model, rather than as a fully 3D model and still obtain valid results, while reducing computational time, and making parametric variation easier. This approach also avoids the necessity of modelling individual details (e.g. bolts or welds in the joints) in detail and remodelling every time a change is required.

While ABAQUS/CAE provides multiple built in features that enable a wide variety of scenarios to be considered there are other factors that limit the size and complexity of model that is created. The larger the model is, with reference to the number of nodes required to make the model, and the more information that is requested at each nodal point, the longer ABAQUS/CAE will take to run the analysis. Therefore a balance needs to be found between the complexity of the model and time available. This restraint must be considered at every stage of the modelling process.

While numerous models will be created and analysed, two core models will form the basis for all the models that are required. These core models are the ‘fixed-base’ response model and the ‘soil-structure interaction’ response model.

3.4.1.1 Fixed-base response model

The fixed-base response model contains only the structural elements of the system. It is used to validate the structural characteristics of the frame and the independent (fixed-base) response of the frame to earthquake shaking, without considering the soil structure interaction. The basic layout of this model is outlined in Figure 3.5. While this will be the general layout, dimensions H and L_b are adapted, as previously outlined in Table 3.2.

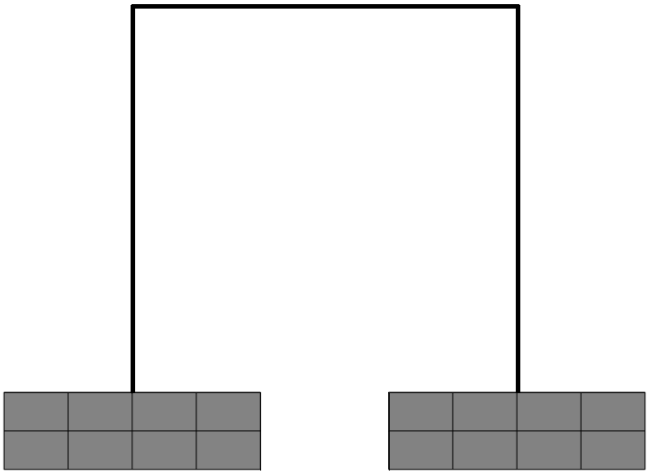

Figure 3.5 Fixed-base response model: layout NTS

3.4.1.2 Soil Structure Interaction Model

The soil structure interaction model takes the ‘fixed-base’ response model described above and places it on a 20 m thick uniform deposit of soil as highlighted in Figure 3.6. The soil in this case is a medium-dense sand with properties described in Section 3.4.3. As before, this is just the core model for the soil structure interaction analyses that are carried out. The dimensions H and L_b are again adapted as per Table 3.2.

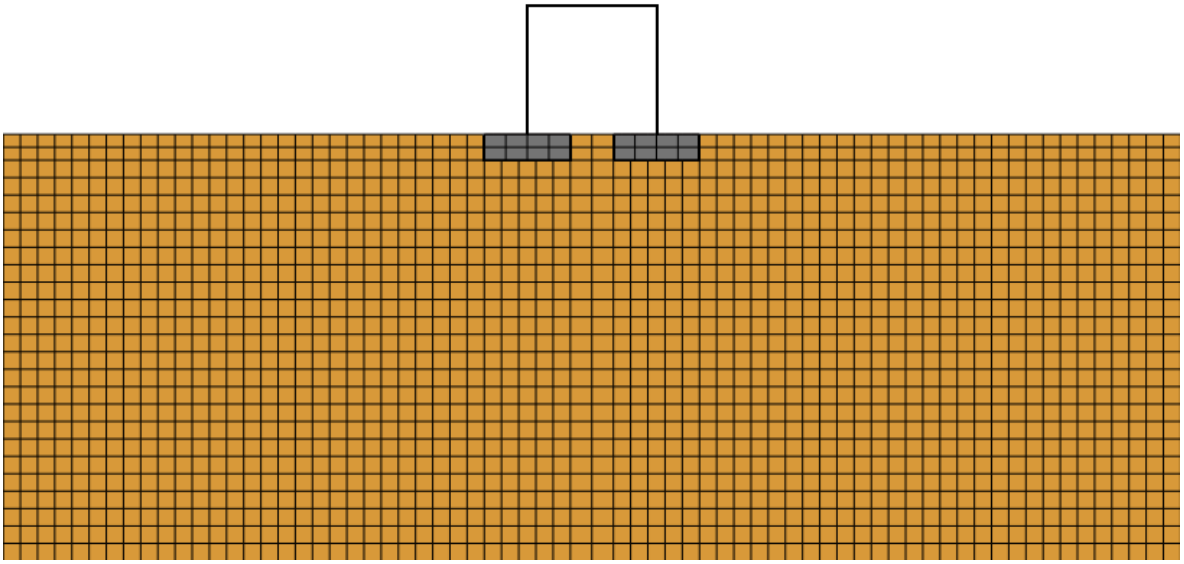

Figure 3.6: Section of the Soil Structure Interaction response model: layout NTS

The static bearing capacity is calculated after Terzaghi (1943), Equation 3.1.

$$q_f = \frac{1}{2}\gamma_s B N_\gamma + cN_c + \gamma_s D N_q \qquad \textbf{Equation 3.1}$$

Where:

q_f is the bearing capacity of the foundation,

B is the width of the foundation

D is the embedment of the foundation

c is the cohesive strength of the soil

γ_s is the unit weight of the soil

N_γ is the bearing capacity factor for self weight

N_q is the bearing capacity factor for embedment

N_c is the bearing capacity factor for cohesion

The bearing capacity factors can be found, for the static bearing case, after Hansen (1970). From these bearing capacities a factor of safety, (FOS), for the foundation can be calculated by dividing the bearing capacity of the foundation by the bearing pressure applied onto that foundation. Considering the structures designed within this research the 3m × 3m frame and the 5m × 3m both have a FOS of 47, while the 5m × 8m frame has a FOS of 31, see Figure 3.7, all well above critical and therefore should experience no bearing capacity failure, see Appendix B for calculations.

However the bearing capacity of a shallow foundation will be reduced as the system is subjected to seismic loading as outlined by Knappett *et al.* (2006). Multiple proposals for reducing the bearing capacity factors in order to accommodate this reduction in the bearing capacity due to seismic loading exist. These methods were analysed by Knappett *et al.* (2006) and compared to the failure mechanisms produced by physical modelling tests. The reduction proposed by Paolucci *et al.* (1997) proved the best match to the physical test results. This method is therefore used within this analysis and the reduction in the FOS for each of the structures, across different levels of peak ground acceleration, a_g (g), is given in Figure 3.7. The FOS for the 3m × 3m frame and the 5m × 3m both reduces to 30 and 2 for the 0.07g and 0.35g earthquakes respectively, while the FOS for the 5m × 8m frame reduces to 20 and 1.5 for the 0.07g and 0.35g earthquakes respectively.

The expected static settlement is calculated after Knappett *et al.* (2012) section 8.6 and presented in Table 3.4.

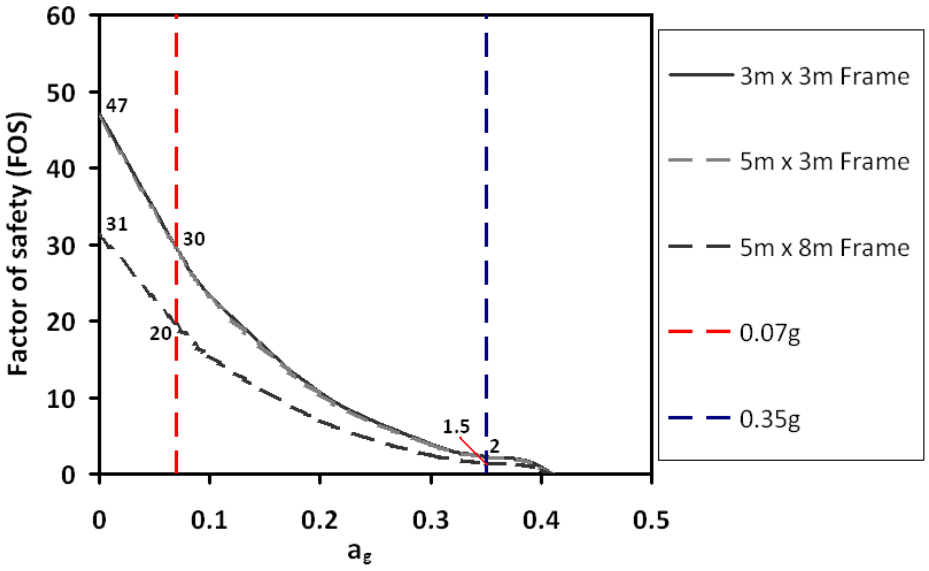

Figure 3.7 Factor of Safety reducing with increased seismic strength (g)

Frame	*Settlement*
3m×3m	1.4mm
5m×3m	1.4mm
5m×8m	2.1mm

Table 3.4 Settlement of foundations

3.4.2 Elements

Within ABAQUS/CAE the frame is built from individual parts (components) which are later assembled to form the soil-structure system that is analysed. The parts that are required to create this model are as follows:

- Foundation (×2)
- Beam
- Slab
- Column (×2)
- Plate – provides a rigid connection between column and foundation (×2)
- Soil

These components are created using beam, continuum or infinite elements, as described below:

i. **Beam Element, (type B21):** A Timoshenko (shear flexible) beam element is used for the Beam, Column, Slab and Plate parts of the system. The B21 beam element (two-dimensional with linear interpolation) is one in which one dimension (the length) is significantly greater than the other two dimensions. As a result it is only the stress in the direction along the axis that is considered, and the element can be represented by a wire (line) feature in ABAQUS.

ii. **Continuum Element, (type CPE4R):** Continuum elements are used to form the soil and foundation parts. This type of element acts as a block of material with two dimensions defined, as opposed to the beam elements which only have a single defined dimension. These blocks can connect to other elements along any of their faces in order to form the complete part. This particular type of element is a four-node linear element for plane strain analysis, with reduced integration and hour-glass control.

iii. **Infinite Element, (CINPE4R):** This element acts similarly to the CPE4R element but the addition of the 'IN' turns this element into an infinite element version of the continuum element. Any stresses or strains that pass through it will be allowed to pass out of the system in the element's infinite direction,

thereby preventing reflection of (dynamically generated) stress waves within the model. While the majority of elements can be generated directly within the CAE module, the infinite elements must be generated manually within the input (.inp) file. By creating an original continuum element (CPE4R) for the area requiring infinite elements, and generating an input file for ABAQUS/CAE, the file can subsequently be edited to replace the CPE4R element definition with that for the CINPE4R element.

Combinations of these three elements are used to form all of the parts within the model, transferring the stresses and strains through adjacent parts within the mesh, in some cases through element connections/interfaces.

3.4.3 Material and sectional properties

The elements described in the previous Section, are assigned sectional, material and profile parameters so that they accurately represent the required structural and geotechnical parts of the system. Columns, beams and plates are considered to be made from steel, the slab and foundations from reinforced concrete, and the soil representative of medium dense sand. The properties of these materials are outlined in Tables 3.5 and 3.6, and justification for their selection is given below:

i. **Steel:** this must have appropriate elastic stiffness which has a controlling effect on the natural period of the structure and the resulting induced shear forces and bending moments. It is also important to capture yielding within either the beam or column elements; non-hardening plasticity, using the Von Mises criterion, (Mises, 1913), was used to represent this, with properties representative of grade S275 steel.

ii. **Concrete:** The slab and foundations are principally required to model the additional bending stiffness due to the floor slab and the weight of the slab (for the correct dynamic frame behaviour), and to correctly model the footing contact pressure distribution. As a result, a linear elastic material model (with self-weight) was used for this material.

iii. **Soil:** Rather than use a complex soil model with a large number of parameters that require definition using complex testing, it was decided to use a simple linear-elastic perfectly plastic idealisation of behaviour. The elastic stiffness is representative of an operative (linear) secant stiffness over a range of dynamic strains induced by an earthquake, i.e. the secant elastic stiffness of the foundation soil which is controlling the degree of soil-structure interaction. The use of a linear elastic stiffness makes the resulting behaviour and interaction between the stiffness of the frame/joints and the stiffness of the soil easier to understand. A Mohr-Coulomb failure criteria is also included for the soil (to allow for bearing capacity failure), using a non-associative flow rule ($\psi \neq \varphi$) which is more representative of the actual strength characteristics of coarse-grained geo-materials. It should also be noted here that both the soil and the structural joints are idealised to the same level of complexity (i.e. linear elastic, perfectly plastic), despite the fact that the true properties of both are non-linear.

The material properties defined in Tables 3.5 and 3.6 represent those that could be obtained for the relevant materials using nothing more than routine material testing.

Property	***Steel***	***Reinforced Concrete***
Density (kg/m^3)	7850	2400
Young's Modulus (Pa)	210×10^9	26×10^9
Poisson's Ratio	0.3	0
Yield stress (MPa)	275	Elastic only
Structural (viscous) damping	0.05 (5%)	Elastic only

Table 3.5 Material properties of structural materials

Property	*Soil*
Density (kg/m³)	1700
Young's Modulus (Pa)	35 x 10^6
Poisson's Ratio	0.3
Mohr Coulomb Plasticity (Non-associative flow)	
Friction angle, φ	35°
Dilation angle, ψ	3°
Hardening	
Cohesion yield stress c' (kPa)	0.3

Table 3.6 Material properties of soil

In addition to the material properties, profile information is applied to each part through the section module. Profile information relates to the physical representation of the individual part. While they appear as 2-D lines in the section sketch the profile information gives the parts their true 3-D shape characteristics (e.g. second moment of area), ensuring realistic behaviour from the parts. An example, showing the dimensions given to the Beam part can be seen in Figure 3.8.

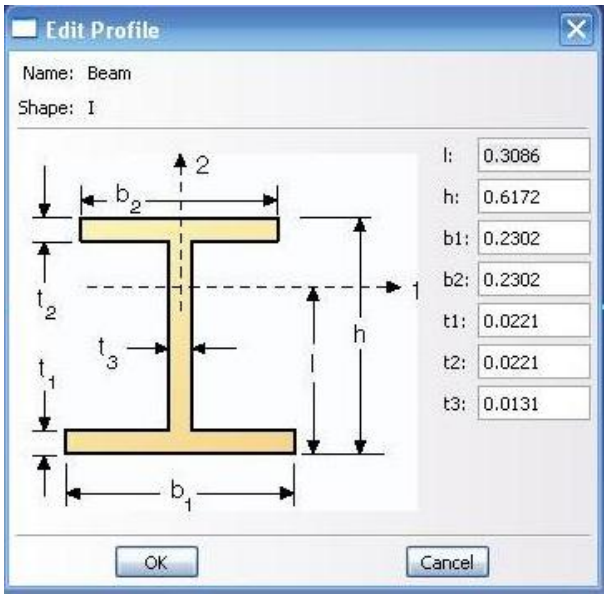

Figure 3.8: Profile dimensions for Beam applied in ABAQUS/CAE

3.4.4 Model assembly and connections/interactions

Once all of the main parts of the frame have been created as described above, they still remain as unconnected individual parts. Connection interactions are defined and applied to the appropriate part at the required location in order to join separate parts together. Wire-based connector elements are used at the beam-column and column-foundation plate connections to represent the moment-rotation behaviour of the desired joint system (as outlined in Section 3.3.2).

The beam and the concrete slab also require connection to one another in a way that ensures they work together as a composite system, as they would in reality. This is carried out through the use of a 'Tie' constraint that is applied to the two individual parts, with the beam set as the 'master' and the slab as the 'slave'. The tie connection ensures that the nodes along each element displace in the same way and essentially represent the shear studs which would link the two elements together in a real structure.

A similar connection to that used to connect the beam and slab, is required between the steel foundation plate and the reinforced concrete foundation part. Again a tie constraint is used in order to connect the two parts. In this case the Foundation is the controlling factor and is therefore the master surface and the plate is the slave surface.

The final interaction between parts that is required to ensure that all the parts are working as one system is the connection between the soil and the foundation. This is defined as a surface-to-surface interaction. This interaction allows the two surfaces to create a frictional bond under gravity loading, with a coefficient of friction of 1 (i.e. fully rough), and also allows them to separate during the analysis (no tension) allowing for uplift and the correct axial force distribution in the columns during any rocking of the foundation. The foundation part is the master surface for this interaction, and the soil the slave.

3.5 Analysis procedures

3.5.1 Overview

The analysis procedure followed, in an idealised way, the sequence of events and loading conditions which the structure would see during its life, using a staged

approach. This stage-by-stage loading is controlled in the Step Module. The Step Module allows for individual steps (subsequent phases of loading) to be created and interactions and loadings to be applied, propagated and deactivated if necessary within each particular step. The rate at which each step is applied is also controlled. Some common steps are created for all analyses run; however, in each case the final step differs depending on the data that is required. Figure 3.9 shows the complete programme of analyses, while the individual steps are described below.

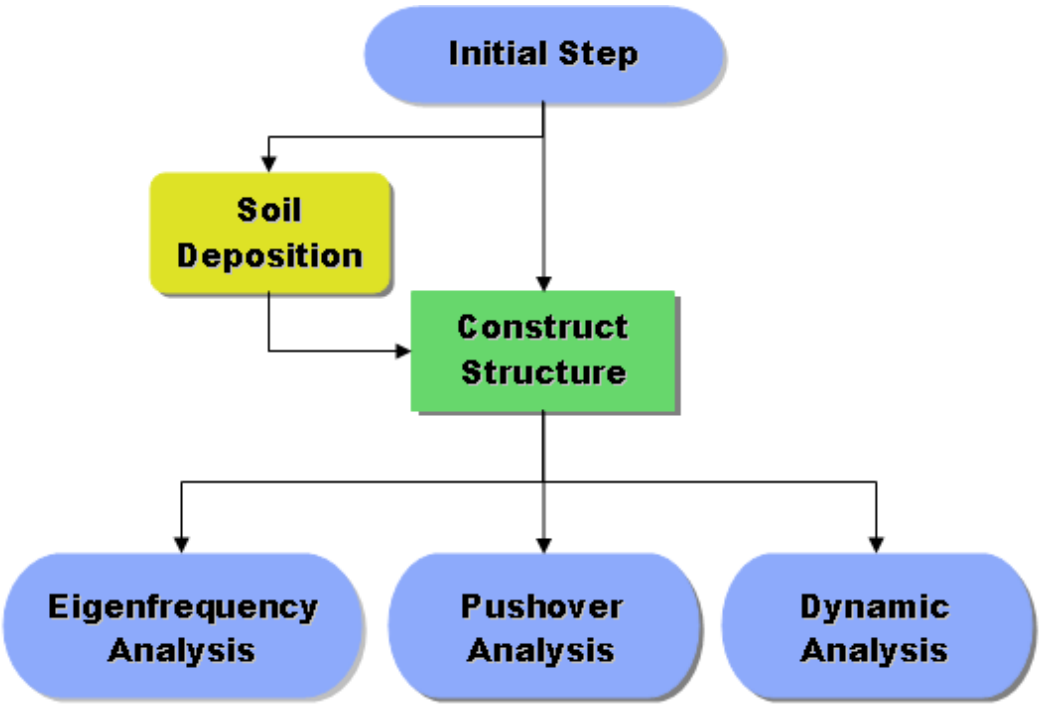

Figure 3.9 Finite element programme of analysis

1. **Initial step:** This is a common first step in all analyses and is a default requirement within ABAQUS/CAE, allowing the model to be initialised and the initial boundary conditions, connections and interactions defined.

2. **Soil deposition/formation and foundation construction:** This is a Geostatic Step. The boundary conditions and interactions that were outlined and applied in the initial step are propagated through to this step. Field and history data output that are required are defined at this stage. Gravity loading on the soil and foundations is applied, using the density of the material, in order to define the initial stress field within the soil mass before the structure is constructed. The profile of the soil is designed to allow for the foundations to be embedded into

the soil, this creates two trenches towards the centre of the soil model; the gravity loading is therefore also applied to the foundations in this step to avoid collapse of the surrounding soil. This action also, through the interactions of the foundations and the rest of the structure, keeps the structure in constant contact with the soil as the soil settles under its own weight (the structure is still weightless in this step). This step models, in an idealised way, the stress history of the soil (Normally-consolidated K_0 condition in this case) and the construction of the foundations. It should be noted that for cases where only the structure is modelled with no soil (i.e. fixed-base), step 2 is redundant and therefore is not applied.

3. **Construct structure:** This is defined as another Geostatic Step. The boundary conditions, interactions, field output definitions, history output definitions and the soil and foundation gravity loading are all further propagated through to this step. The gravity loading for the structure is applied to all of its composite parts. This step simulates the building of the structure and the application of its bearing pressure such that the initial stress field within the soil is correct when the earthquake is applied. This step is also used to check the static suitability of the structure.

4. **Analysis:** The final step consists of either (i) an eigenvalue analysis (Frequency step) to determine natural frequencies of vibration of the system, (ii) a pushover analysis (RIKS load-incrementation step) to determine the backbone lateral load deflection behaviour of the soil-structure system, or (iii) the application of an earthquake ground motion (Dynamic step) to the system. These different stages are described in further detail in the subsequent Sections.

3.5.2 Natural frequency analyses

In order to find the natural frequency of the structure a linear perturbation frequency step is introduced. During this step all relevant previous loadings, boundary conditions, and interactions are propagated. A Lanczos Eigensolver method, (Parlett, 1980), is employed to find the first ten eigenvalues and eigenvectors of the structure or the soil-structure system, depending on the model analysed. Although the first

(fundamental) natural frequency is of primary interest, by determining the higher harmonics, it is possible to check that the modal frequencies are well separated. Within the ABAQUS/CAE finite element model (FEM) it is possible to simply read off the given natural frequency of the fixed base structure and then convert it to natural period. However for the soil structure interaction model a transfer function approach must be carried out, using the data for the dynamic analyses, to accurately obtain the natural period of the soil-structure system, as outlined in Section 3.6.2.

3.5.3 Pushover analyses

The pushover analysis is performed using a static RIKS step, which permits a load-multiplier type analysis to be conducted, (Crisfield, 1981). During this step the boundary conditions, interactions, field output definitions, history output definitions and the soil, foundation and structural gravity loading are all propagated from the previous step. A unit horizontal load vector is then applied to the structure along the line of the concrete slab of the frame, this point being the centre of mass of the independent structure and the height above ground level where the principal structural inertia forces would act during earthquake shaking. This load is automatically incremented via a load factor within the RIKS procedure to a point where it will push over the structure. When applied to the fixed-base structural models this enables the lateral stiffness of the structural frame to be determined; when applied to the soil-structure models the interaction between lateral drift and rotation of the frame can be determined. The Riks procedure is also able to determine the response in the post-failure regime and allows the model to find static equilibrium states during any unstable period of response, (Simulia, 2009). The pushover analyses tested are summarised in Table 3.7.

Test Name	*Foundation Type*	*Joint type*	*Frame H (m)*	*Frame L_b (m)*
POT001	Fixed Base	Fixed	3	3
POT002			5	3
POT003			5	8
POT004		Nominally Fixed	3	3
POT005			5	3
POT006			5	8
POT007		Semi Rigid	3	3
POT008			5	3
POT009			5	8
POT010		Nominally Pinned	3	3
POT011			5	3
POT012			5	8
POT013		Pinned	3	3
POT014			5	3
POT015			5	8
POT016	Strip Foundation on Soil	Fixed	3	3
POT017			5	3
POT018			5	8
POT019		Nominally Fixed	3	3
POT020			5	3
POT021			5	8
POT022		Semi Rigid	3	3
POT023			5	3
POT024			5	8
POT025		Nominally Pinned	3	3
POT026			5	3
POT027			5	8
POT028		Pinned	3	3
POT029			5	3
POT030			5	8

Table 3.7: Summary of pushover analyses conducted

3.5.4 Seismic ground motion analyses

Seismic ground motion is applied by using a Dynamic (implicit) step. At the beginning of this step the boundary condition that has been applied to the sides of the soil is deactivated, and replaced with an alternative displacement/rotation boundary condition allowing for horizontal movement to be introduced into the whole system. This movement is controlled by applying an amplitude curve representing the dynamic ground displacements for a given earthquake time history.

Two different ground motions were selected representing a 0.07g and 0.35g scaled version of the motion recorded at the Takatori recording station in the 1995 Kobe earthquake. The original input motion was downloaded from the PEER (Pacific Earthquake Engineering Research Centre) Ground Motion Database, (PEER, 2010), which contains an extensive record of past shallow crustal earthquake events. Once the unscaled motion was downloaded as an acceleration-time text file it was reformatted into a layout that is compatible with ABAQUS/CAE. The earthquake data was band-pass filtered and integrated to obtain ground velocity, with cut-off frequencies of 0.8 and 8 Hz. This frequency range was selected to allow the same motions to be subsequently used in the centrifuge work reported in Chapters 5 and 6. The velocity data was then re-filtered using the same filter parameters and integrated to obtain ground displacement. The resulting data was saved externally as text files. To apply the seismic ground displacement the amplitude curve is saved in the following format:

```
t1, d1, t2, d2, t3, d3, t4, d4
t5, d5, t6, d6, t7, d7, t8, d8
t9, d9, t10, d10, t11…....etc.
```

Where ‘t’ represents a time datapoint and ‘d’ represents the displacement at the corresponding datapoint.

The time period for the dynamic step is matched to the duration of the earthquake (40.94 seconds) and the incrementation of the time step is set as a fixed value of 0.001s with a maximum number of increments of 100,000.

A comparison is made between the response of two ground types (‘Rock’ – fixed base and ‘Sand’ - SSI) as outlined in Section 3.3.3. Each variation of frame geometry

was analysed with each variation in joint stiffness, both soil types and under both earthquake conditions as highlighted in Tables 3.8 and 3.9.

Test Name	*Earthquake Type*	*Soil Type*	*Joint type*	*Frame H (m)*	*Frame L_b (m)*
SM001	0.07g Kobe	A - Rock	Fixed	3	3
SM002				5	3
SM003				5	8
SM004			Nominally Fixed	3	3
SM005				5	3
SM006				5	8
SM007			Semi Rigid	3	3
SM008				5	3
SM009				5	8
SM010			Nominally Pinned	3	3
SM011				5	3
SM012				5	8
SM013			Pinned	3	3
SM014				5	3
SM015				5	8
SM016		E – Medium Dense Sand	Fixed	3	3
SM017				5	3
SM018				5	8
SM019			Nominally Fixed	3	3
SM020				5	3
SM021				5	8
SM022			Semi Rigid	3	3
SM023				5	3
SM024				5	8
SM025			Nominally Pinned	3	3
SM026				5	3
SM027				5	8
SM028			Pinned	3	3
SM029				5	3
SM030				5	8

Table 3.8: FEM analysis under 0.07g Kobe Earthquake Loading

Test Name	*Earthquake Type*	*Soil Type*	*Joint type*	*Frame H (m)*	*Frame L_b (m)*
SM031	0.35g Kobe	A - Rock	Fixed	3	3
SM032				5	3
SM033				5	8
SM034			Nominally Fixed	3	3
SM035				5	3
SM036				5	8
SM037			Semi Rigid	3	3
SM038				5	3
SM039				5	8
SM040			Nominally Pinned	3	3
SM041				5	3
SM042				5	8
SM043			Pinned	3	3
SM044				5	3
SM045				5	8
SM046		E – Medium Dense Sand	Fixed	3	3
SM047				5	3
SM048				5	8
SM049			Nominally Fixed	3	3
SM050				5	3
SM051				5	8
SM052			Semi Rigid	3	3
SM053				5	3
SM054				5	8
SM055			Nominally Pinned	3	3
SM056				5	3
SM057				5	8
SM058			Pinned	3	3
SM059				5	3
SM060				5	8

Table 3.9: FEM analysis under 0.35g Earthquake Loading

3.6 Post-processing

As the ABAQUS solver performs calculations, it continuously writes output data to an output database, the .odb file. This file becomes a large mass of information that requires suitable processing in order to obtain the relevant information embedded within the data.

3.6.1 Structural movement

Certain physical movements of the structure during the analysis are required in order to fully analyse the response, therefore the vertical and horizontal displacements of each node as well as the stresses building within the elements were extracted from the .odb file.

The settlement of the foundations was obtained from the foundations' vertical displacement during the analysis. The overall sway of the structure can also be obtained easily from the difference in horizontal movement between the top and base of the columns.

The inter-storey drift of the structure requires some additional calculations to be carried out on the data. While the sway of the structure will give an indication of the drift, the mechanism of sway is influenced by the rotations of the structure, both local (foundation rotation) and structural (global rotation), in the SSI models. The structural rotation of the frame can be calculated by using trigonometry, the difference in vertical displacement of the foundations and the distance between the foundations at any given point in the analysis to give the angle of rotation. Once the angle of rotation is known, the horizontal displacement produced by the rotation of the structure can then be calculated. The local rotation is calculated in a similar fashion, by using the difference in vertical displacement of either side of the individual foundations. The rotational value calculated by the vertical displacement in the foundations also contains the structural rotation angle embedded within it and this must be removed in order to obtain the true local angle rotation. The horizontal displacements produced by both the global and local rotations are then subtracted from the sway value to give the true inter-storey drift value (i.e. related to pure column bending).

3.6.2 Natural frequency in SSI models

As mentioned in Section 3.5.2, it is not possible to accurately obtain the natural frequency of the soil structure interaction models directly from ABAQUS/CAE. However the output data in the .odb file can be used to calculate the natural frequency. Taking advantage of the relationship between the input acceleration to the base of the structure during the seismic analysis and the output acceleration at the top of the structure, transfer functions were determined using a MATLAB script, modified after Brennan (2004), to determine the frequency response of the structure from the output data. This same method was subsequently used in the centrifuge tests described in Chapters 5 and 6. A "least squares" data fit was then made to the transfer function data, using a single-degree-of-freedom response curve for absolute response to a ground displacement (Equation 3.2), to determine the best-fit natural frequency, f_n, and overall damping, ζ_{ssi}, of the structure in the SSI model.

$$\left|\frac{output}{input}\right| = \frac{\left\{1+\left(2\varsigma_{ssi}\frac{f}{f_n}\right)^2\right\}^{0.5}}{\left\{\left[1-\left(\frac{f}{f_n}\right)^2\right]^2+\left(2\varsigma_{ssi}\frac{f}{f_n}\right)^2\right\}^{0.5}} \qquad \textbf{Equation 3.2}$$

3.6.3 Predicted structural response

The seismic elastic response spectral analysis allows for a prediction of the acceleration, velocity and displacement of a structure of a given fundamental period to be made, as outlined in Chapter 2, Section 2.2. Based on the ground motion acceleration, obtained by double differentiation of the horizontal ground displacements at the surface of the soil, the damping ratio and the time sampling interval, a further MATLAB script, after Tazarv (2011), was used to produce an earthquake-specific response spectrum.

3.7 Preliminary tests – size of soil domain and boundary conditions

Before undertaking the main programme of numerical analyses, sample analyses were conducted on soil-structure models both with and without infinite elements at the

vertical boundaries of the soil domain, to check the necessity of using infinite elements. In the first model a large far field zone was created in hope that any shear waves reflected from the boundaries would not affect the near field around the structure (the area of interest). In the second model infinite elements were additionally applied to the edge of the soil model. The same seismic loading is applied to both situations and the horizontal displacement of the soil at certain points is recorded. Three sections through the soil are monitored and data collected from them during the analysis, Figure 3.10.

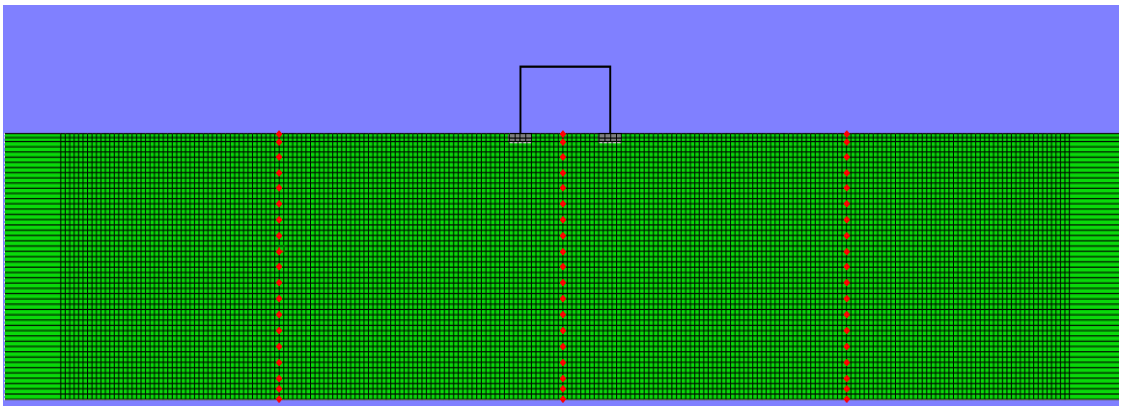

Figure 3.10 Soil nodes at which sine wave was monitored

A 0.08g sine wave, frequency 1Hz, was introduced to both analyses at the bottom of the soil. Comparing the displacement at points close to the surface, as highlighted in Figures 3.11, 3.12 and 3.13, it is clear that sine wave for both the Infinite Element model (IE) and the Finite Element far field model (FE) are identical at the three points, the left far field, the right far field and, most importantly, at the centre of the model directly underneath the structure.

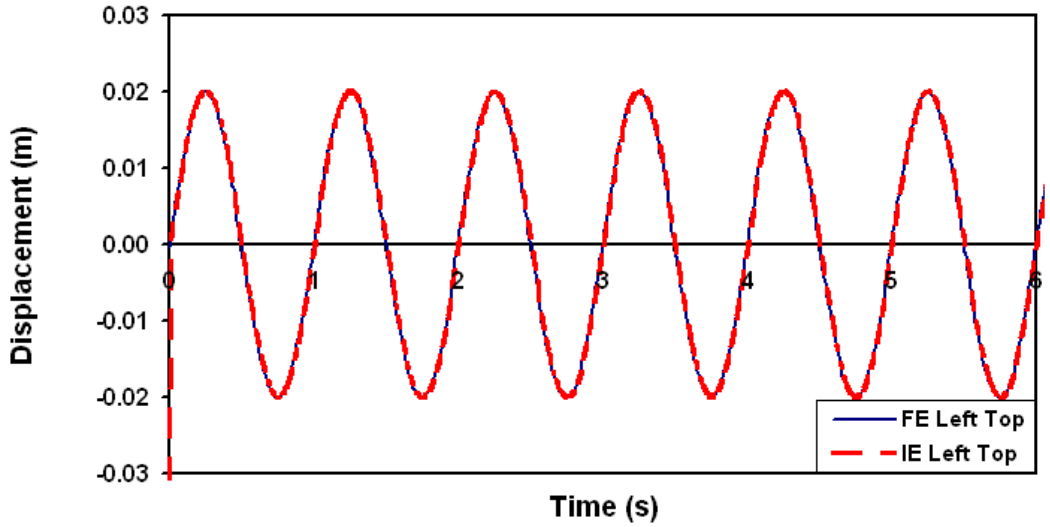

Figure 3.11: Sine wave at surface of soil LHS for both Far Field and Infinite Element Analysis

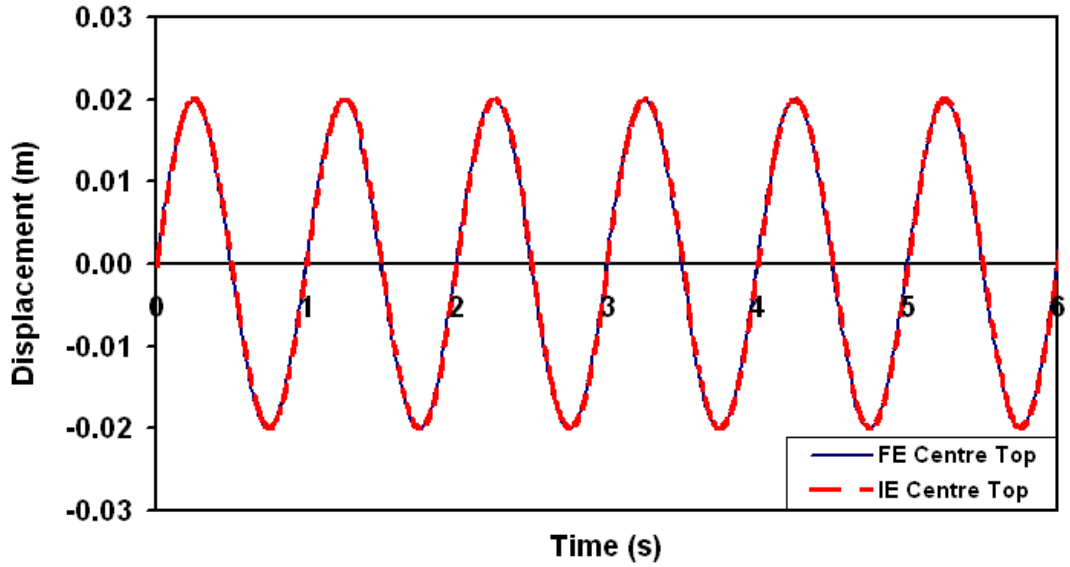

Figure 3.12 Sine wave at surface of soil centre for both Far Field and Infinite Element Analysis

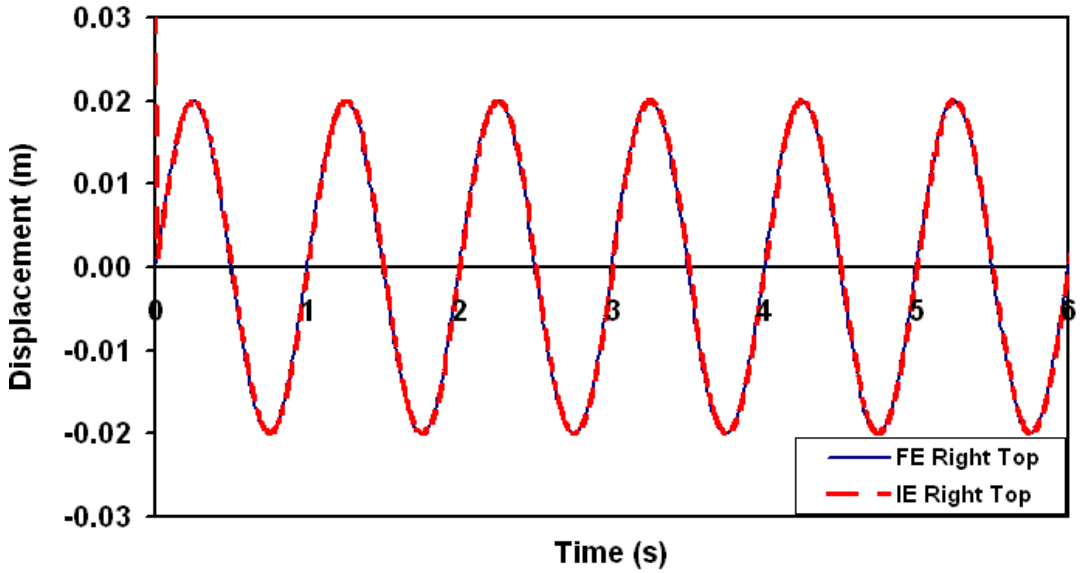

Figure 3.13 Sine wave at surface of soil RHS for both Far Field and Infinite Element Analysis

This comparison indicates that there is little or no reflection of the waves back into the system from the boundary when using either method. It suggests that the size of the soil model chosen for the far field analysis is sufficient enough to dissipate any reflections may have occurred. This size of model is also not so big as to add significant amounts of extra processing time. As a result the far field method is used in all subsequent analyses. This allows the structure to be modelled with its plastic properties, giving a more realistic representation of results; something which is not possible when infinite elements are used.

Chapter 4

Numerical results and analysis

4.1 Introduction

Within chapter three it was outlined how a structural frame, suitable for analysis, was designed and modelled using ABAQUS/CAE. The procedures of analysing the frame's natural frequency, structural strength and stability, and dynamic response, for both a fixed based model and one incorporating soil structure interaction, by using the finite element package, were outlined.

This chapter will begin by outlining a way of improving the current spectra method used to estimate the system's peak seismic response. It will then report, compare and discuss the results from the finite element analyses. These analyses were designed to highlight the effect that the joint stiffness of the frame, the geometry of the frame and the foundation conditions have on the dynamic response of the frame, therefore any effect that these variables may have had, and to what extent, will be discussed. The results will also be used to validate the new spectral prediction method.

4.2 Theoretical prediction method

Eurocode 8, (BSI 2008), provides a 'traditional' spectral method for predicting the fundamental period of a structure, the maximum peak acceleration and the maximum displacement experienced by the structure under seismic loading. In this section the method provided by Eurocode will be presented as well as alterations to this method which help improve the prediction. The new improved method proposed determines

the natural period and effective single degree of freedom damping ratio for semi-rigid structures of varying frame geometry and will including the effects of SSI. This method is a fusion of an existing approach for determining the natural period of a semi-rigid framed structure with flexible beams and columns, (Hellesland, 2008), with an existing method for incorporating SSI, (Veletsos *et al.*, 1974); (Veletsos *et al.*, 1975). When combined the new model can account for both the local rotational stiffness of the individual footings within a frame and the overall global rotational stiffness of the foundation (e.g. to rigid body rotation).

This new method provides a simple way of determining improved input parameters for a routine spectral analysis (without requiring FEM to account for the structural and soil complexities), and will be useful in undertaking rapid parametric studies on the effects of various design features/choices including:

- Joint properties/joint system
- Frame geometry (both height and width of bays)
- Element properties (e.g. changing beam or column section)
- Changes in soil properties

The method will be validated against the FE results later in this Chapter (where the soil is essentially linear elastic), and will be subsequently validated against centrifuge test data in Chapter 6 (following further modifications, described in Chapter 6, to account for the strain dependency of soil stiffness in real soil).

4.2.1 Determination of fundamental period and damping

4.2.1.1 Fixed base structure with flexible joints

In Section 2.2 it was shown how the natural period of a Multi Degree of Freedom (M.D.O.F.) structure is calculated as per Equation 2.7. While this method gives a representative value for the natural period of a pinned or fully fixed structure it does not allow for the additional flexibility applied to the frame by intermediate joint stiffnesses, the flexibility of the beam or the flexibility within the foundation due to soil-structure interaction to be considered.

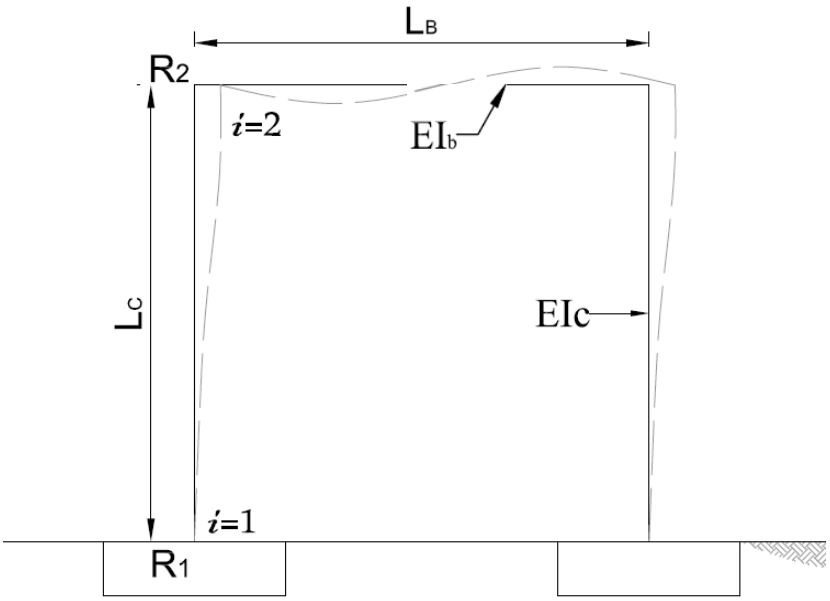

Figure 4.1 Structure Layout

Hellesland (2008) provided an improved method for calculating k_{col} in order to allow for some of this additional flexibility. Considering a frame (Figure 4.1) with flexible columns of bending stiffness EI_c, connected to a flexible beam of bending stiffness EI_b, by flexible beam-column joints of rotational stiffness k_j, and following Hellesland (2008) the sway stiffness of an individual column, k_{col}, is given by Equation 4.1.

$$k_{col} = \frac{H}{\Delta_{hh}} = \left(\frac{12R_m}{3-2R_m} \right) \frac{EI_c}{L_c^3} \qquad \textbf{Equation 4.1}$$

Where R_m is the mean value of the fixity factors at either end of the column, R_1 at the bottom and R_2 at the top, as highlighted in Figure 4.1 ie:

$$R_m = 0.5(R_1 + R_2) \qquad \textbf{Equation 4.2}$$

The fixity factors that are applied to the sway stiffness of the column are defined by Equation 4.3.

$$R_i = \frac{k_j}{k_j + \frac{2EI_c}{L_c}} \qquad \textbf{Equation 4.3}$$

where k_j is the rotational stiffness at an end of the column, *i* being 1 at the base of the structure and 2 at the first storey (Figure 4.1). In the case of a general joint at column end *i* within a frame, in which an elastic beam is connected to an elastic column through an elastic joint, the rotational stiffness is given by:

$$k_j = f_j \sum \left[\frac{12 d_n}{4 - d_n d_f} \left(1 + 0.5 \frac{\theta_f}{\theta_n} d_f \right) \frac{EI_b}{L_b} \right]_i \qquad \textbf{Equation 4.4}$$

In this equation, the summation is conducted for all beams framing into the joint, allowing for the additional flexibility of the beam member to be considered. The subscripts '*n*' and '*f*' represent the near and far ends of the beam under consideration, relative to the column end. In Figure 4.2, the joint on the left is considered, such that:

$$\textbf{(a)}\ d_n = \frac{k_{j,n}}{k_{j,n} + 3\frac{EI_b}{L_b}} \qquad \textbf{(b)}\ d_f = \frac{k_{j,f}}{k_{j,f} + 3\frac{EI_b}{L_b}} \qquad \textbf{Equation 4.5 (a) (b)}$$

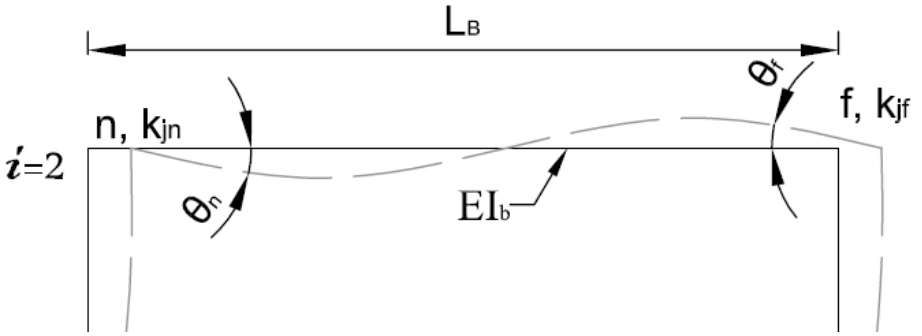

Figure 4.2: Beam layout

The parameter *d*, as calculated in Equation 4.5(a) and 4.5(b), is the degree of rigidity of the connection considered, d_n being the near end connection and d_f being the far end connection. Parameters $k_{j,n}$ and $k_{j,f}$ in Equation 4.5(a) and 4.5(b), are the stiffness of the beam-column joint at the near end and far end of the beam respectively. This allows for a more accurate representation of the joint stiffness to be represented in the final calculation. The parameter f_j, within Equation 4.4, is a 'beam restraint demand' factor, which for a simple S.D.O.F. frame is calculated after Equation 4.6.

$$f_j = \frac{\left(EI_c / L_c\right)}{\left(\frac{EI_b}{L_b}\right) + \left(\frac{EI_c}{L_c}\right)}$$ **Equation 4.6**

For a symmetrical single bay single storey frame, such as that being considered in this research, at the column end at the level of storey 1, ie column end 2, the following simplifications can be made.

$$k_{j,n} = k_j$$

$$k_{j,f} = k_j$$

$$\theta_f = \theta_n$$

$$d_n = d_f = d$$

Therefore the equation for k_2 becomes:

$$k_2 = \frac{12d}{4 - d^2}\left(1 + 0.5d\right)\frac{EI_b}{L_b}$$ **Equation 4.7**

where:

$$d = \frac{k_j}{k_j + 3\frac{EI_b}{L_b}}$$ **Equation 4.8**

This value of k_2 can then be used in Equation 4.3 to find R_i.

Considering column end 1, with a column-foundation joint of infinite stiffness, i.e. a fixed-base frame, k_j and EI_b are infinite, so $k_1 = \infty$ and $R_1 = 1$.

This more advanced method of calculating k_{col} for a 'rigid' structure, given in Equation 4.1, replaces the more simplistic method outlined in Equation 2.10. This new value for k_{col} is then used in Equation 2.9 to calculate the equivalent stiffness of the structure, k_{eq}, which is subsequently used to calculate the natural period of the structure, Equation 2.7.

4.2.1.2 System including soil structure interaction and flexible joints

The previous method refines the prediction of the natural period for a fixed base system, producing a more accurate value of T_n. However the T_n of the structure will similarly be affected by the flexibility that is introduced when a soil base is incorporated instead of a fixed base. The addition of the soil base and the rotational stiffness of the foundation acts like another joint system at the bottom end of the storey 1 column. Allowing for this when considering column end 1, the value for k_j - the local rotational stiffness (of the foundation) – is now calculated from Equation 4.9 for an elastic soil:

$$k_j = k_{fr} = \frac{G\beta_\phi B^2 L_f}{(1-\nu)}\left(1+2\frac{e}{r_x}\right) \qquad \textbf{Equation 4.9}$$

where G is the shear modulus of the soil, ν is the Poisson's ratio of the soil, B is the breadth of the foundation and L_f is its length. β_ϕ is the rectangular footing coefficient from Figure 4.3, taken from Richart *et al.* (1967), and e is the embedment depth of the foundation. The value r_x relates to the area of the foundation and is defined by Equation 4.10.

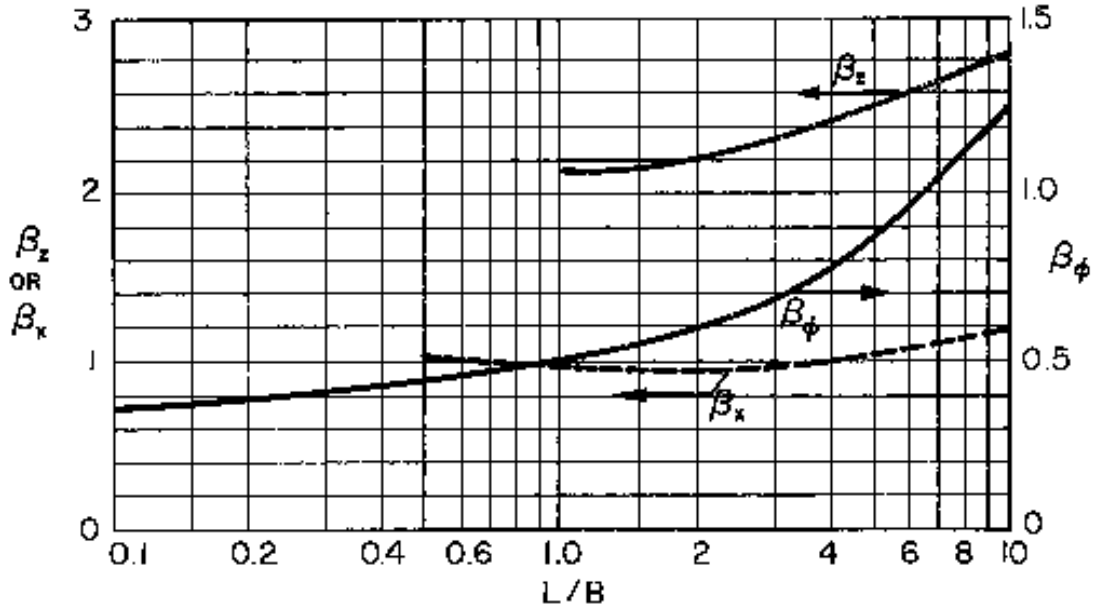

Figure 4.3 Coefficients β_z, β_x, β_ϕ for rectangular footings, from Richart *et al.* (1967)

$$r_x = \sqrt{\frac{BL_f}{\pi}} \qquad \textbf{Equation 4.10}$$

So far, Hellesland's technique, which allows for the flexibility of the columns, beams and joints has been expanded to allow for an additional joint to be considered between the foundation and the soil. Building on this and considering principles from Veletsos *et al.* (1974) and Richart *et al.* (1967) it is possible to generate a more accurate prediction of, $T_{n,ssi}$, the natural period of the structure when it is interacting with an elastic foundation subsoil. $T_{n,ssi}$ can be approximated, after Veletsos *et al.* (1974), as outlined previously by Equation 2.15. In Equation 2.15 k_{fx} is the horizontal stiffness of the foundation system (i.e. for all of the individual footings combined) and is found after Richart *et al.* (1967) using Equation 4.11

$$k_{fx} = 2G(1+\nu)\beta_x\sqrt{BL_f}\left(1+\frac{2e}{3r_x}\right) \qquad \textbf{Equation 4.11}$$

Where β_x is the rectangular footing coefficient from Figure 4.3.

$k_{f\phi}$ in Equation 2.15 relates to the overall (global) rotational response of the combined structure and foundation system and is also defined by Richart *et al.* (1967) as shown in Equation 4.12.

$$k_{f\phi} = \frac{G\beta_\phi B^2 L_f}{(1-\nu)}\left(1+2\frac{e}{r_f}\right) \qquad \textbf{Equation 4.12}$$

However this value considers a single slab foundation and not two independent strip foundations. Considering this parameter in its simplest form it can be represented as a global moment divided by the tilt of the structure, Equation 4.13.

$$k_{f\phi} = k_{f\theta} = \frac{M}{\theta} \qquad \textbf{Equation 4.13}$$

where:

$$M = 2F\left(\frac{L_b}{2}\right) \qquad \textbf{Equation 4.14}$$

where F is the force acting to overturn the structure and L_b is the centre-to-centre distance between the columns/footings.

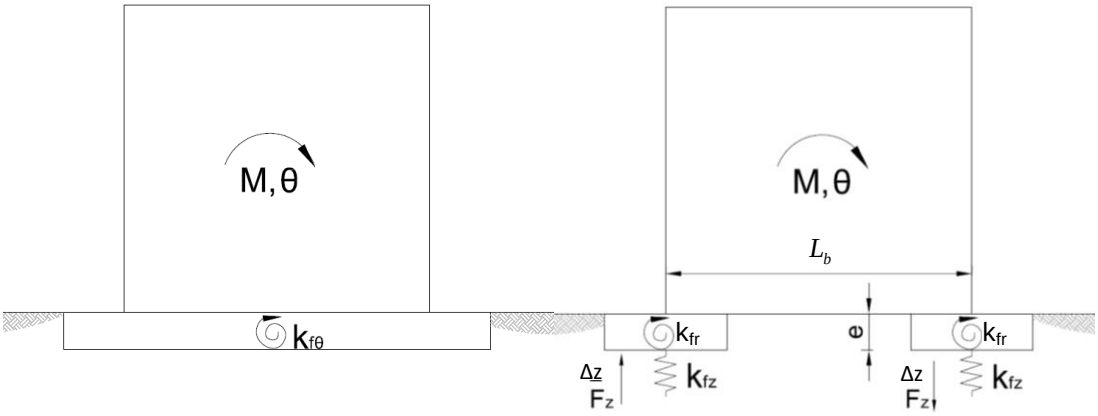

Figure 4.4 Rotational response for raft foundation structure and a strip foundation structure

Considering Δ_z as being the vertical displacement caused by the rotation then the rotation itself, θ, can be defined by Equation 4.15 while the rotations are small, and F_z can be defined by Equation 4.16.

$$\theta = \frac{2\Delta_z}{L_b} \qquad \textbf{Equation 4.15}$$

$$F_z = k_{fz}\Delta_z \qquad \textbf{Equation 4.16}$$

Therefore:

$$k_{f\theta} = \frac{\left(k_{fz}{L_b}^2\right)}{2}\left(1+2\frac{e}{r_f}\right) \qquad \textbf{Equation 4.17}$$

where k_{fz} is defined by Equation 4.18, after Richart *et al.* (1967), and $\left(1+2\frac{e}{r_f}\right)$ is the embedment depth correction factor.

$$k_{fz} = \frac{G}{(1-\nu)}\beta_z\sqrt{BL}_f \qquad \textbf{Equation 4.18}$$

The value of $T_{n,ssi}$ can then be extracted from Equation 2.15. With the values that have been predicted it is now possible to estimate the damping of the system after Veletsos *et al.* (1975), defined by Equation 2.16.

These improved values for period and damping can then be used in the spectral prediction outlined in Section 2.2., where $T_{n,ssi}$ can be substituted for T_n in the equations when SSI is being considered.

4.3 Free vibration response of structures

The natural period of each frame obtained by the Eurocode 8, (BSI 2008), simple method, the improved method from Section 4.2 and the FEM results from the free-vibration analyses are compared in Figure 4.5. The FEM natural period result was obtained through an eigenvalue analysis, as outlined in Section 3.5.2, the results of which were cross-checked with values from two other methods of obtaining the natural period, (i) by obtaining the lateral stiffness of the structure from the pushover analysis and applying Equation 2.7, and (ii) by performing a transfer function on the data from the fully dynamic analysis of the structure.

An improved correlation is shown between the new method and the FEM results. The trend that is present in the FEM data is accurately replicated by the new method for both the fixed base and SSI models. While the magnitude of increase in T_n for the fully pinned case is still not fully replicated, (albeit better than the simple method), this is an extreme, non realistic case and once some joint stiffness is considered the correlation improves. Once the joint stiffness exceeds that of a semi rigid joint the rate of influence of the joint system is minimal. Frames with joint stiffness above the semi rigid threshold respond similar to a fixed joint frame. The consideration of the soil structure interaction increases the fundamental period, $T_{n,ssi,}$ of the structure across all joint stiffness considered. In the case of the models including soil structure interaction the new model accurately predicts the coupled effects that both the joint stiffness and soil structure interaction have on the fundamental period, and therefore, on the seismic response of the structure. The change in the fundamental period of the structure directly related to the stiffness of the joint system is greatest when considering more flexible joints.

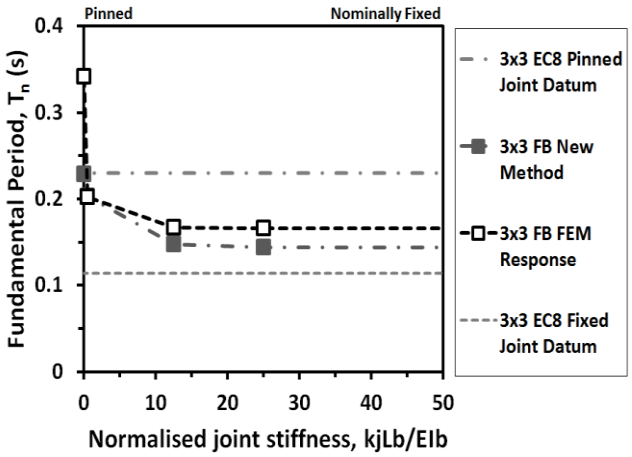

(a) Frame 3m × 3m, fixed base

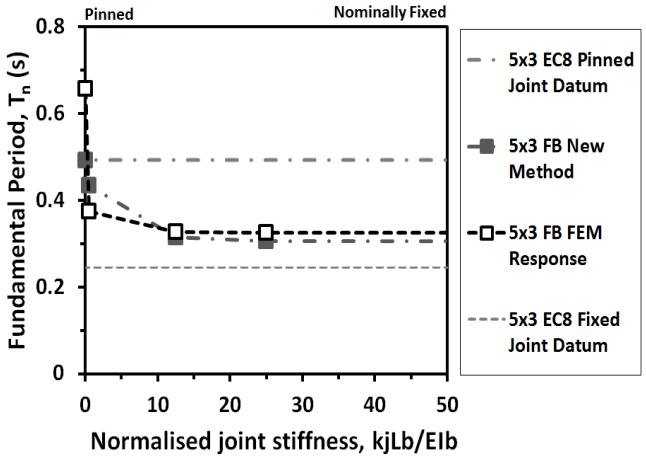

(b) Frame 5m × 3m, fixed base

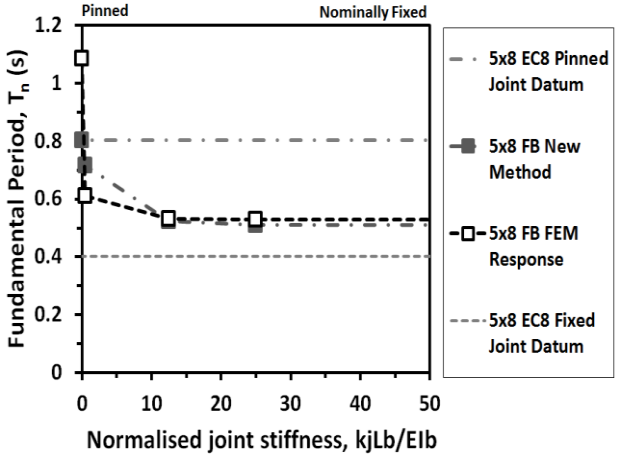

(c) Frame 5m × 8m, fixed base

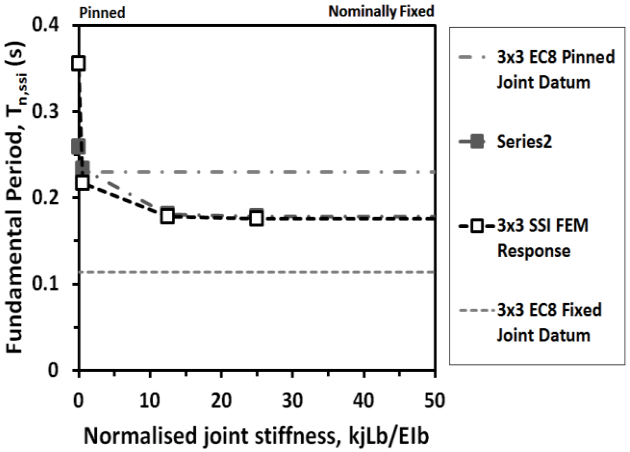

(d) Frame 3m × 3m, soil structure interaction

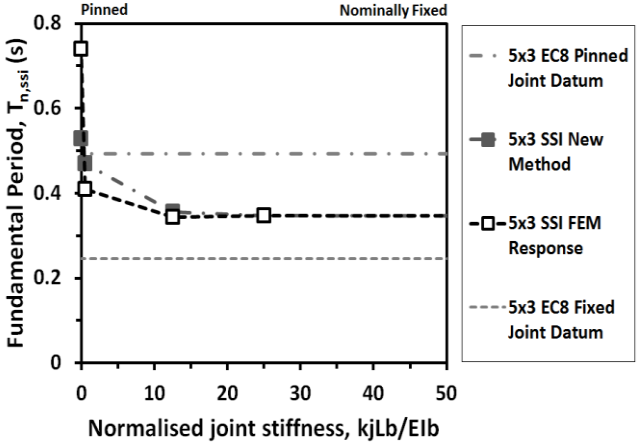

(e) Frame 3m × 3m, soil structure interaction

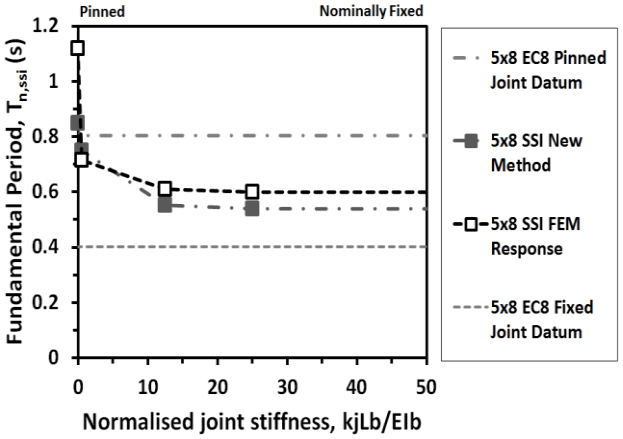

(f) Frame 3m × 3m, soil structure interaction

Figure 4.5 (a) to (f): T_n of structure, by FEM model, the new method and the EC8 simple method

The corresponding mode shape for the first natural period of the single-storey, single bay structures analysed is highlighted in Figure 4.6 using the fully fixed joint case for the 5m (height) × 8m (width) frame as an example. It has been designed to Eurocode 3, (BSI, 2008a), so that the structural capacity of the joints is higher than that of the columns. This can be seen within the mode shape where the plastic hinges are forming in the columns and not elsewhere in the structure, confirming that the structure is responding in a sway mode, as expected.

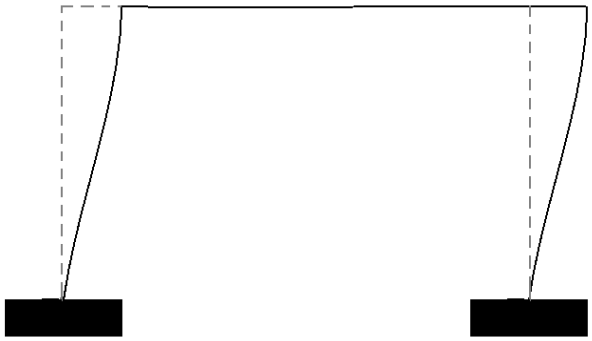

Figure 4.6: Fundamental mode shape for the 5m (height) 8m (width) Fixed Joint Frame (displacements shown at exaggerated horizontal scale)

While it is the first natural period that is of primary importance when considering the response of the structure, the modal separation is also important in order to determine whether the modes are independent of one another. The response of two vibration modes can only be considered as independent of each other when their periods satisfy Equation 2.14, as outlined in Section 2.2. Figure 4.7 shows the natural periods determined for the first five modes for each of the fixed base structural configurations considered from the FEM.

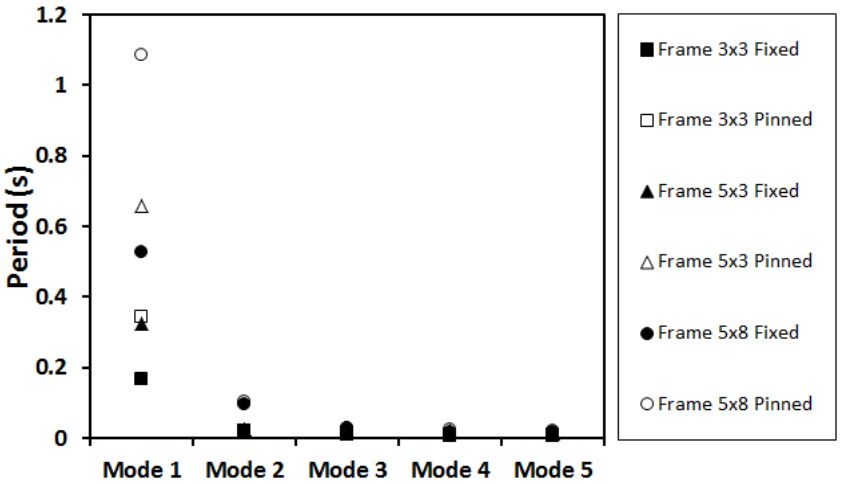

Figure 4.7: Separation of modal periods

From Figure 4.7 it is evident that the primary mode is indeed of most importance when considering the seismic response of the structure, with the subsequent modes adding little to the response in comparison.

For each of the frame configurations the first three modes proved to be fully independent, satisfying Equation 2.14. Modes four and five fell slightly outwith the allowable threshold indicating that these modal responses were not fully independent of the mode that preceeded it. As mode four and five provide very little additional input to the structural seismic response it was considered acceptable that they were not fully independent modes, and that the model will still respond as an equivalent SDOF structure.

4.4 Pushover response

The pushover loading was applied at the top of the structure (to the beam) and it was expected that the strength of the columns would govern the structure's ability to withstand horizontal sway loading. It can be seen, in Figure 4.8(a)–(f), that the structures are loaded to a point at which the moment in the column reaches its maximum threshold, the plastic moment capacity (Mp); at this stage plastic hinges are formed and the structural drift continues with no additional increase in moment. This clarifies that it is the columns that are governing the response of the frame. The change in height of the columns from a 3m high frame to a 5m high frame has a significant effect on the response of an individual frame. Taller frames experience larger drifts under a reduced pushover loading due to their increased flexibility. The pushover force required to reach moment capacity in the 5m high frames is approximately half that required in the 3m high frames.

Similar to the fundamental period response, the structures with fixed, nominally fixed, and semi rigid joint systems all responded almost identically. Only the fixed, nominally pinned and pinned joint cases are shown in Figure 4.8 (a) – (f); this is to allow for clarity. The reduced stiffness cases of the nominally pinned and pinned frames both required more drift to occur in order to reach moment capacity. While the nominally pinned frame required the same force as the fixed frame, albeit with more inter-storey drift occurring, the more flexible pinned frame required only half that force. The flexibility of the frame, either due to the height of the column or

the joint stiffness, clearly governs the ability of the frame to resist lateral loading in the fixed base case. The maximum moment developing within the column occurs initially at the top of the column near the beam connection in the majority of cases, however for the fully pinned joint case the maximum moment develops at the base of the column (where all the resistance is being provided) with very small moments developing at the top of the column, as seen in Figure 4.8. This results in only half the force being required to generate failure.

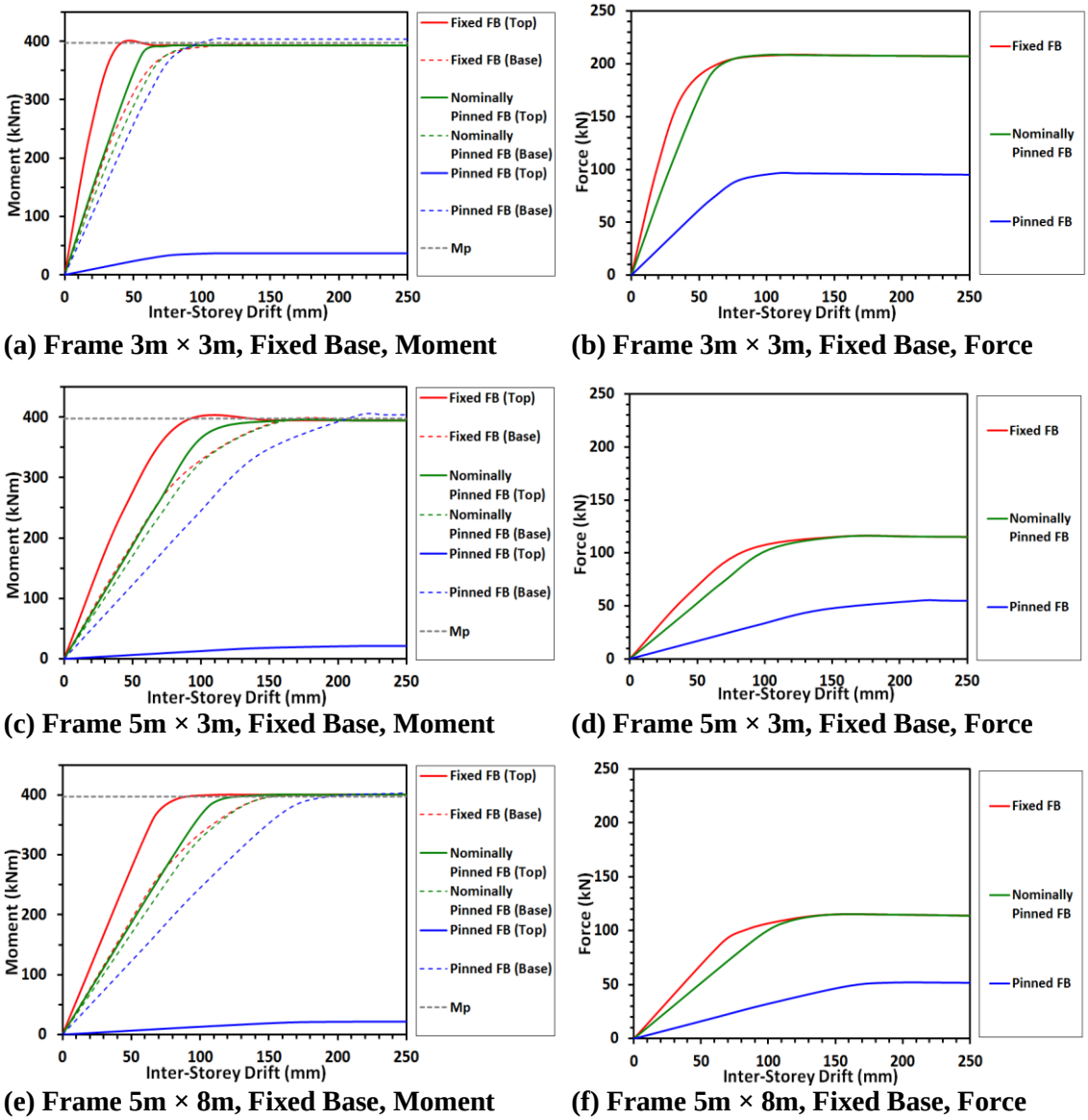

(a) Frame 3m × 3m, Fixed Base, Moment **(b) Frame 3m × 3m, Fixed Base, Force**

(c) Frame 5m × 3m, Fixed Base, Moment **(d) Frame 5m × 3m, Fixed Base, Force**

(e) Frame 5m × 8m, Fixed Base, Moment **(f) Frame 5m × 8m, Fixed Base, Force**

Figure 4.8 (a) – (f): Fixed base pushover response of structures: (a), (c), (e) showing moment generation in columns; (b), (d), (f) showing corresponding force deflection relationship (i.e. overall lateral stiffness of frame).

The introduction of soil to the model (compliant base) changes the system's response. The structure must now work with the soil to resist the pushover force that

is applied. The flexibility of the soil introduces additional mechanisms to the system, namely the global structural rotation (tilt) of the frame and the local foundation rotation, as outlined in Figure 4.9. The occurrence of these new mechanisms is apparent in Figure 4.10 (a)-(i). Frames with closely spaced foundations lend themselves more readily to overall structural rotation, with the 3m wide frames showing significant signs of structural rotation, whereas the 8m wide frames show limited to no structural rotation occurring. At the same time that structural rotation is occurring another rotational mechanism, local foundation rotation, is also developing, this type of local foundation rotation mechanism has been seen before and documented by Gajan *et al.* (2005), Ugalde *et al.* (2007) and Algie *et al.* (2010) among others and was found to reduce structural demand. In the case of the narrow, stiff frames prone to structural rotation this local rotation is a secondary rotational mechanism which develops until the structural rotation takes over to induce the failure, which occurs when structural rotation reaches approximately 0.5deg, at this point the local rotation is seen to begin to reverse. When considering the pinned joint case for each of the frames, the structure does not experience the same structural rotation as is apparent with the other joint stiffness frames. The flexibility of the pinned connection, at the column and beam joint, allows the two combined foundation and column sections of the structure to act independently, allowing the local foundation rotation to develop as the primary rotational effect and limiting the overall structural rotation (tilt).

While moment still builds up within the column of the frames, once the frames rotational mechanisms of failure take over, (possibly due to soil failure beneath the foundations), the moment in the column stops increasing and the frame is pushed over due to a combination of structural and local rotation. The rotational mechanisms prevent the moment capacity of the columns in the rotating frames from being reached.

Considering the 8m wide frame, with the stiffer joints, the failure remains within the structure in the sway mode. The wider spaced footings result in the structural rotational moment capacity of the foundation system increasing significantly due to the longer lever arm (in this case given by the length of the beam). While some rotation does occur it is not large enough to reach the 0.5º threshold and therefore never becomes the controlling mechanism. As seen with the narrower structures, when structural rotation is restrained local rotation is free to continue to

develop. The stiffer jointed frames allow the local rotation to develop while resisting the inter-storey drift induced by the pushover, but this local rotation is not enough to stop the moments within the column building up, moment capacity is eventually reached and a structural failure occurs. The interaction with the soil, and the local rotation, has allowed for slightly more inter-storey drift to occur before failure is reached than when compared to the fixed base case. This mechanism of allowing some rotation to dissipate work/energy within the soil-structure system, while still being stable enough to prevent overturning may prove to be valuable within the seismic loading case, similar to that seen in Gajan *et al.* (2005). In the flexible 8m wide frame with pinned joint more inter-storey drift occurs, (due to the flexibility of the frame), as the local rotation develops. This flexibility allows failure in the soil below the foundations to develop, due to the local rotation, before the moment capacity of the structural elements is reached, therefore protecting the structural elements.

The pushover tests have highlighted that the overall sway response of the system is dependent on three main mechanisms: inter-storey drift, global rotation of the structure and local rotation of the foundations. This is highlighted in Figure 4.9. The amount of sway each mechanism provides is governed by the local flexibility in the footing, the rigidity of the frame (through the joint system) and the overall geometry of the structure. Controlling these mechanisms could prevent the structure from suffering structural collapse (in the columns). This effect will be examined further in Section 4.6 under seismic ground motion.

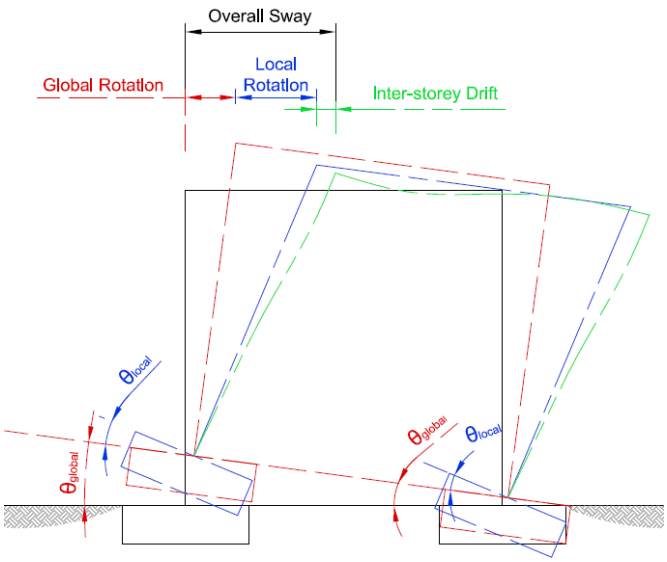

Figure 4.9 Mechanisms controlling overall sway of a structure on soil

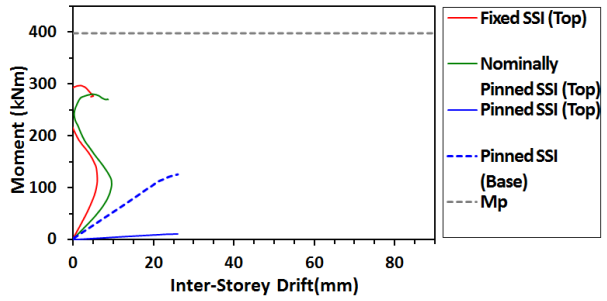

(a) Frame 3m × 3m, SSI moment

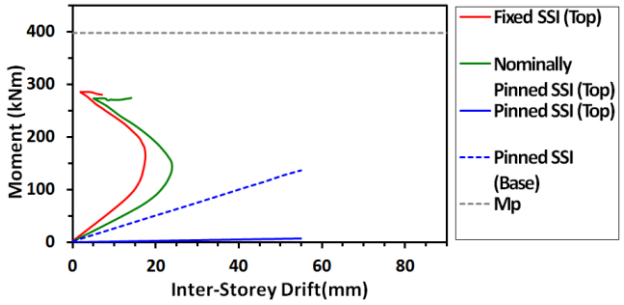

(b) Frame 5m × 3m, SSI moment

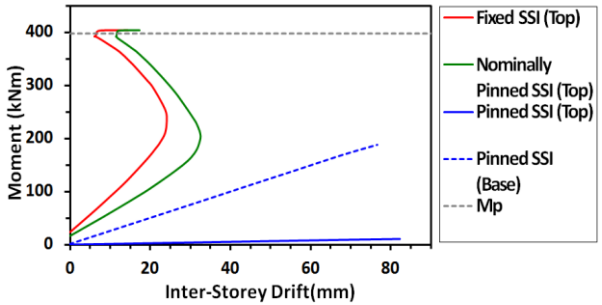

(c) Frame 5m × 8m, SSI moment

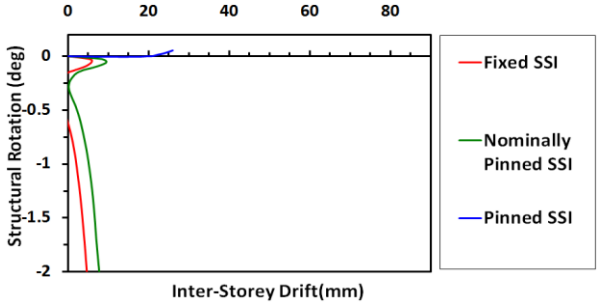

(d) Frame 3m × 3m, SSI structural rotation

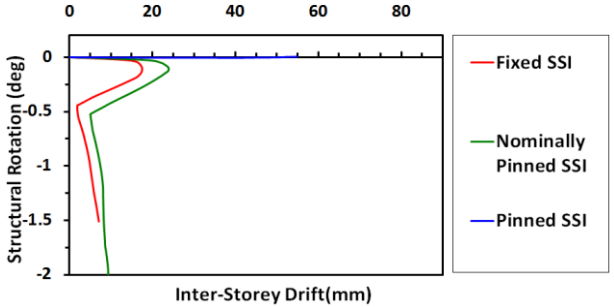

(e) Frame 5m × 3m, SSI structural rotation

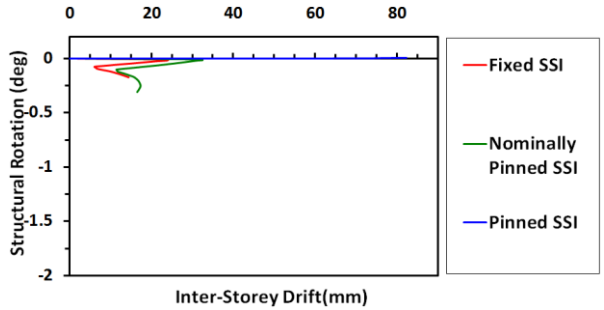

(f) Frame 5m × 8m, SSI structural rotation

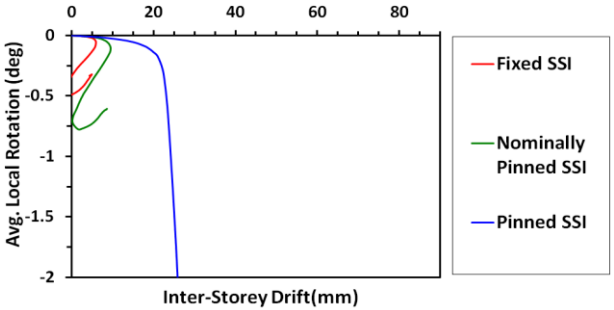

(g) Frame 3m × 3m, SSI local rotation

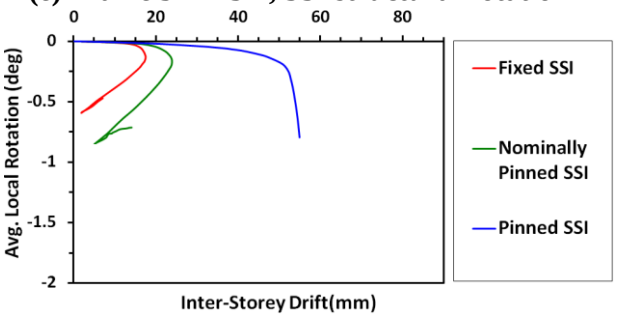

(h) Frame 5m × 3m, SSI local rotation

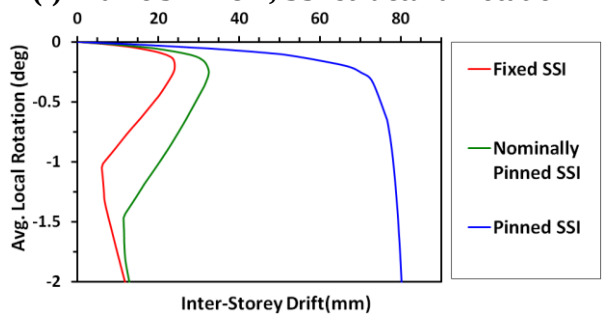

(i) Frame 5m × 8m, SSI local rotation

Figure 4.10 (a) – (i): Soil Structure Interaction, SSI, pushover response of structures

The global and local rotation mechanisms appear to be heavily dependent on one another. While they each generate an individual contribution to the overall sway of the structure, the development of one can directly influence the development of the other. This dependence is highlighted more clearly in Figure 4.11 (a) and (b). In the case of the narrow frame, (a), with some joint rigidity, (nominally pinned and fixed), both mechanisms develop together, with the local rotation developing faster, but once the global rotation reaches 0.5deg its accelerated development halts, and even reverses the local rotation. In the wide frame, (b), the local rotation mechanism remains the controlling mechanism, and while local rotation is free to develop, the global rotation is restricted by comparison. As both mechanisms influence a portion of the overall sway, and therefore can be used to reduce overall structural demand on the columns, an instance where both mechanisms develop together without limiting each other would perhaps be most beneficial, this would allow the local rotation to reduce demand in smaller earthquakes, while the global rocking could be activated in larger earthquakes.

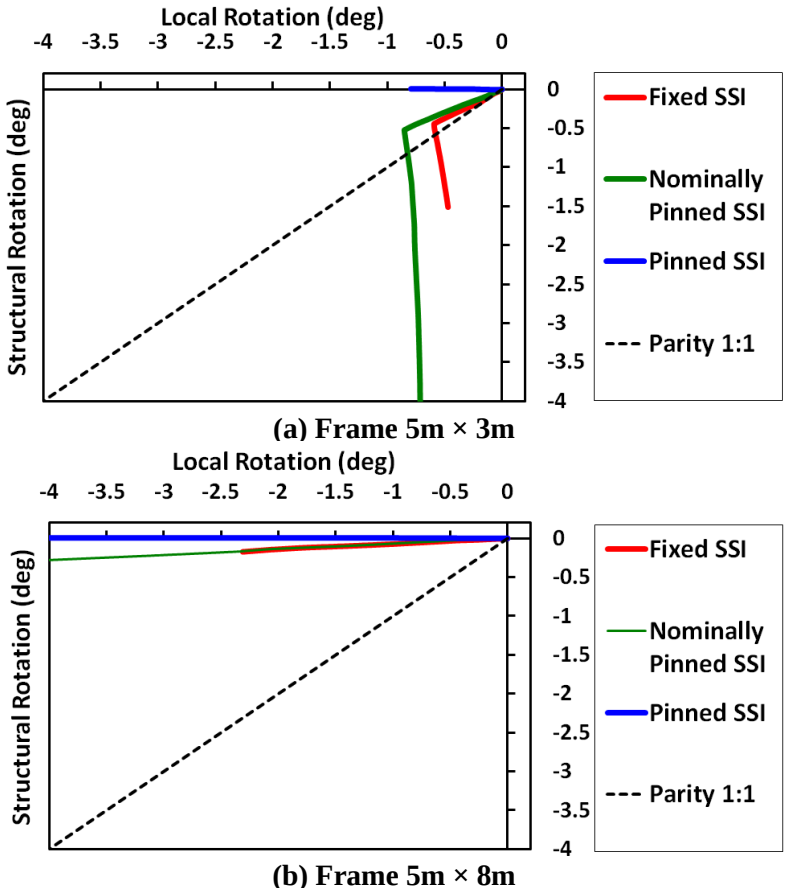

Figure 4.11 Rotational mechanisms (local and global), in the narrow and wide frames

4.5 Seismic structural response

As discussed in Chapter 3, two scaled versions of the seismic recording taken at the Takatori recording station in the 1995 Kobe earthquake are applied to each FEM model assembly. Each model contains a unique frame joint, aspect ratio, ground type combination as outlined in Tables 3.8 and 3.9 of Chapter 3.

Within the pushover loading of the systems the inter-storey drift, local rotation and global rotation of the frames and the resulting moments that built up within the columns were considered. This gave an insight into the possible failure mechanisms that were occurring within the system. The time histories for the 0.35g scaled Kobe earthquake applied to the 5m × 3m frame, for both the fixed and pinned soil structure interaction systems, are presented in Figure 4.12. These plots indicate the displacement input to the foundation of the structure, the overall cyclic rotation of the structure during the earthquake, the cyclic moment that built up within the column and the cyclic drift of the column. While both frames had identical displacements introduced into their foundations through the soil, their seismic response is evidentially different. The more flexible frame rotated in a manner consistent with the input motion, while the more rigid frame however showed less consistent rotation and more extreme spikes in rotation. Overall larger moments were observed in the pinned joint frame resulting from an increase in sway. However the magnitude of increase of both the moment and the sway, compared to that of the fixed joint, was not equal. While the sway observed in the pinned joint frame was almost 5 times that of the fixed joint frame, the moment in the column only doubled, therefore the pinned joint frame seems better at minimising the amount of moment built up in the columns for a given amount of sway experienced. From this data alone it is difficult to get an overall perspective on how exactly the system is being influenced. Elements of this data, from across all frames analysed are extracted and compared further in Section 4.6.

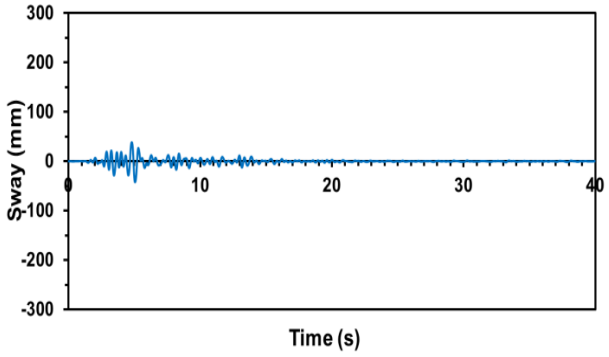

(a) Fixed joint frame, average sway

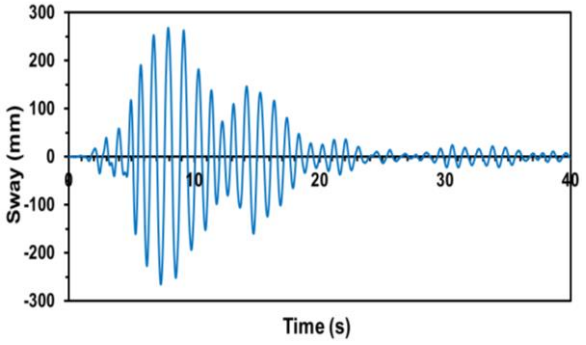

(b) Pinned joint frame, average sway

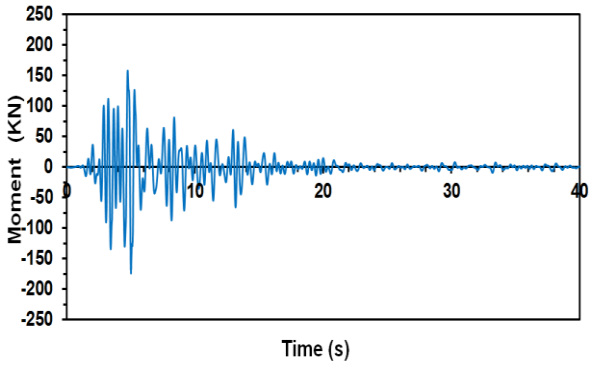

(c) Fixed joint frame, moment column (base)

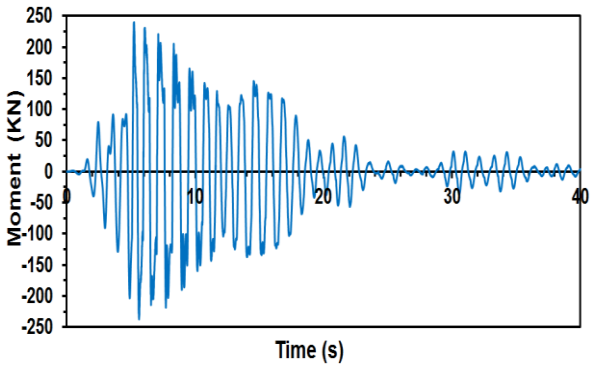

(d) Pinned joint frame, moment column (base)

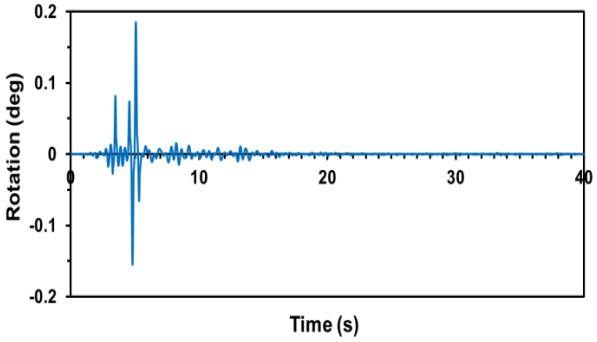

(e) Fixed joint frame, rotation in structure

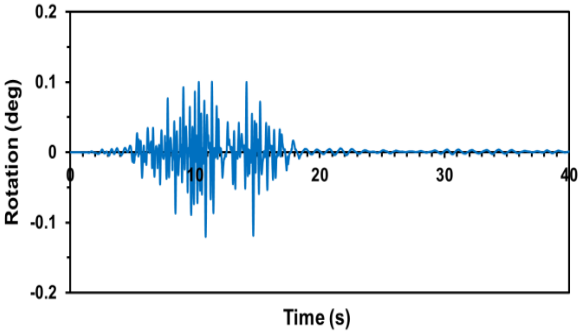

(f)Pinned joint frame, rotation in structure

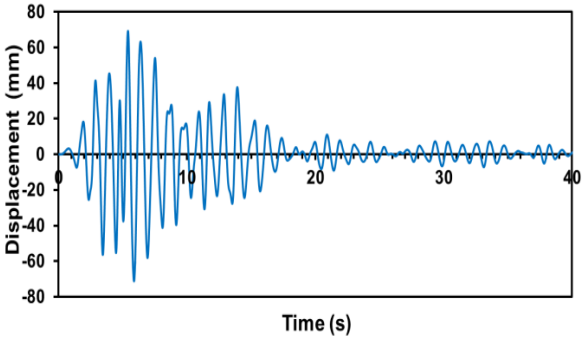

(g) Fixed joint frame, Input to found

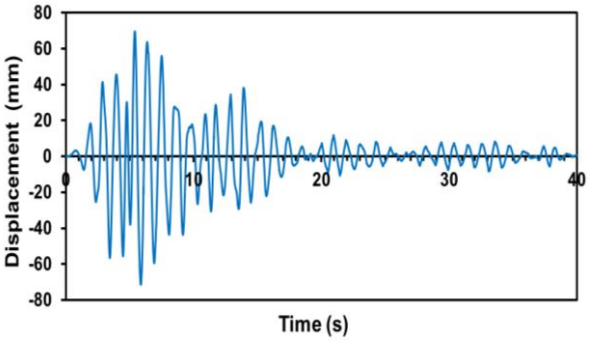

(h) Pinned joint frame, Input to found

Figure 4.12: Time History Response for 0.35g Kobe fixed and pinned frame, fixed base models

4.6 Relative influence of frame stiffness, aspect ratio and SSI

From the initial data, outlined in Section 4.5, it could be understood that the same factors that played an influential part within the static analysis were also important during the seismic analysis. It was immediately evident that the soil structure interaction had a large influence on both how seismic motion was amplified before reaching the foundations and how the structure responded to the cyclic loading. The geometry of the structure was also playing a big part in its response. The joint system appeared to become a greater influencing factor when the more flexible joint systems were considered. In this section these factors are compared with each other and with other system responses in order to try and find important underlying mechanisms within the system.

4.6.1 Peak drift

The level of inter-storey drift experienced in the columns of the structure during the seismic loading is an indicator of the induced seismic shear forces and bending moments acting within the frame (columns). The maximum inter-storey drift achieved during the 0.35g Kobe earthquake for all frames is presented in Figure 4.13 (a)-(c). The difference in the amount of inter-storey drift experienced by the different sized structures is substantial. The level of drift increases with both the increase in height and the increase in width of the structure. Increasing the height increases the length of the column and therefore the flexibility of the frame, allowing greater drift to occur within the member. Increasing the width of the frame also shows a significant increase in the drift achieved within the column. The longer beam and slab that connect the two columns in the 8m wide frame will be more flexible, due to its length, than that in the 3m wide frame. This increase in flexibility of the system also allows for the greater drift to occur. The influence the joint system has does not seem to take great effect until the system stiffness is greatly reduced due to the joint flexibility, far into the lower semi rigid zone.

It would appear that increased flexibility of the system, the factor which also influences the change in period of the structure, increases inter-storey drift of the structure. Moving from a FB case to a SSI case adds a lot more flexibility to the system and therefore it would be natural to assume that this additional flexibility

would again have a negative effect on the amount of inter-storey drift experienced within the structure.

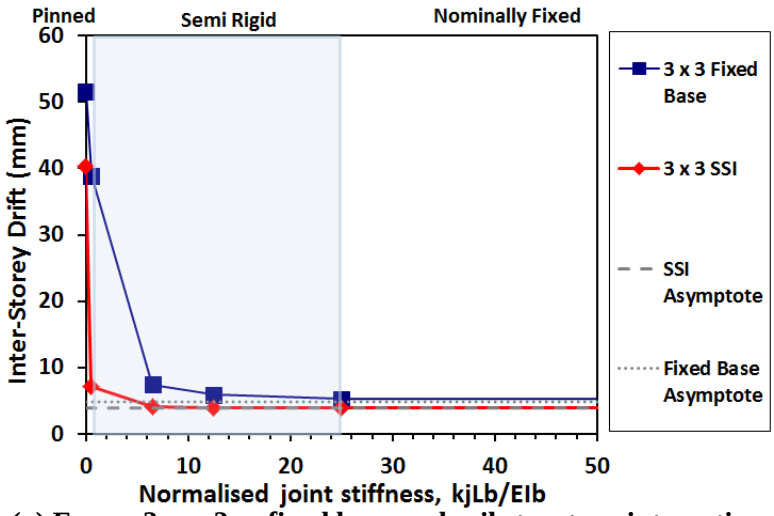

(a) Frame 3m × 3m, fixed base and soil structure interaction

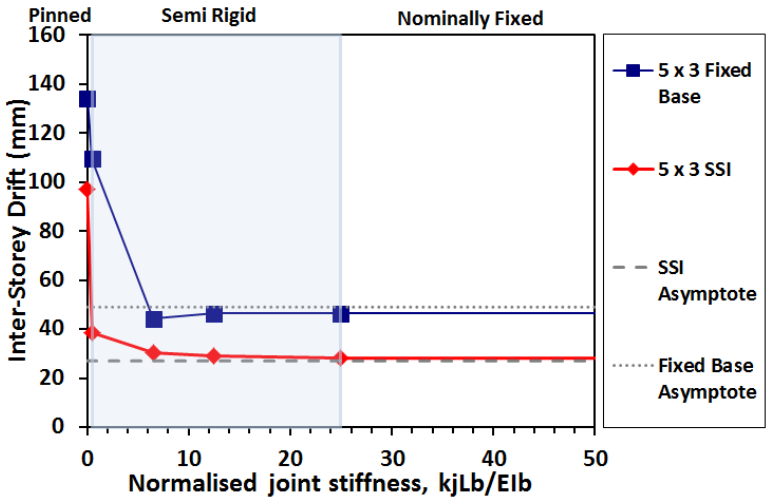

(b) Frame 5m × 3m, fixed base and soil structure interaction

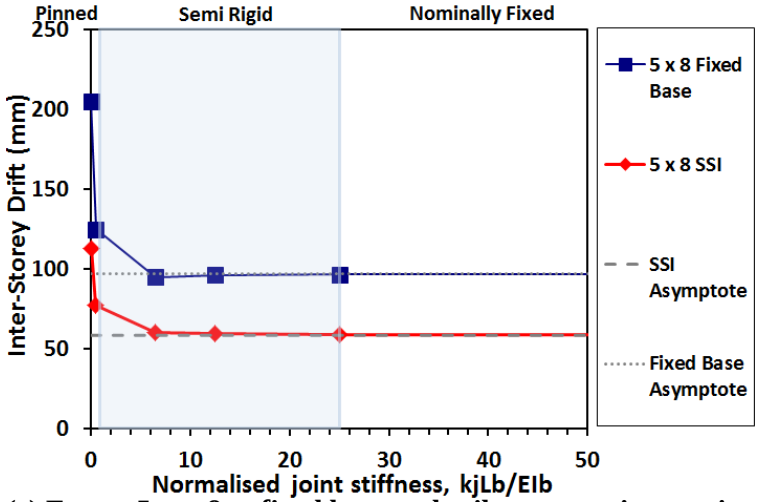

(c) Frame 5m × 8m, fixed base and soil structure interaction

Figure 4.13 (a) – (c): Joint stiffness affecting peak inter-storey drift of frame

However in all frame systems the addition of SSI is seen to actually reduce the amount of inter-storey drift experienced by the frame and therefore reducing the structural demand on the columns of the frame. While the geometry of the structure greatly affects the levels of inter-storey drift the structural columns experience, it is not the only factor that has influence. In all cases, for all geometries and both SSI and FB situations, the stiffness of the joint system shows an effect on the maximum inter-storey drift achieved. This effect pattern is similar to the pattern seen in the change in fundamental period of the frame, as discussed in Section 4.3. This would support the change in period due to the frame rigidity resulting in proportional changes in drift from a spectral analysis, as in Section 2.2.

The inter-storey drift makes up only part of the total response of a frame with SSI, as outlined in Figure 4.9. The full response of the structure, the overall sway, is comprised of the lateral displacement induced by the global rotation, local rotation and the inter-storey drift. These rocking mechanisms are largely responsible for the reduction in inter-storey drift observed between the fixed base and SSI cases. The displacements induced by these rotations have a greater effect over a longer column element than a shorter one; therefore the taller structures are expected to show an increased sway for a given amount of rotation. These rotational mechanisms, as well as the moment within the columns must be analysed before a clear picture of the true response is obtained.

4.6.2 Response mechanisms affecting peak inter-storey drift

While the maximum inter-storey drift of the structure can give an indication of the structural response of the system, as well as some of the factors affecting that response (the geometry, joint stiffness and foundation stiffness), it is not until the level of drift is paired with other response mechanisms that a true response of the structure is revealed. Both the structural rotation mechanism and local foundation rotation mechanism, similar to those observed during the pushover loading analysis, are also observed during the seismic loading analysis.

Figures 4.14, 4.15 and 4.16 present the moment build up in the columns, the structural rotation and the local rotation associated with the corresponding inter-storey drift of the frames. Only the 5m × 3m and the 5m × 8m frames are presented

here as the magnitude of the rotations observed for the 3m × 3m were too small to allow direct visual comparisons with the other frames, but their maximum values will be summarised alongside the other frames later in this section for general comparison. The peak inter-storey drift and peak moment values observed during the fixed base seismic loading of the corresponding frame are also shown, where applicable, as an envelope on each graph in order to observe the beneficial impact of SSI on the response.

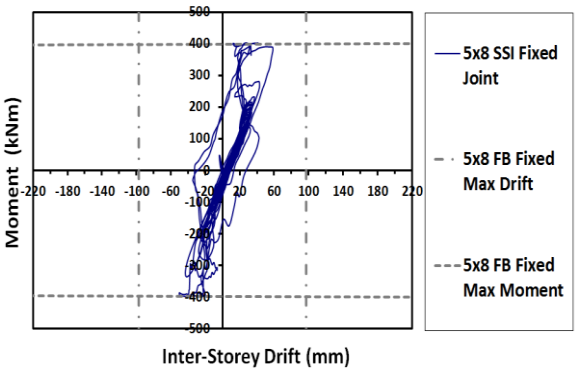

(a) 5m × 8m fixed joint frame moment

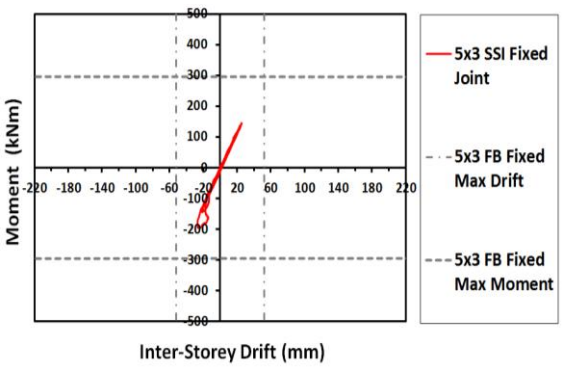

(b) 5m × 3m fixed joint frame moment

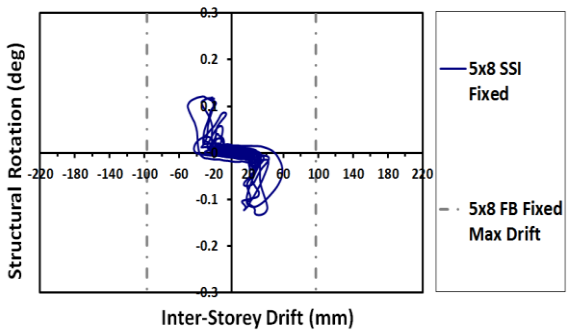

(c) 5m × 8m fixed joint frame structural rotation

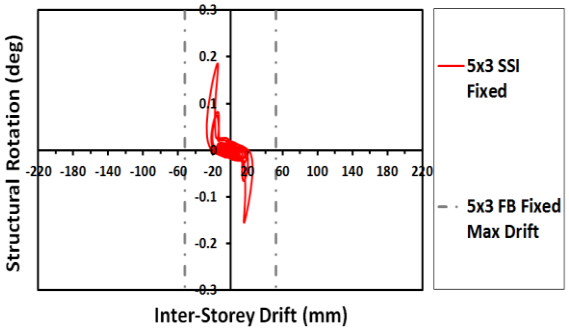

(d) 5m × 3m fixed joint frame structural rotation

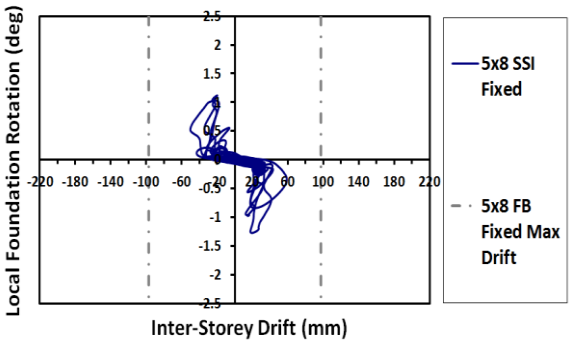

(e) 5m × 8m fixed joint frame local rotation

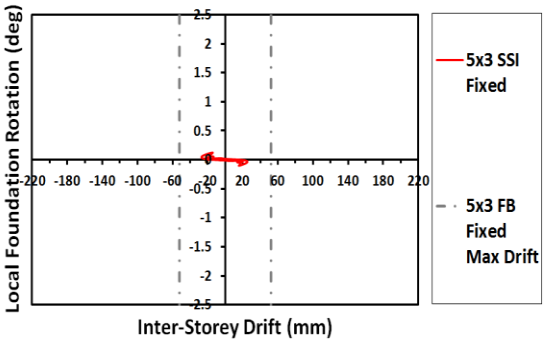

(f) 5m × 3m fixed joint frame local rotation

Figure 4.14 Rotational and Moment response of fixed joint structures

In Figure 4.14, the 5m × 8m fixed joint frame and the 5m × 3m fixed joint frame are compared to show how the structure responds to a change in the geometry

of the structure. It should be noted that if the effects of the beam flexibility were ignored (i.e. stiffness from the columns only), these two frames would be considered to have similar natural period and spectral response through a conventional analysis, albeit with some small difference resulting from differences in the overall mass. The reduction in inter-storey drift, compared to their fixed base counterparts, originally observed in Figure 4.13, is also clear from Figure 4.14, however it is only the 5m × 3m which also sees a reduction in the peak moment within the columns. The 5m × 8m still reaches moment capacity of the column; however the number of hysteresis loops that reach moment capacity, compared to the fixed base case, is reduced suggesting that additional damping, resulting from the rotations, is present, but not enough to prevent moment capacity being reached. The narrower frame lends itself to structural rotation more easily than the wider frame, displaying 0.19 deg of structural rotation compared to 0.13 deg in the wider frame.

The reduced structural rotation in the wider frame, compared to the narrower frame, is due to the frame's structural rotational moment capacity increasing due to a longer lever arm, as seen in Section 4.4 for the pushover response. The wider spaced frame displays much more local rotation in the individual footings, 1.27°, compared to 0.12° for the narrow frame. The longer beam element, which increases the structural rotational moment capacity, also introduces more flexibility to the system allowing the individual footings to be more independent and allowing more local rotation.

It is evident that the geometry can have an effect on controlling which rocking mechanisms are activated during seismic loading, the flexibility provided by the beam and the spacing of the foundations being the major factors. Additional flexibility is also provided by the jointing system within the frame. Figures 4.15 and 4.16 examine how the nominally pinned joint frame and the pinned joint frame respond to the loading. The nominally fixed and semi rigid joint system frames responded similarly to the fully fixed condition and for brevity are not presented here. In the nominally pinned case the narrower structure again shows more structural rotation, 0.25°, compared to the wider frame, 0.15°, and the wider frame showed more local rotation, 1.81°, compared to the narrow frame, 0.21°. This follows the trend seen in the fixed joint case but the magnitude of rotations has increased in all cases.

While there is more inter-storey drift in the nominally pinned frames compared to their fixed frame counterparts, this may be due to the joints' impact on

the overall response, as this increase also occurs in the fixed base case. In the fixed base case for the 5m × 3m frame the moment was seen to reduce between the fixed joint and nominally pinned cases, as outlined by the change in the maximum moment envelope for the fixed base condition in Figures 4.15 and 4.16. With the inclusion of the soil in the system both joint conditions have seen the moment within the columns reduce but to a level which is more in line with one another, suggesting that the joint system plays a lesser role in the response when a flexible soil is considered rather than a fixed base condition. This is also evident from Figure 4.13 where the inter-storey drift appears to be affected more by the joint system in the fixed base case rather than the SSI case.

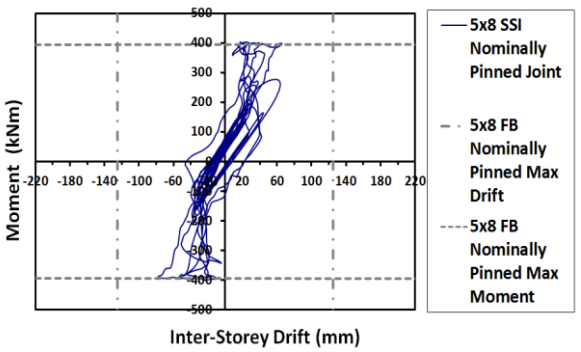

(a) 5m × 8m nominally pinned frame moment

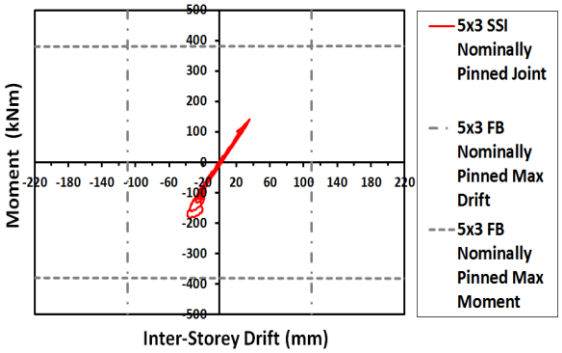

(b) 5m × 3m nominally pinned frame moment

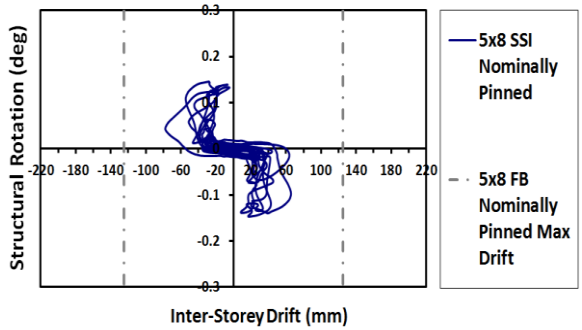

(c) 5m × 8m nominally pinned frame structural rotation

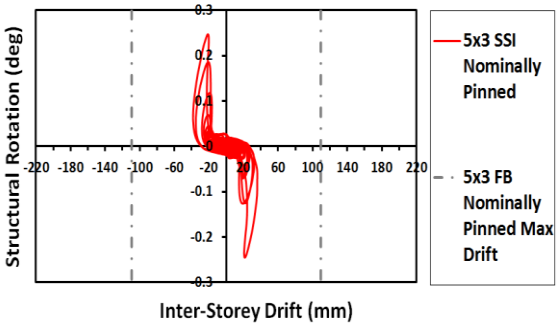

(d) 5m × 3m nominally pinned frame structural rotation

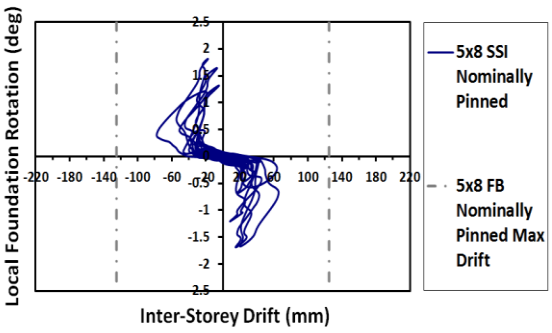

(e) 5m × 8m nominally pinned frame local rotation

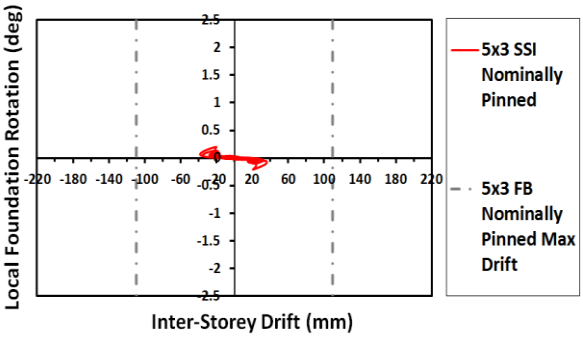

(f) 5m × 3m nominally pinned frame local rotation

Figure 4.15 Rotational and Moment response of nominally pinned joint structures

In Figure 4.16, showing the pinned joint frame case for both the 5m × 8m and the 5m × 3m frame, the maximum inter-storey drift again reduces when compared to the fixed base analysis. The maximum moment, which in the pinned case occurs at the base of the column, for both cases also reduces, a result not fully seen before within the 5m × 8m frame. The reduction in the inter-storey drift within the 5m × 8m frame, compared to its fixed base case, is slightly greater than other joint cases for the first time, while the narrow frame actually sees less of a reduction when compared to its fixed base case. The presence of a fully pinned joint within the structure isolates the columns response, preventing or limiting the structural rotation mechanism taking effect.

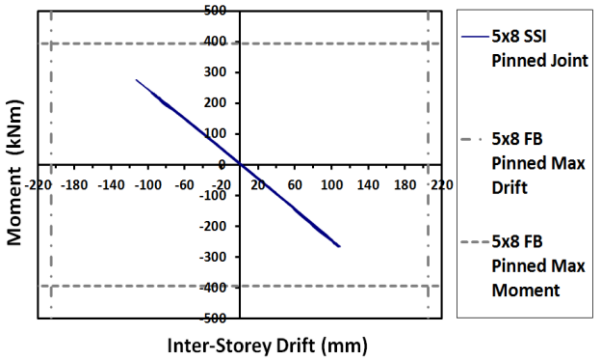

(a) 5m × 8m pinned joint frame moment

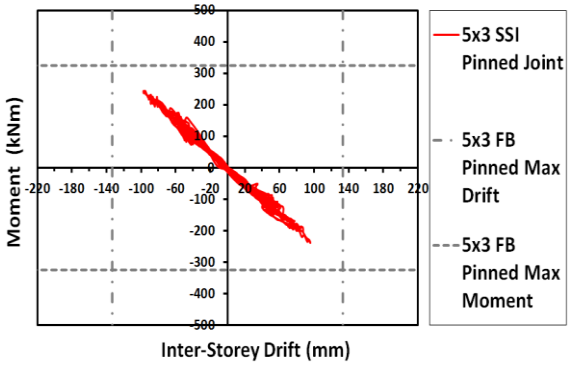

(b) 5m × 3m pinned joint frame moment

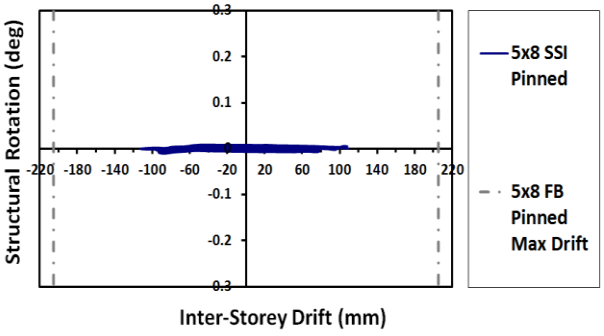

(c) 5m × 8m pinned joint frame structural rotation

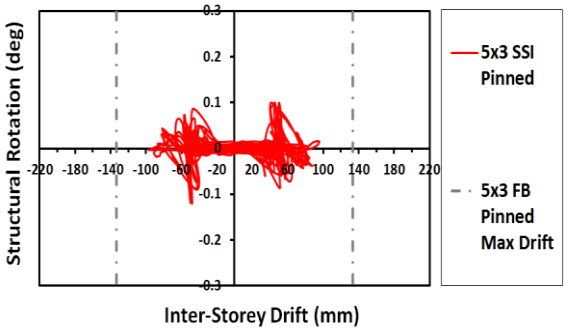

(d) 5m × 3m pinned joint frame structural rotation

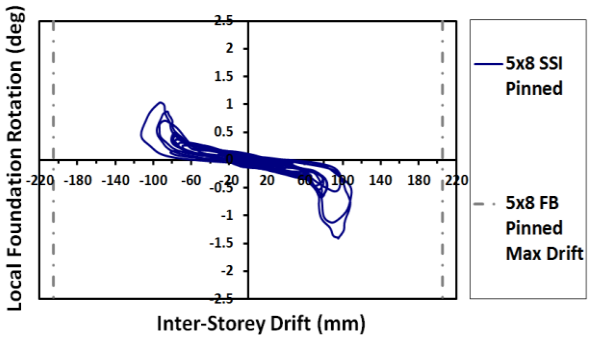

(e) 5m × 8m pinned joint frame local rotation

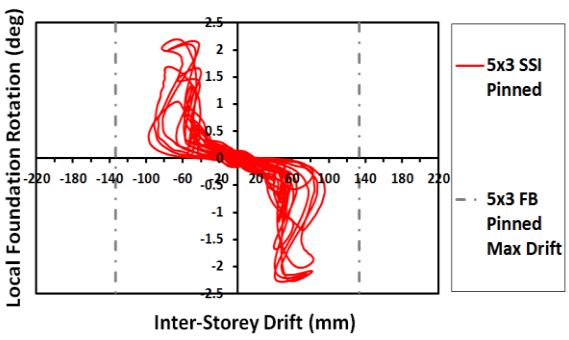

(f) 5m × 3m pinned joint frame local rotation

Figure 4.16 Rotational and Moment response of pinned joint structures

While some structural rotation is observed in the narrow frame the pattern is quite random, suggesting that, instead of an actual rocking mechanism being the cause, the data is showing the difference in independent vertical movement of both columns due to their local rotational movement. A greatly increased level of local rotation occurs in the narrow structure, however without the structural rotation it is unable to generate as much of a reduction in the inter-storey drift on its own compared to cases with both mechanisms.

From Figures 4.14, 4.15 and 4.16 is it evident that the SSI effect of reducing the inter-storey drift, as outlined in Figure 4.13 is heavily influenced by the amount of rotation, both local and global, that is activated during the seismic loading. The rotational mechanisms themselves are governed by both the geometry of the structure and the flexibility of the joints, more clearly summarised in Figure 4.17 for both global and local rotational mechanisms.

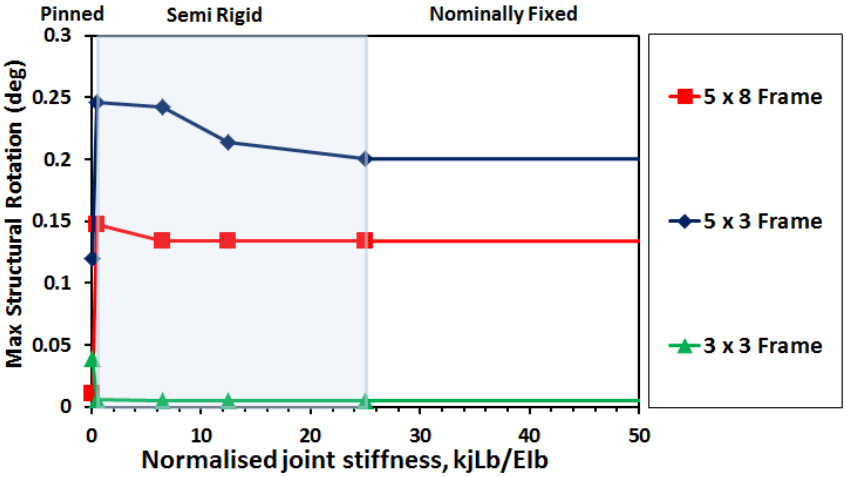

(a) Max Structural Rotation, all SSI frames, all joint stiffness

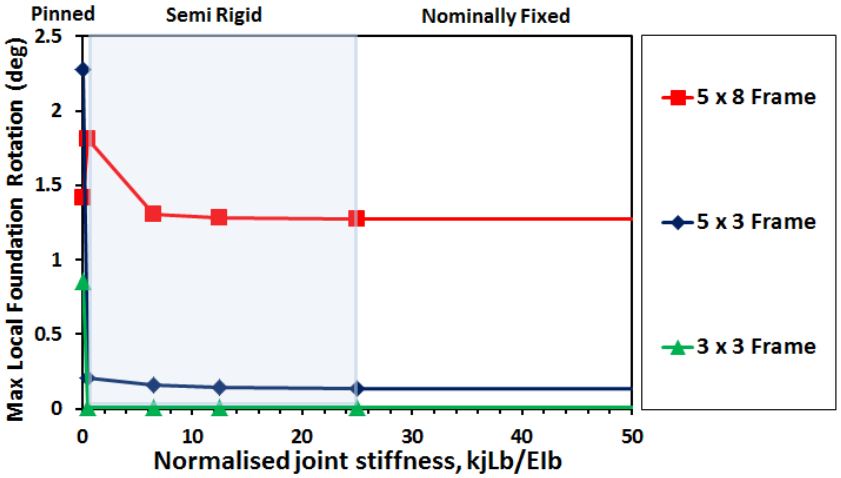

(b) Max Local Rotation, all SSI frames, all joint stiffness

Figure 4.17 Influence of geometry and joint stiffness on rotational mechanisms

It is clear from Figure 4.17 that the major influencing factor for the rotational mechanisms is the geometry of the frame. A tall narrow structure lends itself more readily to structural rotation while a wider frame is more prone to local footing rotation. The joint system has limited effect on the structural rotation of the structure on its own, however when it is combined with the system that is optimised to allow structural rotation, it then begins to influence the amount of the rocking that occurs, the stiffer joints reducing the geometry effect by about one fifth. Local rotation is also affected by the geometry of the system - increasing the width of the structure comparative to its height will greatly increase the amount of local rotation that is activated, the joint systems influence on the mechanism appears limited, until more flexible, nominally pinned and pinned, joints are considered.

Previously it was shown that the overall response, sway, of a SSI system is composed of three mechanisms inducing displacement, inter-storey drift, global rotation and local rotation. From Figure 4.13 it is clear that a flexible joint can affect the overall response of a structure, in line with the increase in natural period of the system. Figures 4.14, 4.15 and 4.16 showed that it can also slightly affect the amount of rotation that occurs in the frame. Interestingly, as shown in Figure 4.18, the amount of sway that is made up of inter-storey drift does not appear to be affected by the joint system, and is generally controlled by the height and width of the structure. The 3m × 3m frame is shown to have the majority of its response comprising of inter-storey drift, 92% - this is due to the limited rotations that occurred. The 5m × 3m frame, which is prone to global rotation, with some additional local rotation, showed that significantly less of its response, 63%, was due to inter-storey drift. For the wider 5m × 8m frame, which is prone to local rotation but also displayed a significant amount of global rotation, even less of its response, 41%, was due to inter-storey drift. The amount of sway that was made up of inter-storey drift appears to be uniform across the joint systems, so while the joint system may influence the initial sway response, its impact on the percentage contribution of each of the mechanisms, inter-storey drift, global rotation and local rotation, to the sway response seems limited.

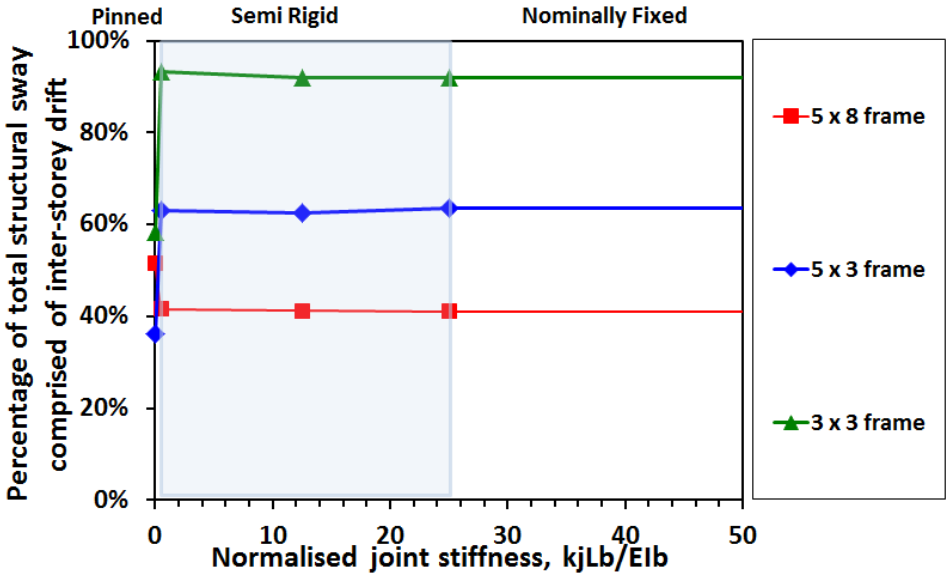

Figure 4.18 Change in percentage of sway comprised of inter-storey drift across the frames

4.7 Validation of improved spectral prediction model

The detailed FEM results in the previous section illustrated the response mechanisms of the systems analysed during seismic loading. Moreover it demonstrated how structural changes within the system, such as geometry, joint stiffness and foundation type, affected these response mechanisms.

While is it possible to account for some of these structural changes (column height effect on stiffness and natural period of the frame) through the current method of prediction, an improved model for determining the dynamic structural parameters accounting for joint stiffness, bay geometry (beam flexibility) and local and global flexibility within the foundation system as developed earlier in Section 4.2. In this section, this new method is validated against the seismic time history FEM results. This will include validation of the equivalent fundamental period of the system, the equivalent damping of the system, peak spectral acceleration and peak drift of the structure.

4.7.1 Prediction of fundamental period, T_n, fixed base structures

Figure 4.19 highlights how accurate the semi-rigid model with beam flexibility presented by Hellesland (2008) is for the fixed base model. By incorporating the flexibility of the system through joint consideration, and structural member length and flexibility, the new method of prediction is able to better represent the natural period

of the structural system. This flexibility was shown, in the FEM. analysis, to influence the response mechanisms of the system to seismic loading. The three markers of the new prediction data that are shown as red squares instead of black squares, in Figure 4.19, represent the fully pinned joint cases - no improvement was seen for these values as their fully pinned state does not allow any influence from the beam rigidity to be transferred through the joint within the Hellesland method. However this is a theoretical state which would not be replicable in real instances; when even a little stiffness is considered within the joint, i.e. the nominally pinned joint case, the new prediction instantly shows improvement. The improved predictions for T_n will later be used in calculations predicting the drift and acceleration of the system in Section 4.7.2. The accuracy of the improved method generally has almost all points within +/- 10% of the actual value determined from FEM for the fixed base model.

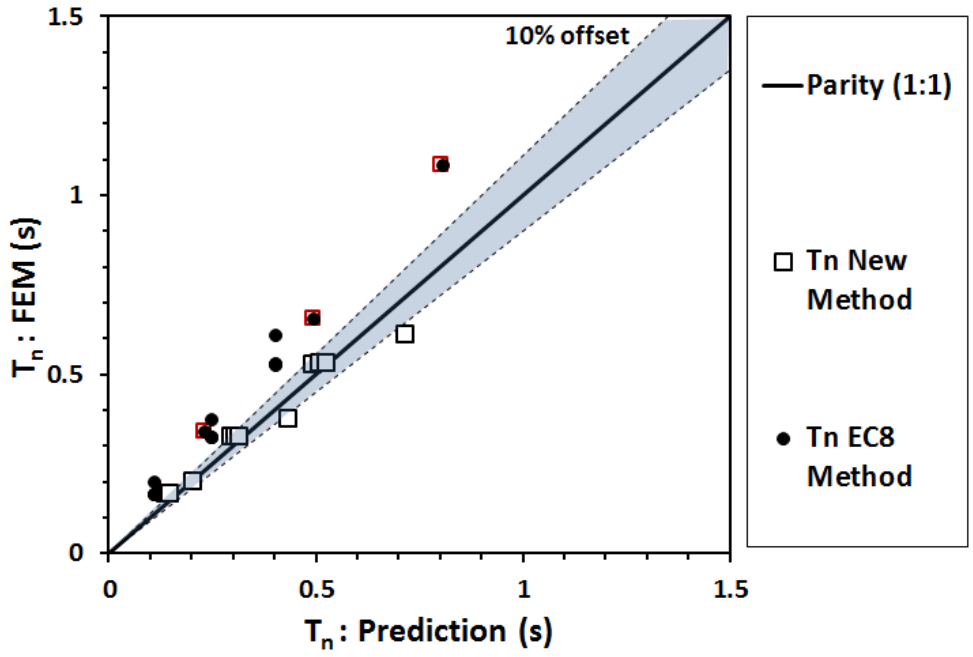

Figure 4.19: Predicted T_n compared to measured FEM values

4.7.2 Fixed Base Structure response

Eurocode 8, (BSI, 2008b) offers a method of utilising the T_n of a system to predict the elastic acceleration response, S_e, of the system, as discussed in Section 2.2. Figure 4.20 compares the acceleration response spectrum that is predicted by Eurocode 8, (BSI, 2008b), with the peak accelerations measured from the FEM analyses for the fixed base model. Values for both the 0.07g and 0.35g earthquakes have been

normalised by their peak input accelerations in order to make them comparable. The measured FEM results, do not fit the Eurocode 8, (BSI, 2008b), spectra of predicted values very well. However it must be considered that the Eurocode 8, (BSI, 2008b), spectra has been generated to predict response to a future unknown seismic event. In this study a specific motion is used and the acceleration response spectra was determined from this input motion. This acceleration response spectrum is overlain on the EC8 one and the FEM data in Figure 4.20 and matches up much better with this response spectra.

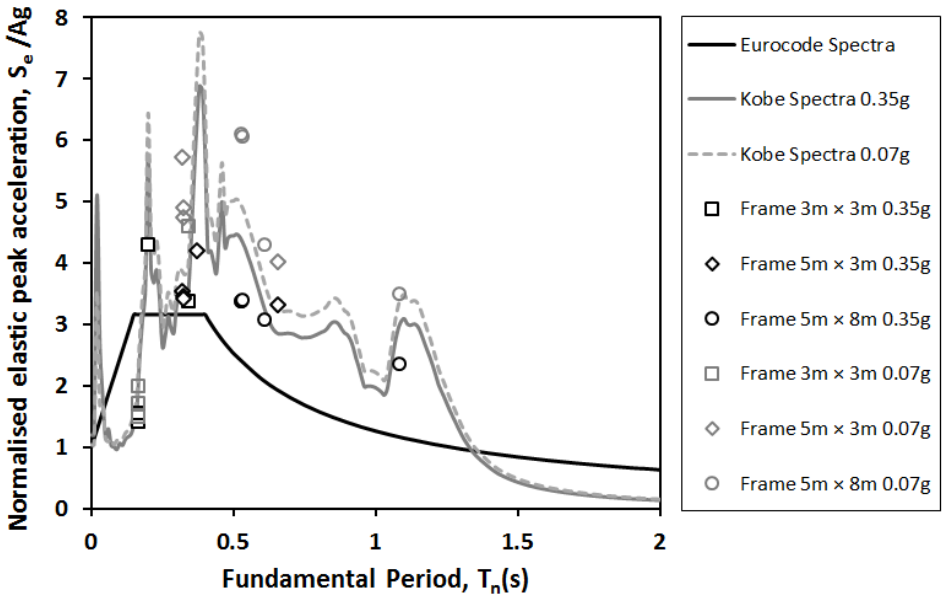

Figure 4.20: Fixed Base Elastic acceleration response, normalised by peak acceleration

Figure 4.21 highlights that, similar to the elastic acceleration response spectrum, the elastic displacement response given by Eurocode 8 does not tie in very well with the measured peak values obtained from the FEM. analysis. Again once the Kobe Takatori response spectrum is overlain on the data the correlation between the predicted data and the measured data improves. While 5% structural damping was input to the steel element for the FEM analysis the transfer function analysis performed in Section 4.3 to determine the T_n of the structure suggested an overall structural damping of 1.25%. Two spectra representing the Kobe Takatori response, each accounting for a different level of structural damping, are therefore shown. A greater correlation between the FEM data and the measured structural damping spectra is evident. Due to this better correlation a structural damping of 1.25% will be used for future predictions.

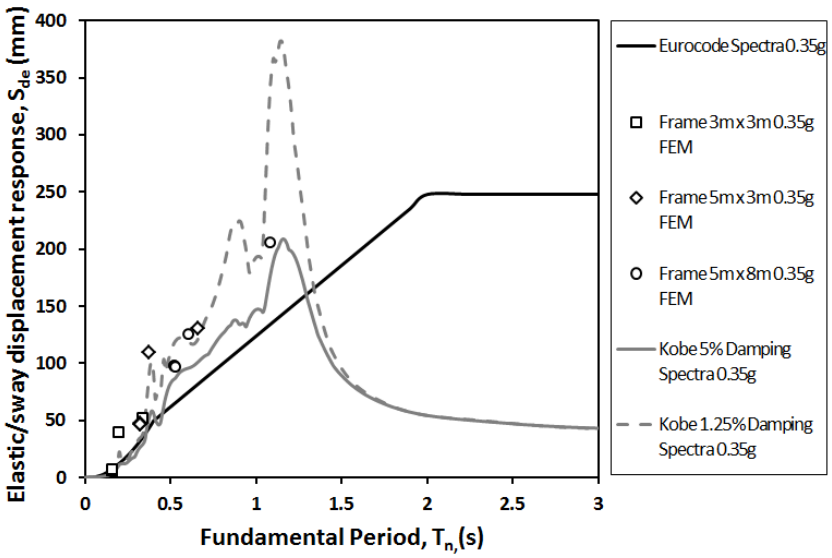

Figure 4.21: Fixed Base Displacement Response Spectra, 0.35g

4.7.3 Predicting fixed base displacement response

Following the Eurocode 8, (BSI, 2008b), method for predicting the elastic displacement response, i.e. the overall sway of the structure, S_{De}, as outlined in Section 2.2, Equation 2.6, and using the new T_n estimated previously with 1.25% structural damping gives the correlation shown in Figure 4.22. In the fixed base case the sway of the structure will be fully comprised of inter-storey drift as no rotational mechanisms occur.

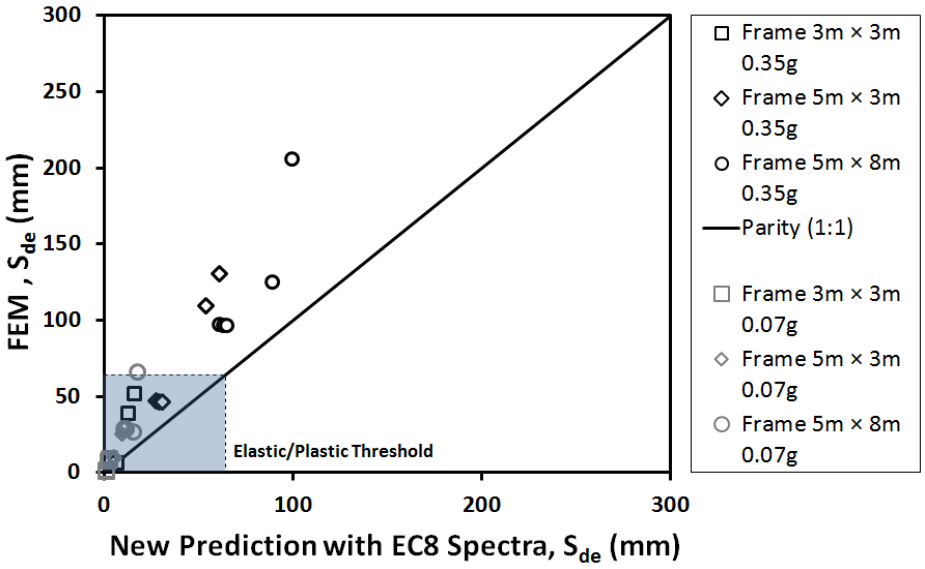

Figure 4.22: Accuracy of the peak S_{De} response and the inter-storey drift response predicted using new T_n and EC8 spectra for fixed base

There is an evident under prediction of the peak sway values using this method. This can be accounted for by the observed divergence between the acceleration/displacement response spectra for the Kobe motion and the Eurocode 8, (BSI, 2008b), elastic displacement response spectra, as shown in Figure 4.21.

Alternatively, predicting the S_{De} response of the structure using the actual response spectrum (1.25% damping) for the Kobe motion gives a better prediction of the FEM results, as shown in Figure 4.23. This highlights the benefit of obtaining a representative spectrum or set of spectra for earthquakes in a particular region when undertaking design.

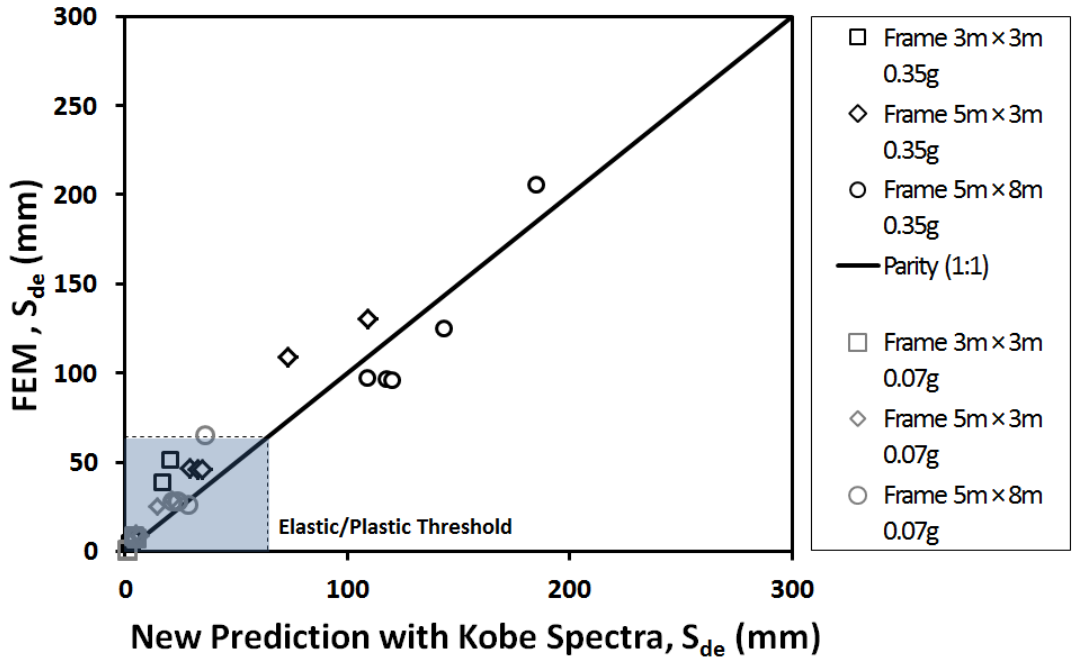

Figure 4.23: Accuracy of the peak S_{De} response predicted using new T_n and the actual Kobe spectra

4.7.4 Structural spectral response – soil structure interaction case

The acceleration response spectrum predicted by Eurocode 8 and the peak accelerations measured from the FEM analyses, for the soil structure interaction models are presented in Figure 4.24. As with the fixed base analysis the values for both the 0.07g and 0.35g earthquakes have been normalised by their peak accelerations in order to make them comparable. A similar mismatch between the Eurocode 8, (BSI, 2008b), spectra of predicted values and the measured values from the FEM analysis, as was seen for the fixed base analysis, also exists here. Using the

actual Kobe spectrum improves the correlation for the systems, however some discrepancy still exists.

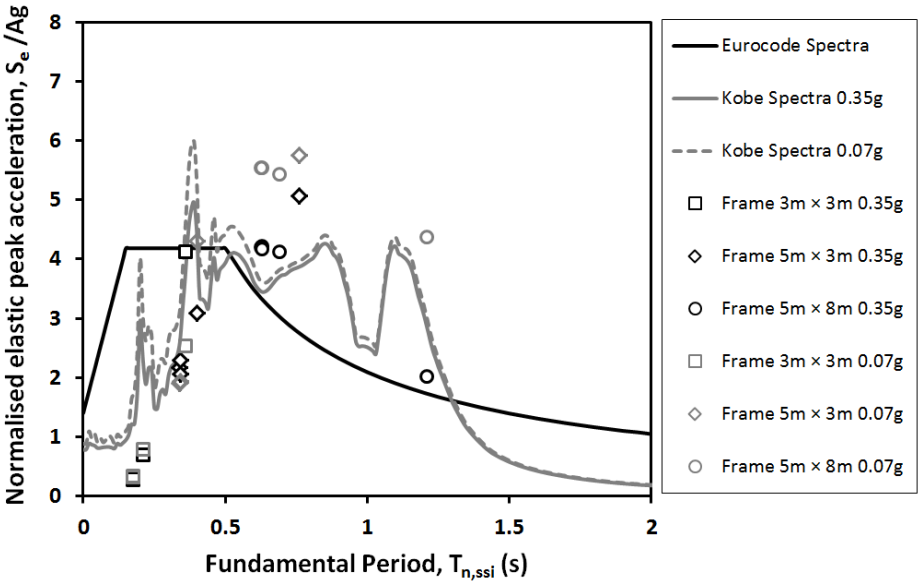

Figure 4.24: SSI Elastic acceleration response, normalised by peak acceleration

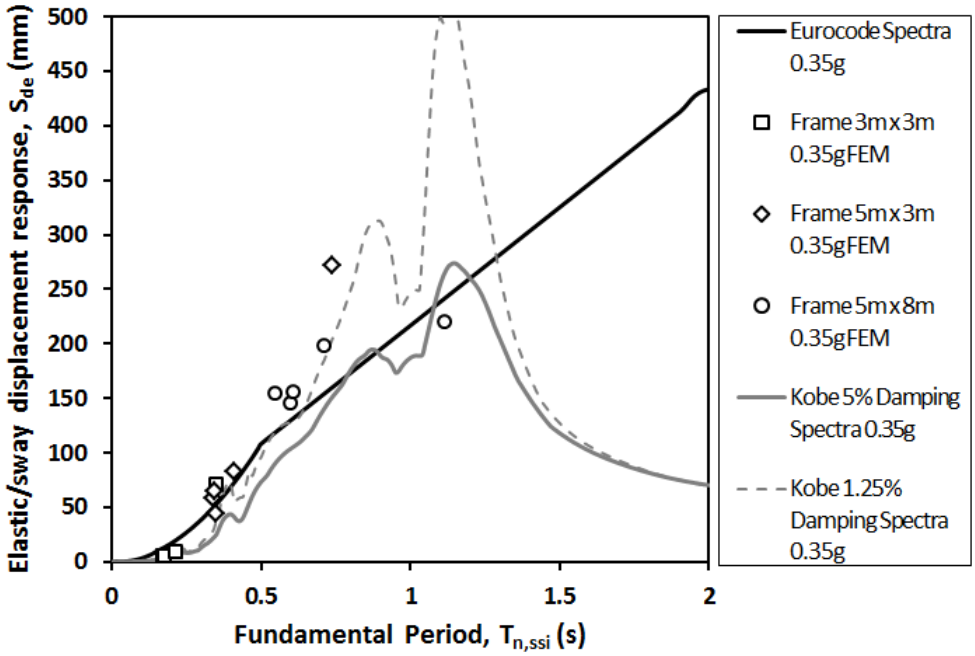

Figure 4.25: SSI Displacement Response Spectra, 0.35g

The elastic displacement response, $S_{De,}$ of the structures measured from the FEM model are shown in Figure 4.25 and compared to the Eurocode 8, (BSI, 2008b), displacement response spectra, the Kobe, 5% structural damping, displacement response spectra and the Kobe, 1.25% structural damping, displacement response spectra. While all spectra correspond well with the data for periods <0.6 s it is only

the Kobe, 1.25% structural damping, spectra that really captures the response of the larger period structures.

4.7.5 Prediction of equivalent fundamental period, $T_{n,\ ssi}$

By incorporating the flexibility of the system through joint consideration, structural member length and flexibility, and the flexibility added through soil structure interaction, the new method of prediction, outlined in Section 4.2.1, can incorporate the effects of all of these effects on the equivalent fundamental period $T_{n,ssi}$. Figure 4.26 highlights how accurate this prediction method is for the soil structure interaction (SSI) cases compared to the FEM results. The accuracy of the prediction, similar to the fixed base case, generally falls close to 10% of the value from the FEM. A clear improvement to the prediction can be seen between the simple Eurocode 8 method (which limits its inclusion of structural flexibility and does not include SSI effects) and the new method.

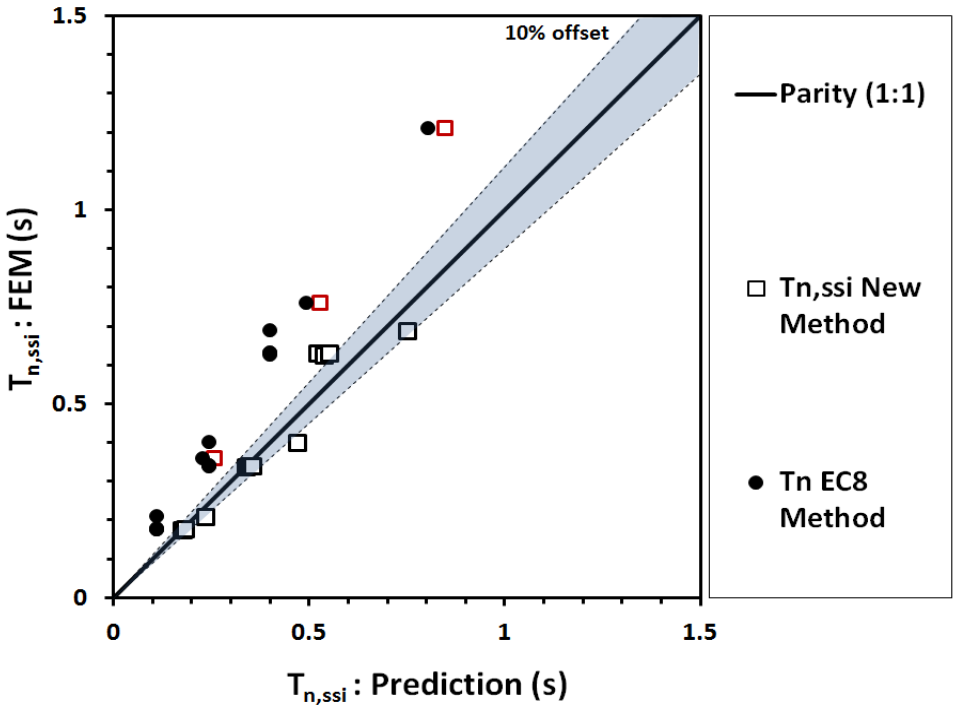

Figure 4.26: Predicted T_n , T_{nssi} compared to measured FEM values

4.7.6 Prediction of equivalent damping

In the soil-structure interaction case, consideration must also be given to the equivalent damping of the system and not just the structural element damping.

Analysing the results obtained for the soil structure interaction model from the FEM analysis through a transfer function calculation, the method of which is outlined in Section 3.6.2, and the results presented in Figure 4.27, highlights that there is more single degree of freedom damping being provided than just the structural element damping which in this case is about 1.25%. The damping changes with the fundamental period of the system, $T_{n,ssi.}$ This suggests that, broadly speaking, the effects of frame flexibility on the equivalent damping can be incorporated via Tn,ssi.

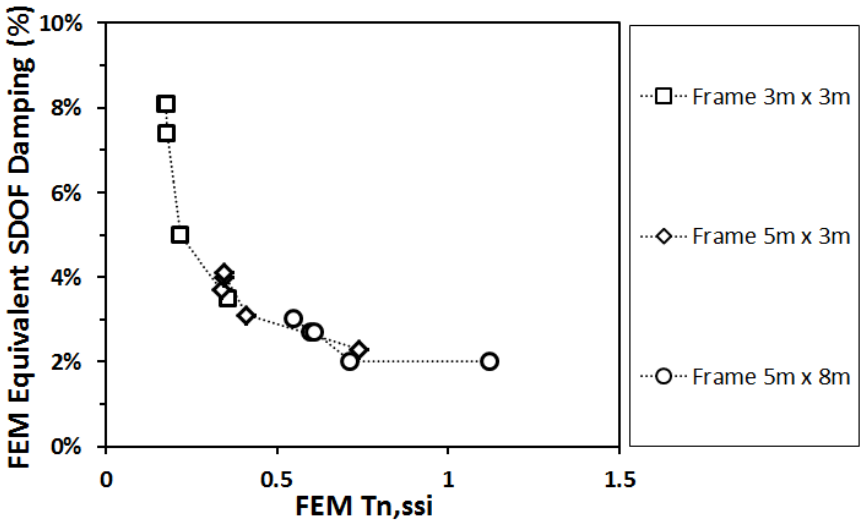

Figure 4.27: SDOF damping changing with $T_{n,ssi}$ (linear elastic soil)

.

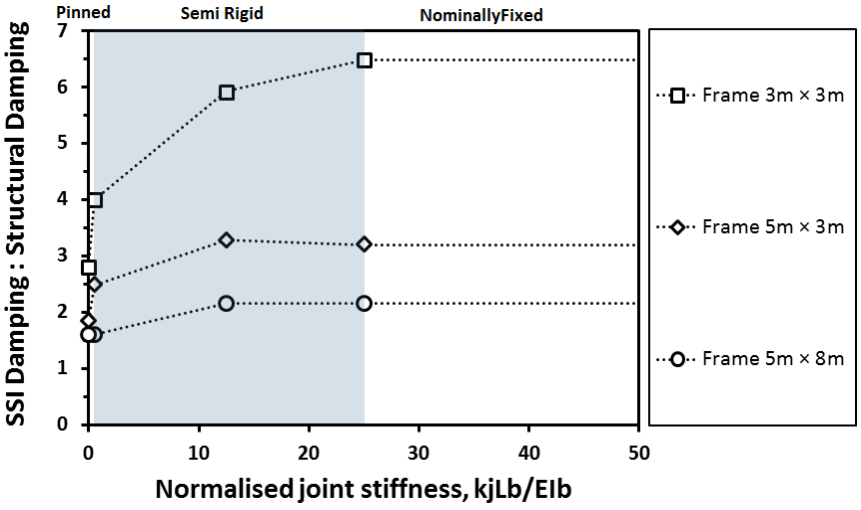

Figure 4.28: Joint stiffness and geometry affecting equivalent (SSI) damping

Normalising the equivalent system damping by the structure-only damping and comparing the result across the range of joint stiffness, as presented in Figure 4.28, shows that as the rigidity of the frame increases, with both geometry and joint

stiffness, so too does the overall damping effect, with the most rigid frame (the 3m × 3m fixed frame) behaving with almost six times as much equivalent damping compared to just the structural damping alone. A comparison of the equivalent damping using the new estimation method with the equivalent damping obtained from the FEM analyses is given in Figure 4.29 (a) and (b), showing a strong correlation between results.

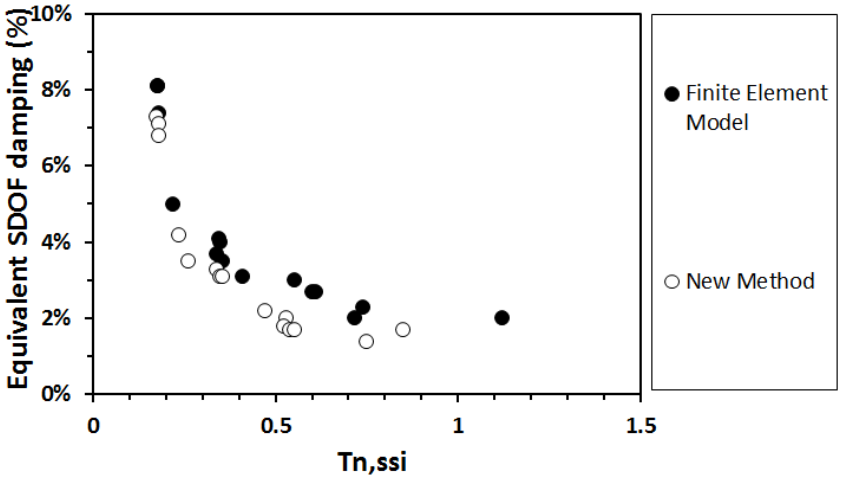

(a) Prediction and FEM damping for Tn,ssi value

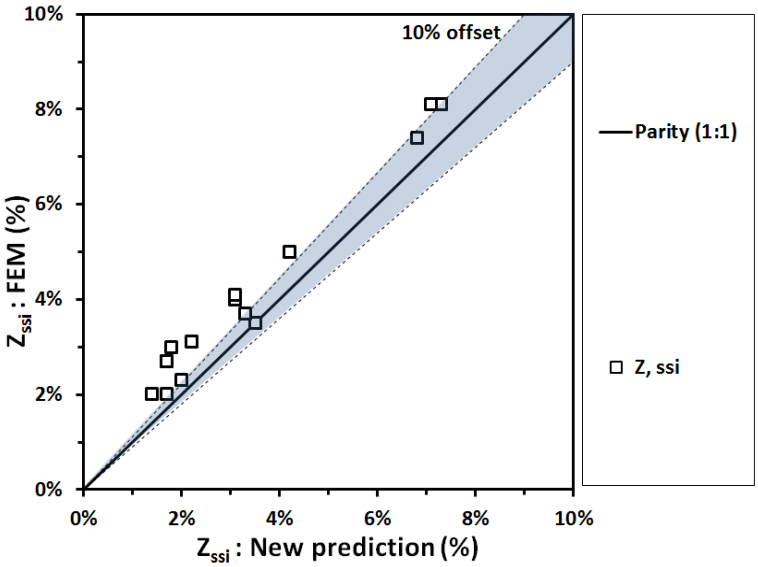

(b) Correlation between prediction and measured data.

Figure 4.29 (a) (b): Damping prediction

4.7.7 Predicting displacement response

Incorporating the joint system, structural flexibility and soil structure interaction of the system into the prediction of $T_{n,ssi}$ gives an enhanced indication of how the

structure will respond during a seismic event. Combining the new Tn,ssi estimation method with the Eurocode 8, (BSI, 2008b), method for predicting the elastic displacement response, sway, of the structure, S_{De}, as outlined in Section 2.2, Equation 2.6 produces the correlation, between predicted and measured response, shown in Figure 4.30 (a).

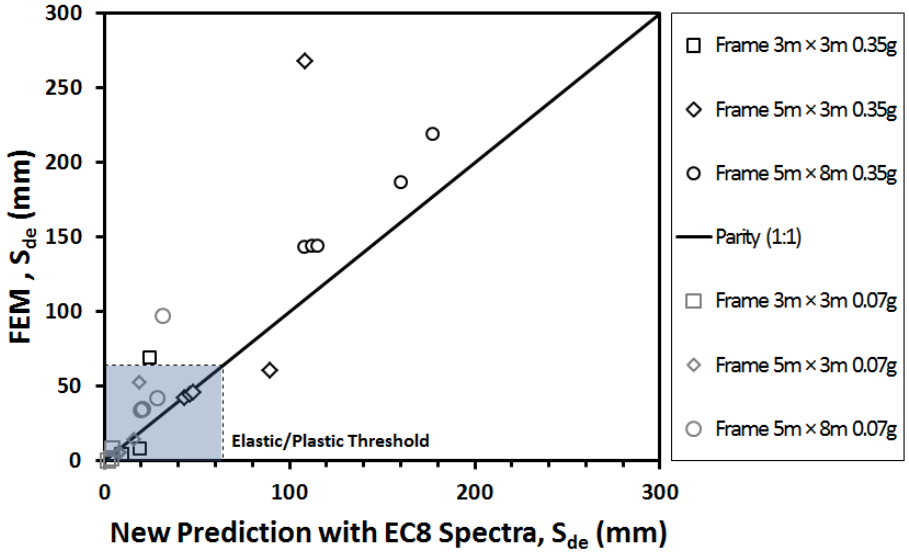

(a) SSI, S_{de}, prediction using EC8 Spectra

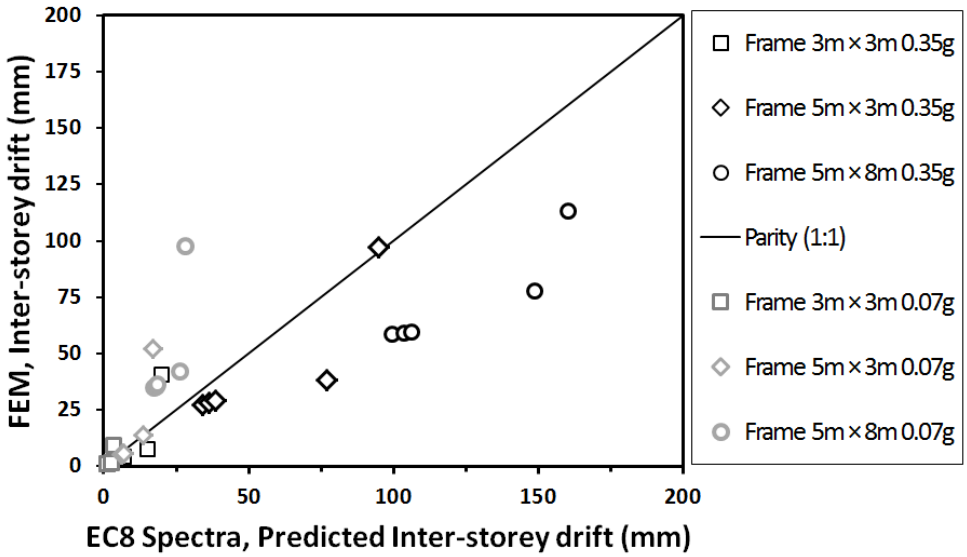

(b) SSI, inter-storey drift prediction (using EC8 Spectra S_{de} as base)

Figure 4.30 (a) (b): Newly predicted values for peak sway and peak drift using EC8 spectra for SSI structures.

Using the EC8 spectra method with the new predictions of $T_{n,ssi}$ and z_{ssi} gives a close prediction of the sway response of the structure. This close prediction, better than the fixed base prediction using EC8 spectra, is as a result of the measured elastic

displacement response from the FEM lying close to the line of the EC8 spectra for many of the frames, as seen in Figure 4.25. Those values that were under predicted correlate with the sections of the Kobe spectra that the EC8 spectra did not accurately replicate.

Figure 4.30 (b) presents a correlation between the inter-storey drift measured in the FEM analysis with a prediction of the inter-storey drift made based on the overall sway of the structure predicted in Figure 4.30 (a). This prediction is based on the principle of adding the effect of springs in sequence, with the spring stiffness provided by:

- the lateral stiffness of the structure as calculated for a fixed base frame from Equation 4.1 is the representative stiffness relating to the inter-storey drift component of the sway,
- the lateral stiffness of the structure as calculated from Equation 4.9 including the local rotational stiffness of the foundations represents the combined stiffness for the inter-storey drift and the local rotation components of the lateral drift (i.e. the effect of two representative lateral springs in series). Using this and the known stiffness for the inter-storey component (see above) the equivalent lateral stiffness relating to the local footing rotation component can be determined,
- the lateral stiffness relating to the displacement due to global rotation is given by $k_{f\theta}/H^2$

The overall lateral stiffness incorporating all three components can be determined by considering the three springs in series. The lateral displacement associated with any specific component is then found by multiplying the combined response, S_{De}, by the stiffness of the component in question, divided by the overall lateral stiffness. The accuracy of this prediction is therefore governed by the accuracy of the initial sway response prediction.

The inter-storey drift prediction assumes that a rotational response does occur, therefore in the 0.07g earthquake, where limited rotational response was observed, the prediction under predicts the inter-storey drift response in line with the under prediction of the equivalent sway response. However in cases where the earthquake is strong enough to induce a rotational response the prediction proves accurate for

frames which have global rotation as their primary rotational mechanism. In cases where local rotation is the primary rotational mechanism, all 5m × 8m frames, the prediction is not as accurate, instead it produces a conservative over prediction of the inter-storey drift response. A prediction was also made by using the actual Kobe spectra with the new predictions of $T_{n,ssi}$ and $z_{ssi,}$ as shown in Figure 4.31.

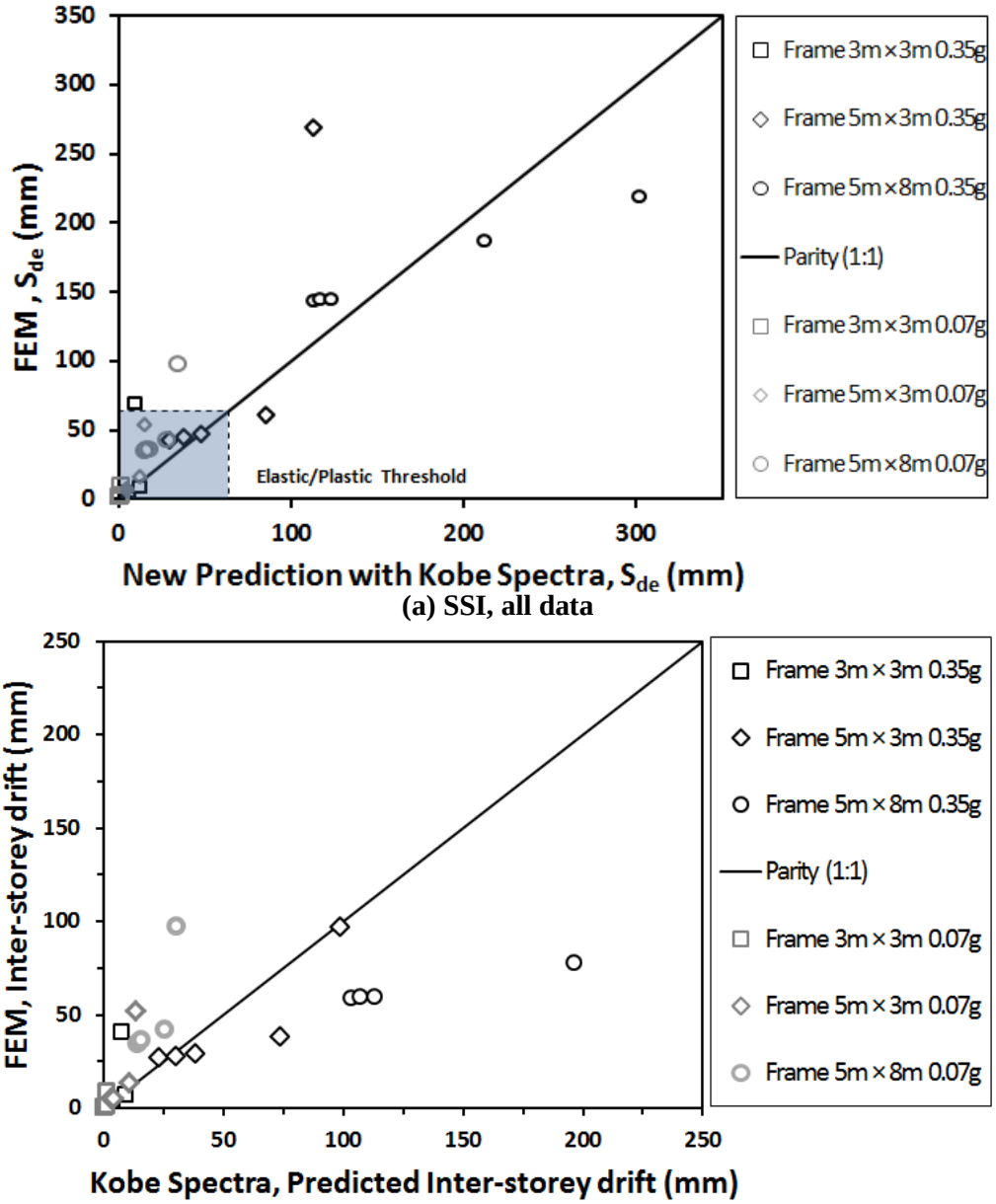

(a) SSI, all data

(b) SSI, elastic zone

Figure 4.31 (a) (b): Improved peak drift, S_{de}, prediction with F.E.M. data for SSI model

Even when an actual elastic displacement spectra from the given seismic motion is used an exact match cannot be guaranteed. The Kobe spectra used is generated from the free field data assuming the new structural damping of 1.25% and

while it is a reasonable fit for the data generated it is not an exact match. Obtaining an exact spectra for a future earthquake would not be possible and this comparison, between the EC8 spectra method prediction and the Kobe spectra method prediction, shows that even without an exact spectra, Eurocode 8, (BSI, 2008b), can generate results similar to those obtained when a "close" spectral match is obtained. Again the accuracy of the inter-storey drift prediction is based on the accuracy of the sway response, with frames undergoing structural rotation more accurately being represented than those undergoing local rotational mechanisms. Obtaining an accurate natural period and damping value is important in obtaining an accurate sway, $S_{De,}$ response prediction and a direct effect of using these new, more accurate values is outlined in Section 4.7.8.

4.7.8 Effect of frame rigidity and SSI effects compared to traditional analysis

The new estimation method, which included advances in predicting the fundamental period of the structure and of the entire system, has been proven to give a good prediction of the actual seismic response of the different structural frames. The changes as a result of using this new prediction method compared to the traditional prediction method for maximum sway, $S_{De,}$, is shown in Figure 4.32. The traditional method, based on the Eurocode 8 spectra method of prediction using the basic natural period prediction method, was unable to fully incorporate the flexibility of the system brought about by changes within the geometry, jointing and foundation aspects of the system, and hence results in under-prediction compared to the new prediction method, which used the new advanced method of predicting the natural period, which has been shown in Section 4.7.5 to produce a close correlation with the FEM results.

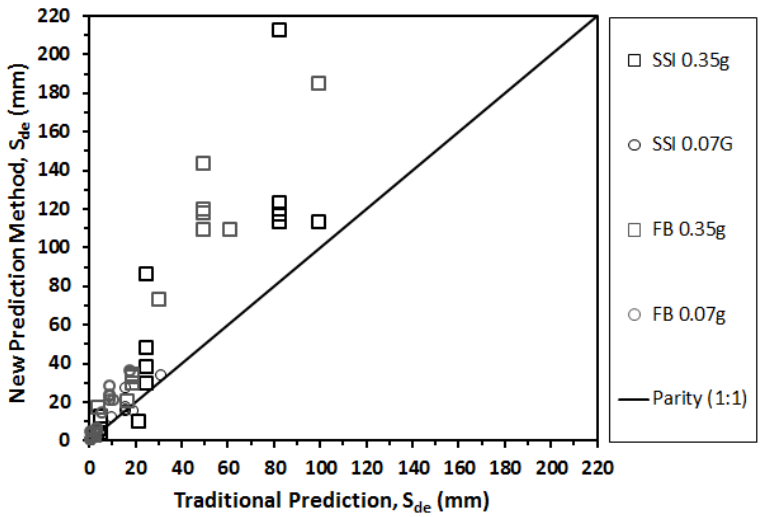

Figure 4.32: Improvement to the sway prediction method

In the case of the fixed base frames this sway value prediction will be the same as the inter-storey drift prediction. However for frames with SSI, which undergo additional rotational response mechanisms, it was shown to be possible to obtain a estimate of the actual inter-storey drift experienced within the columns of the frame. Figure 4.33 compares this new prediction of inter-storey drift with the traditional method (which would have assumed that inter-storey drift and sway response were the same), this shows that the traditional method under predicts the inter-storey response compared to the new method prediction which was shown to be accurate for most frames.

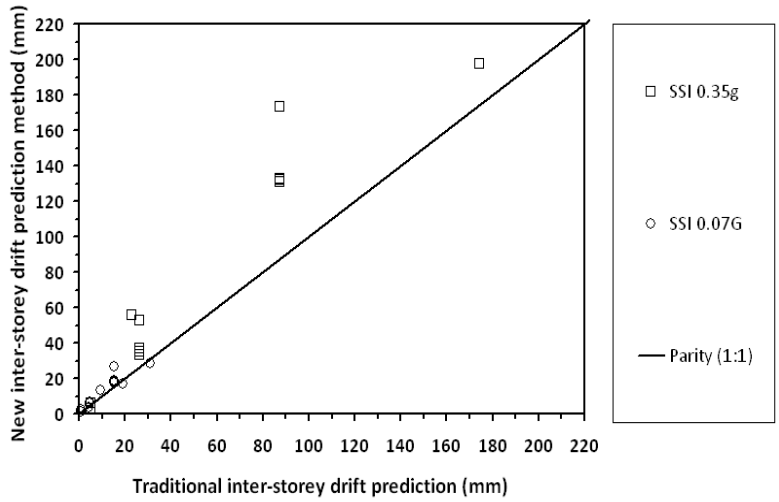

Figure 4.33 Improvement to the inter-storey drift prediction method

4.8 Summary

In this chapter the FEM results were presented and discussed to highlight the changes in structural response due to changes in frame geometry, joint stiffness and the foundations (fixed base or compliant base). It was shown that:

- Increasing the flexibility of the system, either by increasing the height or length of a structural frame, by reducing the joint stiffness or by introducing a compliant base as opposed to a fixed base, will increase the overall response (sway) of the structure. This increase in response falls in line with the increase in natural period of the system.
- While the overall response of the frame, sway, increases with flexibility, the introduction of soil to the system will also introduce new mechanisms of damping and energy dissipation. These new mechanisms will act to protect the structural elements of the frame by reducing inter-storey drift. These additional mechanisms are:
    - A global structural rotation mechanism, whereby the full structure rocks on its foundations. The magnitude of rotation is heavily dependent on the geometry of the system, with joint flexibility having a minor effect except for structures optimised for global rotation (i.e. frames/bays which are tall compared to their width).
    - A local rotation mechanism, whereby the foundations themselves rock. In narrow/tall frames it produces rotations similar in magnitude to their global rotations. In wider frames, larger magnitudes of local rotation occur compared to the magnitude of global rotation, further increasing the reduction in the amount of sway attributed to inter-storey drift.
- The joint flexibility can influence the overall response, sway, of the frame. However the percentage influence of each of the mechanisms, global rotation, local rotation and inter-storey drift, on the sway response appears to be dependent on the geometry of the structure and not the joint stiffness.

A method for improving the prediction of the natural period of a structure, developed by Hellesland (2008), was outlined and validated against FEM results for a fixed base structure case. The predicted natural period was then combined with the

spectral analysis method outlined by Eurocode 8, (BSI, 2008a), in order to predict the structural response to a seismic event and results compared with the FEM simulation results.

The Hellesland (2008) method was expanded to allow for the inclusion of a compliant base with SSI considered. Again this method was validated against FEM results, showing a strong correlation with the FEM. This method also allows for an improved prediction of the equivalent damping of the SSI system. The natural period and damping were again used with the spectral analysis method to predict their response to a seismic event and the results compared to a FEM analysis.

Improved predictions of the natural period for both fixed base and SSI cases, an equivalent damping prediction for the SSI case, and improved predictions of the overall, sway, response for structures were obtained. A method of obtaining a prediction of the inter-storey drift, from the predicted sway response, for the SSI models was also presented.

In Chapter 6, this method will be further extended to be applicable to cases where the soil response is non-linear (rather than the linear elastic simplifications used in the validation in this chapter) and also allowing spectral prediction of settlement.

Chapter 5

Centrifuge methodology

5.1 Introduction

This Chapter details the centrifuge model tests that were carried out on both independent and adjacent buildings on soil, subjected to seismic loading. This testing will be used to:

1. highlight the key aspects of SSI behaviour of low rise building structures, including their behaviour under multiple sequential strong earthquakes (e.g. an earthquake 'storm', or a mainshock followed by strong aftershocks),
2. act as a validation dataset for the response spectra model which includes the effects of real non-linear soil and extends the model to also include a spectral prediction of settlement.
3. investigate the limitations of SSI analysis (i.e. of isolated structures) when applied to adjacent structures (where the interaction may be better described as Structure-soil-structure interaction, SSSI).

This Chapter will outline the centrifuge modelling principles that were adhered to, the facility that was utilised, the modelling techniques required for the testing to be carried out and the method of analysis.

5.2 Centrifuge modelling principles

In order to accurately analyse the response of a physical soil-structure interaction model that is subjected to seismic loading, certain constraints must be taken into consideration. The large scale of the overall system that is being considered

necessitates that a scaled down version of the system is required for practical investigation. Analysing a scaled version of the structural elements of the system would give representative (scalable) results even under normal 1g analysis. However the mechanical properties of soil are strongly related to its stress state, therefore a reduced scale model of soil, analysed under 1g conditions, will not produce representative prototype stresses within the model. This is due to the reduced self weight of the soil sample. The additional gravitational load created within a geotechnical centrifuge overcomes this issue by recreating the same stresses within the small scale model as would be present at the corresponding point of the full scale prototype system. Modelling the soil at the required prototype density but to a depth equivalent to that of the prototype depth reduced by a factor of N, and increasing the gravitational load on the model by a factor of N will restore the stress field to the required representative state. This technique of geotechnical centrifuge modelling is well documented in various sources including Taylor (1995) and Muir Wood (2004).

As the physical parameters are reduced, in line with the increased gravitational loading applied, certain scaling laws must be obeyed. These laws are described in detail by Schofield (1980); Taylor (1995); Muir Wood (2004) and Stone *et al.* (2007) and a summary of the laws that are of particular interest in this study are presented in Table 5.1.

Parameter	***Model : Prototype***
Length	1 : N
Mass	1 : N^3
Density	1 : 1
Stiffness	1 : 1
Force	1 : N^2
Stress	1 : 1
Strain	1 : 1
Dynamic time	1 : N
Acceleration	1 : N^{-1}
Velocity	1 : 1
Displacement	1 : N
Frequency	1 : N^{-1}

Table 5.1 Scaling laws for dynamic centrifuge modelling, after Taylor (1995)

5.3 Centrifuge facility

All of the experiments were carried out in the centrifuge facility at the University of Dundee. A brief introduction to the facility will be presented here; a more detailed description can be found in Davies *et al.* (2001) and Muir Wood (2004). The facility contains a type C67, 3.5 m radius, computer-controlled beam centrifuge manufactured by Actidyn Systems, Figure 5.1. A beam centrifuge is balanced on a central spindle. A gondola, which contains the model, has a working radius of 3.5m and is located at one end of the centrifuge arm. During operation the gondola swings upwards into position as the centrifuge gains speed and the resultant acceleration acts normal to the base of the gondola. By 10g the model is in a position whereby the additional gravitational loading provided by the centrifuge acts close to radial. The centrifuge arm is balanced by a counterweight at the opposite end to the gondola. The distance between the counterweight and the spindle is adjustable, enabling accurate balance to be achieved dependant on the mass of the model and actuator under test.

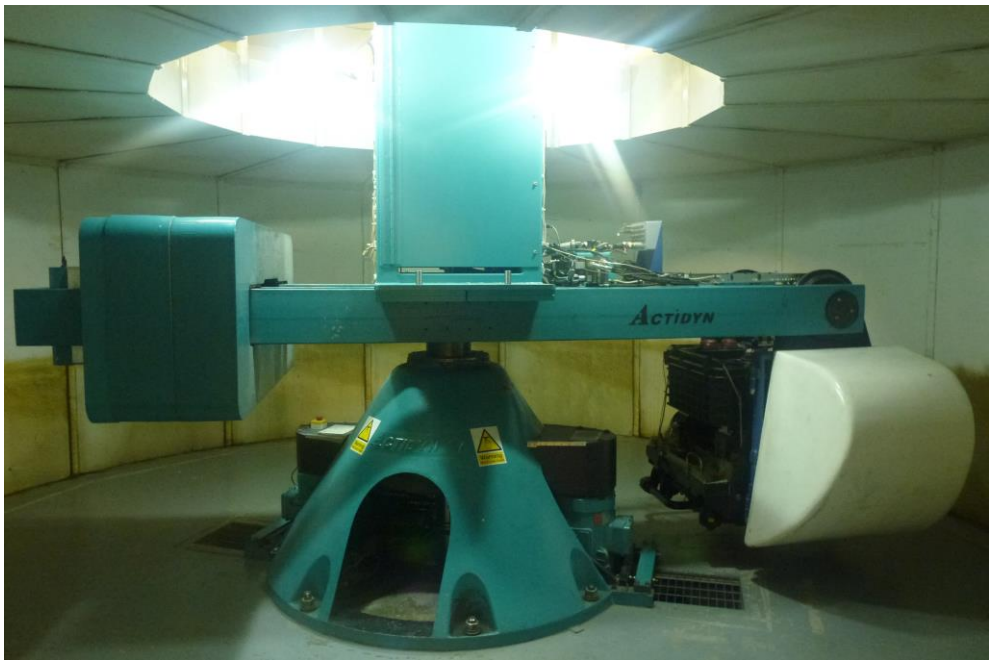

Figure 5.1 Centrifuge facility at University of Dundee

In its original state (with a standard gondola attached) the centrifuge is capable of supporting a 1 tonne payload, with a maximum dimension of 1m length, 0.8m width and 0.8m height. In this configuration the centrifuge is capable of a maximum centripetal acceleration of 130g. Due to the addition of the earthquake simulator (EQS), which is built into a second gondola, the maximum operational capabilities are reduced (currently) to 80g. The overall size and weight of the simulator constrains the

space and weight tolerance available within this gondola. With this addition the maximum dimensions available for the model is 0.8m length, 0.4m width and 0.6m height, with a maximum allowable mass of 400kg.

The EQS (described in more detail in Section 5.4.1) has some internal instrumentation for measuring the response of the servo-hydraulic actuators and the X-Y-Z accelerations of the shaking table; however, the centrifuge is additionally equipped with a 64 channel high speed data acquisition system. This allows for additional instruments to be employed within the model during the test; these instruments are further discussed in Section 5.7. An onboard PC logs and stores this data which can be accessed remotely from the control room, for monitoring purposes during flight, via a fibre optic data transfer slip ring.

5.4 Model earthquakes

5.4.1 Servo-hydraulic earthquake simulator (EQS)

The addition of the Actidyn EQS (model Q67-2) to the centrifuge gondola allows for historic earthquakes and other dynamic ground motions to be simulated and applied to the model in flight. A visual representation of the simulator attached to the centrifuge gondola is shown in Figure 5.2. The simulator utilises a dynamic balancing principle, as outlined in Actidyn (2008), which enables it to accurately reproduce both sinusoidal and real earthquake time histories without transmitting potentially damaging vibrations to the other centrifuge components.

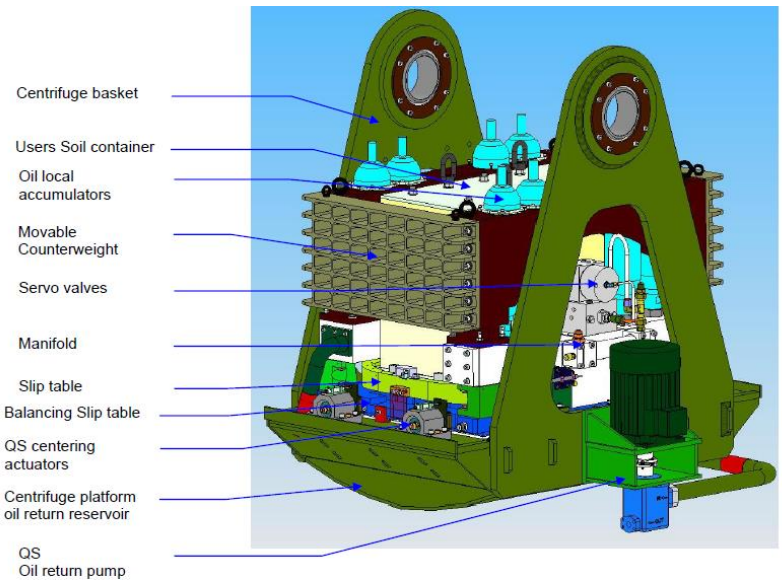

Figure 5.2: Actidyn EQS model Q67-2 on centrifuge gondola Actidyn (2008)

The dynamic balancing principle works by simultaneously and automatically actuating both the model and a pair of movable counterweights, Figure 5.3, in opposite directions such that the net dynamic inertia forces are cancelled-out. Two parallel servo-hydraulic actuators, governed by independent acceleration loop controllers, simultaneously actuate the slip table, along the length of the model, through hydrostatic bearings that provide friction free movement. The actuators are controlled by a programmable logic controller (PLC) with feedback control, which ensures that motions are uniaxial, with very small parasitic movements in the out-of-plane directions.

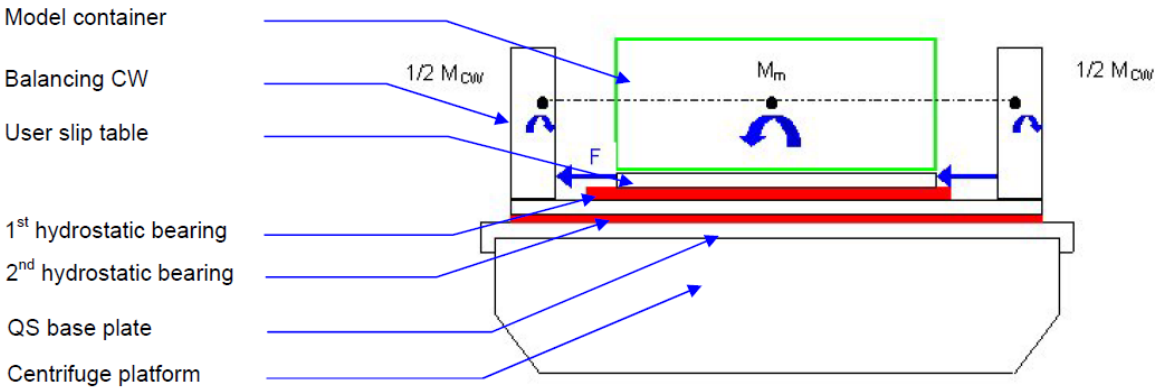

Figure 5.3: Actidyn Earthquake simulator– dynamic balancing principle (Actidyn, 2008)

The limitations of the simulated motions that can be reproduced by the EQS are outlined in Table 5.2.

Shaker capabilities		***Unit***
Controllable frequency range	40 to 300	Hz
Max Acceleration Peak	40	g
Max Velocity Peak	0.75	m/s
Max Displacement Peak	2.5	mm

Table 5.2 EQS limiting operational envelope (properties given at model scale)

While the EQS does have some limitations, the range of frequencies and complexity of earthquake time history it can accurately replicate are vast, and more than adequate for the purpose of this research. In order to accurately and repeatably reproduce the required time history a calibration learning stage is required; this is further discussed in Section 5.4.2.

5.4.2 Replication of Kobe (Takatori station) input motion

The same earthquake time histories that were utilised for the finite element modelling, in Chapters 3 and 4, are used in the centrifuge testing. The time history of the 1995 Kobe event (Takatori station) was obtained and filtered as outlined in Chapter 3.

In order to replicate this motion within the model the simulator must first undergo a calibration test. During this test a model was created having the same mass and geometry as the one that was to be tested (i.e. the model container was filled with soil to the test density). The model was first brought to the required g level – all testing reported in this Chapter was conducted at 50g. Once the calibration commences the control software initially generates sixteen white noise motions and applies them to the model. This information is used to determine the system dynamics (via transfer functions between the input control signals and the resulting table motion).

The earthquake time history to be replicated is then checked to ensure that it complies with the limitations of the shaker, given in Table 5.2, before it is triggered. The EQS has a built in learning facility which enables it to analyse past attempts, learn from the results and correct for the errors during future attempts; this facility is activated during the calibration test. A scaled-down version of the earthquake (-20dB) is initially applied to the model during the calibration phase. Once an adequate replication is achieved through repeating the event, the motion is increased in magnitude in stages of 2-3dB, with repeated motions at each stage until, finally, the motion can be simulated at 0dB scaling (actual size) with small (< 1%) RMS errors compared to the demand motion. Once a sufficiently accurate version of the earthquake has been produced, (Figure 5.4), it is saved and this input is used directly for all future tests.

The great benefits of the EQS are its accuracy and repeatability. The earthquake motion that enters the model is a very close representation of the original demand motion that was input to the system. The accuracy is demonstrated in both the time domain and the frequency domain in Figure 5.4 (a) and (b). While some additional peak acceleration values are present in the replication, Figure 5.4 (b), the majority of the time domain follows closely that of the original earthquake, Figure 5.4 (a). These additional peak accelerations make the large earthquake a 0.46g and the small earthquake a 0.1g seismic event, which is how they will be referred to henceforth. The

frequency response characteristics match well in terms of the dominant range of frequencies

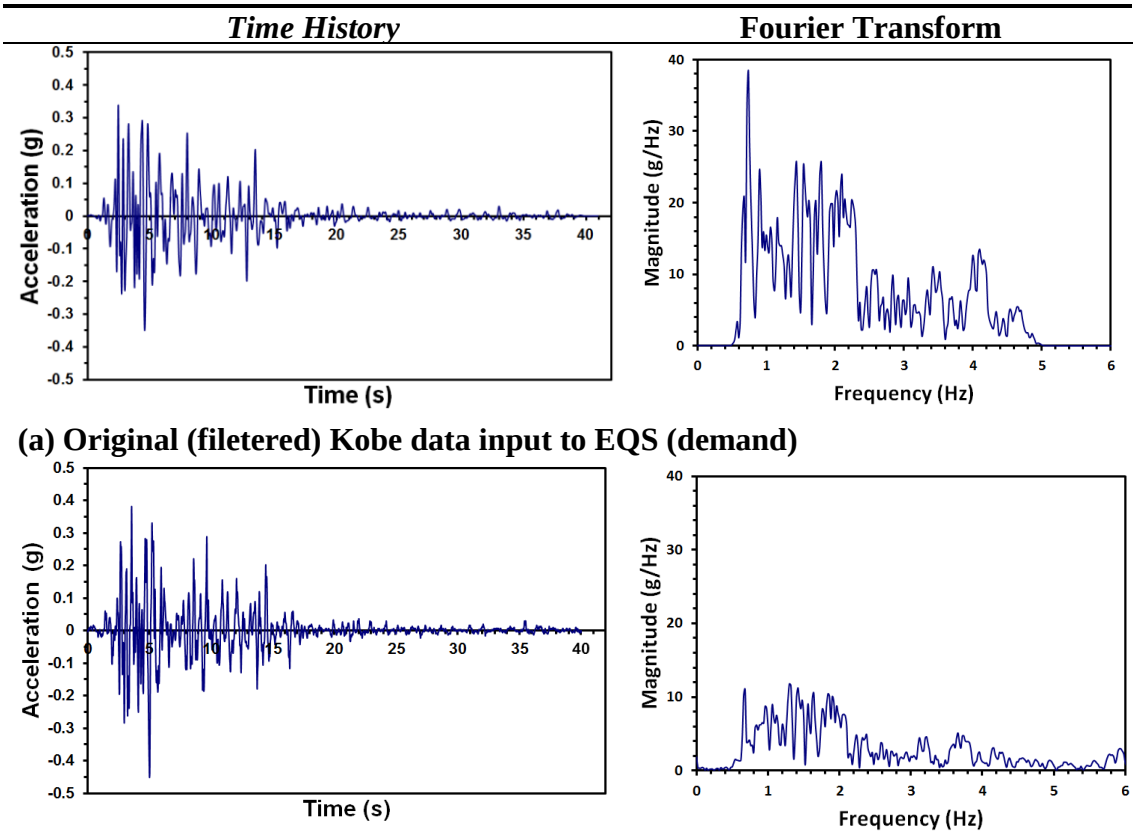

Figure 5.4 Replication of Kobe motion using EQS

The acceleration spectra, obtained from the motion input to the system at the base of the soil (considering a nominal 5% structural damping), for all 16 earthquakes applied to the independent structure tests, (PM001 – PM004), is highlighted in Figure 5.5.

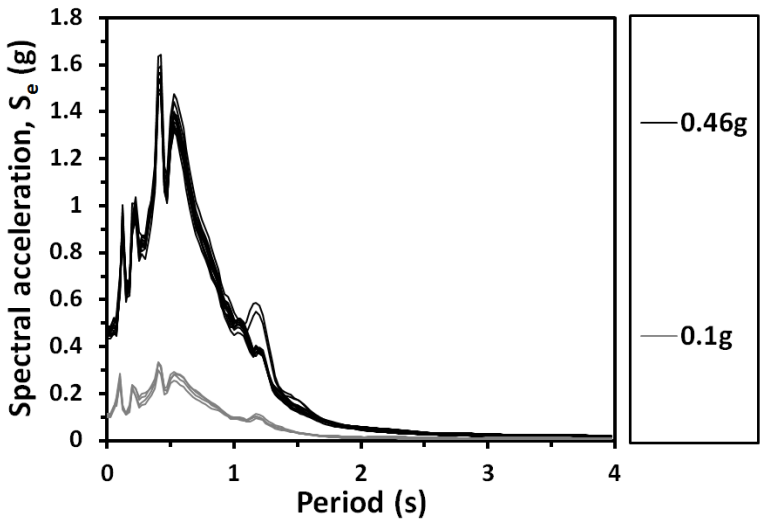

Figure 5.5 Acceleration spectra for 16 earthquakes in tests PM001 – PM004 plotted for 5% structural damping

The consistency between each of the individual acceleration spectras, for both the 0.1g and 0.46g earthquakes highlights the ability of the system to reproduce the same earthquake, to a high level of accuracy and on demand.

5.5 Modelling the ground

5.5.1 Model container (ESB)

As stated previously in Section 5.2, one of the main purposes of the centrifuge testing is to accurately model the stresses that build up within the soil. One of the main obstacles with centrifuge modelling for seismic events is that of boundary effects being introduced to the model via the interaction between the moving soil and the container within which it is held. The base shaking of the container during the simulation will cause vertically propagating shear waves within the soil. In the presence of a rigid boundary these S-waves would interact with the boundary resulting in a P-wave reflection back into the model (Zeng *et al.*, 1996). A similar problem was highlighted within the earlier finite element (FE) analysis part of this research (Chapter 3). Within the FE analysis it was possible to increase the field of soil so that these effects did not interfere with the model, Section 3.7. Due to space limitations of the centrifuge this is not possible. Instead, an alternative solution, namely a flexible container, was used.

An Equivalent Shear Beam (ESB) box, was designed at University of Dundee by Bertalot (2013), in order to overcome the boundary effect issue. This box proved suitable for the work within the scope of this research and the design of this system will be summarised here; it is outlined in more detail in Bertalot (2013).

The ESB container has flexible walls made up of a stack of alternating machined aluminium rings and rubber interlayers. The rubber interlayers provide the flexibility to the system. The thickness and flexibility of the rubber layers, and the mass of the aluminium rings are designed so that the container dynamic properties model those of a column of soil at a specific density and g-level, as highlighted in Table 5.3. The optimum performance of the container is achieved when the soil model and imparted motion exactly matches that which it was designed for. However even though the soil model used in this case is different from the design soil of the container, it will still mitigate boundary effects compared to a rigid wall container.

Parameter	
Soil:	
Max Soil Column Height	0.3348m
Unit Weight	22 kN/m³
Friction Angle (deg)	33º
K_0 Coefficient	0.44
Earthquake:	
Peak Acceleration Ratio	0.3g
g-level	50g

Table 5.3 ESB container model design parameters.

The ESB container, which is shown in Figure 5.6, has a plan size of 674.8mm × 280mm and a depth of 334mm and an overall mass of 65kg. These parameters control the maximum size and layout of the model that can be tested.

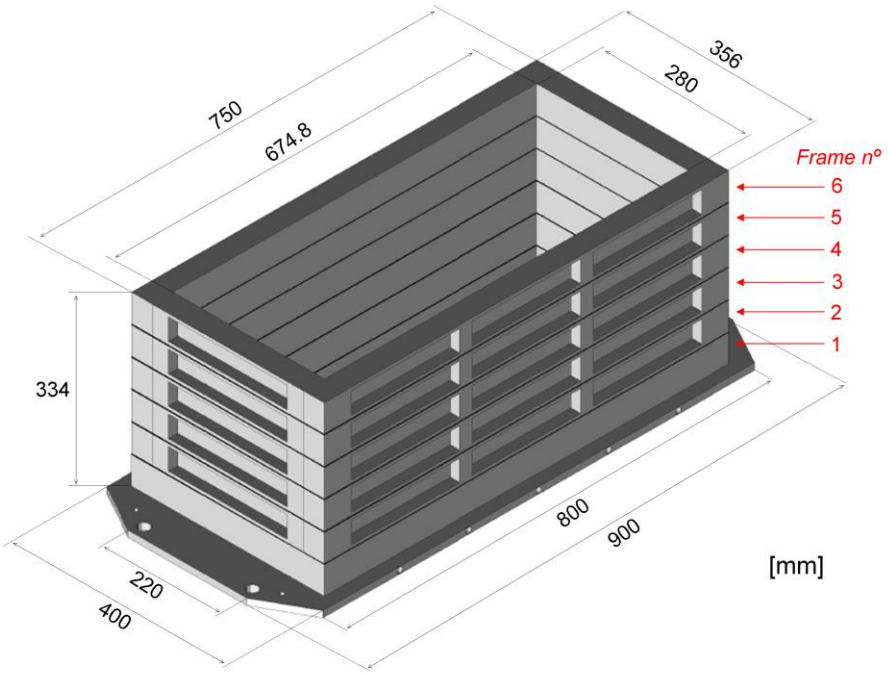

Figure 5.6 Equivalent shear beam box, (ESB), as designed by (Bertalot, 2013)

5.5.2 Soil properties and preparation

For this analysis sand, HST95 from Bent Farm in Congleton, Cheshire, is used to model the soil. This sand has undergone extensive analysis at the University of Dundee and is well classified, (Lauder, 2010). The main properties of this sand are presented in Table 5.4.

Property	*Value*
$Ø_{crit}$	32°
D_{10}	0.10mm
D_{30}	0.12mm
e_{max}	0.769mm
e_{min}	0.467mm
G_s	2.63
Shape	Rounded

Table 5.4: Properties of HST95 sand, (Lauder, 2010)

The sand is uniformly graded and has a particle size distribution curve as outlined in Figure 5.7. The data used to produce the curve in Figure 5.7 was taken from CDS (2006) analysis of the soil, an identical curve is produced from independent analysis by Lauder (2010).

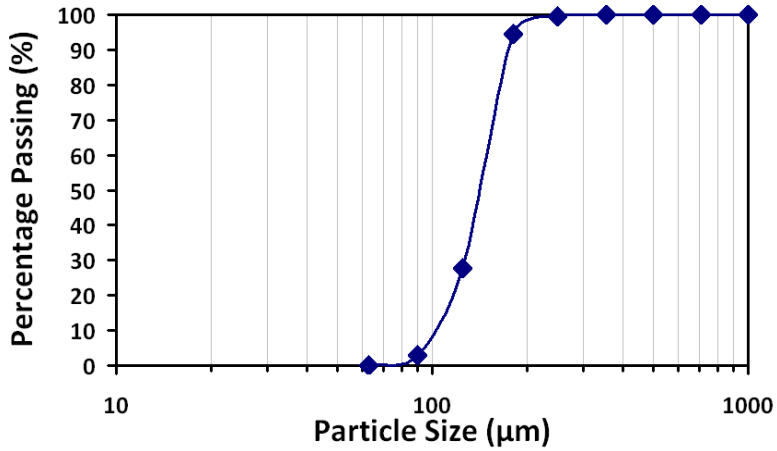

Figure 5.7 Particle size distribution of HST95 sand after CDS (2006)

The sand is prepared to have a relative density of 55-60%, producing a medium dense sand layer 200mm deep. This represents a 10m deep deposit of soil at prototype scale. The sand model is built up by air pluviating from an overhead slot pluviator. The relative density of the sand resulting from this method of pluviation is directly related to the width of the slot in the base of the hopper and the corresponding flow rate of the sand, as outlined by Lauder (2010). The accuracy of the density achieved in the centrifuge models was found to vary by no more than +2.5% and -1.9% around an average value of 58%, as shown in Table 5.5.

Analysis Ref:	*Density (kg/m³)*	*Relative Density (%)*
PM001	1655	60.4
PM002	1653	60.5
PM003	1735	57.7
PM004	1706	58.6
PM005	1767	56.6
PM006	1727	57.9
PM007	1759	56.9
PM008	1732	57.7
PM009	1703	58.7
PM010	1769	56.5
PM011	1782	56.1

Table 5.5: Relative Density of sand model in each analysis

While a dry medium dense sand is not necessarily the most common soil strata found in the field, it does have certain characteristics that make it more suitable for this analysis than other soil types. As multiple models are to be analysed a certain level of repeatability needs to be obtained; the use of a dry homogenous sand strata makes it possible to recreate the same soil model multiple times and to a high accuracy. It also isolates the behaviour of SSI and SSSI without including interference from other mechanisms such as liquefaction.

5.6 Modelling the structure(s)

5.6.1 Selection of representative structural models

As the aim of this thesis is partially to investigate how structural design decisions affect seismic performance, it was decided to model two different structural models in the centrifuge testing. This allowed for both similar and dissimilar structural combinations to be investigated in the case of the adjacent buildings. Each structure was a one-storey one-bay sway frame, similar to those designed for the finite element analysis in Chapter 3, founded on strip foundations. The first structure had a shorter natural period and a lower centre of mass, representing the fundamental characteristics of a short 2 storey building, while the second was taller, with a longer natural period, representing a 5 storey building. Two models of each structural type were constructed. The structures were not tested to structural failure (they were

designed to remain as elastic oscillators); therefore four structures were sufficient to satisfy the requirements of this research.

The strip foundations were made from mild steel, aluminium-alloy (6063-T6) plates were used to model the equivalent SDOF stiffness of the frame and a set of mild steel plates were used to model the lumped mass at the top of the structures allowing for the mass to be varied (though this feature was not used in the testing reported herein).

5.6.2 Short period structure

The short period structure was designed to represent a two storey frame structure or an equivalent SDOF system. The required fundamental period, T_n, of the structure was calculated based on the height of the structure, as per Eurocode 8 Clause 4.3.3.2.2., (BSI, 2008b), for buildings with heights of up to 40m, where the natural period can be approximated by Equation 5.1.

	Model	***Prototype***
No. of Storey	1 (equivalent SDOF)	2
Height of Structure	N/A	6m
Height of centre of mass	0.06m	3m
Natural period	0.0065s	0.33s
Structural damping	5%	5%
Foundation:		
Type	2 No. Strip Foundations	
Width, B	0.04m	2m
Length, L	0.1m	5m
Mass/foundation	0.374kg	46.80t
Slab:		
Mass	1.88kg	234.64t
Plan area	0.1m × 0.1m	5m × 5m
Thickness	0.024m	1.2m
Columns:		
Total lateral sway stiffness	1.7447 MN/m	87.235 MN/m
Thickness of sheet per column	3mm	N/A
Bearing Pressure	161kPa	

Table 5.6: Structural properties of the short period structure

$$T_n = C_t \times H^{3/4} \qquad \textbf{Equation 5.1}$$

Where C_t is 0.085 for moment resisting steel frames and H is the height of the structure from the top of the foundation. The structural elements of the model, the thickness of the aluminium sheets for the columns and the mass required, were then designed to produce a structure matching that natural period by utilising Equation 2.7 from Chapter 2.

The structural parameters of the short structure, for both model and prototype scale are highlighted in Table 5.6. The column elements of the structure are rigidly fixed using epoxy resin into custom-machined grooves in both the foundation and slab elements creating fixed joints. The additional plates of steel that make up the total mass for the slab are bolted on top, as shown in Figures 5.8 and 5.9.

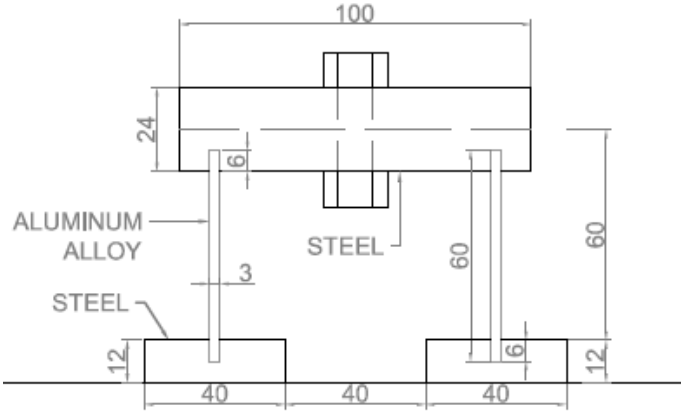

Figure 5.8 Structural elevation of short period structure (dimensions in mm at model scale)

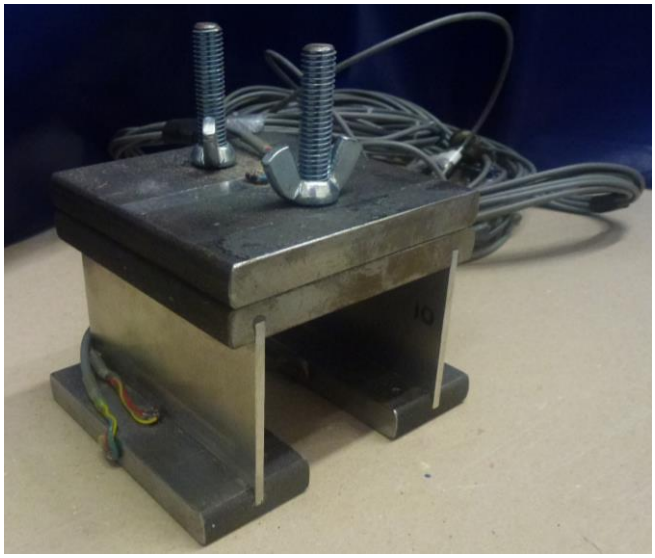

Figure 5.9: Short period structure, showing attached accelerometers

5.6.3 Long period structure

The long period structure was designed to represent the basic characteristics of a five storey frame structure. The overall width of the frame was kept the same as for the short period structure; therefore this represents a structure with a much larger aspect ratio (H/L_b), where rocking effects are likely to be more dominant. The structural parameters of this structure, in both model and prototype scale are highlighted in Table 5.7. The long period structure follows the same design procedure and assembly method as the short period structure, outlined in Section 5.6.2, and detailed in Figures 5.10 and 5.11

	Model Scale	***Prototype Scale***
No. of Storey	1 (equivalent SDOF)	5
Height of Structure	N/A	15m
Height of centre of mass	0.15m	7.5m
Fundamental period	0.013s	0.65s
Structural damping	5%	5%
Foundation:		
Type	2No. Strip Foundations	
Width, B	0.04m	2m
Length, H	0.1m	5m
Mass/foundation	0.374kg	46.80t
Slab:		
Mass	3.75kg	469.09t
Plan area	0.1m × 0.1m	5m × 5m
Thickness	0.048m	2.4m
Column:		
Total lateral sway stiffness	0.88 MN/m	44.12 MN/m
Thickness of sheet per column	6mm	N/A
Bearing Pressure	276kPa	

Table 5.7: Structural properties of long period structure

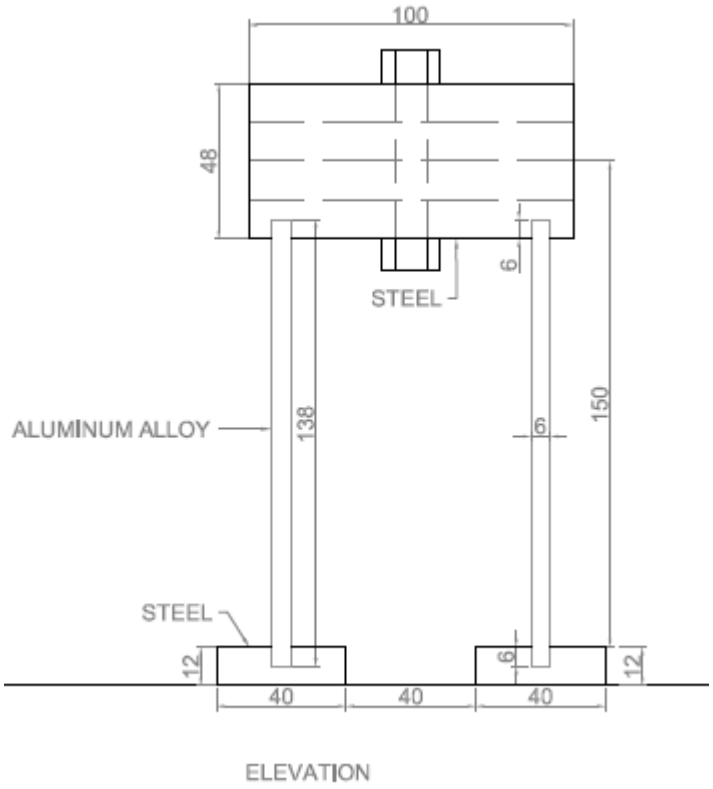

Figure 5.10: Structural elevation of long period structure (dimensions in mm at model scale)

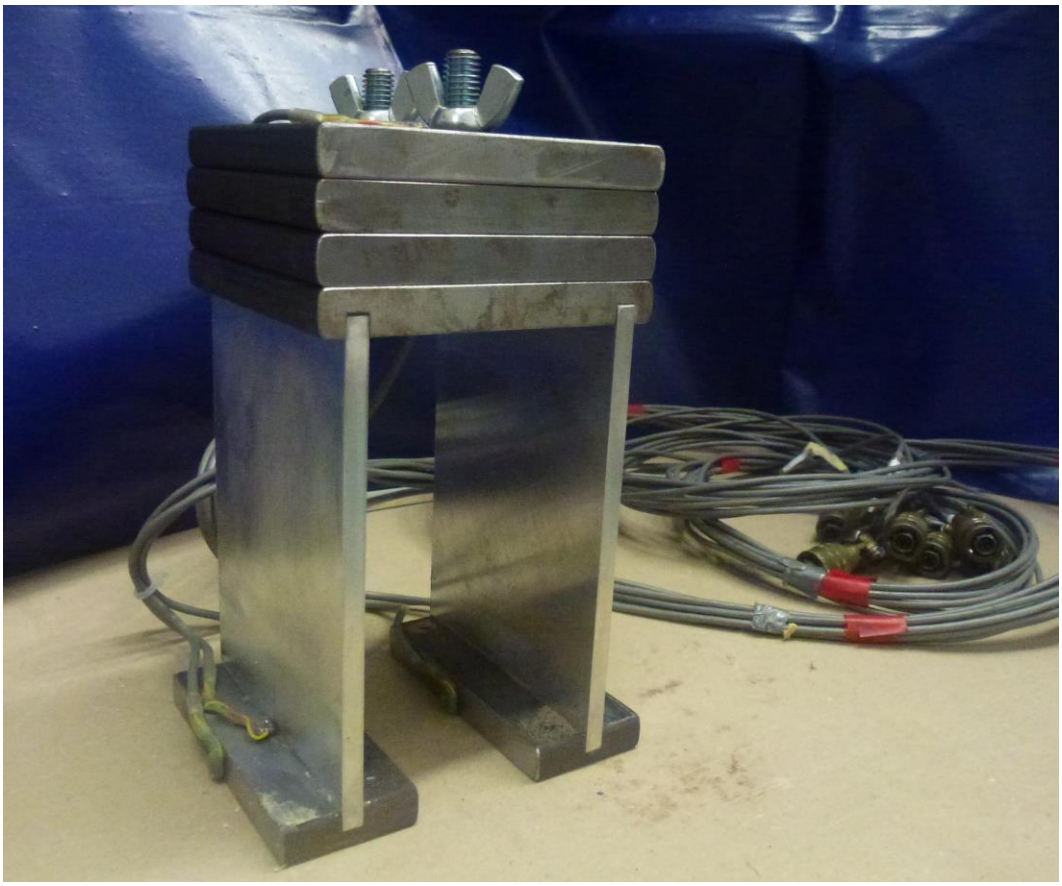

Figure 5.11: Long Period Structure

5.7 Instrumentation and data acquisition

For the purpose of this research it is imperative that the response of the structure and the soil can be recorded during the analysis. This analysis is taking place while the centrifuge is spinning at 128 revolutions per minute (RPM). The data acquisition system, along with the fibre optic slip ring cable system, allows a constant monitoring of the model to take place throughout the analysis. Additional instruments are required to be attached to and embedded within the model, these are highlighted in Sections 5.7.1 and 5.7.2.

5.7.1 Accelerometers

ADXL78 low power, single-axis, high-g accelerometers, manufactured by Analog Devices (model type AD22281-R2) were used to measure dynamic motions within the structure and soil during the tests, Figure5.12. The accelerometers can record accelerations of ±70g with a typical sensitivity of 27mV/g, (Analog Devices, 2010). The accelerometers were calibrated for sensitivity and assigned an individual calibration factor in order to ensure uniformity of readings across the range of accelerometers used. Their small size, plan 5mm × 5mm and depth 1.98mm, make them ideal for use on the structures as they can be easily positioned directly onto the frame without interfering with the behaviour of the structural elements. When used within the sand, their size ensures that they cause minimal disturbance to the soil continuum behaviour, however their size can also make them difficult to place, and remain, horizontal. To help overcome this, and also to ensure a good connection with the sand, a small PVC disk was applied to the top of the accelerometers being used in the sand. This disk was just big enough to help with placing and the accelerometer/sand interaction but was not of sufficient size or mass to interfere with the continuum behaviour of the soil.

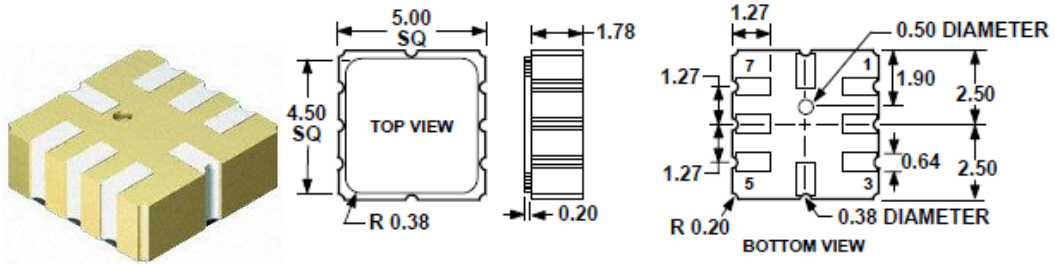

Figure 5.12: Dimensions (NTS) and layout of AD22281-R2 accelerometer (Analog Devices, 2010)

This data obtained from the accelerometers was subsequently processed by band-pass filtering in order to carefully remove parts of the signal that were not due to the applied shaking. This data was then integrated twice to obtain the displacements and the dynamic drift is calculated from the difference between the displacement in the mass and the displacement in the foundation at any given time step.

5.7.2 Linear Variable Differential Transformers [LVDT]

While accelerometers provide accurate data for the dynamic displacement of the structure, initial tests indicated that they were not suitable in providing information about the permanent settlement or rotation of the structures. In order to ensure accurate measurement of this settlement two Linear Variable Differential Transformers, LVDT's, were used per structure, which enabled both overall settlement and overall rotation (tilt) in the plane of shaking to be determined.

An LVDT is made up of a hollow cylinder static transformer through which a magnetic rod can pass. The outer transformer consists of one primary coil, connected to an AC supply, and two secondary coils, Figure 1.13. The magnetic rod provides a path for linking the primary coil with the secondary coils via a magnetic flux, thus the output from the secondary coils is directly linked to the position of the rod, see Figure 1.13. The LVDT's allow a displacement of up to 50mm to be accurately recorded.

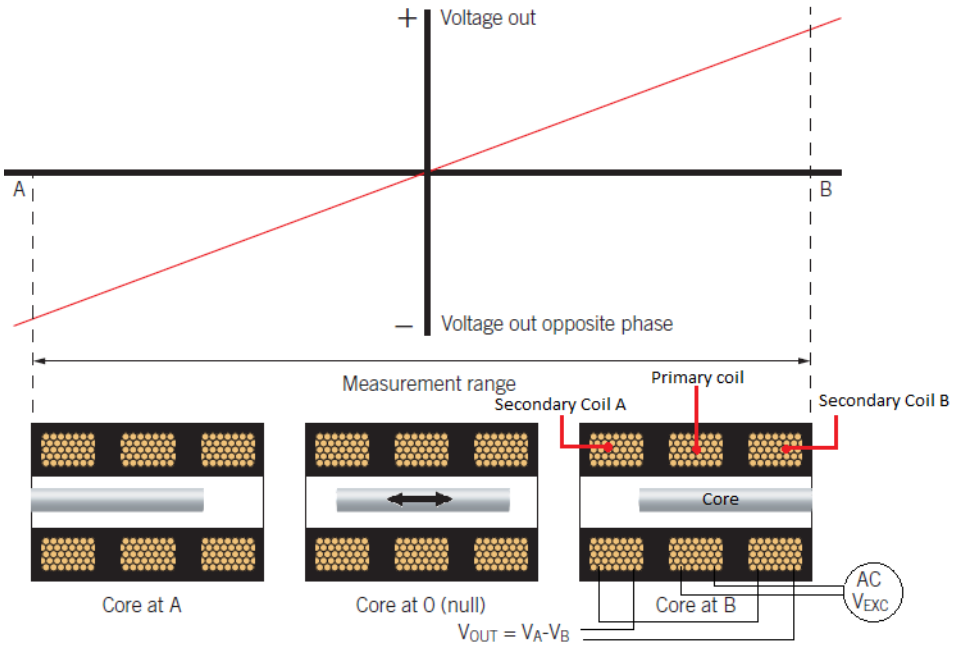

Figure 5.13 LVDT displacement transformer internal components and principle of operation after Solartron Metrology (2013)

The LVDT's monitored the vertical movement of both sides of the structures throughout the earthquake storm. A direct reading was taken from both LVDT's on each structure and filtered through a low pass filter in MATLAB in order to remove noise introduced by electrical interference. The readings were obtained in model scale and scaled up to prototype scale in post processing. Each LVDT gave the settlement of its corresponding footing on the structure and an average of these settlements gave the average structural settlement at a given time step.

The rotations of the structure were also obtained from this data. An inverse Sine calculation was carried out on the difference between the vertical movements of both foundations divided by the distance between the foundations. This was done at each recorded time step of the earthquake.

5.7.3 Data acquisition system

As mentioned previously a 64 channel high sampling frequency data acquisition system is built into the centrifuge facility. This system supplies the instruments with the relevant supply voltage and also collects and sends their output signals through the signal conditioning unit and on to the PC where they are stored.

LabView software was used to control, monitor and log the instruments, remotely from the centrifuge control room, during the tests. Once the model had reached 50g, LabView was used to trigger logging at a sample rate of 2kHz at model scale, equating to 40Hz at prototype scale. This results in 1600 data points being recorded over the course of the 40second earthquake, which is adequate to monitor the response to a high level of accuracy, given the low frequency input of the earthquake and low natural frequencies of the model structures. LabView recorded the data over a 10 second window. During this time the earthquake was triggered manually, such that pre- and post-earthquake data was also captured.

5.8 Testing programme

The test sequence and the structural combinations and layouts for each test are outlined in Table 5.8 and 5.9 and in Figures 5.14, 5.15 and 5.16. The first two analyses, PM001 and PM002 did not contain LVDT's to monitor the settlement and therefore the same structural set up was tested again in test PM003 and PM004 with the addition of LVDT's, and a slightly different earthquake sequence. Tests PM007

and PM010 suffered malfunctions of key instrumentation during the analysis and therefore were retested as PM008 and PM011 respectively.

Analysis ref:	*Layout*
PM001	Independent Short Model
PM002	Independent Tall Model
PM003	Independent Short Model
PM004	Independent Tall Model
PM005	Tall Model, Tall Model (2m spacing between)
PM006	Tall Model, Tall Model (1m spacing between)
[PM007	Short Model, Short Model (1m spacing between)]
PM008	Short Model, Short Model (1m spacing between)
PM009	Tall Model, Short Model (1m spacing between)
[PM010	Short Model, Tall Model (1m spacing between)]
PM011	Short Model, Tall Model (1m spacing between)

Table 5.8: Structural Layout of the models

Analysis	*Earthquake sequence*										
ref:	1	2	3	4	5	6	7	8	9	10	11
PM001	0.1g	0.46g	0.44g	0.44g							
PM002	0.1g	0.46g	0.47g	0.48g							
PM003	0.45g	0.45g	0.47g	0.1g							
PM004	0.47g	0.47g	0.48g	0.11g							
PM005	0.09g	0.46g	0.47g	0.49g	0.11g	0.45g	0.45g	0.47g	0.47g	0.46g	0.08g
PM006	0.09g	0.46g	0.49g	0.46g	0.09g	0.48g	0.47g	0.47g	0.46g	0.44g	0.1g
PM007	0.1g	0.46g	0.46g	0.49g	0.09g	0.47g	0.47g	0.46g	0.45g	0.46g	0.09g
PM008	0.1g	0.47g	0.46g	0.49g	0.09g	0.46g	0.43g	0.43g	0.45g	0.46g	0.09g
PM009	0.09g	0.43g	0.42g	0.44g	0.1g	0.48g	0.44g	0.44g	0.46g	0.42g	0.08g
PM010	0.1g	0.46g	0.47g	0.45g	0.09g	0.46g	0.48g	0.48g	0.46g	0.47g	0.1g
PM011	0.09g	0.43g	0.44g	0.46g	0.1g	0.48g	0.47g	0.47g	0.47g	0.43g	0.09g

Table 5.9 Earthquake sequence carried out for each test with measured acceleration input to base of model

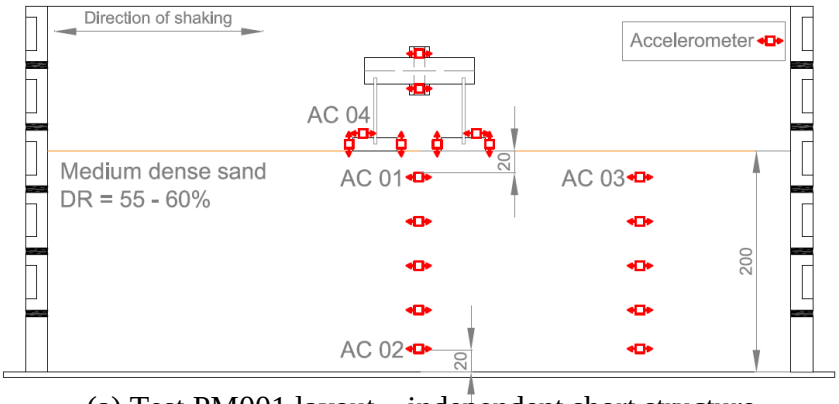

(a) Test PM001 layout – independent short structure

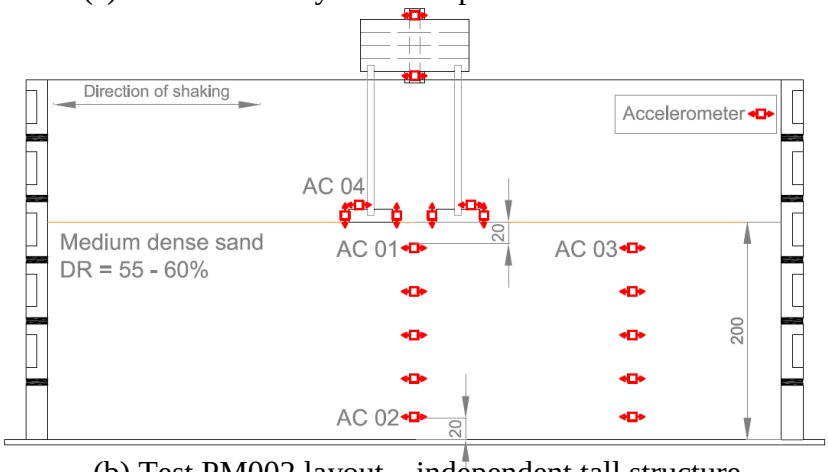

(b) Test PM002 layout – independent tall structure

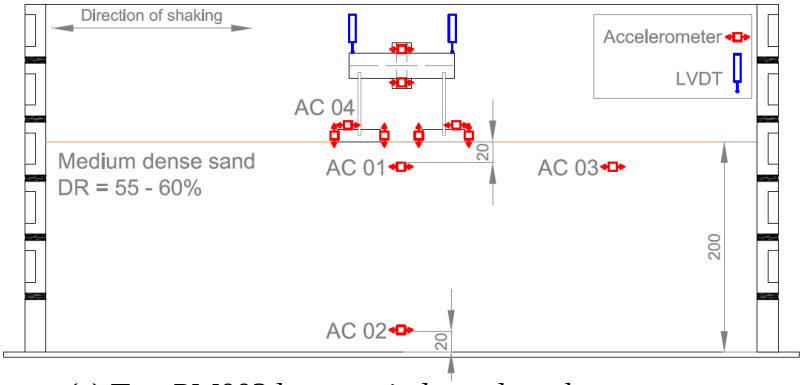

(c) Test PM003 layout – independent short structure

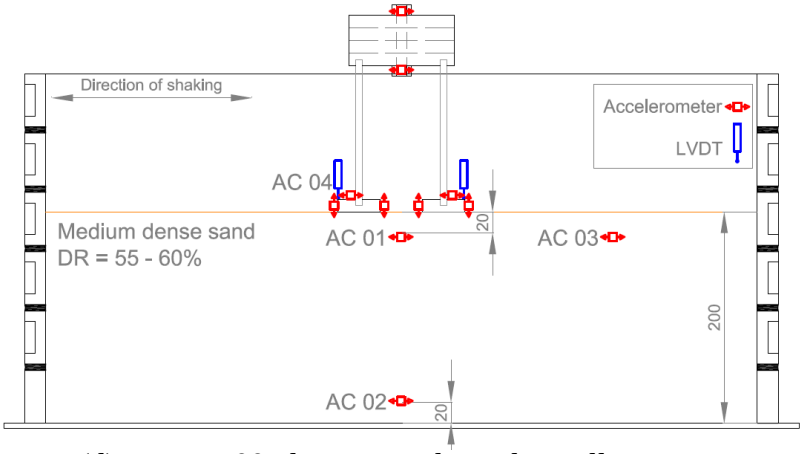

(d) Test PM004 layout – independent tall structure

Figure 5.14 Independent structure tests layout (PM001 – PM004)

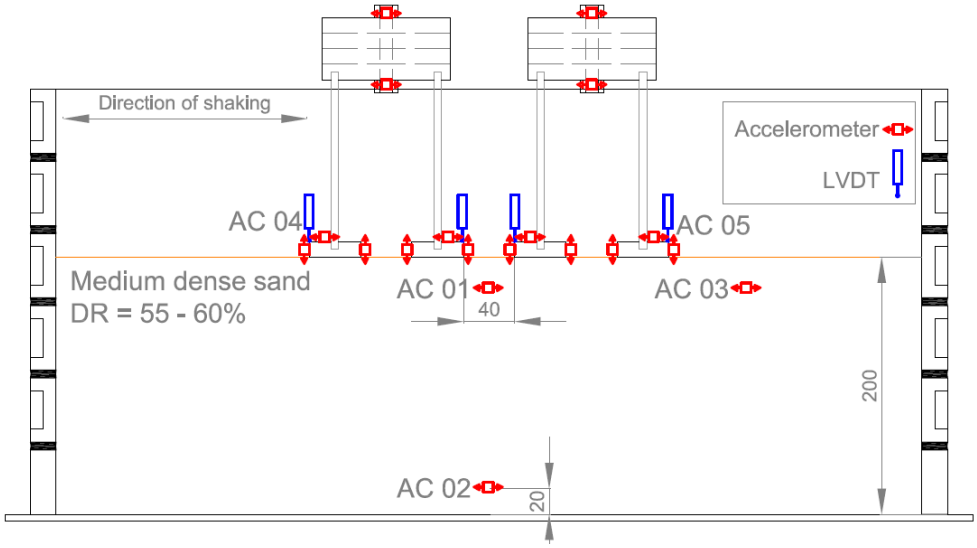

(a) Test PM005 layout – Adjacent tall structures 2m spacing

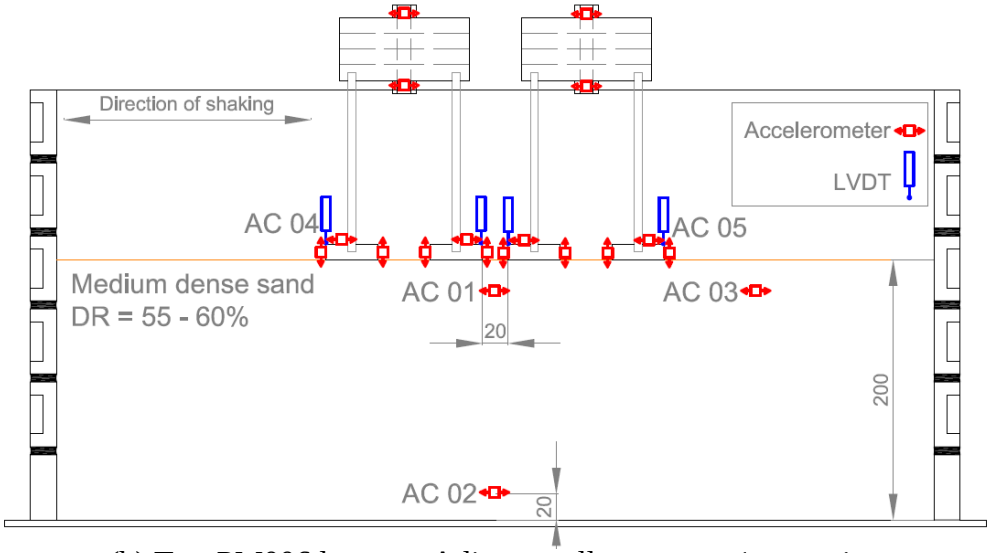

(b) Test PM006 layout – Adjacent tall structures 1m spacing

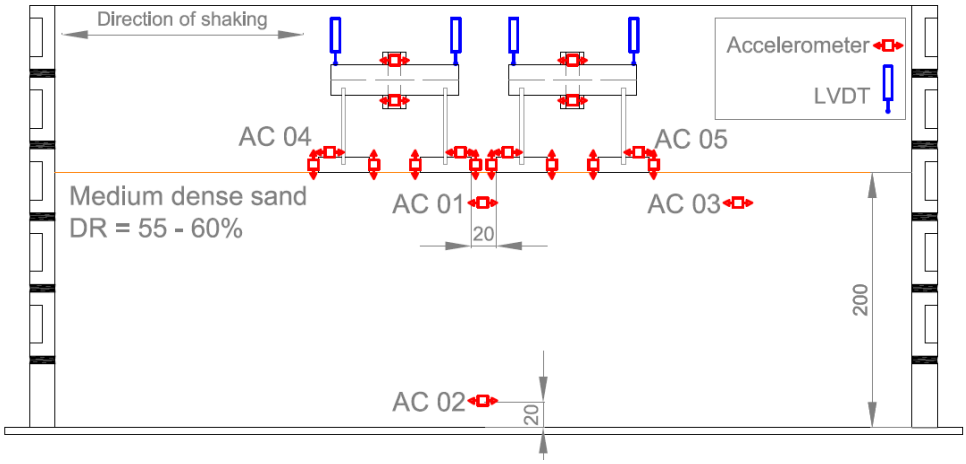

(c) Test PM007 & PM008 layout – Adjacent short structures 1m spacing

Figure 5.15 similar adjacent structures (PM005 – PM008)

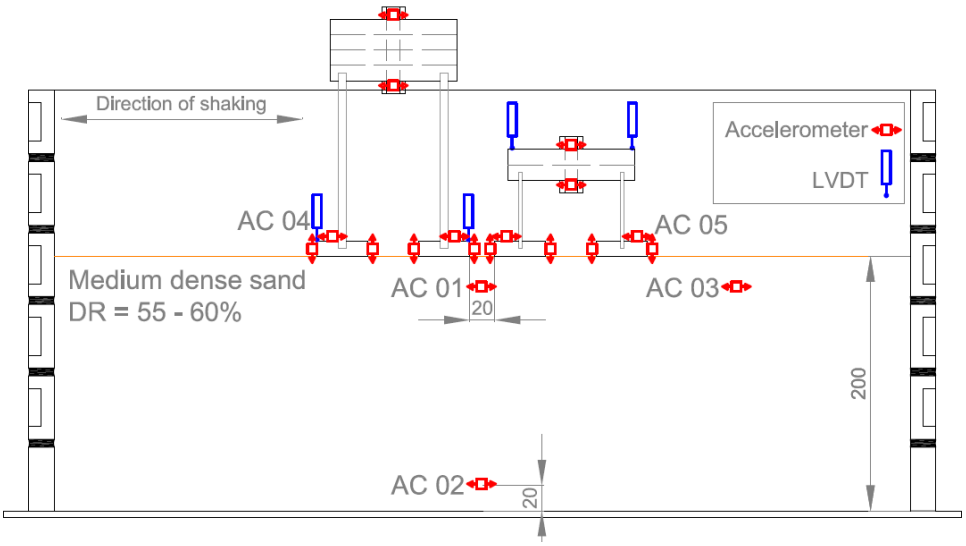

(a) Test PM009 layout – Adjacent tall and short structures 1m spacing

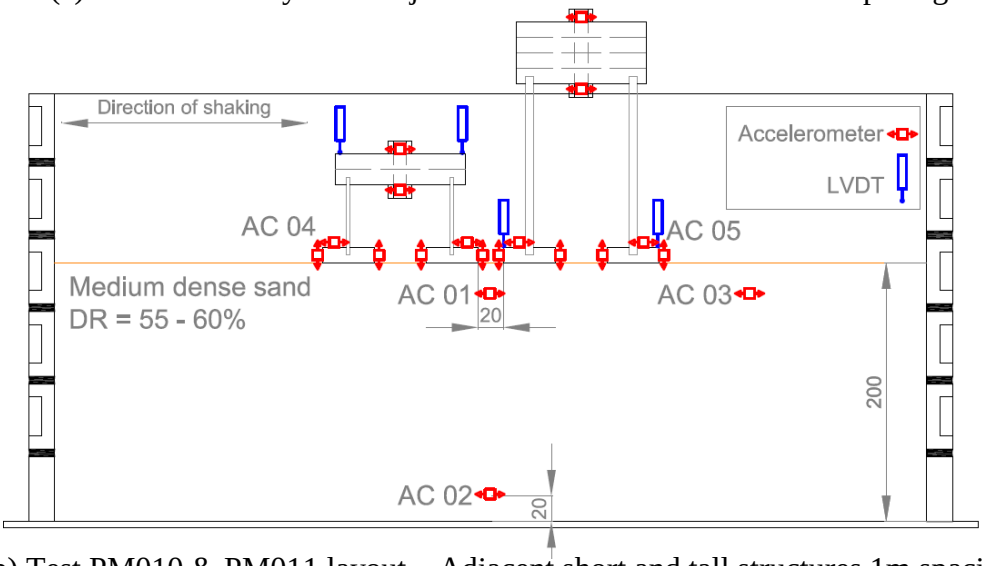

(b) Test PM010 & PM011 layout – Adjacent short and tall structures 1m spacing

Figure 5.16 dissimilar adjacent structures layout (PM009 – PM011)

Chapter 6

Centrifuge Results

6.1 Introduction

Chapter 5 outlined a series of tests to be carried out on the earthquake simulator, EQS, on a set of designed structures, with a view to highlight key aspects of soil structure interaction, SSI, and structure soil structure interaction, SSSI, behaviour on low rise structures under an earthquake "storm" scenario.

This chapter will discuss the observations of these tests, the response of the structures and the factors affecting the response. The response of the soil itself will be considered followed by an in-depth look at the SSI response of isolated structures. The spectral method of predicting the response of structures to earthquake loading, presented in Chapter 4, will be expanded to incorporate the non-linear behaviour of real soil as an improvement of the simplified linear elastic model used in the FEM. The validation of this improved method against the centrifuge data will be presented. Finally a look at how SSSI affects the response of the structures will be discussed.

6.2 Soil response

6.2.1 Natural frequency

The equivalent shear beam, ESB, container introduced in chapter 5 was tested by Bertalot (2013) to determine its natural frequency. The empty container proved to have a natural frequency of 1.6Hz, however through his analysis, Bertalot determined that the dynamic behaviour of the container was heavily reliant on the soil model it contained, with the soil influencing the container and not vice versa. Bertalot (2013)

analysed the container frequency using a loose dry HST95 sand deposit at an approximate relative density of 30% and determined that the natural frequency of the container increased to between 2.4 and 2.6Hz, Figure 6.1, due to the soil deposit. The soil deposit added additional stiffness to the container and thus increased its natural frequency.

In test PM001 a similar soil deposit, a dry HST95 sand, was added to the container, but this time with a higher relative density of 57%. Figure 6.1 shows the transfer function determined between the input motion to the soil, recorded at the accelerometer closest to the base of the soil (instrument AC02 Figure 5.14) and output of the soil, recorded at the accelerometer closest to the surface of the soil in the free field (instrument AC03 Figure 5.14), together with its spectral coherence. Only the data with a high coherence within the range of frequencies controllable by the EQS is plotted for clarity. Two distinct peaks can be seen in the data. The first peak occurs at around 3.6Hz and this can be attributed to the natural frequency of the container. With a stiffer sand deposit the stiffness of the container increased further and thus increased its natural frequency to higher than that measured by Bertalot (2013). The second peak occurs at 5.45Hz which corresponds well with the predicted natural frequency 5.7Hz, from Equation 6.1, for a H_s = 10 m deep layer of uniform sand with an average shear wave velocity, V_s, of 228m/s.

$$f_n = \frac{V_s}{4H_s} \qquad \textbf{Equation 6.1}$$

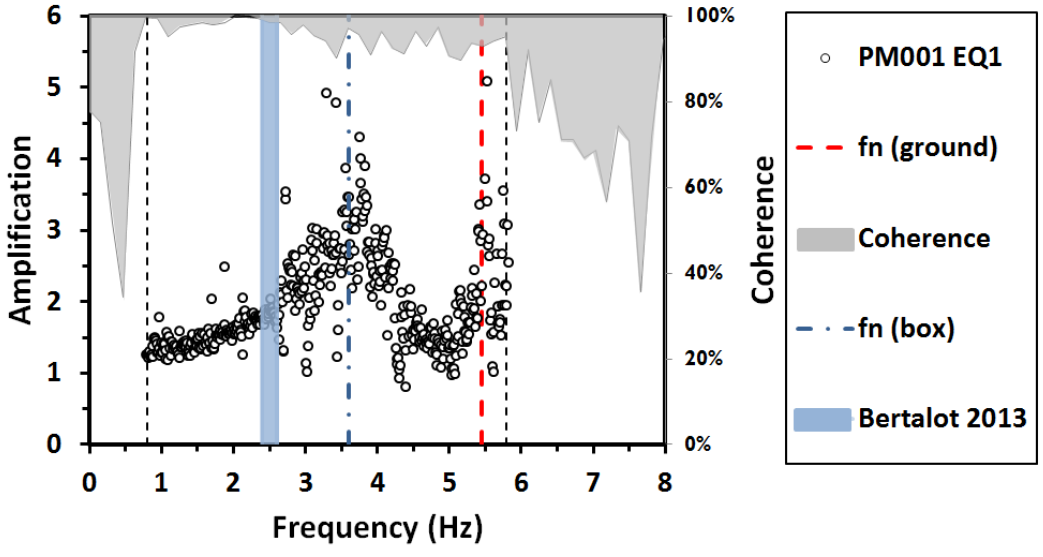

Figure 6.1 Frequency response of E.S.B. containing medium-dense sand

6.2.2 Free-field motion (site effect)

The EQS applied the replicated Kobe (Takatori station) seismic event to the base of the model, equivalent to the bedrock beneath the soil in the prototype. The soil medium itself will have an effect on this motion as it moves through it. The exact effect will depend on the composition of the soil, its density and uniformity; the peak ground motion will be either amplified or attenuated which can be represented by a site amplification factor, *S*. In the case of these analyses the soil is prepared so that it is a homogenous sand of uniform density, as outlined in Section 5.5.2. As the seismic motion reaches the surface of the soil it should therefore remain uniform across the surface of the model (in the absence of any structures or boundary effects).

Each seismic motion that is passed through the soil will have a densifying effect. This may cause the resulting site amplification, *S*, to be changed for each subsequent earthquake (aftershock) applied to a model. Eurocode 8 suggests that the level of site amplification experienced should be dependent on the ground type; for this particular ground type, (type E), the site amplification should be $S = 1.4$. Figure 6.2 presents the measured site amplification experienced in all of the adjacent structure models (in the free-field) and compares them directly with the Eurocode 8 recommended value. The increased number of earthquakes applied to the system makes the adjacent structure models more suitable for monitoring any change in amplification due to soil densification. The isolated structures are omitted from the figure as they had a different sequence applied.

The Eurocode 8 prediction appears to work well for the larger magnitude earthquakes, including for strong aftershock earthquakes where the soil will be expected to have densified. Generally, the measured amplification in the smaller earthquakes is larger than in the stronger earthquakes, which is likely due to the soil response being predominantly elastic in the smaller motions, compared to a likely elasto-plastic response, which potentially induces more hysteretic damping, in the larger ones. The Eurocode 8 prediction remains reasonable for the initial smaller earthquake; however there is a divergence from the trend when smaller aftershocks are considered. The amplification increases to a value closer to 2 for both of the 0.1g Kobe aftershock cases. This divergence is likely due to the soil remaining elastic (as described above) but with increased density (therefore better ability to transmit shear waves) as a result of the numerous strong previous earthquakes.

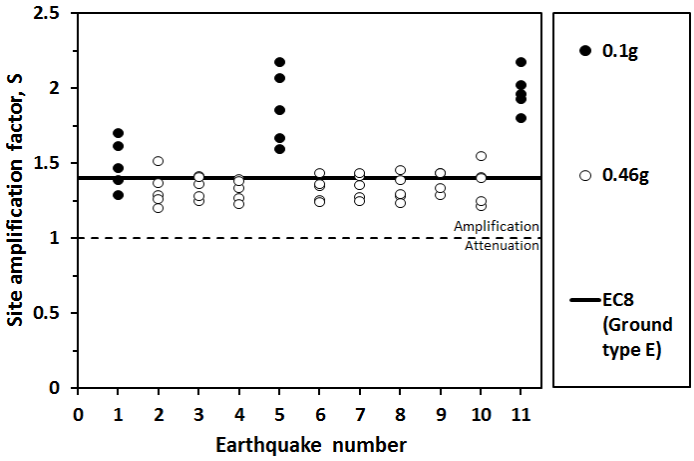

Figure 6.2 Free field site amplification

6.2.3 Near field motion

The addition of structures to the surface of the soil will also change the density of the soil directly underneath them due to the additional contact pressure of the foundations resulting in increased confining stress and a greater densification in these areas. This may therefore also influence the site amplification.

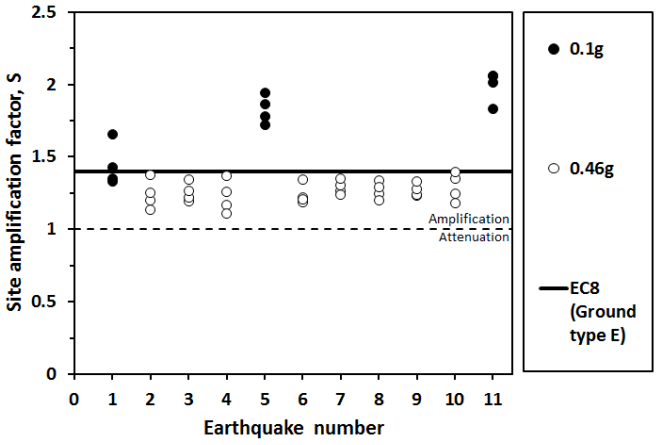

(a) Short Structure

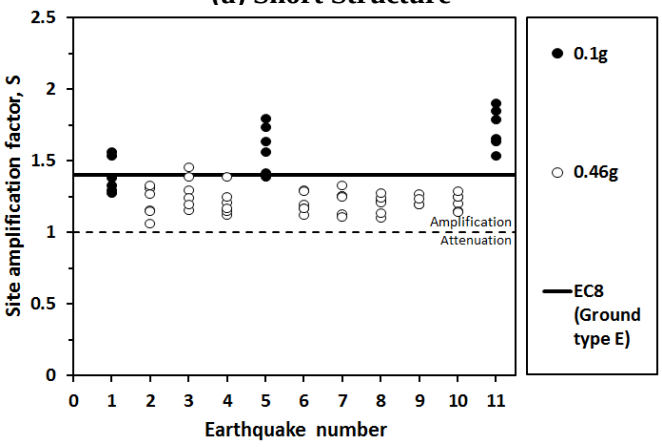

(b) Tall Structure

Figure 6.3 (a) (b) Near field site amplification, short (a) and tall (b) structure

Considering both the small and large structure used in this research, Figure 6.3 (a) and (b) visualises the response, similar to that presented for the free field case. As before, only the adjacent structure models are shown as these all have the same shaking history. While in the free field case the Eurocode 8 prediction for the larger earthquakes fell close to the average response measured, in the near field case it is very much at the top end of the amplification measured for both the short and the tall structures during the larger earthquakes, suggesting that the presence of the structures reduces the peak magnitude of seismic ground motion at foundation level. The smaller magnitude earthquakes again appear to show a similar divergence as with the free field though this effect is slightly reduced at these locations.

The reduction in the peak magnitude of seismic ground motion under the structures compared to the free field may be the result of multiple mechanisms interacting. It would be expected that the additional confining stress within the soil due to the presence of the structures will improve the transmittance of the shear wave through the soil and therefore increase the peak magnitude. However, destructive interference between the responses of the adjacent structures may be acting to reduce the site amplification and therefore proving beneficial to the system, similar to the 'group effect' outlined in Section 2.5.2.

6.3 Soil Structure Interaction (Isolated Structures)

Tests PM001 through PM004 concentrated on the soil structure interaction (SSI) of isolated structures. Compared to the finite element analyses described in Chapters 3 & 4, these tests allow SSI to be observed where the structure is simpler (having 'rigid' joints, which approximately represent a wide range of real/semi-rigid conditions as shown in Chapter 4) but with more representative non-linear soil behaviour (as the soil is real). As the seismic excitation was applied in the tests, a series of accelerometers and LVDT's monitored the soil and structural response, as outlined in Chapter 5 (Figures 5.14 -5.16).

The simple analytical prediction method developed in Chapter 4 is modified in this chapter in order to determine representative soil properties for use in the analysis, accounting (in an approximate way) for the non-linear strain dependency of the soil shear modulus. Both the observations of the physical test and the improved prediction method are presented in this Section.

6.3.1 Observations from centrifuge tests

Considering both the long and short period isolated structures, the observations highlighted in Figure 6.4 were made during this analysis. Time histories for the bedrock input motion, the cumulative settlement of the structure, the total sway of the structure (rocking of the structure due to seismic motion including the effect of permanent global structural rotation), and the earthquake induced sway (rocking of the structure due to the seismic motion and not including the movement due to rotation) are presented.

While both models had nominally identical seismic motions input to the base of the soil, the response of the structures was evidently different. The seismic input under consideration consisted of a strong Kobe motion, followed by two strong aftershocks of the same magnitude and one final small aftershock. The long period (tall) structure showed increased earthquake induced sway (due to the longer period); however this was not as large an increase as was expected given the large increase in period. The long period structure also displayed an increase in settlement (due to the higher bearing pressure) and permanent sway (due to the larger aspect ratio/higher centre of mass) when compared directly to the short period (short) structure. In both cases the resulting settlement for a given strength of earthquake shaking reduced as each preceding earthquake densified the soil under the structure. This had a slight effect on the earthquake induced sway of the structure as a slight increase was observed with each subsequent earthquake; this effect is further demonstrated in Figure 6.5 and discussed later.

The earthquake induced sway that was observed in the taller structure was not very much greater than the shorter structure. The short period structure, PM003, showed little permanent total sway during the test once the initial permanent total sway had occurred, however the long period structure showed more significant total sway, which increased with every seismic motion. This shows the potential for damage accumulation (in terms of excessive settlement and tilt) due to a sequence of strong aftershocks. The strong global rotation mechanism responsible for the permanent total sway, particularly for the tall structure, may be reducing the amount of energy dissipated in the earthquake due to the structural frame effect, thus limiting the earthquake induced inter-storey drift and protecting the structural elements.

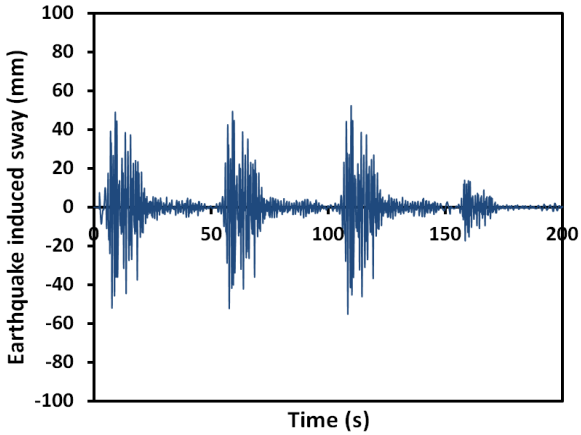

(a) PM003 Short Structure EQ sway

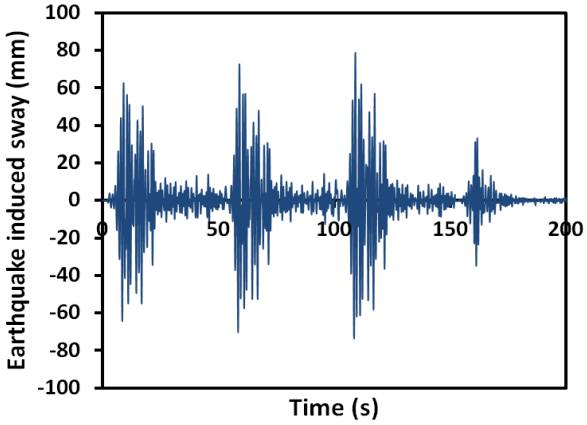

(b) PM004 Tall Structure EQ sway

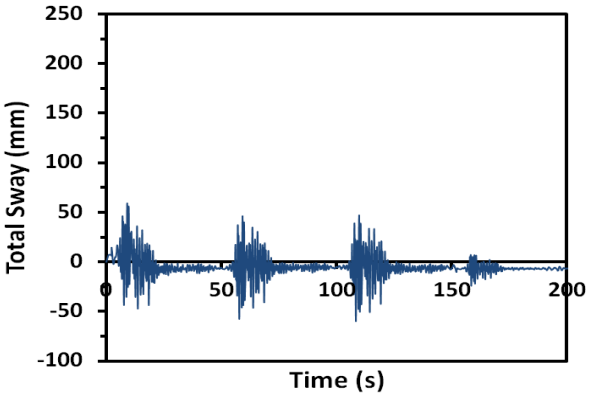

(c) PM003 Short Structure Total sway

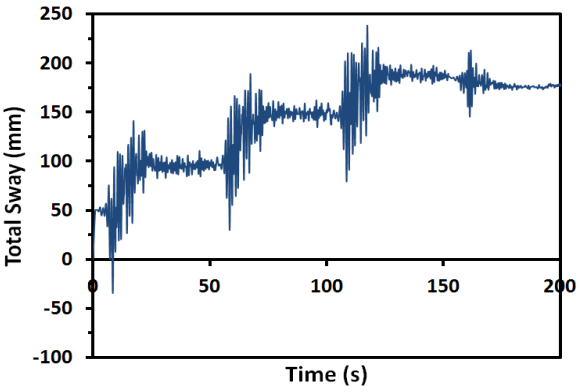

(d) PM004 Tall Structure Total sway

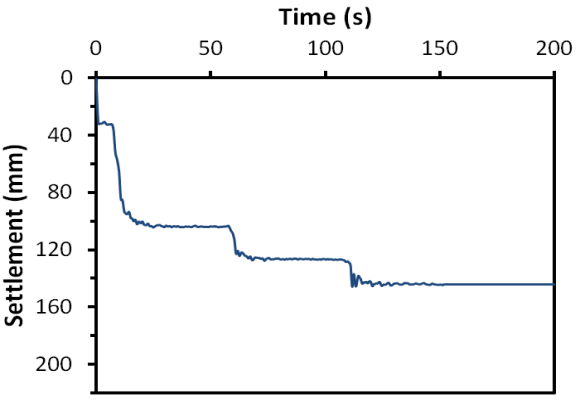

(e) PM003 Short Structure Settlement

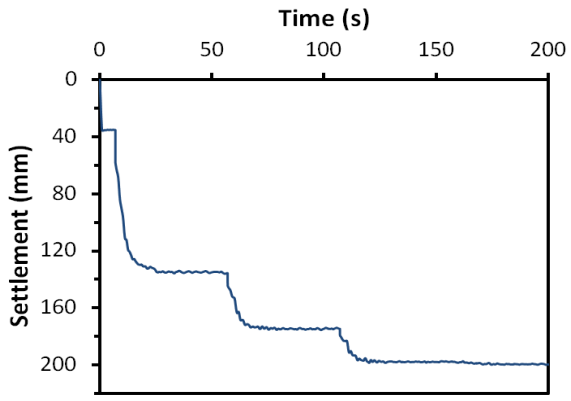

(f) PM004 Tall Structure Settlement

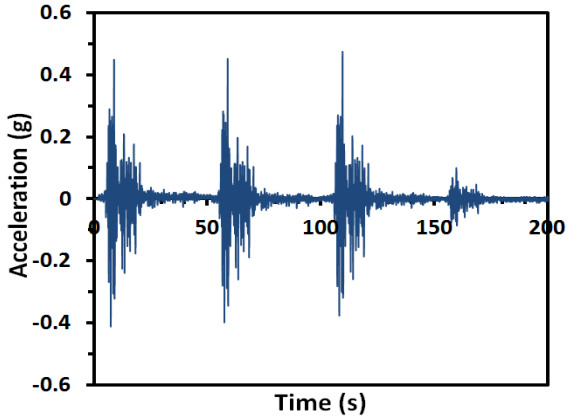

(g) PM003 Short Structure Bedrock Input

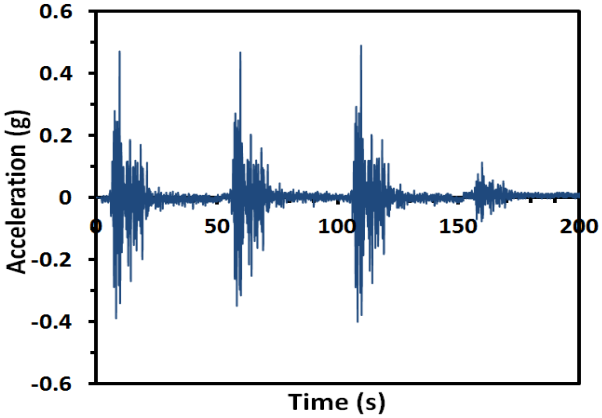

(h)PM004 Tall Structure Bedrock Input

Figure 6.4(a-f) Seismic response of Isolated structure, PM003 and PM004, (g-h) input motions at base of models

The horizontal sway (S_{de}) of the structure may be affected by multiple external factors. The difference in the natural period of the structure, the damping of the structure, the strength of the seismic event and the soil amplification of the seismic motion can all have an effect on the structural response. By normalising each of the sway values, the earthquake induced sway (measured from accelerometers and labelled as "EQ Sway" in future graphs due to space restraint) and the total sway (an accumulation of the EQ Sway and the horizontal movement due to the permanent global rotation), by all of these factors, a clearer understanding of how each of the sway mechanisms are affected by the settlement and rotational initial conditions that exist prior to the earthquake can be obtained. Figure 6.5 compares both sway mechanisms to the settlement and rotation conditions pre-earthquake (i.e. the structure's initial conditions). It should be noted that in this Figure, the fixed-base natural period and damping of the structures were used in the normalisation, and Sa_g was taken from centrifuge measurements in the free-field (Sa_g is the surface acceleration at AC03, Figure 5.14). Therefore the figure accounts for any difference in input motion magnitude, but not any effects due to SSI (i.e. in terms of altering the natural period, damping or near-field motion of the soil-structure system between events). The first thing to note is how the normalisation of the total sway for both the short and tall structures are more directly comparable than the normalisation of the EQ sway, indicating that a large part of the divergence in the normalised EQ sway results as a direct consequence of the global rotation mechanism. The remainder will be due to the SSI effect. This global rotational mechanism, larger in the tall structure, reduces the magnitude of normalised EQ sway experienced by the taller structure, therefore reducing the demand on its structural elements.

Both the EQ sway and total sway show slight increases with increased settlement for both structures, but more prominent in the tall structure. The increased settlement results in a denser soil model which in turn could result in the increase in sway experienced by the structure as a result of improved transmission of seismic motions to the structure through the denser soil.

When considering the total sway of the tall structure with settlement it is also interesting to note that the final earthquake introduces significantly more normalised total sway than the others. This final earthquake is in fact the smaller aftershock motion and its large increase in normal total sway is due to the permanent rotation induced by the preceding earthquakes being much larger than any sway the

earthquake itself could induce (as this now has a small magnitude); however there is still a reduction in the normalised EQ sway experienced by the tall structure during this earthquake compared to its short structure equivalent. With that said it should also be noted that there is an increase in normalised EQ sway experienced for the tall structure during this earthquake, compared to the previous earthquakes experienced by this structure, indicating that there is greater beneficial effect on soil structure interaction in the larger earthquakes, potentially due to increased energy dissipation through elasto- plastic global rotation in a framed structure, in addition to the local rotation investigated by previous authors,(Kutter *et al.* 2006; Anastasopoulos *et al.* 2012; Kourkoulis *et al.* 2012).

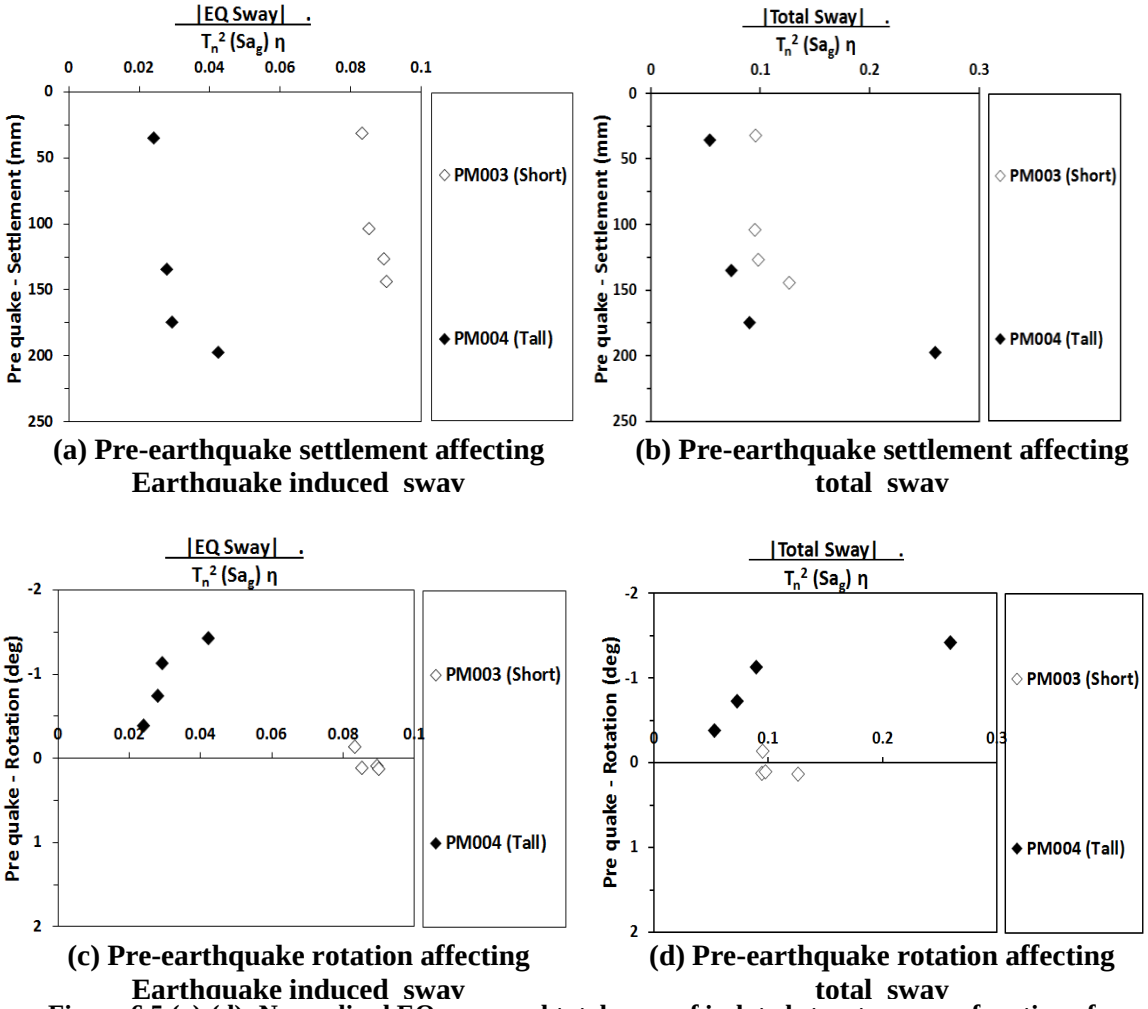

(a) Pre-earthquake settlement affecting Earthquake induced sway

(b) Pre-earthquake settlement affecting total sway

(c) Pre-earthquake rotation affecting Earthquake induced sway

(d) Pre-earthquake rotation affecting total sway

Figure 6.5 (a)-(d): Normalised EQ sway and total sway of isolated structures as a function of initial conditions

The normalised total sway and the EQ sway of the tall structure are also directly affected by the initial condition rotation of the structure, increasingly so for the smaller earthquake for reasons outlined previously. This is not seen so strongly in

the short structure due to the lower magnitude of settlement and low permanent rotations for this case.

The permanent global rotation, as well as any elastic global rotation will be directly linked to the bearing capacity of the soil. Table 6.1 gives estimated bearing capacities, calculated as shown in Appendix C (as outlined in Chapter 3 Section 3.4.1.2), for both the 0.1g and 0.46g earthquakes considered in the tests. It is clear that the 0.46g seismic bearing capacity of the soil is greatly reduced. It falls below the amount of pressure applied by both the tall and short structures and results in a very low factor of safety for both structures' foundations. Once the factor of safety falls below a value of 1, instantaneous failure of the soil can occur.

Considering both the tall and short structure separately, Figure 6.6(a) and (b) shows the seismic motion that is input to the structures. It also divides this motion into two areas. The first area, sway response, is the area within which the factor of safety of the soil is above 1. The second area, rotational response, is the area where the factor of safety against footing failure falls below 1 for that particular structure allowing sequential failure of alternate foundations to occur resulting in permanent rotation (and settlement). This global rocking would dissipate some of the energy from the earthquake, reducing that which is available to excite the sway mode.

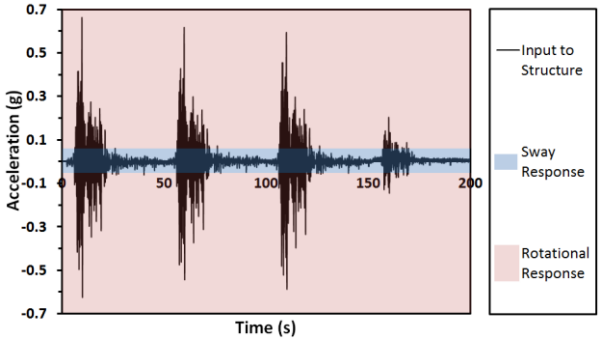

(a) Tall structure

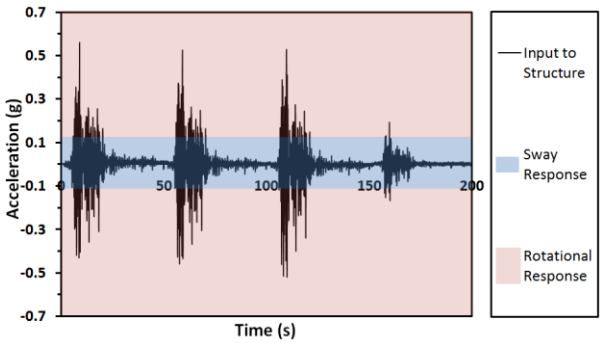

(b) Short structure

Figure 6.6: Response mechanism predicted for structures during seismic event

	Static	*0.1g*	*0.46g*
Critical Bearing capacity:	476 kPa	170 kPa	1.7 kPa
Factor of Safety:			
Tall Structure	1.72	0.62	0.004
Short Structure	2.96	1.1	0.007
Peak Bearing capacity:	1054 kPa	493 kPa	5.1 kPa
Factor of Safety:			
Tall Structure	3.8	1.79	0.02
Short Structure	6.55	3.06	0.03

Table 6.1 Bearing Capacity of soil with factors of safety for structures

6.3.2 Improvements to Chapter 4 analytical model

6.3.2.1 Determination of operational shear modulus in non-linear soil

In Chapter 4 a method for predicting the seismic response of the structures on soil was outlined. This method however was developed for a linear elastic soil. While this accurately represents the simplified elasto-plastic soil model used in the finite element modelling of Chapter 4, it is not clear how a suitable value of shear modulus may be estimated for response on real soil where the shear modulus may vary with cyclic shear strain (and therefore on the strength of the earthquake).

Yi (2010) describes a method for evaluating seismic settlement in free-field dry sand based on shear wave velocity or relative density. In this method, an estimate of peak cyclic shear strain is obtained and it is here proposed that this value (selected at an appropriate depth) and modified to account for the additional confining stresses beneath the building could be used to determine $[G/G_0]$ which can in turn be used to estimate a linearised *G* for the soil for use in determining the effects of SSI on natural period and damping.

From Yi (2010) the shear strain, γ, for a non-linear material under seismic loading is, related to shear modulus by:

$$\frac{G}{G_0} = \left[\frac{\tau_{av}}{G_0}\right].\frac{\gamma}{1} \qquad \textbf{Equation 6.2}$$

Yi (2010) recommends following the Pradel (1998) method for calculating γ, outlined in Equation 6.3:

$$\gamma = \left[\frac{1 + a.\exp\left(b.\tau_{av}/G_0\right)}{1+a}\right].\frac{\tau_{av}}{G_0} \times 100(\%) \qquad \textbf{Equation 6.3}$$

where:

$$a = 0.0389\left(p'/p_a\right) + 0.124 \qquad \textbf{Equation 6.4}$$

and

$$b = 6400\left(p'/p_a\right)^{-0.6} \qquad \textbf{Equation 6.5}$$

where p' is the mean confining stress defined in Equation 6.6 and p_a is a reference stress of 100kPa:

$$p' = \frac{1}{3}\left(\sigma'_{v0} + 2\sigma'_{h0}\right) \qquad \textbf{Equation 6.6}$$

In Equations 6.7 and 6.8 the vertical and horizontal effective stresses in the soil beneath the structure are here modified to include the effect of the soil self-weight and the bearing pressure from the overlying structure (using the Boussinesq stress distribution, as reported in Poulus *et al.* (1980)), which in dry sand gives:

$$\sigma'_{v0} = \gamma_s z + \left[\frac{\alpha + \sin\alpha\cos\left(\alpha + 2\beta\right)}{\pi}\right]\cdot q \qquad \textbf{Equation 6.7}$$

$$\sigma'_{h0} = K_0\gamma_s z + \left[\frac{\alpha - \sin\alpha\cos\left(\alpha + 2\beta\right)}{\pi}\right]\cdot q \qquad \textbf{Equation 6.8}$$

where

$$\alpha = \left[\tan^{-1}\left(\frac{x + B/2}{z}\right)\right] - \beta \qquad \textbf{Equation 6.9}$$

and

$$\beta = \tan^{-1}\left(\frac{x - B/2}{z}\right) \qquad \textbf{Equation 6.10}$$

Where γ_s is the unit weight of soil and K_o is the lateral earth pressure as outlined by Mayne *et al.* (1982). The geometric parameters x, z, α, β are defined in terms of a single footing as shown in Figure 6.7, and for the single bay frames considered in this thesis, the effects of both footings are superimposed.

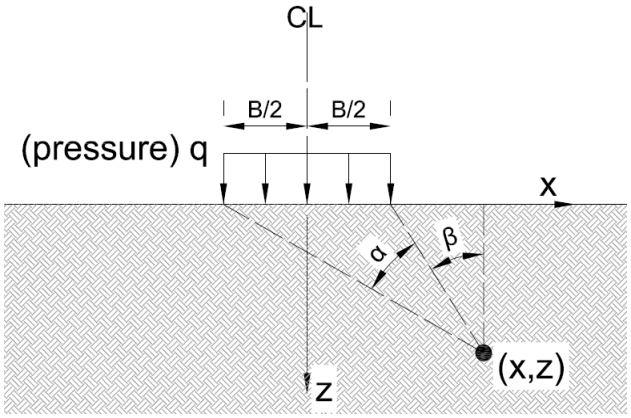

Figure 6.7 Geometric parameters for a single footing

The average shear stress, τ_{av}, in Equation 6.2 is defined by Equation 6.11:

$$\tau_{av} = 0.65\left(\frac{a_{\max}}{g}\right)\sigma_{v0}.r_d \qquad \textbf{Equation 6.11}$$

where $a_{\max}$ is the peak ground acceleration for free field soil, σ_{vo} is the total effective overburden stress (assumed here to be given by Equation 6.7 as $\sigma_{vo} = \sigma'_{vo}$ in dry sand) and r_d is a stress reduction coefficient defined by Equation 6.12 after Idriss (1999):

$$r_d = \exp\left[\alpha(z) + \beta(z).M_s\right] \qquad \textbf{Equation 6.12}$$

where M_s is the moment magnitude of the earthquake,

$$\alpha(z) = -1.012 - 1.126\sin\left(z/11.73 + 5.133\right) \qquad \textbf{Equation 6.13}$$

and

$$\beta(z) = 0.106 + 0.118\sin\left(z/11.28 + 5.142\right) \qquad \textbf{Equation 6.14}$$

In which the sine terms are in radians. Equation 6.2 still requires a value for G_0, this is obtained from Equation 6.15

$$G_0 = \frac{(3 - e_0)^2}{1 + e_0}\sqrt{p} \qquad \textbf{Equation 6.15}$$

as suggested by Hardin *et al.* (1969) where e_0 is the initial void ratio of the soil (determined from relative density, $e_{\max}$ and $e_{\min}$) With values for both $[G/G_0]$ and

G_0 a value of *G* can be determined for any required depth of the soil. It is proposed to use the value of *G* calculated at a representative position (in this case, beneath the centre of the structure, midway between the foundations and at a depth of *B*/2) in the prediction method outlined in Chapter 3 in order to predict the seismic response incorporating SSI in real soil. In order to evaluate the accuracy of this proposed prediction method it is used in Section 6.3.3 to determine the dynamic characteristics of the soil-structure system ($T_{n,ssi}$, ζ_{ssi}) and validated against the centrifuge test observations.

6.3.2.2 Determination of structural settlement and use in aftershocks

The method outlined above not only provides a method of estimating the shear modulus of the soil at any given depth, it also allows predictions of the seismically induced settlement, ΔH , at any depth, *z*, to be predicted, as outlined in Equation 6.16.

$$\Delta H = \int_{bedrock}^{z} \varepsilon_{vc} dz \qquad \textbf{Equation 6.16}$$

with ε_{vc} being the volumetric strain (as a function of depth) within the soil, defined by Equation 6.17

$$\varepsilon_{vc} = 0.658\left(0.26M_s - 0.96\right)\left(\frac{D_r}{100}\right)^{-2.68}\gamma(z) \qquad \textbf{Equation 6.17}$$

These Equations were originally proposed by Yi (2010) for estimating the settlement of free-field soil. It is here proposed that by using the shear strains from Equation 6.3, which include the additional confining stresses beneath the foundation (Equations 6.7 and 6.8), the volumetric strain and settlement beneath the foundation can be estimated. This therefore may provide a spectral method of estimating the total structural settlement, in addition to drift (via $T_{n,ssi}$ and ζ_{ssi}).

Furthermore, once the volumetric strain has been found, the change in void ratio throughout the depth of the soil can be found as:

$$\Delta e = -\varepsilon_{vc}\left(1 + e_0\right) \qquad \textbf{Equation 6.18}$$

By adding this change in void ratio to the initial void ratio, e_0, the updated post-earthquake density profile can be found and used as a starting point for further

calculations conducted for an aftershock. In this way, the effects of previous shaking can be accounted for in the determination of settlement, G, $T_{n,ssi}$ and ζ_{ssi} for aftershocks.

6.3.3 Validation of improved analytical model

6.3.3.1 Dynamic characteristics ($T_{n,ssi}$, ζ_{ssi})

The new prediction method considers the effect the soil will have on the structure's response and how this will change as the structure is subjected to subsequent earthquakes. It allows for this effect through its prediction of the $T_{n,ssi}$ of the structure. Figure 6.8 highlights how accurate this prediction method is in calculating $T_{n,ssi}$ for both the long and short period structures. By incorporating the flexibility of the system through a strain and density-dependent G which can be modified by previous shaking, the model adapts to the changes in subsoil properties and therefore provides a good estimation, even in the aftershocks. The accuracy of the prediction generally falls close to within 10% of the actual measured values from the centrifuge analysis, determined through curve fitting to the measured transfer function across the structure from the centrifuge test data. This is an improvement on the EC8 method (which does not consider SSI), also plotted in Figure 6.8, which under predicts the natural period of the structure by not considering the soil effect. The predicted value of $T_{n,ssi}$ will subsequently be used to estimate the peak drift and spectral acceleration of the system; it is therefore important that an accurate representation of the fundamental period is used for future calculations.

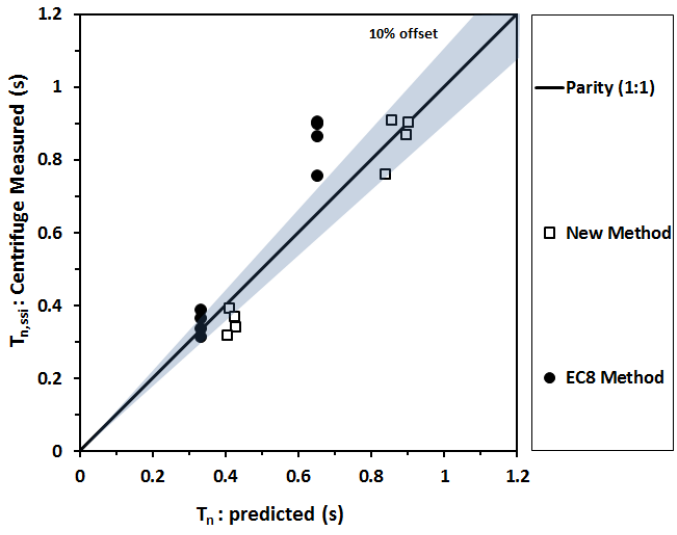

Figure 6.8 Prediction of $T_{n,ssi}$

The other major factor that requires accurate prediction is the damping of the system, this will subsequently be used within the seismic response spectrum determination. The new prediction of ζ_{ssi} , Figure 6.9, improves on the EC8 method of prediction (without SSI) which only considers structural damping.

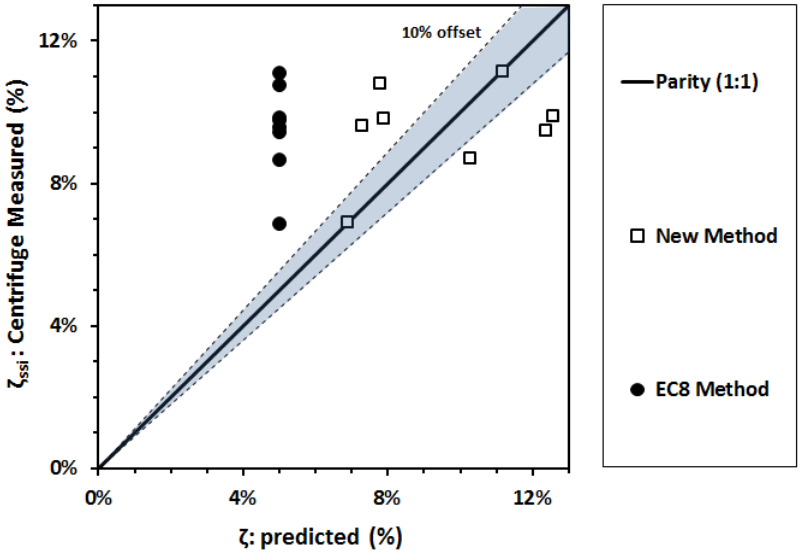

Figure 6.9 Damping prediction

The new method does still include some deviation from the centrifuge analysis, though it should be noted that the experimental data from the centrifuge was much noisier in the magnitude of the peak of the transfer function than that from the finite element models in Chapter 4, and the additional scatter may be due to the greater uncertainty in determining the measured damping due to this effect.

Section 6.3.1 discussed the normalised EQ sway and normalised total sway responses of the structure. This used the fixed-base T_n and η value for the fixed base structure. With the new adaptations to the prediction method a more comprehensive normalisation of both the sway responses can be made by using $T_{n,ssi}$ and η_{ssi}, thereby removing not only any effect of input motion magnitude, but also any effects due to the true dynamic characteristics of the soil-structure system. This is shown in Figure 6.10. The short structure, which is less affected by rocking, now shows a stronger correlation between the pre-earthquake settlement and both sway responses. This would suggest that the initial earthquakes densify the soil, alter the equivalent period and damping and amplify the structural response within a subsequent aftershock.

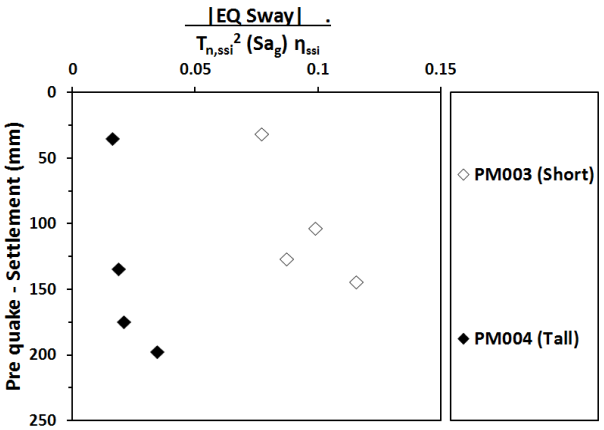

(a) Pre-earthquake settlement affecting Earthquake induced sway

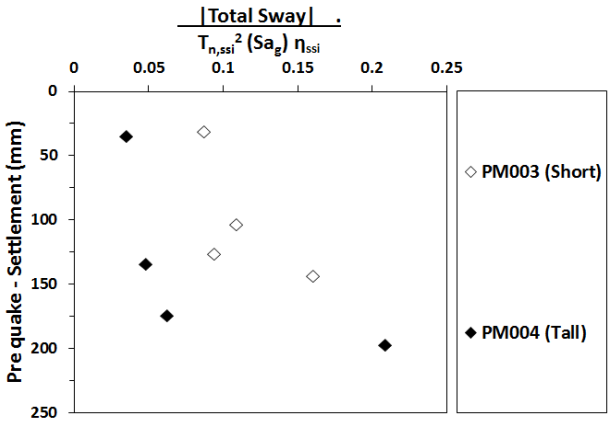

(b) Pre-earthquake settlement affecting total sway

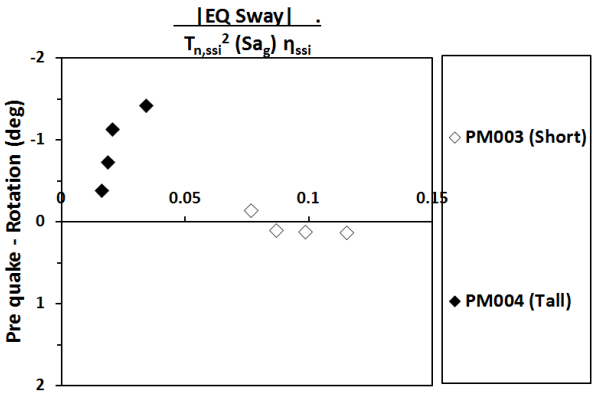

(c) Pre-earthquake rotation affecting Earthquake induced sway

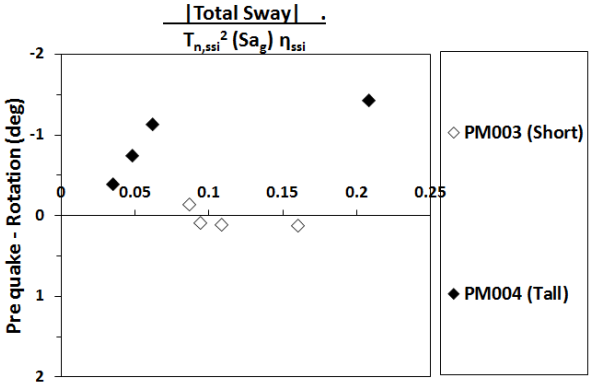

(d) Pre-earthquake rotation affecting total sway

Figure 6.10 Normalised drift as a function of initial conditions, using improved parameters

6.3.3.2 Prediction of spectral quantities

The Eurocode 8, (BSI 2008), spectral method of predicting the response of the structure, as outlined in Chapter 4, does give an indication of the structural response. However as shown in Chapter 4 the accuracy of this prediction decreases when elements that add flexibility to the system are included, either through structural joints or through the foundation. The new model, using the new prediction of $T_{n,ssi}$ to account for this additional flexibility proved very successful when validated against the finite element analyses.

Considering now the centrifuge test data, Figure 6.11 compares the measured elastic displacement response (EQ sway = S_{De}) of the structure to the Eurocode spectral prediction using a nominal structural damping of 5% (reasonable for the structural models alone). The actual response spectra for the Kobe earthquake that was applied, considering both 7 and 13% equivalent damping, is also overlain on the

graph. The equivalent damping of the structure and soil system changed with each earthquake, but from the measured transfer functions it generally fell between the thresholds of ζ_{ssi} = 7 and 13% (shown shaded), as predicted in Figure 6.9. Therefore it would be expected that the response measured from the centrifuge tests would fall within this shaded area. This highlights how important it is to accurately predict the damping as it has a large effect on the design spectrum. In this case the Eurocode 8 prediction for the 0.46g earthquake and 5% damping, appears to work very well for the short structure (where the response is pure sway with little rotation, Figure 6.4, and the equivalent damping is towards the lower end of the range); however once the tall structure is considered the measured EQ sway response lies well below the prediction area (shaded grey area). Considering instead the total sway of the tall structure, including the plastic deformation, this provides an accurate prediction for the initial 0.46g earthquake, falling within the shaded spectra area. This suggests that in a situation with mainly elastic and limited permanent rotation response, similar to that seen in the short structure case, the elastic sway prediction works well. However in a situation permanent structural rotation occurs, i.e. the tall structure case, the sway response is dampened by this permanent structural rotation. If the response for the tall structure was an entirely elastic sway response the prediction may have been more accurate. However the current method of prediction does not account for permanent deformation response of the structure.

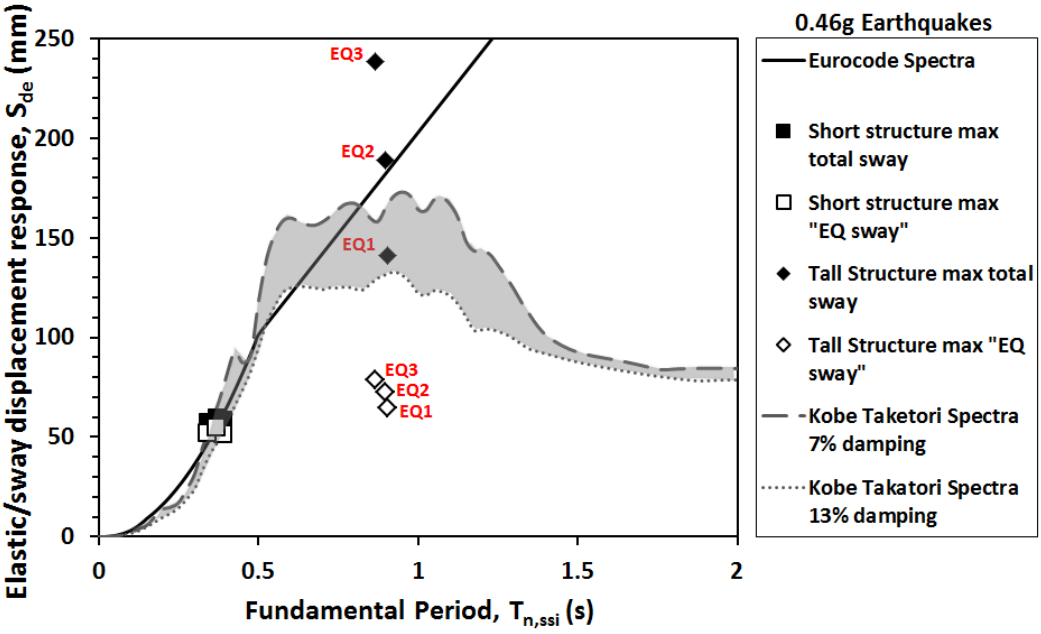

Figure 6.11 Elastic displacement response measured compared to spectral prediction, 0.46g

Figure 6.12 directly compares the new model's predicted values with the measured data from the centrifuge tests for all seismic events and for both tall and short structures. As in Figure 6.11, a strong correlation between the predicted and measured EQ sway values for the short model is clear. When considering the tall structure the level of EQ sway predicted for the small magnitude earthquake, matches up very well with the measured value from the centrifuge tests. It is only when considering the larger earthquakes, when the significant permanent rotation occurred (Figure 6.4), that the prediction method over predicts the EQ sway response.

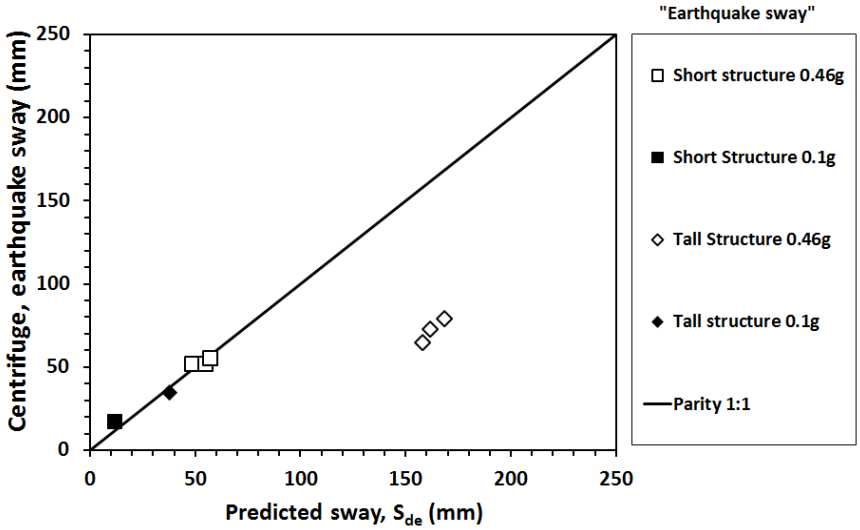

(a) Predicted EQ sway

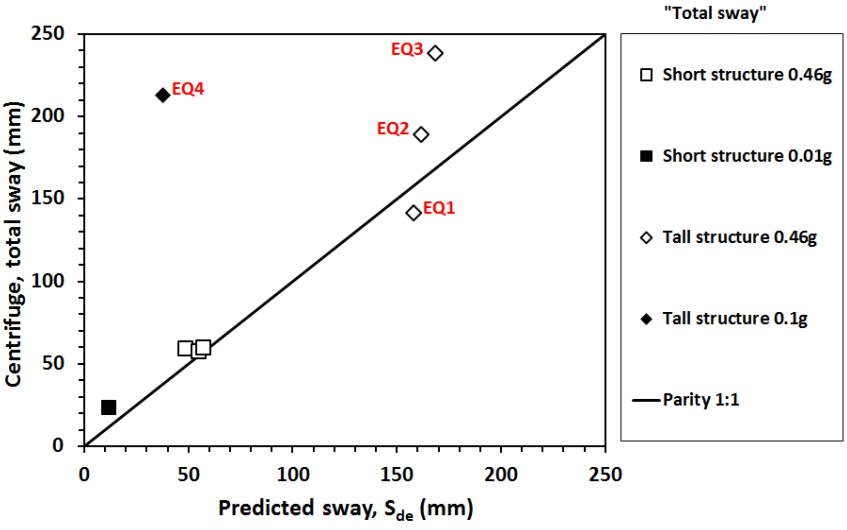

(b) Predicted total sway

Figure 6.12 Displacement response prediction compared to that measured

The prediction method appears to line up with the total sway response of the tall structure for the initial earthquake, with the correlation reducing with each subsequent earthquake due to larger magnitudes of initial condition rotation. This

could suggest that the total sway response, inclusive of permanent sway deformation due to permanent rotation, may be limited to a horizontal displacement similar in magnitude to the peak predicted elastic response. Further research into this mechanism would be required in order to make a conclusive observation and in order to fully understand the relationship.

Now that a prediction of the sway has been made a prediction of the inter-storey drift can also be made, through the method outlined in Section 4.7.7. Again as this prediction is based on the predicted sway values its accuracy is dependent on the accuracy of the sway prediction. Therefore the result, presented in Figure 6.13, for the tall structure under 0.46g seismic loading over predicts the inter-storey drift response. The other predictions however show a very good correlation. This is largely due to global rotation being the major rotational mechanism recorded, with negligible local rotations observed. In the FEM prediction frames with much greater global rotation compared to local rotation were shown to be easier to predict.

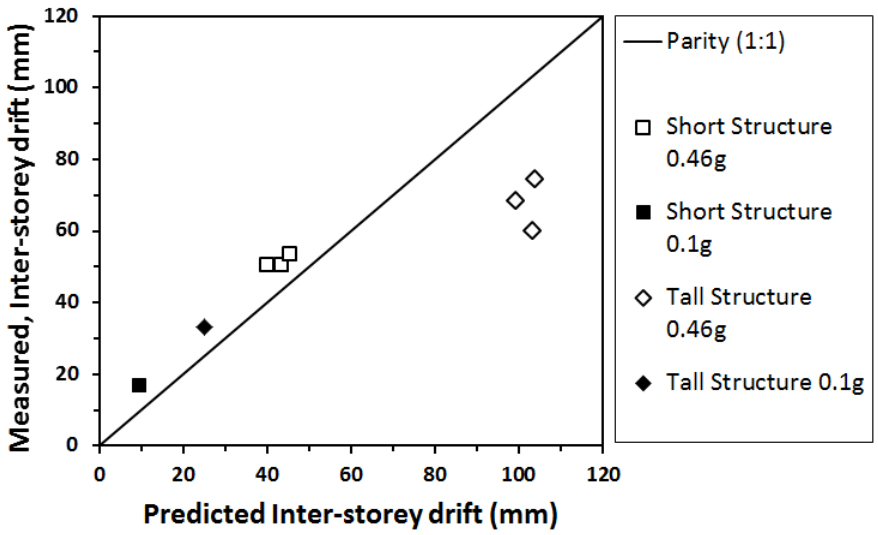

Figure 6.13 Max inter-storey drift prediction compared to that measured

As mentioned in Section 6.3.2.2, the modified Yi (2010) method also allows for estimation of overall seismic settlement. The settlement of the structure is assumed to be equal to the surface settlement of the soil beneath the structure, which is what is actually computed using the method outlined previously. Comparing the prediction of this settlement with the settlement recorded during the centrifuge tests, Figure 6.14 demonstrates that the new model is highly accurate, even at estimating the reduced settlements in the strong aftershocks. Almost all of the predictions fall within 10% of

the actual settlement recorded. This new spectral peak settlement prediction ability, along with the improved estimations of the dynamic properties, will prove very useful to a structural engineer when designing structures for seismically active areas.

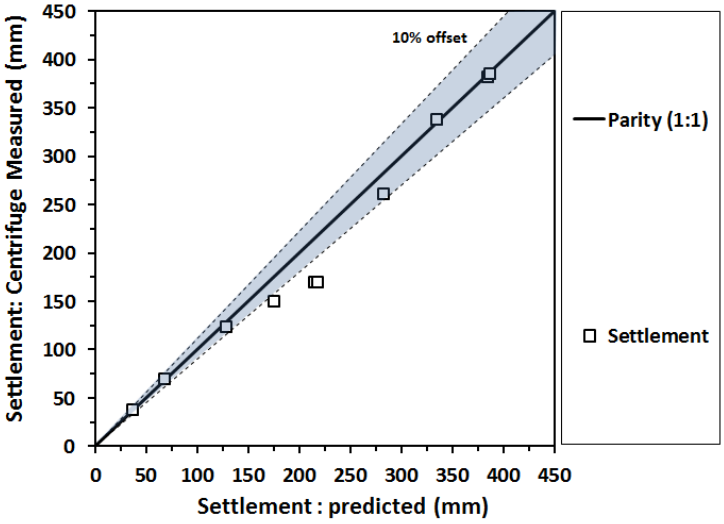

Figure 6.14 Predicted Settlement compared to that measured.

6.4 Structure Soil Structure Interaction (Coupled Structures)

Tests PM005 through PM011 focus on the structure-soil-structure interaction, SSSI, response of coupled structures. They take advantage of the real non-linear soil used in the tests to observe how these structures interact with each other through the soil when a seismic excitation is applied to the system. Similar to the isolated structures, the response of these structures was monitored by a series of accelerometers and LVDT's, as outlined in Chapter 5. A comparison between the response of the isolated structures and the response of the coupled structures will be made to highlight whether SSSI has a significant effect on how a structure responds. Multiple aftershock earthquakes are also applied to each grouping of structures in order to evaluate the cumulative effect that multiple earthquakes can have on the response.

6.4.1 Effects of aftershocks

In Section 6.3.3.1 the isolated structures displayed some correlation between the pre-earthquake settlement and both normalised sway responses, especially when considering the smaller, short period, structures. They also displayed a correlation between the normalised total sway response and the pre-earthquake rotation of the structure. Figure 6.15 presents a similar comparison, the effect that the pre-earthquake

settlement and the pre-earthquake rotation have on the normalised sway responses, for the coupled structures. While there is a slight increase in the normalised EQ sway for the dissimilar coupled structures compared to the similar structures, the slight correlation between pre-quake settlement and normalised EQ sway, which was seen in the isolated structures, is no longer evident. Similarly the pre-earthquake rotation appears to have limited influence on the EQ sway response.

Considering the total sway response, the effect of the pre-earthquake settlement appears to generally increase the total sway response with depth, being most evident in the similar structures. A stronger correlation exists between the total sway and the pre-earthquake rotation, with all structures' normalised total sway increasing (from their initial normalised total sway levels) with increased pre-quake rotation magnitudes. This is to be expected considering that the total sway is more strongly influenced by permanent rotation.

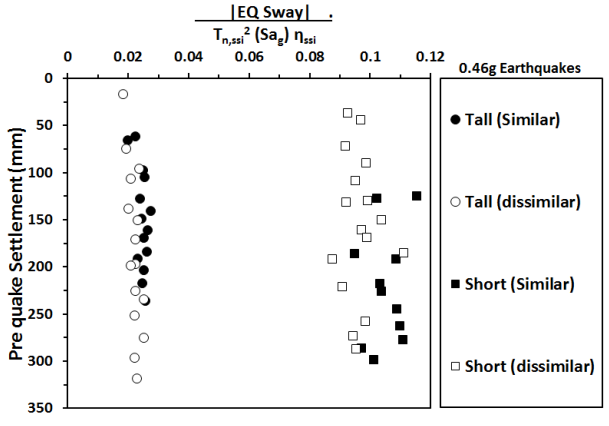

(a) Pre-earthquake settlement affecting Earthquake induced sway

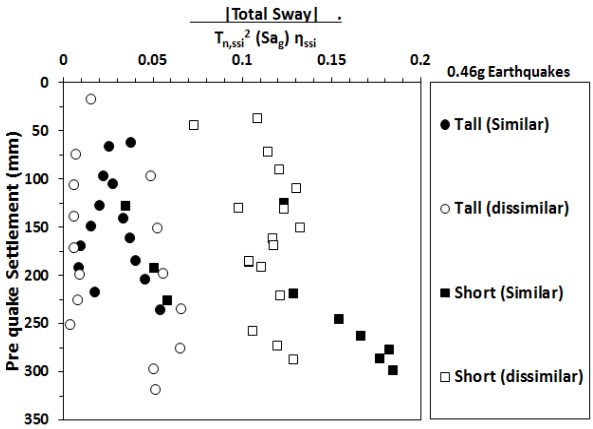

(b) Pre-earthquake settlement affecting total sway

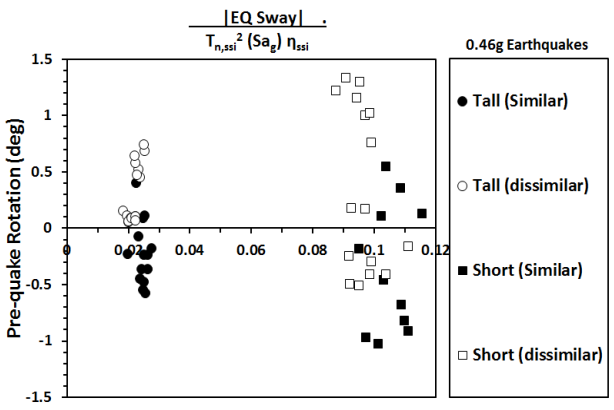

(c) Pre-earthquake rotation affecting Earthquake induced sway

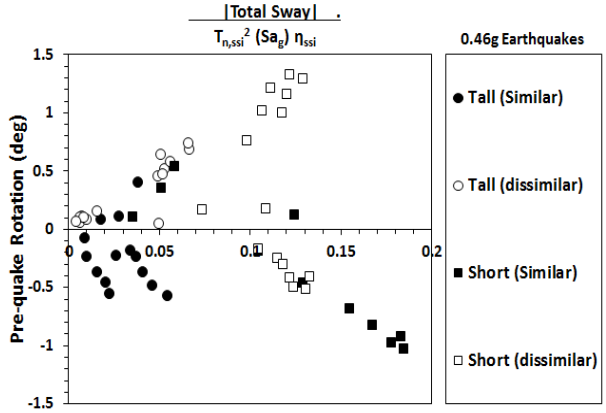

(d) Pre-earthquake rotation affecting total sway

Figure 6.15 Coupled structures normalised drift as a function of initial conditions for settlement and rotation.

The response in Figure 6.15 would indicate that the response due to an aftershock earthquake can be considered to be the same as that of the initial earthquake when considering normalised EQ sway. The settlements and rotations experienced in the preceding earthquakes do not seem to affect the EQ sway response. When the total sway response is being considered it will be heavily dependant on the pre-earthquake rotational condition, resulting in the cumulative rotation of the structure.

Figure 6.16 considers how the initial conditions, i.e. the pre-earthquake settlement and rotations, affect the incremental settlement and incremental rotation experienced during each earthquake. The incremental settlements and incremental rotations are normalised by the normalised free field peak ground acceleration, a_{gf}, to account for any disparity in the size of the motion input between events.

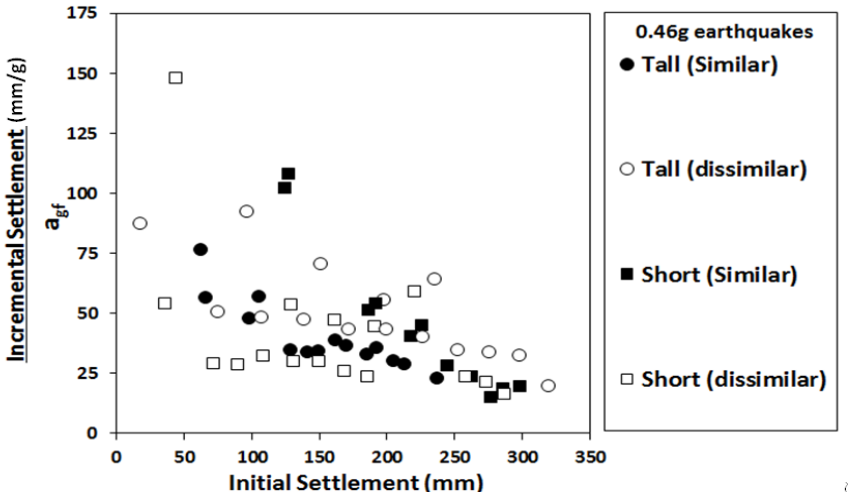

(a) Initial settlement affecting incremental settlement

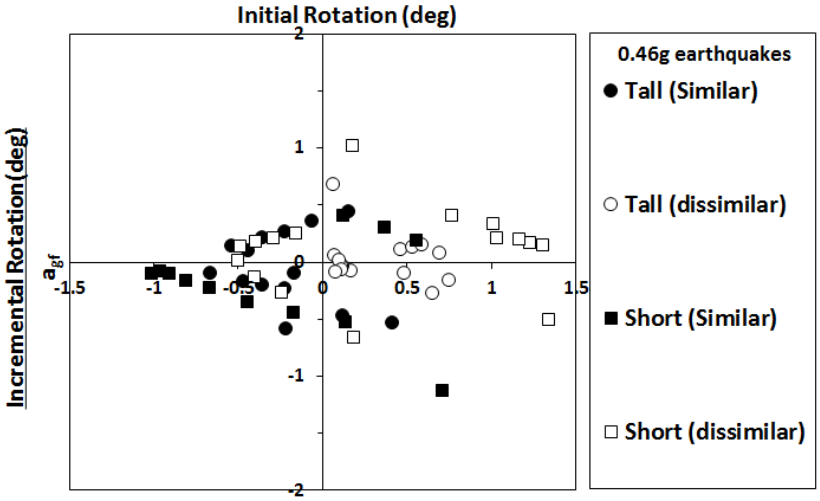

(b) Initial rotation affecting incremental rotation

Figure 6.16 Coupled structures (a) incremental settlement and (b) incremental rotation response as a function of initial conditions.

The initial settlement greatly affects the incremental settlement experienced by structure during the seismic loading. The incremental settlement reduces as more earthquakes are applied and the structure begins with a greater initial settlement which is consistent with the soil densifying and approaching e_{min}. This is consistent with the modifications made to the analytical model in Section 6.3.2.

The initial rotation has an interesting effect on the rotational response in that the structures with limited or no initial rotation appear to be more prone to larger incremental rotations, whereas if the structure has already experienced some rotations its incremental rotation response is reduced. This may suggest that while the initial earthquake may cause the structure to rotate the following aftershocks may not continue to make the rotation worse, however this was only observed for cases here, where initial rotations were < 1.5º. It should be noted however that there is not a strong trend in Figure 6.16(b), suggesting that the spectral prediction of rotation woud be difficult.

6.4.2 Comparative response of isolated and coupled structures

The coupled structures have shown that their response to the seismic motions is not the same as when they are isolated. This would imply that the SSSI may be having some effect on the response but the amount it is affecting it and how it is introducing this affect still is not clear. Figure 6.17 considers the coupled structures' normalised sway responses for a given configuration as a percentage of its isolated equivalent's normalised sway responses, for the 0.46g case the isolated equivalent value is taken as the average of the three 0.46g earthquakes applied to the isolated structure, whereas the 0.1g was only applied once to the isolated structures. This gives an indication of whether SSSI is beneficial or detrimental to the drift response of the structure.

Considering first the effect of SSSI on the EQ sway of the structures, the SSSI effect on similar structural coupling for both the large and small earthquakes is clearly detrimental for the taller structure. It does however prove beneficial to the shorter structure. When the structures are arranged dissimilarly, the effect of SSSI proves either beneficial or negligible. This would suggest that in the cases where two structures are to be built side by side it would be more beneficial to have two different structures rather than identical structures.

Now considering the effect SSSI has on the total sway of the structures, generally this can be seen to be beneficial, apart from for the short structure in a dissimilar configuration for the smaller earthquake. This response is similar to that reported by Aldaikh *et al.* (2011), whereby the smaller structure's response is amplified when it is coupled with a larger structure, acting like a tuned mass damper and further reducing the response of the tall structure, as seen in Figure 6.17 (d).

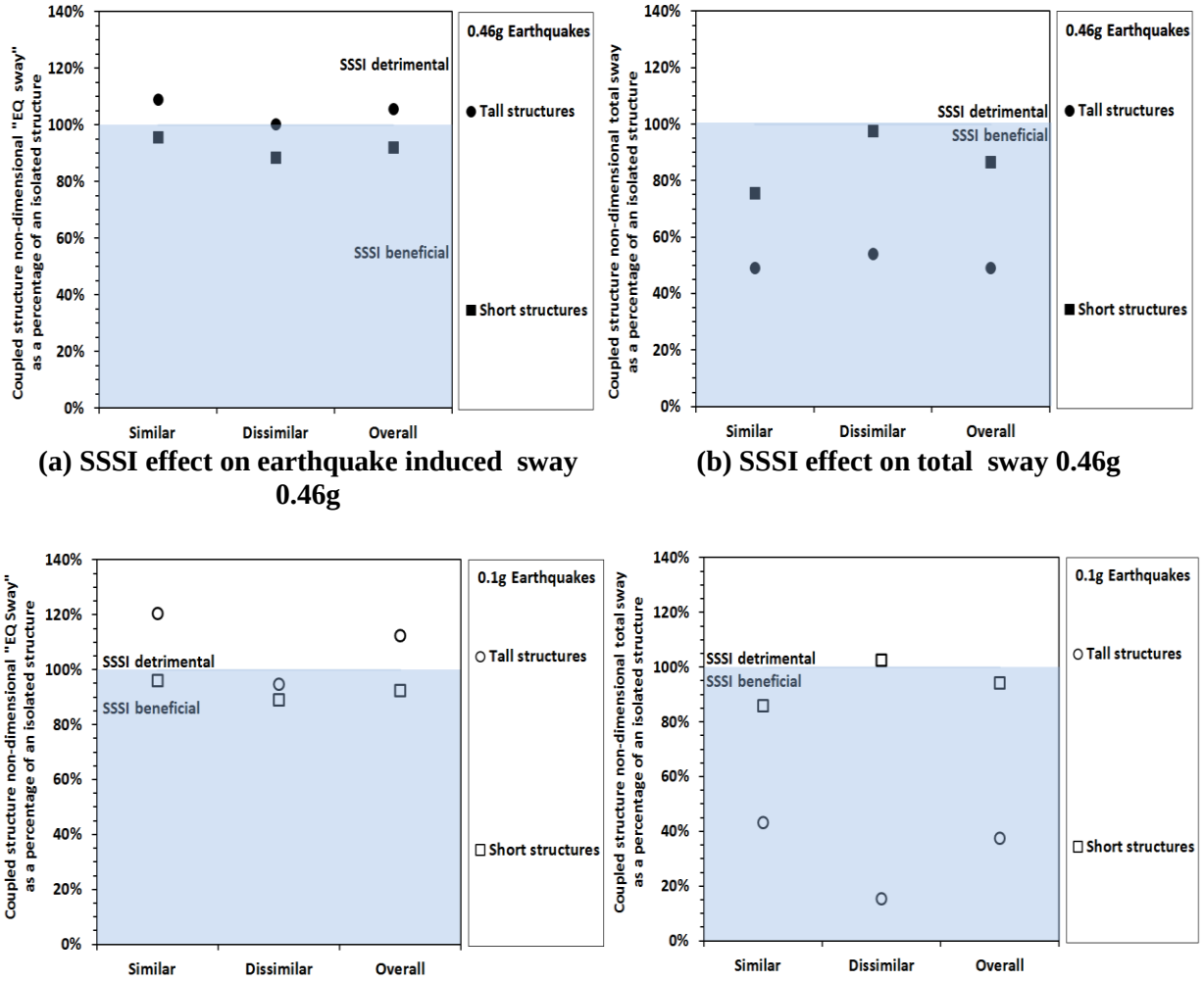

(a) SSSI effect on earthquake induced sway 0.46g

(b) SSSI effect on total sway 0.46g

(c) SSSI effect on earthquake induced sway 0.1g

(d) SSSI effect on total sway 0.1g

Figure 6.17 (a) (d) Coupled structures' average normalised sway response as a percentage of the isolated normalised sway response.

The normalised sway responses that are considered in Figure 6.17 are normalised by three factors, the peak bedrock input acceleration with soil amplification considered in the free field (Sa_g), the natural period of the structure ($T_{n,ssi}$) and the damping (η_{ssi}). The soil amplification was presented in Figure 6.2 and did not show any signs of a significant divergence between the similar structures and dissimilar structures. Figure 6.18(a)(b) presents the equivalent natural period of the

structure ($T_{n,ssi}$) and the equivalent damping (η_{ssi}) for each configuration considered across all earthquakes; in each case this was determined through fitting of a SDOF transfer function across the structure for the centrifuge accelerometer data. The same values for the isolated structures are overlaid on top of the coupled structure data in red. It should be noted that the isolated structures underwent a different sequence of earthquake magnitudes compared to the coupled structures, with a 0.46g earthquake being the first applied in the isolated case, therefore in order to provide a direct comparison between equivalent earthquake magnitudes their sequence has been staggered to suit. Although there is some scatter in the data, it appears that the natural period is shortened in the case of the tall structures, but largely unaffected in the case of the short structures. The equivalent damping appears largely unaffected in the stronger earthquakes and increased by SSSI in the small earthquakes. Neither of these effects would appear to explain the differences in Figure 6.17.

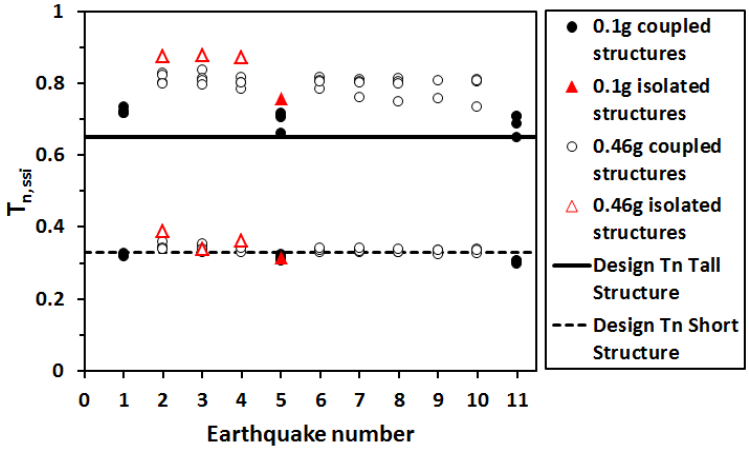

(a) $T_{n,ssi}$

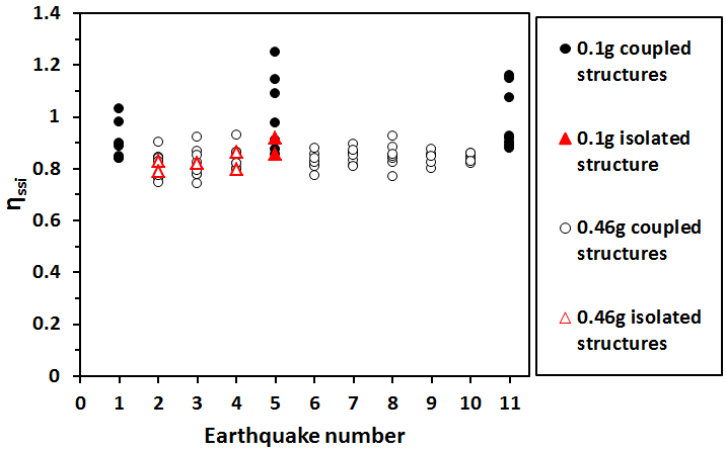

(b) η_{ssi}

Figure 6.18 Changes in (a) natural period ($T_{n,ssi}$) and (b) damping (η_{ssi}) across all tests

A third factor may provide a clue as to how the SSSI is affecting the drift response. While the input to the bedrock and the soil amplification to the free field have been considered, the change in amplification between the free field and the near field may be enough to change the input to the base of the structures and therefore affect the drift response. Determination of a transfer function between the acceleration in the free field and the acceleration directly underneath the structures describes how the amplitude of shaking is modified across the frequency range considered. Finding the ratio between the adjacent structure transfer function and its isolated equivalent then indicates how the response is amplified or dampened by the SSSI. Figures 6.19, 6.20 show this effect.

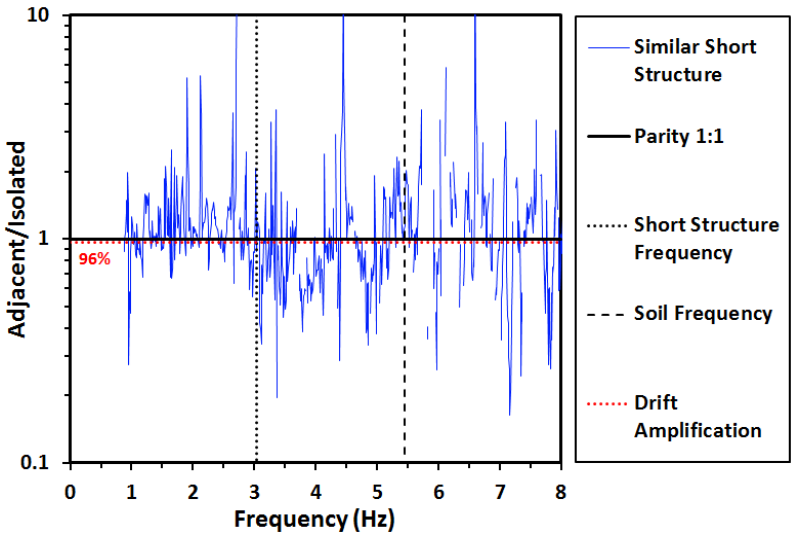

(a) Similar short structure

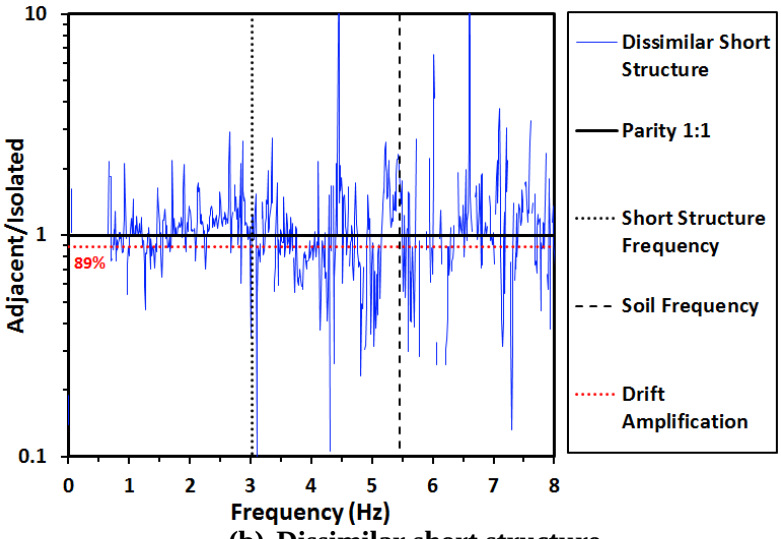

(b) Dissimilar short structure

Figure 6.19 Change in peak ground acceleration due to SSS Interaction for short structures

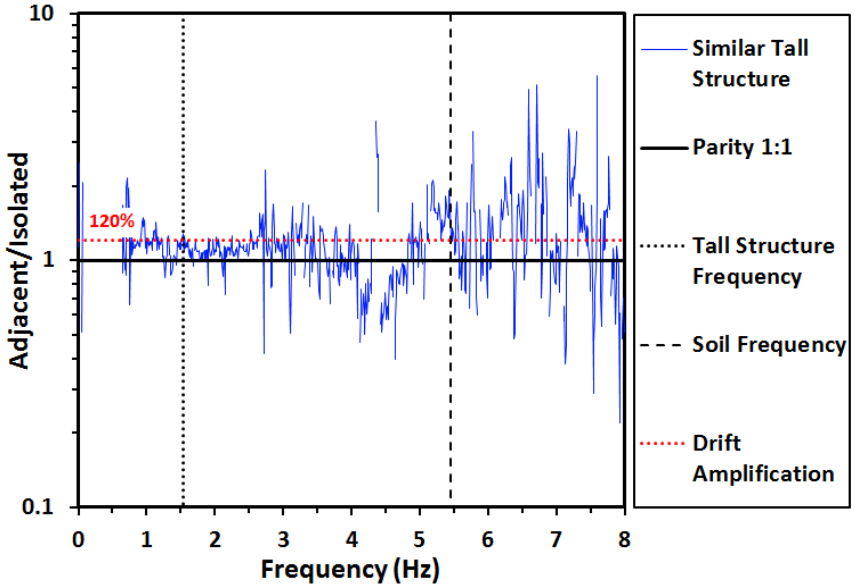

(a) Similar tall structure

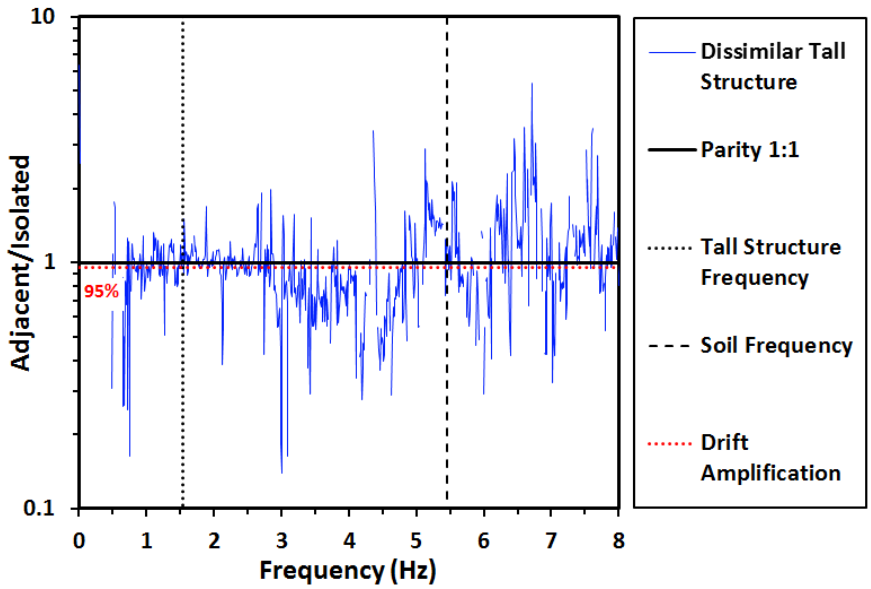

(b) Dissimilar tall structure

Figure 6.20 Change in peak ground acceleration due to SSS Interaction for tall structures

The ratios shown in Figures 6.19 – 6.20 are not uniform and are highly sensitive to the frequency considered. However, the earthquake induced sway amplification factors from Figure 6.17 have been added as red dashed lines and these show some degree of correlation with the size of the transfer function ratio. This suggests that it may be the modification of the input motion to the structure (i.e. that in the near field) which is responsible for the change in earthquake induced sway due to SSSI; however this comparison is not definitive and does not guarantee causation of the effect. While it could provide an explanation for effect of SSSI on the

earthquake induced sway it does not explain the SSSI effect on the total sway. Further research into this response is needed in order to fully classify its cause.

6.5 Summary

The centrifuge tests carried out provided a large amount of data on how both isolated and coupled low rise structures respond to earthquakes, including a "storm" of strong aftershocks. This Chapter assessed this data, picking out key elements of interest and constructing a comparative analysis of how both soil structure interaction, SSI, and structure soil structure interaction SSSI, affect structural response. Adaptations to the response prediction outlined in Chapter 4 were also made in order to account for non-linear soil behaviour. Through this analysis it was observed that:

- The soil amplification under the structure, based on peak values, was actually less than that experienced in the free field. This would suggest that other factors such as destructive interference may be having a large enough effect to overcome the additional amplification that would have been expected due to the settlement of the structure densifying the soil underneath it and therefore being better able to transfer the shear waves.
- Less normalised earthquake induced sway and less normalised total sway was experienced by the taller structure compared to the short structure. This appears to have resulted from incremental bearing capacity failure during the seismic loading causing the structure to rock globally and therefore dissipate energy that would otherwise have been used to induce greater sway.
- The advances to the prediction method, first outlined in Chapter 4, to incorporate a real soil model, proved to be a good match with the centrifuge test data when predicting sway responses. These advances also allowed for a good prediction of peak seismically induced structural settlement to be made.
- The total sway response, inclusive of permanent sway deformation due to permanent rotation, may be limited in total horizontal displacement

to a magnitude similar to the peak predicted elastic response displacement.

- Structure soil structure interaction was shown to be beneficial in terms of earthquake induced sway when considering a pair of dissimilar adjacent structures, however it could also prove detrimental in the case of similar, taller structures.
- SSSI was also shown to be generally beneficial in terms of total sway experienced by a structure except for a small structure paired with a tall structure, in which case it sometimes proved detrimental for the small structure while at the same time increasing its beneficial effect on the tall structure. More research is required into how the SSSI effect changes the response of the structures.

Chapter 7

Conclusions & future work

7.1 Overview

Accurately predicting the response of simple frame structures to seismic loading is important in order to adequately design the structure to survive the event with limited structural and response damage. The response spectral analysis, outlined in Eurocode 8, (BSI, 2008b), can give a good estimate of the elastic displacement response of the structure, provided that its initial rotational conditions are neutral. However in order for this estimate to be representative of the structure concerned, the parameters it is based on, namely the natural period of the structure and the overall system damping, require accurate prediction. Current methods often over simplify these predictions, ignoring factors which can influence their predicted values. The work presented in this thesis aims to outline the additional factors which influence this prediction, and therefore influence the response of the structures to seismic loading, through both finite element analysis and physical centrifuge model analysis. The factors that have been investigated are the joint stiffness of the structural frame (from fully pinned to fully fixed conditions), the foundation conditions (both a fixed base condition and a shallow foundation with soil structure interaction condition have been investigated), the geometry of the frame, and the impact of adjacent structures on the response of a structure. The mechanisms of response which combine to form the total response of the structures are outlined and their influence discussed.

7.2 New spectral model

A detailed method of predicting the natural period of semi rigid frames, as developed by Hellesland (2008), is further developed to account for the influence of the soil structure interaction on both the natural period, and the damping of the system. This advanced method also allows for the prediction of the earthquake induced settlement of the structures to be predicted, and can be applied to a sequence of strong ground vibrations. This method is entirely spectral and does not require the use of complex FE analysis. It has been validated extensively against FE and centrifuge test data.

7.3 Response mechanisms

The finite element analysis showed that while the sway response of a fixed base frame is composed entirely of its inter-storey drift, the sway response of a frame with soil structure interaction is more complex and composed of three response mechanisms. These response mechanisms are:

- A global structural rotation mechanism, whereby the full structure rocks on its foundations, induces some damping to the system.

- A local rotation mechanism, whereby the foundations themselves rock, further dampens the system.

- Inter-storey drift. This is the same mechanism seen in the fixed base case, whereby the top of the column moves in relation to the base of the column. This puts a lot of strain on the column, with moments within the column increasing until moment capacity is reached.

The presence of the rotational mechanisms were shown to dissipate some of the energy of the earthquake resulting in a reduction in the amount of inter-storey drift experienced by the frame, compared to its fixed base counterpart. Both rotational mechanisms appeared to have ‘self centring’ properties in the finite element case, however this was undertaken on an elastic soil.

In the centrifuge analysis it was not possible to monitor the local foundation rotation with high enough accuracy. However the earthquake induced sway response of the structure and the permanent global rotation was monitored. The total sway response, a combination of the earthquake induced sway and the horizontal displacement due to the permanent global rotation may be limited in total horizontal displacement to a magnitude similar to the peak predicted elastic response displacement. This results in the damping of the elastic EQ sway response of the structure.

7.4 Factors influencing the response

The effect of increasing the flexibility of the system, by increasing the height or length of the structural elements, by reducing the joint stiffness or by introducing a compliant base as opposed to a fixed base, will increase the overall response, sway, of the structure. This increase in response falls in line with the increase in natural period of the system that would be introduced by making the same changed to the system.

Soil structure interaction introduces the additional rotational mechanisms to the response of the structure. The main factor controlling the magnitude of the rotational mechanisms induced by SSI was the geometry of the structure. The magnitude of both the elastic global rotation observed in the finite element analysis and the permanent global rotation observed in the centrifuge analysis are heavily dependant on geometry of the system, with taller narrower structures being more susceptible. Narrow/tall frames were also seen to produce local rotation, in the finite element analysis, similar in magnitude to the same frames global rotation. In wider frames it was able to induce larger magnitudes of rotation, compared to the same frames magnitude of global rotation. Both of these mechanisms help reduce the amount of inter-storey drift experienced by the frame and therefore protecting the structural elements of the frame, however the global rotation mechanism was seen to produce some permanent rotations (in cases where some initial rotation was already present) in the centrifuge tests, a response which my leave the structure exposed to cumulative rotation during future earthquakes.

Structure soil structure interaction was shown to be beneficial in terms of earthquake induced sway when considering dissimilar adjacent structures; however it

could also prove detrimental as was the case for the similar tall structures. SSSI was also shown to be generally beneficial in terms of total sway (inclusive of the global rotation induced lateral displacement) experienced by a structure except for a small structure paired with a tall structure, in which case it sometimes proved detrimental for the small structure while at the same time increasing its beneficial effect on the tall structure.

7.5 Prediction method

The spectral analysis method outlined by Eurocode 8, (BSI, 2008b), was used as the method of predicting the seismic response of the structures. The advanced model, proposed by Hellesland (2008), was chosen to form the basis of the natural period prediction. The finite element models showed that increased flexibility of a structure, provided by the lengthening of both the columns and beams of the structure, along with the flexibility of the joint system, had an influence on the structural response to seismic loading. The Hellesland method accounts for the influence of a flexible beam, column and joint system in its prediction and was therefore ideal to form the basis of the prediction method used in this research.

The original Hellesland method is firstly validated against the finite element analysis results for the fixed base case, Figure 4.4 and Figure 4.18, providing a strong correlation. The method is then adapted in order to account for a flexible base and soil structure interaction with an elastic soil, as used in the finite element model, Section 4.2.1.2., and subsequently validated against the finite element results in Figure 4.25. This again shows a good correlation with the results and also an improvement compared to traditional methods of predicting the natural period. The method of including the soil to the prediction also allows for a more accurate prediction of the damping of the system to be made, Figure 4.28.

In Chapter 6 the method is further adapted to account for a real soil response and validated against the results obtained from the centrifuge analysis, Figure 6.8. The inclusion of the real soil increases the benefits of this method by allowing for an accurate prediction of the settlement of the structure induced by an earthquake, even after multiple preceding earthquakes inducing settlement, Figure 6.13.

Increasing the accuracy of the prediction of natural period improves the elastic displacement prediction made by using the Eurocode 8, (BSI, 2008b), spectral method.

7.6 Implications and further research

A more accurate prediction of the natural period of the structure, the system damping and the settlement resulting from seismic activity allow for a more accurate prediction of the overall response of a system during a seismic event to be made.

Understanding the response mechanisms, the benefits they introduce to the systems response, and the factors controlling their magnitudes, will enable engineers to design structures which maximise the benefits from these mechanisms. Further research is required into the relationship between the local and global rotational mechanisms so that a structure which maximises the benefits of both mechanisms can be determined. Finite element models which better replicate the plastic deformation of soil, or a physical model with better instrumentation which more accurately reports each of the mechanisms separately would be required; unfortunately both of these were outside the scope of this research.

A more detailed analysis of the response of frames which undergo permanent rotational displacement is required in order to be able to expand the prediction to include this mechanism. Initial observations suggested that the magnitude of displacement would be similar to that induced by the elastic response prediction but much more analysis would be required in order to validate this observation.

More research is also required into how the SSSI effect changes the response of the structures. Additional finite element analysis of the interaction may shed some light on how the mechanism effects changes but again a more realistic soil model would prove beneficial.

References

Abdalla, K. M. and W.-F. Chen (1995). "Expanded database of semi-rigid steel connections." Computers & Structures **56**(4): 553-564.

Actidyn (2008). Model Q67-2 Earthquake Simulator Design Review Report. Trappes, France, Actidyn Systems.

Aggarwal, A. K. (1990a). Behavior of Flexible Beam-to-Column Connections. The Institution of Engineers Australia Structural Engineering Conference**:** 462-467.

Aggarwal, A. K. (1990b). "Behaviour of flexible end plate beam-to-column joints." Journal of Constructional Steel Research **16**(2): 111-134.

Aldaikh, H., N. Alexander and E. Ibraim (2011). Exploration of structure-soil-structure interaction dynamics. The Thirteenth International Conference on Civil, Structural and Environmental Engineering Computing. Chania, Crete, Greece.

Algie, T., M. Pender, R. Orense and L. Wotherspoon (2010). Dynamic field testing of shallow foundations subject to rocking. New Zealand Society for Earthquake Engineering Conference, Paper No.

Analog Devices (2010). ADXL78 Datasheet http://www.analog.com/static/imported-files/data_sheets/ADXL78.pdf.

Anastasopoulos, I., R. Kourkoulis, F. Gelagoti and E. Papadopoulos (2012). "Rocking response of SDOF systems on shallow improved sand: An experimental study." Soil Dynamics and Earthquake Engineering **40**(0): 15-33.

Barakat, M. A. K. (1988). Simplified Design Analysis of Frames with Semi-rigid Connections. School of Civil Engineering. West Lafayette, Purdue University.

Bard, P. Y., J. L. Chazelas, P. Guéguen, M. Kham and J. F. Semblat (2006). Site-City Interaction. Assessing and Managing Earthquake Risk. C. Oliveira, A. Roca and X. Goula, Springer Netherlands. **2:** 91-114.

Bertalot, D. (2013). Seismic behaviour of shallow foundations on layered liquefiable soils. Department of Civil Engineering. Dundee, University of Dundee. **Ph.D Thesis**.

Bielak, J. (1974). "Dynamic behaviour of structures with embedded foundations." Earthquake Engineering & Structural Dynamics **3**(3): 259-274.

Bolisetti, C. and D. A. Whittaker (2011). Seismic Structure-Soil-Structure Interaction in Nuclear Power Plant Structures. SMIRT 21 - 21st International Conference on Structural Mechanics in Reactor Technology. New Delhi.

Boulanger, R., C. Curras, B. Kutter, D. Wilson and A. Abghari (1999). "Seismic Soil-Pile-Structure Interaction Experiments and Analyses." Journal of Geotechnical and Geoenvironmental Engineering **125**(9): 750-759.

Boutin, C. (2004). "Assessment of the Urbanization Effect on Seismic Response." Bulletin of the Seismological Society of America **94**(1): 251-268.

Brennan, A., N. Thusyanthan and S. Madabhushi (2005). "Evaluation of Shear Modulus and Damping in Dynamic Centrifuge Tests." Journal of Geotechnical and Geoenvironmental Engineering **131**(12): 1488-1497.

Brennan, A. J. (2004). Transfer function MATLAB script P. Madden.

BSI (2008a). Eurocode 3: Design of steel structures, BSI Standards.

BSI (2008b). Eurocode 8. Design of Structures for Earthquake Resistance. Foundations, Retaining Structures and Geotechnical Aspects, BSI Standards.

CCBFC (2010). Canadian Commission on Building and Fire Codes : The National Building Code of Canada. National Research Council, Ottawa.

CDS, C. (2006). Congleton HST 95 Washed, Surface Treated and Graded Silica Sand Partical Size Distribution report GWYNEDD, C.D.S. Consultants.

Chen, W. and N. Kishi (1989). "Semirigid Steel Beam-to-Column Connections: Data Base and Modeling." Journal of Structural Engineering, ASCE **115**(1): 105-119.

Chen, W. F. and E. M. Lui (1986). Recent developments in structural connections. Advances in Tall Buildings. L. S. Beedle. New York, Van Nostrand Reinhold**:** 353-365.

Chen, W. F. and E. M. Lui (1991). Stability Design of Steel Frames, Taylor & Francis.

Chen, Z., N. W. Trombetta, T. C. Hutchinson, H. B. Mason, J. D. Bray and B. L. Kutter (2013). "Seismic System Identification Using Centrifuge-based Soil-Structure Interaction Test Data." Journal of Earthquake Engineering **17**(4): 469-496.

Chopra, A. K. (2011). Dynamics of Structures: Theory and Applications to Earthquake Engineering, Prentice Hall/Pearson Education.

Clouteau, D. and D. Aubry (2001). "Modifications of the ground motion in dense urban areas." Journal of Computational Acoustics **09**(04): 1659-1675.

Crisfield, M. A. (1981). "A fast incremental/iterative solution procedure that handles "snap-through"." Computers & Structures **13**(1–3): 55-62.

Davies, M. C. R., T. A. Newson and M. F. Bransby (2001). Geotechnical centrifuge modelling at the University of Dundee. Proceedings of the International Symposium on Geotechnical Centrifuge Modelling and Networking. B. Kutter. Hong Kong University of Science and Technology**:** 15-16.

Davison, J. B., P. A. Kirby and D. A. Nethercot (1987). "Rotational stiffness characteristics of steel beam-to-column connections." Journal of Constructional Steel Research **8**(0): 17-54.

Dowrick, D. J. (1977). Earthquake resistant design: a manual for engineers and architects, Wiley.

Dutta, S. C. and R. Roy (2002). "A critical review on idealization and modeling for interaction among soil–foundation–structure system." Computers & Structures **80**(20–21): 1579-1594.

Fiorakis, A. (2011). Seismic performance of adjacent multi-storey structures, University of Dundee. **Masters**.

Gajan, S. and B. L. Kutter (2008). Numerical simulations of rocking behavior of shallow footings and comparisons with experiments. British Geotechinical Association (BGA) International Conference on Foundations. Dundee, Scotland.

Gajan, S., B. L. Kutter and J. Thomas (2005). Physical and numerical modeling of cyclic moment-rotation behavior of shallow foundations. 16th Intl. Conf. Soil Mechanics and Geotechnical Engineering. Osaka Japan.

GFD (2004). Government of the Federal District: Complementary technical norms for seismic design. Mexico, Official gazette of the federal district.

Ghergu, M. and I. R. Ionescu (2009). "Structure–soil–structure coupling in seismic excitation and "city effect"." International Journal of Engineering Science **47**(3): 342-354.

Ghosh, B. and S. P. G. Madabhushi (2007). "Centrifuge modelling of seismic soil structure interaction effects." Nuclear Engineering and Design **237**(8): 887-896.

Glardini, D., G. Grunthal, K. Shedlick and P. Zhang (1999). The GSHAP Global Seismic Hazard Map, Annali di Geoisica 42 (6), 1225-1228.

Goverdhan, A. V. (1983). A Collection of Experimental Moment Rotation Curves and Evaluation of Prediction Equations for Semi-Rigid Connections. Nashville, TN., Vanderbilt University. **Masters:** 490.

Groby, J.-P. and A. Wirgin (2008). "Seismic motion in urban sites consisting of blocks in welded contact with a soft layer overlying a hard half-space." Geophysical Journal International **172**(2): 725-758.

Grondin, M. (2004). Advance Simulation Tools Soil-Structure Interaction Damage Synthesis Project DS-3, Michigan State University.

Hansen, J. B. (1970). A revised and extended formula for bearing capacity. Tests and formulas concerning secondary consolidation. Copenhagen, The Danish Geotechnical Institute.

Hardin, B. O. and W. L. Black (1969). "Vibration modulus of normally consolidated clay." Journal of the soil mechanics and foundations division, ASCE **95**(6): 1531-1537.

Hellesland, J. (2008). Approximate second order analysis of unbraced frames reflecting inter-storey interaction in single curvature regions, University of Oslo**:** 26.

Hellesland, J. (2009). "Extended second order approximate analysis of frames with sway-braced column interaction." Journal of Constructional Steel Research **65**(5): 1075-1086.

Hellesland, J. and R. Bjorhovde (1996). "Restraint Demand Factors and Effective Lengths of Braced Columns." ASCE **122**(10): 1216-1224.

Housner, G. W. (1963). "The behavior of inverted pendulum structures during earthquakes." Bulletin of the Seismological Society of America **53**(2): 403-417.

Hügel, H., S. Henke and S. Kinzler (2008). High-performance Abaqus simulations in soil mechanics. Proceedings of Abaqus users conference.

Hung, H.-H., K.-Y. Liu, T.-H. Ho and K.-C. Chang (2011). "An experimental study on the rocking response of bridge piers with spread footing foundations." Earthquake Engineering & Structural Dynamics **40**(7): 749-769.

ICC (2009). International code council: International Building Code. Washington D.C. .

Idriss, M. (1999). An update to the Seed-Idriss simplified procedure for evaluating liquefaction potential. TRB Workshop on New Approaches to Liquefaction Washington D.C. , Federal Highway Administration.

Jennings, P. C. (1970). "Distant motions from a building vibration test." Bulletin of the Seismological Society of America **60**: 2037 - 2043.

Jennings, P. C. and J. Bielak (1972). Dynamics of Building-soil Interaction, Earthquake Engineering Research Laboratory.

Kanamori, H., J. Mori, D. L. Anderson and T. H. Heaton (1991). "Seismic excitation by the space shuttle Columbia." Nature **349**(6312): 781-782.

Kausel, E. (2010). "Early history of soil–structure interaction." Soil Dynamics and Earthquake Engineering **30**(9): 822-832.

Kham, M., J.-F. Semblat, P.-Y. Bard and P. Dangla (2006). "Seismic Site–City Interaction: Main Governing Phenomena through Simplified Numerical Models." Bulletin of the Seismological Society of America **96**(5): 1934-1951.

Kim, W. Y. and G. R. Baum (2001). Seismic Observations during September 11, 2001, Terrorist Attack, Lamont-Doherty Earth Observatory of Columbia University, New York and Environmental Geology and Mineral Resources Program, Maryland Geological Survey, Baltimore.

Knappett, J. A. and R. F. Craig (2012). Craig's soil mechanics. Abingdon, Spon Press.

Knappett, J. A., S. K. Haigh and S. P. G. Madabhushi (2006). "Mechanisms of failure for shallow foundations under earthquake loading." Soil Dynamics and Earthquake Engineering **26**(2–4): 91-102.

Kourkoulis, R., I. Anastasopoulos, F. Gelagoti and P. Kokkali (2012). "Dimensional Analysis of SDOF Systems Rocking on Inelastic Soil." Journal of Earthquake Engineering **16**(7): 995-1022.

Kutter, B. L. and D. L. Wilson (2006) Physical Modelling of Dynamic Behavior of Soil-foundation-superstructure Systems. International Journal of Physical Modelling in Geotechnics **6**, 1-12

Lauder, K. (2010). The performance of pipeline ploughs Department of Civil Engineering. Dundee, University of Dundee. **Ph.D Thesis**.

Lee, T. H. and D. A. Wesley (1973). "Soil-structure interaction of nuclear reactor structures considering through-soil coupling between adjacent structures." Nuclear Engineering and Design **24**(3): 374-387.

LeMessurier, W. M. (1977). "A practical method of second order analysis." ENG J AISC **14**(2): 49-67.

Luco, J. E. and L. Contesse (1973). "Dynamic structure-soil-structure interaction." Bulletin of the Seismological Society of America **63**(4): 1289-1303.

Maxwell, S. M., J. H. Howlett and W. M. Jenkins (1981). A realistic approach to the performance and application of semi-rigid jointed structures Joints in structural steelwork. J. H. Howlett, W. M. Jenkins and S. R., Pentech Press**:** 2.71-72.98.

Mayne, P. W. and F. H. Kulhawy (1982). "K0-OCR Relationships in Soil." Journal of the Geotechnical Engineering Division, ASCE **108**(GT6): 851-872.

Menglin, L., W. Huaifeng, C. Xi and Z. Yongmei (2011). "Structure–soil–structure interaction: Literature review." Soil Dynamics and Earthquake Engineering **31**(12): 1724-1731.

Mises, R. V. (1913). "Mechanik der festen Körper im plastisch- deformablen Zustand." Nachrichten von der Gesellschaft der Wissenschaften zu Göttingen, Mathematisch-Physikalische Klasse.

Moore, D. B. and P. A. C. Sims (1986). "The influence of backing plates on the behaviour of extended end plate connections." Journal of Constructional Steel Research **6**(2): 95-122.

Muir Wood, D. (2004). Geotechnical modelling. London and New York, Spon Press.

Mylonakis, G. and G. Gazetas (2000). "SEISMIC SOIL-STRUCTURE INTERACTION: BENEFICIAL OR DETRIMENTAL?" Journal of Earthquake Engineering **4**(3): 277-301.

Padrón, L. A., J. J. Aznárez and O. Maeso (2009). "Dynamic structure–soil–structure interaction between nearby piled buildings under seismic excitation by BEM–FEM model." Soil Dynamics and Earthquake Engineering **29**(6): 1084-1096.

Pala, M., N. Caglar, M. Elmas, A. Cevik and M. Saribiyik (2008). "Dynamic soil–structure interaction analysis of buildings by neural networks." Construction and Building Materials **22**(3): 330-342.

Paolucci, R. and A. Pecker (1997). "Seismic bearing capacity of shallow strip foundations on dry soils." Soils and Foundations **37**(2): 97-105.

Parlett, B. N. (1980). The symmetric eigenvalue problem, SIAM.

PEER (2010). Ground Motion Database University of California. **http://peer.berkeley.edu/peer_ground_motion_database/**.

Philips, J. and J. A. Packer (1981). The effect of plate thickness on flush end-plate connections. Joints in structural steelwork. J. H. Howlett, W. M. Jenkins and R. Stainsby, Pentech Press**:** 677-692.

Pitilakis, D., M. Dietz, D. M. Wood, D. Clouteau and A. Modaressi (2008). "Numerical simulation of dynamic soil–structure interaction in shaking table testing." Soil Dynamics and Earthquake Engineering **28**(6): 453-467.

Poulus, H. G. A. and E. H. Davis (1980). Pile Foundation Analysis and Design, John Wiley and Sons.

Pradel, D. (1998). "Procedure to evaluate earthquake-induced settlements in dry sandy soils." Journal of Geotechnical and Geoenvironmental Engineering **124**(4): 364-368.

Richart, F. E. and R. V. Whitman (1967). "Comparison of footing vibration tests with theory." Journal of Soil Mechanics & Foundations Div **93**(SM6): 143-168.

Schofield, A. N. (1980). "Cambridge geotechnical centrifuge operations." Geotechnique **30**(3): 227-268.

Shakib, H. and A. Fuladgar (2004). "Dynamic soil–structure interaction effects on the seismic response of asymmetric buildings." Soil Dynamics and Earthquake Engineering **24**(5): 379-388.

Simulia (2009). Abaqus 6.9 User Documentation.

Solartron Metrology (2013). "LVDT, Half Bridge and Digital Transducer Theory " http://www.solartronmetrology.com/service-support/knowledge-base/theory.aspx. 2013.

Spyrakos, C. C., I. A. Koutromanos and C. A. Maniatakis (2009). "Seismic response of base-isolated buildings including soil–structure interaction." Soil Dynamics and Earthquake Engineering **29**(4): 658-668.

Stewart, J. P., R. B. Seed and G. L. Fenves (1999). Seismic soil-structure interaction in buildings. II: Empirical findings, ASCE.

Stone, K. J. L. and V. Merrien-Soukatchoff (2007). Physical and numerical modelling of chalk slopes. Landslides and Climate Change: Challenges and Solutions, Taylor & Francis.

Tata Steel (2011). Interactive Blue Book - Steel section design data, section properties and member capacities.

Taylor, R. N. (1995). Geotechnical centrifuge technology. London, Blackie Academic & Professional

Tazarv, M. (2011). SPEC MATLAB Script. P. Madden.

Terzaghi, K. (1943). Theoretical soil mechanics. New York, John Wiley & Sons.

Tsogka, C. and A. Wirgin (2003). "Simulation of seismic response in an idealized city." Soil Dynamics and Earthquake Engineering **23**(5): 391-402.

Uenishi, K. (2010). "The Town Effect: Dynamic Interaction between a Group of Structures and Waves in the Ground." Rock Mechanics and Rock Engineering **43**(6): 811-819.

Ugalde, J. A., B. L. Kutter, B. Jeremic and S. Gajan (2007). Centrifuge modeling of rocking behavior of bridges on shallow foundations. Proc., 4th Intl. Conf. Earthquake Geotechnical Engineering.

Veletsos, A. S. and J. W. Meek (1974). "Dynamic behaviour of building-foundation systems." Earthquake Engineering & Structural Dynamics **3**(2): 121-138.

Veletsos, A. S. and V. V. Nair (1975). "Seismic interaction of structures on hysteretic foundations." Journal of Structural Engineering, ASCE **101**(1): 109-129.

Wang, C. K. (1983). Intermediate Structural Analysis, Mcgraw-Hill Book Comp.

Weissman, K. and J. H. Prevost (1989). "Centrifugal modelling of dynamic soil-structure interaction." Earthquake Engineering & Structural Dynamics **18**(8): 1145-1161.

Wirgin, A. and P.-Y. Bard (1996). "Effects of buildings on the duration and amplitude of ground motion in Mexico city." Bulletin of the Seismological Society of America **86**(3): 914-920.

Wolf, J. P. (1985). Dynamic soil-structure interaction, Prentice-Hall.

Wong, H. L. and M. D. Trifunac (1975). "Two-dimensional, antiplane, building-soil-building interaction for two or more buildings and for incident planet SH waves." Bulletin of the Seismological Society of America **65**(6): 1863-1885.

Xu, L. and Y. Liu (2002). "Story stability of semi-braced steel frames." Journal of Constructional Steel Research **58**(4): 467-491.

Yahyai, M., M. Mirtaheri, M. Mahoutian and A. S. Daryan (2008). "Soil structure interaction between two adjacent buildings under earthquake load." American Journal of Engineering and Applied Sciences **1**(2): 121.

Yazdchi, M., N. Khalili and S. Valliappan (1999). "Dynamic soil–structure interaction analysis via coupled finite-element–boundary-element method." Soil Dynamics and Earthquake Engineering **18**(7): 499-517.

Yi, F. (2010). Procedure to evaluate seismic settlement in dry sand based on shear wave velocity. 9th US National and 10th Canadian Conference on Earthquake Engineering: Reaching Beyond Borders. Toronto.

Zandonini, R. and P. Zanon (1988). Experimental analysis of end plate connections. Connections in Steel Structures; Behavior, Strength and Design. R. Bjorhovde, J. Brozzetti and A. Colson. London, Elsevier Applied Science Publishers Ltd**:** 41-51.

Zeng, X. and A. N. Schofield (1996) Design and performance of an equivalent-shear-beam container for earthquake centrifuge modelling. Geotechnique **46**, 83-102

Appendix A

Design of structural frame elements

Initially more frame geometries were planned to be analysed. These included a 5m high 10m wide frame supporting a 5m slab. Unfortunately due to time restraints some of the original planned geometries were not analysed, including this, the largest, frame. However as outlined in Chapter 3, the frame was designed so that the structural elements would be able to support all of the frame geometries without having to change the structural element sizes', this was to prevent additional factors such as slenderness of the structural elements and differential moment capacities of the elements influencing the response. Therefore the frame element was designed to be suitable for a 10m wide frame. By the time the decision was made to reduce the number of frame geometries to be used a vast amount of the analysis had already been carried out for both the 5m × 8m frame and the 3m × 3m frame, it was therefore decided that a redesign of the elements to suit the new largest frame was not practical due to time restraints.

The design of the slab, beam and column elements for the 10m × 3m frame to Eurocode 3 design, are presented in the following pages.

Civil Engineering Department	CONTRACT Simple Frame DESIGN			JOB REF.
The University DUNDEE	Drawing Ref.	Calculations by	Checked by	Calc. Sheet No. 1
	Part of Structure 10m span Slab			Date

Ref.	CALCULATIONS	OUTPUT

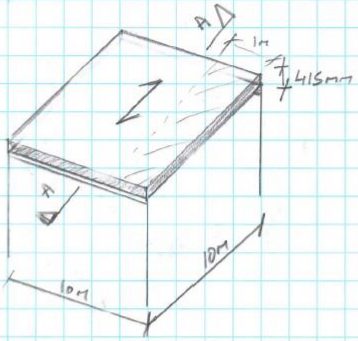

SECTION A-A

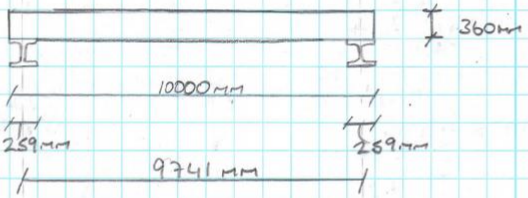

Assume $f_{ck} = 30 N/mm^2$
$f_{yk} = 460 N/mm^2$

Environment conditions : Exposure class 1

Assume Reinforcement, ρ, is 0·5%

Check From Table 4.14 basic span/depth ratios for lightly stressed member correspond to $\rho = 0.5\% = 25$

Table 4.14 Minimum effective depth $(d) = \frac{\text{span}}{\text{basic ratio}} = \frac{9741}{25} \approx 390\,mm$

$d = 390mm$ and assume ϕ of main steel as 10mm and cover to reinforcement $(c) = 20mm$

Overall slab depth, h, is

$$h = d + \frac{\phi}{2} + c = 390 + \frac{10}{2} + 20 = 415mm$$

Civil Engineering Department	CONTRACT FRAME DESIGN			JOB REF.
The University DUNDEE	Drawing Ref.	Calculations by	Checked by	Calc. Sheet No. 2
	Part of Structure 10M SPAN SLAB			Date

Ref.	CALCULATIONS	OUTPUT

LOADING

Permanent

Self-weight of slab (g_k)

$= 0.415 \times 24\ (kN/m^3) = 9.96\ kN/m^2$

ULTIMATE LOAD for 1M width of span, total ultimate load is

$(1.35 g_k + 1.5 q_k)$ span

$(1.35 \times 9.96)\ 9.741 = 130.98\ kN$

Design Moment

Max design moment $(M) = \frac{WL}{8} = \frac{130.98 \times 9.741}{8}$

$M = 159.5\ kNM$

Ultimate Moment

Ultimate moment resistance, M_u is

$M_u = 0.167\ f_{cu}\ b\ d^2$

$= 0.167 \times 30 \times 1000 \times 390^2 \times 10^{-6}$ (1m of slab)

$= 762\ kNM$

Since (M_u) 762kNM > 159.5 kNM (M)

no compression reinforcement is required.

Civil Engineering Department	CONTRACT Frame Design			JOB REF.
The University DUNDEE	Drawing Ref.	Calculations by	Checked by	Calc. Sheet No. 3
	Part of Structure 10m Span Slab			Date

Ref.	CALCULATIONS	OUTPUT

MAIN REINFORCEMENT (A_{s_1})

$$K_o = \frac{M}{f_{ck}\, b\, d^2} = \frac{159.5 \times 10^6}{30 \times 1000 \times 390^2} = 0.035$$

$$z = d\left[0.5 + \sqrt{(0.25 - 3K_o/3.4)}\right]$$

$$= 390\left[0.5 + \sqrt{(0.25 - 3 \times 0.035/3.4)}\right]$$

$$z = 275.5 \text{ MM}$$

$$A_{s_1} = \frac{M}{0.87 f_y k_z} = \frac{159.5 \times 10^6}{0.87 \times 460 \times 275.5} = 1446.65 \text{ MM}^2$$

Hence from bar size/spacing chart

T10 @ 75MM spacing (A_s 1050) are NOT SUITABLE

But

T10 @ 50MM spacing (A_s 1570) is SUITABLE

Max bar spacing $< 3h = 3 \times 415 = 1245 \text{ MM} > 500 \text{ MM}$ ok

Minimum reinforcement area = $0.0015bd =$

$0.0015 \times 10^3 \times 390 = 585 \text{ MM}^2/\text{M}$

$\therefore$ ok

Reinforcement Ratio, ρ, in this case is

$$\rho = \frac{A_s}{bd} = \frac{1570}{1000 \times 390} = 0.00403$$

$$= 0.403\%$$

Civil Engineering Department	CONTRACT FRAME DESIGN			JOB REF.
The University DUNDEE	Drawing Ref.	Calculations by	Checked by	Calc. Sheet No. 4
	Part of Structure 10m SPAN SLAB			Date

Ref.	CALCULATIONS	OUTPUT

ESTIMATED EFFECTIVE DEPTH OF SLAB

Design service stress, $\sigma_s = \frac{5 f_{yk} A_{req}}{8 A_{prov}}$

$= \frac{5 \times 460 \times 1446.65}{8 \times 1570}$

$= 264.91 \ N/mm^2$

Modification factor $= \frac{250}{\sigma_s} = \frac{250}{264.91} = 0.944$

Hence modified span/depth ratios for

$\rho = 0.5\% = (25 \times 0.944) = 23.6$

$\rho = 0.15\% = (34 \times 0.944) = 32.096$

Interpolate for $\rho = 0.403\%$ = 29.741

Hence minimum depth, d, is

$d = \frac{\text{span}}{\text{span/depth ratio}}$

$= \frac{9741}{29.741} = 327.5 \text{ mm} < \text{assumed} (= 390 \text{ mm})$

∴ use a depth d = 335 mm

New overall depth $= 335 + \frac{\phi}{2} + c$

$= 335 + 5 + 20 =$ 360 mm thick slab.

Civil Engineering Department	CONTRACT FRAME DESIGN			JOB REF.
The University DUNDEE	Drawing Ref.	Calculations by	Checked by	Calc. Sheet No. 5
	Part of Structure 10m Span Slab			Date

Ref.	CALCULATIONS	OUTPUT

New updated Loadings for smaller slab

(g_k) Self weight of slab

$= 0.360 \times 24\ (kN/m^3) = 8.64\ kN/m^2$

ULTIMATE LOAD
For 1m width of span

$(1.35 g_k + 1.5 q_k)$ span

$(1.35 \times 8.64)\ 9.741 = 113.62\ kN/m^2$

Design Moment

Max design moment $(M) = \frac{wL}{8} = \frac{113.62 \times 9.741}{8}$

$M = 138.35\ kNm$

ULTIMATE Moment Resistance (M_u)

$M_u = 0.167 f_{cu} b d^2$

$= 0.167 \times 30 \times 1000 \times 335^2 \times 10^{-6}$

$= 562.25\ kNm$

Since (M_u) $562.25\ kNm > 138.35\ kNm$ (M)

∴ no compression reinforcement required.

Main Reinforcement (A_{si})

$k_o = \frac{M}{f_{cu} b d^2} = \frac{138.35 \times 10^6}{30 \times 1000 \times 335^2} = 0.0411$

$z = d\left[0.5 + \sqrt{(0.25 - 3k_o/3.4)}\right]$

$z = 335\left[0.5 + \sqrt{(0.25 - (3 \times 0.0411)/3.4)}\right]$

$z = 322.38\ mm$

$A_{si} = \frac{M}{0.87 \times f_y \times k_z} = \frac{138.35 \times 10^6}{0.87 \times 460 \times 322.38} = 1072.84\ mm^2$

Civil Engineering Department	CONTRACT FRAME DESIGN			JOB REF.
The University DUNDEE	Drawing Ref.	Calculations by	Checked by	Calc. Sheet No. 6
	Part of Structure 10M SPAN SLAB			Date

Ref.	CALCULATIONS	OUTPUT

BAR SIZE SPACING CHART

USE T10 @ 50 mm spacing (As 1570)

Max bar spacing $< 3h = 3 \times 360 = 1080 > 500$
Actual = 50 mm ∴ ok

Min Reinforcement area = $0.0015\ b\ d = 0.0015 \times 1000 \times 335$
$= 502.5\ mm^2/m$ ∴ ok.

Reinforcement Ratio, ρ, in this case is

$$\rho = \frac{A_s}{bd} = \frac{1570}{1000 \times 335} = 0.00469 = 0.469\%$$

ESTIMATED EFFECTIVE DEPTH OF SLAB

DESIGN SERVICE STRESS, $\sigma_s = \frac{5\ f_{yk}\ A_{req}}{8\ A_{prov}}$

$$= \frac{5 \times 460 \times 1072.34}{8 \times 1570}$$

$$= 196.37\ N/mm^2$$

Modification factor $= \frac{250}{\sigma_s} = \frac{250}{196.37} = 1.273$

Hence modified span/depth ratios for

31.9	$\rho = 0.5\% =$	$25 \times 1.273 =$	31.825
	$\rho = 0.15\% =$	$34 \times 1.273 =$	43.282
	$\rho = 0.469 =$	=	32.84

∴ Min depth, d, is = $d = \frac{\text{Span}}{\text{span/depth ratio}}$

$$= \frac{9741}{32.84} = 297.6$$

USE effective depth $d = 300$

LEAVE AS $d = 335$ mm $h = 360$ mm

Civil Engineering Department	CONTRACT FRAME DESIGN			JOB REF.
The University DUNDEE	Drawing Ref.	Calculations by	Checked by	Calc. Sheet No. 7
	Part of Structure 10M SPAN SLAB			Date

Ref.	CALCULATIONS	OUTPUT

SECONDARY REINFORCEMENT

Provide T10 @ 75mm centres As(trans) 1050 mm²/m

As(trans) ⩾ 0.2 As(main) = 0.2 × 1570 = 314 mm²/m ∴ ok.

MAX spacing < 3h = 3×360 = 1080 mm ⩾ 500 mm ∴ ok

SHEAR REINFORCEMENT

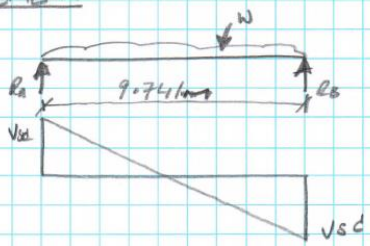

ULTIMATE LOAD = 113.62 kN

Shear force - (Vsd)

$$V_{sd} = \frac{W}{2} = \frac{113.62}{2} = 56.81 \text{ kN} = 56810 \text{ N}$$

EC2 Table 4.2

SHEAR Resistance of Concrete Alone (Ved.)

$f_{ck} = 30 \text{ N/mm}^2$ $\tau_{RD} = 0.34 \text{ N/mm}^2$

$k = 1.6 - d$ ⩾ 1 $\{d \text{ in (m)}\} = 1.6 - 0.335 = 1.265$

Assuming that 50% of the midspan steel does not extend to the supports $A_{si} = \frac{1570}{2} = 785 \text{ mm}^2/\text{m}$

$$\rho_l = \frac{A_{si}}{b_w d} = \frac{785}{1000 \times 335} = 0.00234$$

$\sigma_{cp} = 0$

$$V_{cdi} = [\tau_{cd} \, k (1.2 + 40 \rho_l) + 0.15 \sigma_{cp}] b_w d$$

$$= 0.34 \times 1.265 (1.2 + 40 \times 0.00234) + 0.15 \times 0] 1000 \times 335$$

$$= 186386 \text{ N}$$

V_{cdi} 186386 N > 65480 V_{sd}, no SHEAR reinforcement required

Civil Engineering Department	CONTRACT FRAME DESIGN			JOB REF.
The University DUNDEE	Drawing Ref.	Calculations by	Checked by	Calc. Sheet No. 8
	Part of Structure 10m SPAN SLAB			Date

Ref.	CALCULATIONS	OUTPUT

CRACKING

360mm Slab Thickness > 200mm.

Minimum Reinforcement provides
Bar size and spacing limited in accordance with provisions in sizes TABLE 4.12 EC2

where σ_s = 265.9

∴ crack width limited to 0.3mm.

Reinforcement Details (NTS)

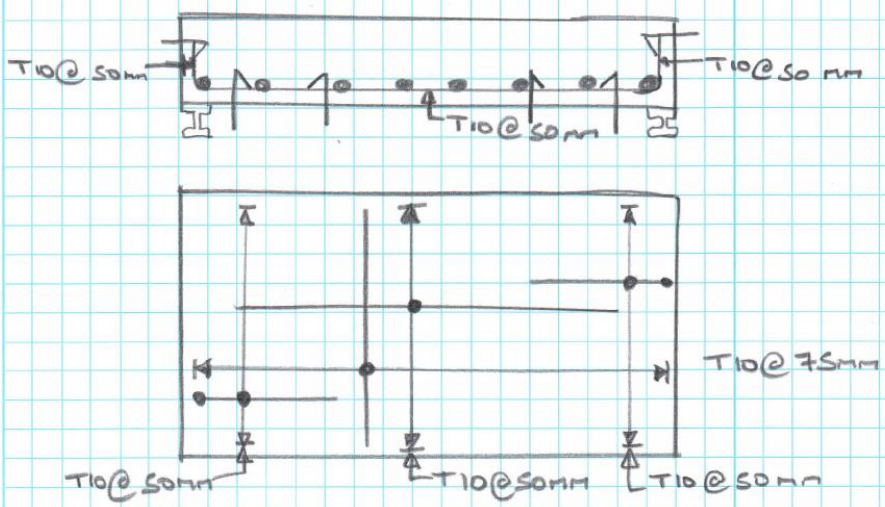

Civil Engineering Department	CONTRACT			JOB REF.
	FRAME DESIGN			
The University DUNDEE	Drawing Ref.	Calculations by	Checked by	Calc. Sheet No. 9
	Part of Structure	10M SPAN SLAB		Date

Ref.	CALCULATIONS	OUTPUT

SUMMARY

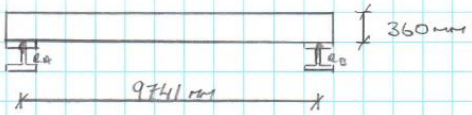

f_{ck} = 30 N/mm²
f_{yk} = 460 N/mm²

ULTIMATE LOAD 113.62 kN

DESIGN MOMENT (M) 138.35 kNm
MOMENT RESISTANCE (M_u) 562.25 kNm

MAIN REINFORCEMENT T10 @ 50mm spacing ((As 1570) mm²/m)

SECONDARY REINFORCEMENT T10 @ 75mm spacing (As 1050 mm²/m)

$R_A = R_B$ = 56.81 kN

Civil Engineering Department	CONTRACT Simple Frame Design Pinned Joints			JOB REF.
The University DUNDEE	Drawing Ref.	Calculations by	Checked by	Calc. Sheet No. 1
	Part of Structure 10m Long Beam. 610 x 229 x 140 UB			Date

Ref.	CALCULATIONS	OUTPUT

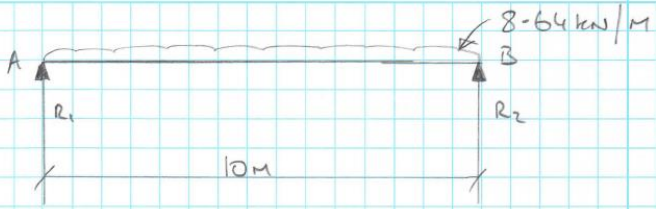

$$R_1 = R_2 = \frac{8.64 \times 10}{2} = 43.2 \text{ kN}$$

Design load on column

Reaction to beam + Self weight

$43.2 + 1.49 = \underline{44.69 \text{ kN}}$

Design Moment

Bending Moment

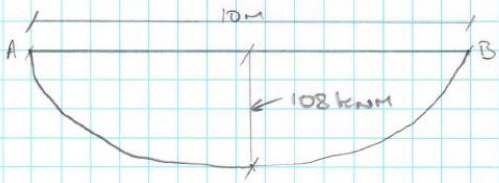

$$\frac{wL^2}{8} = \frac{8.64 \times 10^2}{8}$$

$= 108 \text{ kNM}$

Shear force diagram

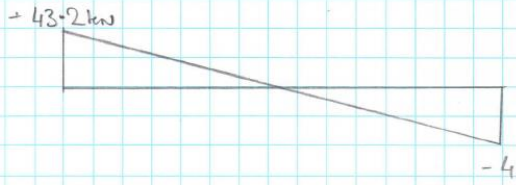

* Hence design moment (M) = 108 kNM which occurs @ mid-span @ zero point of shear force
* Design shear force (V) = 43.2 kN occuring @ supports

Civil Engineering Department	CONTRACT			JOB REF.
The University DUNDEE	Drawing Ref.	Calculations by	Checked by	Calc. Sheet No. 3
	Part of Structure			Date

Ref.	CALCULATIONS	OUTPUT

Resistance of cross Section

Bending moment

S.4.5.2

$$M_{pl,Rd} = \frac{W_{pl} f_y}{\gamma_{M0}}$$

$$= \frac{4142 \times 10^3 \times 275}{1.05}$$

$$= 1084.81 \times 10^6 \text{ Nmm}$$

$$= 1084.81 \text{ kNm} > M_{sd}\ 108 \text{ kNm}$$

$\therefore$ ok

Shear

S.4.6 Design shear force, V_{sd} is

$$V_{sd} = 43.2 \text{ kN}$$

$$V_{sd} \leq V_{pl,Rd}$$

$$V_{pl,Rd} = \frac{A_v (f_y / \sqrt{3})}{\gamma_{M0}}$$

Point (4) For simplicity A_v for rolled section, load parallel to web, may be taken as.

$$A_v = 1.04\, h t_w$$

$$= 1.04 \times 617.2 \times 13.1$$

$$= 8408.7 \text{ mm}$$

$$V_{pl,Rd} = \frac{8408.7 \left(275/\sqrt{3}\right)}{1.05}$$

$$= 1282 \text{ kN}$$

$$V_{sd} \leq V_{pl,Rd}$$

$$43.2 \text{ kN} \leq 1282 \text{ kN}$$

$\therefore$ ok

Civil Engineering Department	CONTRACT			JOB REF.
The University DUNDEE	Drawing Ref.	Calculations by	Checked by	Calc. Sheet No. 4
	Part of Structure			Date

Ref.	CALCULATIONS	OUTPUT

Bending and shear.

5.4.7 M_{pLRD} is reduced if

$V_{Sd} > 0.5 V_{pLRD}$

$43.2\,kN \not> 641\,kN$

∴ no reduction required.

5.6 **Shear buckling Resistance**

$$\frac{d}{t_w} \leq 69\varepsilon$$

$41.8 \leq 63.76$

∴ no check required.

5.7.7 **Flange induced buckling**

$$\frac{d}{t_w} = k(E/f_{yf})[A_w/A_{fc}]^{0.5}$$

A_w = area of web $= (h-2t_f)\,t_w$

$= 7506.3\,mm^2$

A_{fc} = area of compression flange

$= b \times t_f = 5087.4\,mm^2$

for class 1 flanges $k = 0.3$

E = Modulus of elasticity $= 210,000\,N/mm^2$

$41.8 = 0.3(210\times10^3/275)[7506.3/5087.4]^{0.5}$

$41.8 < 278.27$

∴ ok

Civil Engineering Department	CONTRACT			JOB REF.
The University DUNDEE	Drawing Ref.	Calculations by	Checked by	Calc. Sheet No. 5
	Part of Structure			Date

Ref.	CALCULATIONS	OUTPUT

5.7 Resistance of web to transverse forces

5.7.3 Crushing resistance

$$R_{yed} = (S_s + S_y)\, t_w f_{yw} / \gamma_M$$

Fig 5.7.2 from before (previous beam check)

$S_y = 212\,mm$

5.7.3 use half $\therefore \frac{S_y}{2} = 106\,mm$

$$R_{yed} = \frac{(70 + 106)\, 13.1 \times 275}{1.05}$$

$= 603848\,N$

$= 603.8\,kN > V_{sd} = 43.2\,kN$

$\therefore$ ok

5.7.4 Crippling Resistance

$$R_{red} = 0.5\, t_w^2 (E f_{yw})^{0.5} \left[(t_f/t_w)^{0.5} + 3(t_w/t_f)(S_s/d) \right] / \gamma_{M1}$$

$$R_{red} = \frac{0.5 \times 13.1^2 \left(210 \times 10^3 \times 275\right)^{0.5} \left[22.1/13.1 \right)^{0.5} + 3(13.1/22.1)(70/547.6) \right]}{1.05}$$

$R_{red} = 947799.145\,N$

$= 947.8\,kN > V_{sd} = 43.2\,kN$

$\therefore$ ok

Civil Engineering Department	CONTRACT			JOB REF.
The University DUNDEE	Drawing Ref.	Calculations by	Checked by	Calc. Sheet No.
	Part of Structure			Date

Ref.	CALCULATIONS	OUTPUT

4.2 **Deflection**

$$M_{max} = \frac{wL^2}{8} = 108 \text{ kNm}$$

5.4.5.2 $$(M_c R_d)_{cl} = \frac{W_{el} f_y}{\gamma_{M0}}$$

$$= \frac{3622 \times 10^3 \times 275}{1.05} = 949 \times 10^6 \text{ Nmm}$$

$$= 949 \text{ kNm} > M_{max}$$

∴ ok.

Hence deflection can be calculated elastically

Deflection due to permanent and variable loading ie.

$$w = 8.64 \text{ kN/m}$$

$$\delta_{max} = \frac{5 w L^4}{384 EI}$$

$$= \frac{5}{384} \frac{8.64 \times 10000^4}{210 \times 10^3 \times 111777 \times 10^4}$$

$$= 4.8 \text{ mm} < \frac{\text{Span}}{250} = \frac{10000}{250} = 40 \text{ mm}$$

∴ ok

∴ UB 610 x 229 x 140 is ok

Civil Engineering Department	CONTRACT			JOB REF.
The University DUNDEE	Drawing Ref.	Calculations by	Checked by	Calc. Sheet No. 1
	Part of Structure Column 254×254×107 UC Simple construction, pinned.			Date

Ref.	CALCULATIONS	OUTPUT

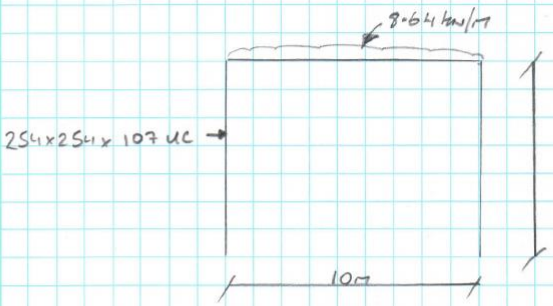

UC 254×254×107 UC unit mass = 107·1 kg/m

unit weight of column = 107·1 × 10 = 1071 N/m

= 1·1 kN/m

1·1 × 1·35 = 1·5 kN/m

1·5 × 5m = 7·5 kN

Design Loading and moments.

ULTIMATE REACTION from beam = 45 kN

self weight = 7·5 kN

ULTIMATE Axial load, F is

45 + 7·5 = 52·5 kN

Load eccentricity for beam

$e_x = D/2 + 100 = \frac{266.7}{2} + 100 = 233.35$ mm

Moment due to beam

$M_x = R_{AC_x} = 45 \times 10^3 \times 233.35 = 10.5 \times 10^6$ N mm

10·5 kNm

Civil Engineering Department	CONTRACT			JOB REF.
The University DUNDEE	Drawing Ref.	Calculations by	Checked by	Calc. Sheet No. 2
	Part of Structure			Date

Ref.	CALCULATIONS	OUTPUT

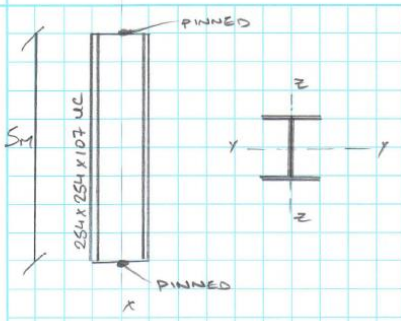

SECTION PROPERTIES

AREA of section (A) 13600 mm²

D = 266.7 mm		r = 12.7 mm	
B = 258.8 mm		d = 200.3 mm	
t_w = 12.8 mm		d/T_f = 6.31	
T_f = 20.5 mm		b/t_w = 15.6	

Radius of gyration — yy axis = 113 mm; zz axis = 65.9 mm

Factored axial loading is

$$N_{Sd} = 45 \times 1.35 = 60.75 \text{ kN}$$

Factored bending moment at top, middle and bottom of column:

$$M_{Sd.t} = 10.5 \times 1.5 = 15.75 \text{ kNm}$$

$$M_{Sd.m} = 7.875 \text{ kNm}$$

$$M_{Sd.b} = 0 \text{ kNm}$$

EC3 STRENGTH CLASSIFICATION

T. 3.1 FLANGE THICKNESS = 20.5 mm
STEEL GRADE = Fe430

HENCE FROM TABLE 3.1, $f_y = 275 \text{ N/mm}^2$

SECTION CLASSIFICATION

T S. 3.1 $\varepsilon = \sqrt{235/275}$

$\varepsilon = 0.924$

T S. 3.1 Sheet (3) $c/t_f \leq 10\varepsilon$

$6.312 \leq 9.24$

T. S. 3.1 Sheet (1) $d/t_w \leq 33\varepsilon$

$15.65 \leq 30.49$

HENCE FROM TABLE 5. 3.1, SECTION BELONGS TO CLASS 1

Civil Engineering Department	CONTRACT			JOB REF.
The University DUNDEE	Drawing Ref.	Calculations by	Checked by	Calc. Sheet No. 4
	Part of Structure			Date

Ref.	CALCULATIONS	OUTPUT

BS 5950 Table 24

RESISTANCE OF MEMBER : COMBINED BENDING + AXIAL COMPRESSION

Effective length of column = $1.0L$
= 5000 mm

EC3

THE COLUMN WILL BUCKLE ABOUT THE WEAK AXIS (z-z)
SLENDERNESS RATIO ABOUT z-z AXIS, λ_z is:

5.5.1.4 (3)

$$\lambda_z = \frac{L_{eff\,z}}{i_z} = \frac{5000}{65.9} = 75.87$$

i is the Radius of gyration about z-z

5.5.1.1 (1) Here β_A = 1 for class 1 sections

5.5.1.2

$$\lambda_1 = 93.9\varepsilon = 93.9 \times 0.924$$

$$\underline{\lambda_1 = 86.76}$$

$$\bar{\lambda}_z = \left(\frac{\lambda_z}{\lambda_1}\right)(\beta_A)^{1/2}$$

$$= \left(\frac{75.87}{86.76}\right)(1)^{1/2}$$

$$\bar{\lambda}_z = 0.874$$

Table 5.5.3

Rolled I section

$$\frac{h}{b} = \frac{266.7}{258.8} = 1.03 < 1.2$$

$$t_f = 20.5 \leq 100\,mm$$

∴ from TABLE 5.5.3 for buckling about the z-z axis Buckling curve "b" is appropriate.

Table 5.5.1

$$\alpha = 0.34$$

5.5.1.2

$$\phi = 0.5\left[1 + \alpha(\bar{\lambda} - 0.2) + \bar{\lambda}^2\right]$$

Civil Engineering Department	CONTRACT			JOB REF.
The University DUNDEE	Drawing Ref.	Calculations by	Checked by	Calc. Sheet No. 5
	Part of Structure			Date

Ref.	CALCULATIONS	OUTPUT

$$\phi = 0.5\left[1 + 0.34(0.874 - 0.2) + 0.874^2\right]$$

$$\phi = 0.997$$

5.5.1.2

$$X = \frac{1}{\phi + \left[\phi^2 - \bar{\lambda}^2\right]^{0.5}}$$

$$= \frac{1}{0.997 + \left[0.997^2 - 0.874^2\right]^{0.5}}$$

$$X = \underline{0.677} \leq 1 \quad \therefore \text{ok}$$

$N_c Rd = N_{pl.Rd} = 3562$ kN

$M_{ply.Rd} = M_{pl.Rd} = 389$ kNm

5.5.4 Check (eqn 5.51)

$$\frac{N_{Sd}}{X_{min}\, N_{c.Rd}} + \frac{k_y . M_{y.Sd}}{M_{pl.y.Rd}} \leq 1$$

$$\frac{60.75}{0.677 \times 3562} + \frac{1 . 15.75}{389} \leq 1$$

$$0.066 \leq 1$$

$\therefore$ OK

HENCE THE SELECTED SECTION IS SUITABLE

Appendix B

Static & seismic bearing capacity (FEM model)

The hand calculations used to determine the static and seismic bearing capacities and factors of safety for the finite element analysis models is presented here.

Civil Engineering Department	CONTRACT			JOB REF.
The University DUNDEE	Drawing Ref.	Calculations by	Checked by	Calc. Sheet No. 001
	Part of Structure F.E. Model Bearing Capacity Check			Date

Ref.	CALCULATIONS	OUTPUT

Strip Footing

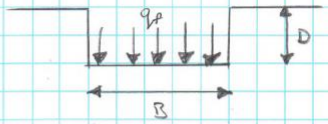

B = 2m

D = 0.6m

Properties of Sand

	Sand
γ	17
c'	0.3
ϕ	35°

Static Loading

Bearing Capacity factors

$N_\gamma = 40$ $N_c = 46$ $N_q = 34$

$q_{ff} = (0.5 \times 17 \times 2 \times 40) + (0.3 \times 46) + (17 \times 0.6 \times 34)$

$q_{ff} = 1040.6$ kPa

Static Bearing Capacity = 1041 kPa

Dynamic analysis

Bearing Capacity factors

Knappett et al (2006)

For $K_h = 0.07g$ $N_\gamma = 23$ $N_q = 25$ $N_c = 31$

$q_{ff} = (0.5 \times 17 \times 2 \times 23) + (0.3 \times 31) + (17 \times 0.6 \times 25) =$

Bearing capacity for 0.07g earthquake 655.3kPa

Civil Engineering Department	CONTRACT			JOB REF.
The University DUNDEE	Drawing Ref.	Calculations by	Checked by	Calc. Sheet No. 002
	Part of Structure FE MODEL BEARING CAPACITY CHECK			Date

Ref.	CALCULATIONS	OUTPUT

for $k_h = 0.35g$ $N_\gamma = H$ $N_q = 3$ $N_c = 5$

$q_f = (0.5 \times 17 \times 2 \times 1.1) + (0.3 \times 5) + (17 \times 0.6 \times 3)$

$= 50.8$

Bearing Capacity for 0.35g earthquake **50.8 kPa**

Force Applied by Frame (q)

5x8 Frame

Slab $(8 \times 8 \times 0.36 \times 2400) \frac{1}{4}$	=	13824 kg
Beam $(149.2 \times 8) \frac{1}{2}$	=	597 kg
Column (107.1×5)	=	536 kg
Plate $(2 \times 1 \times 0.05 \times 7800)$	=	780 kg
Found $(2 \times 0.6 \times 4 \times 2400)$	=	11520 kg
		27257 kg

Bearing Pressure applied $\frac{27257}{2*4} \times 9.81$ **33.4 kPa**

5x3 Frame

Slab $(8 \times 3 \times 0.36 \times 2400) \frac{1}{4}$	=	5184 kg
Beam $(149.2 \times 3) \frac{1}{2}$	=	224 kg
Column (107.1×5)	=	536 kg
Plate $(2 \times 1 \times 0.05 \times 7800)$	=	780 kg
Found $(2 \times 0.6 \times 4 \times 2400)$	=	11520 kg
		18244 kg

Bearing Pressure Applied $\frac{18244}{2 \times 4} \times 9.81$ **22.4 kPa**

Civil Engineering Department	CONTRACT			JOB REF.
The University DUNDEE	Drawing Ref.	Calculations by	Checked by	Calc. Sheet No. 003
	Part of FE MODEL Structure BEARING CAPACITY CHECK			Date

Ref.	CALCULATIONS	OUTPUT

3×3 Frame

Slab $(8 \times 3 \times 0.36 \times 2400) \frac{1}{4}$ = 5184 kg

Beam $(149.2 \times 3) \frac{1}{2}$ = 224 kg

Column (107.1×3) = 321 kg

Plate $(2 \times 1 \times 0.05 \times 7800)$ = 780 kg

Found $(2 \times 0.6 \times 4 \times 2400)$ = 11520 kg

18029 kg

Bearing Pressure Applied = $\frac{18029}{2 \times 4} \times 9.81$ 22.1 kPa

Factor of Safety (q_f / q)

	Static	0.07g	0.35g
5×8	31	20	1.5
5×3	46	29	12
3×3	47	30	2

Civil Engineering Department	CONTRACT			JOB REF.
The University DUNDEE	Drawing Ref.	Calculations by	Checked by	Calc. Sheet No. 004
	Part of Structure FE MODEL - BEARING CAPACITY CHECK - SETTLEMENT			Date

Ref.	CALCULATIONS	OUTPUT

CRAIG'S SOIL MECHANICS Section 8.6 Eqn 8-53

$$s = \frac{qB}{E}\left(1 - \nu^2\right) I_s$$

$B = 2$
$E = 35\ \text{MPa}$
$\nu = 0.3$

$\frac{L}{B} = 2 \quad \therefore I_s = 1.2$ (from table 8.6, CSM8)

5x8 frame

$q = 33.4\ \text{kPa}$

$s = \frac{33.4 \times 2}{35000}\left(1 - 0.3^2\right) 1.2 = 0.0021\ \text{m}$ — **2.1 mm**

5x3 frame

$q = 22.4\ \text{kPa}$

$s = \frac{22.4 \times 2}{35000}\left(1 - 0.3^2\right) 1.2 = 0.0014\ \text{m}$ — **1.4 mm**

3x3 frame

$q = 22.1\ \text{kPa}$

$s = \frac{22.4 \times 2}{35000}\left(1 - 0.3^2\right) 1.2 = 0.0014$ — **1.4 mm**

Appendix C

Static & seismic bearing capacity (centrifuge model)

The hand calculations used to determine the static and seismic bearing capacities and factors of safety for the centrifuge analysis models is presented here.

Civil Engineering Department	CONTRACT CENTRIFUGE MODEL			JOB REF.
The University DUNDEE	Drawing Ref.	Calculations by	Checked by	Calc. Sheet No. 001
	Part of Structure BEARING CAPACITY CHECK			Date

Ref.	CALCULATIONS	OUTPUT

STRIP Footing

B = 2m
D = 0 (no embedment)

Soil Properties

$\gamma = 17$ $c' = 0$ ϕ_{crit} 32° ϕ_{peak} 38°

Static Loading q_f

CRIT $N_\gamma = 28$ $N_c = 38$ $N_q = 26$

$q_f = (0.5 \times 17 \times 2 \times 28) + (0 \times 38) + 0 =$ 476 kPa

Peak $N_\gamma = 62$ $N_c = 82$ $N_q = 51$

$q_f = (0.5 \times 17 \times 2 \times 62) + 0 + 0 =$ 1054 kPa

Dynamic Analysis

For $K_h = 0.1g$

CRIT $N_\gamma = 10$ $N_c = 18$ $N_q = 15$

$q_f = (0.5 \times 17 \times 2 \times 10) + 0 + 0$ 170 kPa

Peak $N_\gamma = 29$ $N_c = 32$ $N_q = 30$

$q_f = (0.5 \times 17 \times 2 \times 29) + 0 + 0$ 493 kPa

For $K_h = 0.46g$

CRIT $N_\gamma = 0.1$ $N_c = 0.5$ $N_q = 0.35$

$q_f = (0.5 \times 17 \times 2 \times 0.1) + 0 + 0$ 1.7 kPa

Peak $N_\gamma = 0.3$ $N_c = 1.8$ $N_q = 0.6$

$q_f = (0.5 \times 17 \times 2 \times 0.3) + 0 + 0$ 5.1 kPa

Civil Engineering Department	CONTRACT CENTRIFUGE MODEL			JOB REF.
The University DUNDEE	Drawing Ref.	Calculations by	Checked by	Calc. Sheet No. 002
	Part of Structure BEARING CAPACITY CHECK			Date

Ref.	CALCULATIONS	OUTPUT

FORCE APPLIED BY FRAMES (q)

TALL STRUCTURE = 276kPa

SMALL STRUCTURE = 161 kPa

FACTOR OF SAFETY (q_f/q) for ϕ CRIT

	STATIC	0.1g	0.46g
TALL STRUCTURE	1.72	0.62	0.004
SHORT STRUCTURE	2.96	1.1	0.007

FACTOR OF SAFETY q_f/q for ϕ peak

	STATIC	0.1g	0.46g
TALL STRUCTURE	3.8	1.79	0.02
SHORT STRUCTURE	6.55	3.06	0.03